

This document is provided as an academic material for personal use only. Any use of parts of this text, figures, or results is subject to copyright rules and warrants a proper authorization from the author.

Analysis and Synthesis of Parallel Robots for Medical Applications

Nabil Simaan

Analysis and Synthesis of Parallel Robots for Medical Applications

RESEARCH THESIS

SUBMITTED IN PARTIAL FULFILLMENT
OF THE REQUIREMENTS FOR THE DEGREE OF
MASTER OF SCIENCE IN MECHANICAL ENGINEERING

by

Nabil Simaan

SUBMITTED TO THE SENATE OF
THE TECHNION – ISRAEL INSTITUTE OF TECHNOLOGY

This research was conducted under the supervision of Prof. Moshe Shoham in the Faculty of Mechanical Engineering , Technion – Israel Institute of Technology.

Acknowledgments

I am grateful for the dedicated supervision of Prof. Moshe Shoham. I spent about three busy years working with him in which I learned to appreciate his perseverance in research. I appreciate the time he spent with me on realizing this work both theoretically and especially practically in the stage of developing the prototype.

I thank Mrs. Hanna Maller for her patience in answering all my endless questions regarding the bureaucratic procedures during my study period.

I would like to thank the technical staff of the workshop in the robotics and manufacturing building of the Mechanical Engineering faculty for their work in preparing the prototype. Special thanks are dedicated to Yossi Barzily who expressed in stages of manufacturing his critical thoughts about my design and made me think about design issues repeatedly.

I appreciate the work done by Avi Suliman who prepared the electrical system. Without his professional work, the electrical setup for the prototype would have been still missing.

The generous financial support of the Technion, Mitchell-Sorf Foundation, and Marco and Louise Mitrani Memorial Fellowship is gratefully acknowledged.

Finally, I would like to thank my family for their support and encouragement.

*Dedicated to my father, Butros, and my mother, Mariam, who spent
endless efforts in bringing me up to be what I am today.*

Contents

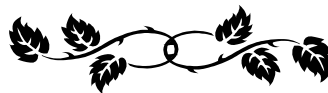
Abstract	1
List of Symbols.....	3
1 Introduction to Parallel Manipulators.....	7
1.1	Three
robotic architectures	7
1.2	Fully
parallel and non-fully parallel manipulators.....	11
2 Parallel Robots in Research and Industry: A Brief Review of the Literature	13
3 Robots for Medical Applications.....	19
3.1 Medical robots and parallel robots in medical applications	19
3.2 The fundamental requirements from a medical robot	20
3.3 Advantages of parallel robots in medical applications.....	21
4 Formulation of the Design Problem	23
5 Type Synthesis.....	26
5.1 Introduction	26
5.2 Synthesis of a class of parallel manipulators.....	28
5.3 Selecting architectures based on design guidelines.....	30
5.4 A family of parallel manipulators	36
5.5 The RSPR and the USR manipulators.....	38
5.5.1 The USR manipulator	38
5.5.2 The RSPR manipulator	39
6 Kinematics of the USR and the RSPR Robots	41
6.1 Introduction	41
6.2 Inverse kinematics of the RSPR robot	44
6.3 Inverse kinematics of the USR robot	49
7 Jacobian Formulation of A Class of Parallel Robots.....	54
7.1 Introduction	54
7.2 The Jacobian matrix for parallel manipulators.....	54
7.3 Jacobian formulation of a class of parallel Robots.....	57
7.3.1 Jacobian of the tripod mechanism	57
7.3.2 Jacobian matrix of the RSPR robot	61

7.3.3	Jacobian matrix of the USR robot	62
7.4	Conclusions	64

Contents – (continued)

8	Dimensional Synthesis of the USR and the RSPR Robots and Performance-Based Comparison.....	65
8.1	Introduction	65
8.2	Dimensional synthesis.....	65
8.3	Selecting a prototype candidate.....	72
8.4	Work volume of the selected RSPR robot.....	73
8.5	Conclusion.....	77
9	Introduction to Line Geometry	78
9.1	Introduction	78
9.2	Homogeneous coordinates of points, planes and lines in space.....	78
9.2.1	Homogeneous coordinates of a point in space	78
9.2.2	Homogeneous coordinates of a plane in space.....	79
9.2.3	The principle of duality	79
9.2.4	Homogeneous coordinates of a line.....	80
9.3	The basic geometric forms	82
9.4	Line families and linear dependence of line.....	86
9.4.1	The linear complex	86
9.4.2	The linear congruence	88
9.4.3	The regulus	90
9.5	Line varieties	92
10	Singularity Analysis	96
10.1	Introduction	96
10.2	A
	analysis of Parallel singularities for a class of non-fully	
	
	parall
	el manipulators	100
10.2.1	The method of analysis	100
10.2.2	Preliminary definitions.....	100

10.2.3	Point singularities (1a)	103
10.2.4	Flat pencil singularities (2b).....	103
10.2.5	Planes singularities.....	113
10.2.6	Linear Congruence singularities.....	119
10.2.7	Linear complex singularities	124
Contents – (continued)		
10.2.8	Concluding remarks	128
10.2.9	Design guidelines for minimizing the parallel singularities.....	130
10.3	Analysis of serial singularities for the RSPR and USR robots	131
10.3.1	Serial singularities of the RSPR robot	131
10.3.2	Serial singularities of the USR robot	133
10.4	Conclusions	136
11	The RSPR Prototype robot	137
11.1	Introduction	137
11.2	The RSPR prototype robot – design characteristics and specifications	137
11.3	Mechanical properties of the prototype.....	140
11.4	Experimental setup	140
11.5	Future work and experimentation.....	142
11.6	Conclusion.....	142
12	Conclusions	144
12.1	Perspective overview of the work	144
12.2	Future work	145
Appendix A.....		146
References.....		153



List of Figures

Figure 1.1:	Serial manipulator	7
Figure 1.2:	Parallel manipulator	9

Figure 1.3: Hybrid manipulator	9
Figure 1.4: A hybrid manipulator [Shainpoor, 1992]	10
Figure 1.5: The ASEA industrial robot as an example of a hybrid architecture.....	10
Figure 2.1: The original flight simulator concept presented by [Stewart, 1965].....	13
Figure 2.2: Two common types of the Stewart platform	14

Contents – (continued)

Figure 2.3: The parallel robot presented by Tsai and Tahmasebi [1993]	15
Figure 2.4: The parallel robot presented by Ben-Horin and Shoham [1996]	15
Figure 2.5: The Double-Tripod.....	16
Figure 2.6: The uncoupled 6-Dof 2-Delta robot	16
Figure 2.7:The	
Double Circular Triangular robot	17
Figure 3.1: The fundamental requirements from a medical robot	22
Figure 4.1: Laser beam laparoscopic surgery	23
Figure 4.2: Symbolic representation of the design goal	25
Figure 5.1: (a) The Bennett linkage. (b) The Spherical crank	27
Figure 5.2: Mobility and connectivity in the Stewart 6-6 platform with two spherical joints at the extremities of each extensible link	28
Figure 5.3: The robot presented by Behi [1988].....	33
Figure 5.4: The robot presented by Kholi et al. [1988]	33
Figure 5.5: The robot presented by Romiti and Soreli [1990].....	33
Figure 5.6: The kinematic chain of the robot presented by Soreli, et al. [1997]	34
Figure 5.7: The robot presented by Zlatanov, et al. [1992]	34
Figure 5.8: The robot presented by Alizade, Tagiyev, and Duffy [1994]	34
Figure 5.9: The robot presented by Collins and Long [1995(a)]	35
Figure 5.10: The parallel robot presented by Mimura and Funahashi [1995]	35
Figure 5.11: The parallel robot presented by Ebert and Gosselin [1998]	35
Figure 5.12: The parallel robot presented by Byun and Cho [1997]	36
Figure 5.13: The parallel robot presented by Cleary and Uebel [1994]	36
Figure 5.14: A family of 14 manipulators with common kinematic features.....	37
Figure 5.15: USR parallel robot.....	38
Figure 5.16: The RSPR parallel robot	39

Figure 6.1: Common symbols used for the RSPR and the USR robots.....	43
Figure 6.2: The RSPR with the kinematic model for one kinematic chain	45
Figure 6.3: Top view of the base platform and the notation system of the rotating links' angles	45
Figure 6.4: The first four out of eight solutions of the inverse kinematics problem for the RSPR robot.....	48

Contents – (continued)

Figure 6.5: The remaining four out of eight solutions of the inverse kinematics problem for the RSPR robot.....	49
Figure 6.6: USR robot with the kinematic model for one kinematic chain	50
Figure 6.7 The eight solutions of the inverse kinematics problem for the USR robot	53
Figure 7.1: Common tripod mechanism	57
Figure 7.2: Force transmission from link B_i to A_i and from link A_i to the moving platform	59
Figure 7.3: Geometrical interpretation of the rows of the tripod's Jacobian matrix	60
Figure 7.4: The actuators' moments and the forces transmitted through the spherical joints	61
Figure 7.5: USR robot with the kinematic loop	63
Figure 8.1: A parallel robot in central configuration and the correspondence of this configuration with the center of the required work volume.....	66
Figure 8.2: Characteristic dimensions of the RSPR robot (a) and the USR robot (b)	66
Figure 8.3: Geometric presentation of the symbols in table 8.2	68
Figure 8.4: Geometric representation of the symbols in table 8.3	68
Figure 8.5: RSPR selected robot actuator forces along the diagonal path.....	72
Figure 8.6: USR selected robot actuator forces along the diagonal path.....	73
Figure 8.7: The RSPR in an initial position and its associated coordinate system.....	74
Figure 8.8: Sections of the RSPR robot work volume with parallel platforms and an initial position of $[0, 0, 0.16]$ [m]	75
Figure 8.9: The RSPR robot work volume boundary surface with parallel platforms and an initial position of $[0, 0, 0.16]$ [m].....	75
Figure 8.10: Work volume sections of the RSPR robot with the moving platform rotated 20° about the $[1, 1, 0]$ axis.....	76

Figure 8.11:	Work volume boundary surface of the RSPR robot with the moving platform rotated 20° about the $[1, 1, 0]$ axis.....	76
Figure 9.1:	Physical interpretation of the Plucker coordinates	81
Figure 9.2:	Mutual moment of two lines	83
Figure 9.3:	Four parameters define every line in space	84

Contents – (continued)

Figure 9.4:	Six independent lines span the space	85
Figure 9.5:	The special complex	87
Figure 9.6:	The hyperbolic congruence	89
Figure 9.7:	The Parabolic congruence as a subset of lines of the General complex	89
Figure 9.8:	The degenerate congruence and its associated general complex	90
Figure 9.9:	The regulus and the conjugate regulus	91
Figure 9.10:	The three types of degenerate reguli	102
Figure 10.1:	Geometrical interpretation of $\tilde{\mathbf{J}}$ and its associated lines $\mathbf{l}_1.. \mathbf{l}_6$	104
Figure 10.2:	15 flat pencils defined by six lines in space	104
Figure 10.3:	Flat pencil groups	105
Figure 10.4:	Singular configuration S1	105
Figure 10.5:	Singular configuration S2	107
Figure 10.6:	Singular configuration S3	108
Figure 10.7:	Singular configuration S4	109
Figure 10.8:	Side view of singular configuration S5	110
Figure 10.9:	Singular configuration S5	110
Figure 10.10:	Singular configuration S6	112
Figure 10.11:	Singular configuration S7	112
Figure 10.12:	Singular configuration S8	115
Figure 10.13:	Special case of singular configuration S7	116
Figure 10.14:	Special Case of Singular configuration S6	117
Figure 10.15:	Singular configuration S9	118
Figure 10.16:	Singular configuration S10	121

Figure 10.17: Singular configuration S11	122
Figure 10.18: The lines of Γ belong to the same general complex if and only if lines \mathbf{l}_7 , \mathbf{l}_8 , and \mathbf{l}_9 belong to a common flat pencil.....	125
Figure 10.19: A simplified case study	126
Figure 10.20: Top view of the initial configuration (a) and the sectors of lines \mathbf{l}_7 and \mathbf{l}_8 (b).....	127
Figure 10.21: Singular configuration S13	128
Figure 10.22: Serial singularities of the RSPR robot – cases a..c	132

Contents – (continued)

Figure 10.24: Carnot maps for registering the configurations in which \mathbf{B} is singular	133
Figure 10.25: The five serial singularities of the USR robot.....	135
Figure 11.1: The RSPR prototype robot demonstrating surgical tool positioning	138
Figure 11.2: Top view of the RSPR prototype robot showing weight reduction voids in the base platform	139
Figure 11.3: A block diagram of the robot's control units	141
Figure 11.4: The imaginary circle for collision detection between the linear actuators and the centrally mounted motors.....	142

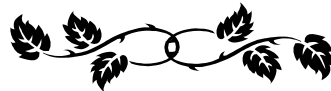
List of Tables

Table 1.1: Comparison between Serial and Parallel manipulators.....	11
Table 5.1: The possible parallel manipulators with identical kinematic chains.....	30
Table 5.2: Listing of known parallel manipulators with three kinematic chains	31
Table 7.1: Jacobian definition for Parallel and Serial manipulators.....	56
Table 8.1: The scanned range of characteristic dimensions of the RSPR and USR robots	67
Table 8.2: Simulation results for the RSPR robot	69
Table 8.3: Simulation results for the USR robot- The first 20 robots out of 95 admissible robots.....	70
Table 9.1: Duality of geometric basic elements	81
Table 9.2: Linear dependence relations between the lines in Fig. 9.4 (a) and the lines in Fig. 9.4 (b).....	70

Table 9.3:	Synthetic representation of the six line varieties reproduced from [Dandurand, 1984].....	80
Table 9.4:	All possible ways of adding an independent line to a group of one to five lines. [Dandurand, 1984].....	86
Table 9.5:	Combinatorially equivalent cases. [Dandurand, 1984]	95
Table 10.1:	15 line quadruplets and their separation into four categories.....	114
Table 10.2:	Complete listing of all 20 line-triples and their separation into six groups ...	123
Table 10.3:	Summary of parallel singular configurations	128

Contents – (continued)

Table 10.4.	Design guidelines for minimizing parallel singularities.....	129
Table 10.5:	The cases in which $C_{n_{1i}}=0$, $C_{n_{2i}}=0$, $C_{r_{1i}}=0$, $C_{r_{2i}}=0$ are fulfilled separately ...	133
Table 11.1:	Characteristic dimensions of the RSPR prototype.	137
Table 11.2:	Physical properties of the RSPR prototype	140



Abstract

Parallel manipulation is relatively a new field in robotics. The development in this field intensified during the last two decades; however, there are still unsolved problems to be investigated in this field. These problems include kinematic modeling and synthesis of new parallel architectures and singularity analysis. The solution of the forward kinematics of a general 6 DOF fully parallel manipulator is only three years old and the first example of a general 6 DOF fully parallel manipulator with 40 real solutions is only one year old. Although during the last decade there were many attempts for implementation of parallel robots, the full merits of these architectures were not fully understood and exploited.

Robot assisted surgery is also a new trend of development in surgery. Assimilating a robotic assistant in the surgical arena as an additional smart and precise tool bears numerous advantages. These advantages include broadening the capabilities of the surgeon in performing precise procedures and uplifting the burden of routine tasks. The intrinsic characteristics of parallel robots are discussed in this work and shown to suit the requirements of a robotic assistant better than the characteristics of serial robots.

Based on these facts, we aim our work towards developing a mini parallel robot for medical applications and exploring new parallel architectures. The work presents a task-oriented synthesis and design of a mini parallel robot for medical applications. Two robotic architectures (the RSPR and the USR robots), which are modifications of known structures, are presented in detail and compared in terms of required actuator forces, minimal dimensions, workspace, and practical design considerations. The work includes type and dimensional synthesis for the suggested architectures, Jacobian formulation, and singularity analysis for a class of non-fully parallel robots.

The Jacobian formulation presented in this work provides a method for classifying the non-fully parallel robots and grouping several architectures in families with common Jacobian formulation and singularity analysis. In particular, the formulation presented here groups 14 non-fully parallel robots into one family. This formulation also shows that all these 14 manipulators share the same parallel singularities due to a tripod mechanism common to all these manipulators. The singularity analysis and Jacobian formulation are based on geometrical understanding of the system, thus, providing easy method for physical interpretation of singularities and deducing conclusions regarding possible elimination of singularities by altering the geometrical characteristics of the robots.

The comparison between the USR and the RSPR robots shows that the RSPR robot better suits the procedure in hand than the USR robot in terms of smaller required actuator forces. The singularity analysis highlights an additional advantage of the RSPR over the USR robot in terms of having less singular configurations.

Based on the results of the comparison and the dimensional synthesis we constructed a prototype of a medical robotic assistant. We also implemented position control and wrote the control program that allows activating the prototype in a Master-Slave mode. This prototype features a new parallel architecture based on the RSPR concept, low weight, compactness, and accuracy. These characteristics promise successful future implementation of this prototype for laparoscope manipulation and knee surgery.

List of Symbols

Font setting

Throughout the entire work, we use small bold letter font setting for vectors, capital bold letters for matrices, and capital or small letters for scalars.

General symbols

- i : An index indicating a specific kinematic chain, $i = 1, 2, 3$.
- \mathbf{o}_p : Center point of the moving platform.
- r_p : Radius of the moving platform.
- \mathbf{t} : Position vector of the center of the moving platform.
- \mathbf{p}_i : Position vector of the upper extremity of the i 'th kinematic chain.
- \mathbf{pp}_i : Position vector of the upper extremity of the i 'th kinematic chain in the central platform-attached coordinate system.
- ξ_{pi} : An angle measured from the x-axis of the central platform-attached coordinate system, \mathbf{x}_p , to \mathbf{pp}_i according to the right-hand rule about \mathbf{z}_p .
- \mathbf{e}_i : Position vector of the lower extremity of the i 'th kinematic chain.
- e : The eccentricity measure (equal to the Euclidean norm of \mathbf{e}_i).
- ξ_{bi} : An angle measured from the x-axis of the world coordinate system, \mathbf{x}_0 , to \mathbf{e}_i according to the right-hand rule about \mathbf{z}_0 .
- \mathbf{b}_i : Position vector of the spherical joint of the i 'th kinematic chain.
- \mathbf{n} : A unit vector normal to the moving platform.
- $\hat{\mathbf{r}}_i$: A unit vector along the axis of the upper revolute joint in the i 'th kinematic chain.
- \mathbf{h}_i : A vector specifying the height of the i 'th kinematic chain upper extremity relative to the base plane.
- ${}^w\mathbf{R}_p$: Rotation matrix transforming vectors from the central platform-attached coordinate system to world coordinate system.
- ${}^p\mathbf{R}_{C_i}$: Rotation matrix from the C_i coordinate system to the central platform-attached coordinate system.
- \mathbf{l}_{bi} : A vector from the i 'th joint located on the base platform to the spherical joint of the i 'th kinematic chain.

- x:** Six-dimensional vector of the position and orientation variables of the output link.
- $\dot{\mathbf{x}}$:** Six-dimensional vector of the linear/angular velocities of the output link.
- q:** Six-dimensional vector of the active joints values.
- $\dot{\mathbf{q}}$:** Six-dimensional vector of the active joints' speeds.
- A_i:** The link of the i'th kinematic chain, which is connected to the moving platform.
- B_i:** The link of the i'th kinematic chain, which is connected to the base platform and to link A_i.
- $\hat{\mathbf{s}}_{1i}$:** A unit vector along link A_i.
- s_{1i}:** A vector from the spherical joint center to the upper extremity of the i'th kinematic chain along link A_i.
- $\hat{\mathbf{s}}_{2i}$:** A unit vector through the center of the spherical joint of the i'th kinematic chain and parallel to the axis of the upper revolute joint $\hat{\mathbf{r}}_i$.
- f_{1i}:** The magnitude of the force transmitted along link A_i.
- f_{2i}:** The magnitude of force acting on the tripod link, A_i, along $\hat{\mathbf{s}}_{2i}$.
- \mathbf{f}_1 :** Three-dimensional vector of the force intensities f_{1i}.
- \mathbf{f}_2 :** Three-dimensional vector of the force intensities f_{2i}.
- \mathbf{f}_e :** The resultant external force applied by the moving platform on its environment.
- \mathbf{t}_e :** The resultant external moment applied by the moving platform on its environment.
- s_e:** Six-dimensional vector of the external wrench applied by the moving platform on its environment.
- $\boldsymbol{\tau}$:** Six-dimensional vector of the active joints' force/torque intensities.
- A:** Instantaneous direct kinematics matrix.
- B:** Instantaneous inverse kinematics matrix.
- $\tilde{\mathbf{J}}$:** Jacobian matrix of the tripod mechanism.
- \mathbf{J}_s :** Jacobian matrix of the serial chains.
- \mathbf{J} :** Jacobian matrix of a complete manipulator.
- $\hat{\mathbf{s}}_{ni}$:** A unit vector along the yaw rotation axis of link B_i.
- $\hat{\mathbf{s}}_{ri}$:** A unit vector along the pitch rotation axis of link B_i.
- t_{ni}:** Torque intensity of the yaw actuators.
- t_{ri}:** Torque intensity of the pitch actuators.
- h_c:** Initial height parameter.
- P_i:** The plane defined by the normal, \mathbf{n} , and point \mathbf{p}_i , i=1,2,3.
- P₀:** The plane defined by points \mathbf{p}_i , i=1,2,3.

- B0:** The tripod base plane, which is defined by points \mathbf{b}_i , $i=1,2,3$.
- (\mathbf{l}, \mathbf{m}):** Mutual moment operator defined in Eq. 9.12.
- \mathbf{p}_{jk} :** Plucker ray coordinate of a line. $j, k \in \{(4, 1), (4, 2), (4, 3), (2, 3), (3, 1), (1, 2)\}$, Eq. (9.4).
- \mathbf{jk} :** A flat pencil generated by lines \mathbf{l}_j and \mathbf{l}_k . $k, j \in \{1,2,3,4,5,6\}$, $k \neq j$.
- X_{jk} :** A flat pencil generated by lines \mathbf{l}_j and \mathbf{l}_k that belongs to category of flat pencils X.
- $^P X_{jk}$:** The plane defined by a flat pencil X_{jk} .
- $^c X_{jk}$:** The center point of flat pencil X_{jk} .
- $\mathbf{p}_j \mathbf{p}_k$:** The line defined by points \mathbf{p}_j and \mathbf{p}_k .
- \mathbf{l}_j :** A line of the Jacobian, $\tilde{\mathbf{J}}$, of the tripod mechanism. $j = 1..6$.
- Γ :** The complete group of Jacobian lines. $\Gamma = \{\mathbf{l}_1, \mathbf{l}_2, \mathbf{l}_3, \mathbf{l}_4, \mathbf{l}_5, \mathbf{l}_6\}$.
- C_{jk} :** The group of Jacobian lines other than the Jacobian lines \mathbf{l}_j and \mathbf{l}_k .
 $C_{jk} = \{\mathbf{l}_n: \mathbf{l}_n \in \Gamma, n \neq j, n \neq k\}$.

Note: All the vectors, unless otherwise noted, are expressed in world coordinate system and treated as column vectors.

Symbols used for the RSPR robot only

- r_b :** The length of the rotating links.
- γ_i :** The angle between the normal, \mathbf{n} , and the normal to the base plane.
- \mathbf{v}_i :** The line of intersection between the plane P_i and the base plane.
- P_i :** The plane in which the i 'th extensible link rotates about the revolute joint, $\hat{\mathbf{r}}_i$.
- θ_i :** The rotation the i 'th rotating link.
- l_i :** The length of the i 'th extensible link.

Symbols used for the USR robot only

- α_i :** The yaw angle of the lower rotating link, B_i .
- β_i :** The pitch angle of the lower rotating link, B_i .
- \mathbf{l}_{i1} :** A vector pointing from the center of the active Hook's joint to the center of the spherical joint.

- \mathbf{l}_{i2} : A vector pointing from the center of the spherical joint to the upper extremity of the kinematic chain.
- l_1 : The length of the lower rigid links in the kinematic chains.
- l_2 : The length of the upper rigid links in the kinematic chains.
- t_{ri} : Torque intensity of the pitch actuators.
- θ_{ni} : The yaw angle of link B_i .
- θ_{ri} : The pitch angle of link B_i .
- ${}^w\boldsymbol{\omega}^{B_i}$: Angular velocity of link B_i relative to world coordinate system.
- ${}^w\boldsymbol{\omega}^p$: Angular velocity of the moving platform relative to world coordinate system.

Chapter 1

Introduction to Parallel Manipulators

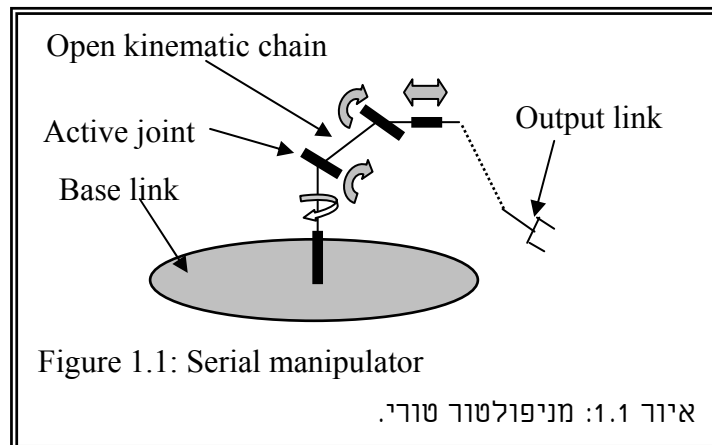
1.1 Three robotic architectures

This chapter presents the three basic architectures for robot manipulators. These architectures are characterized by the type of the kinematic chains connecting the output link of the manipulator to the base link. The three basic robot architectures are:

- a) Serial architecture
- b) Parallel architecture
- c) Hybrid architecture.

The serial architecture

This is the classical anthropomorphic architecture for robot manipulators, Fig. 1.1. In this architecture, the output link is connected to the base link by a single open loop kinematic chain. The kinematic chain is composed from a group of rigid links where each pair of adjacent links are interconnected by an active kinematic pair (controlled joint).



Serial manipulators feature a large work volume and high dexterity, but suffer from several inherent disadvantages. These disadvantages include low precision, poor force exertion capability and low payload-to-weight ratio, motors that are not located at the base, large number of moving parts leading to high inertia.

The low precision of these robots stems from cumulative joint errors and deflections in the links. The low payload-to-weight ratio stems from the fact that every actuator supports the weight of the successor links. The high inertia is due to the large number of moving parts that are connected in series, thus, forming long beams with high inertia.

Another disadvantage of serial manipulators is the existence of multiple solutions to the inverse kinematics problem. The inverse kinematics problem is defined as finding the required values of the active joints that correspond to a desired position and orientation of the output link. The solution of the inverse kinematic problem is a basic control algorithm in robotics; therefore, the existence of multiple solutions to the inverse kinematics problem complicates the control algorithm. The direct kinematics problem of serial manipulators has simple and single-valued solution. However, this solution is not required for control purposes. The direct kinematics problem is defined as calculating the position and orientation of the output link for a given set of active joints' values.

The low precision and payload-to-weight ratio lead to expensive serial robots utilizing extremely accurate gears and powerful motors. The high inertia disadvantage prevents the use of serial robots for applications requiring high accelerations and agility, such as flight simulation and very fast pick and place tasks.

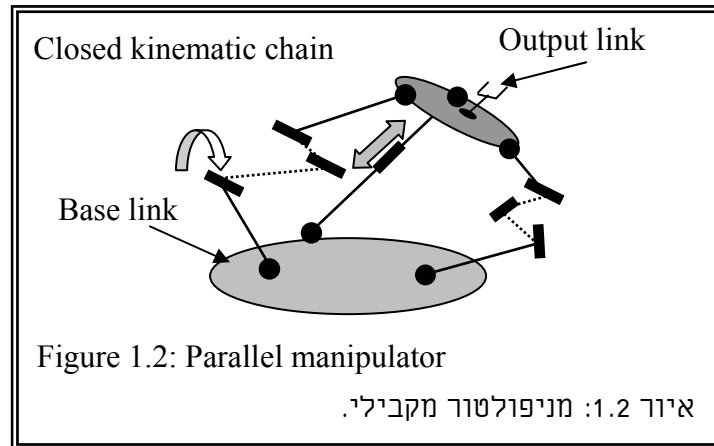
The parallel architecture

This non-anthropomorphic architecture for robot manipulators, although known for a century, was developed mainly during the last two decades. This architecture is composed of an output link connected to a base link by several kinematic chains, Fig 1.2. Motion of the output link is achieved by simultaneous actuation of the kinematic chains' extremities. Similarly, the load carried by the output link is supported by the various kinematic chains; therefore, this architecture is referred to as parallel architecture. In contrast with the open-chain serial manipulator, the parallel architecture is composed of closed kinematic chains only and every kinematic chain includes both active and passive kinematic pairs.

Parallel manipulators exhibit several advantages and disadvantages. The disadvantages of the parallel manipulators are limited work volume, low dexterity, complicated direct kinematics solution, and singularities that occur both inside and on the envelope of the work volume. However, the parallel architecture provides high rigidity and high payload-to-weight ratio, high accuracy, low inertia of moving parts, high agility, and simple solution for the inverse kinematics problem. The fact that the load is shared by several kinematic chains results in high payload-to-weight ratio and rigidity. The high accuracy stems from sharing, not accumulating, joint errors.

Based on the advantages and disadvantages of parallel robots it can be concluded that the best suitable implementations for such robots include requirements for limited workspace,

high accuracy, high agility, and a lightweight and a compact robot. These ideal implementations exploit both the disadvantages and advantages of the parallel architecture.



The hybrid architecture

The combination of both open and closed kinematic chains in a mechanism leads to a third architecture, which is referred to as the hybrid architecture. This architecture combines both advantages and disadvantages of the serial and parallel mechanisms. Fig. 1.3 presents an example of a hybrid manipulator constructed from two parallel manipulators connected in series.

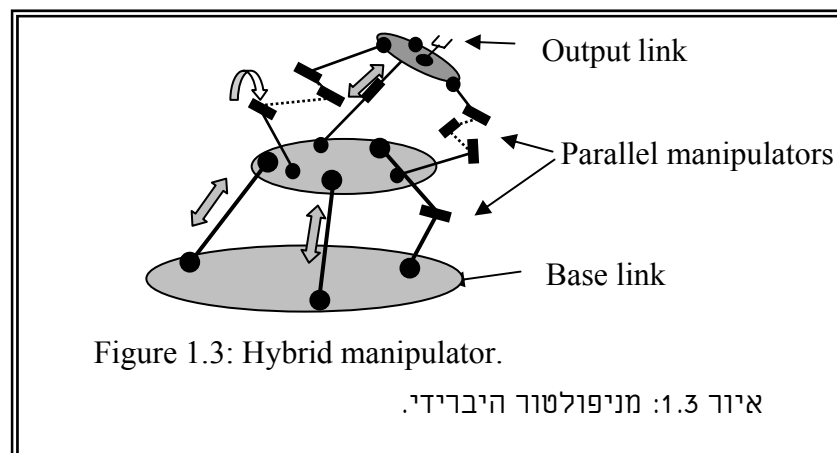
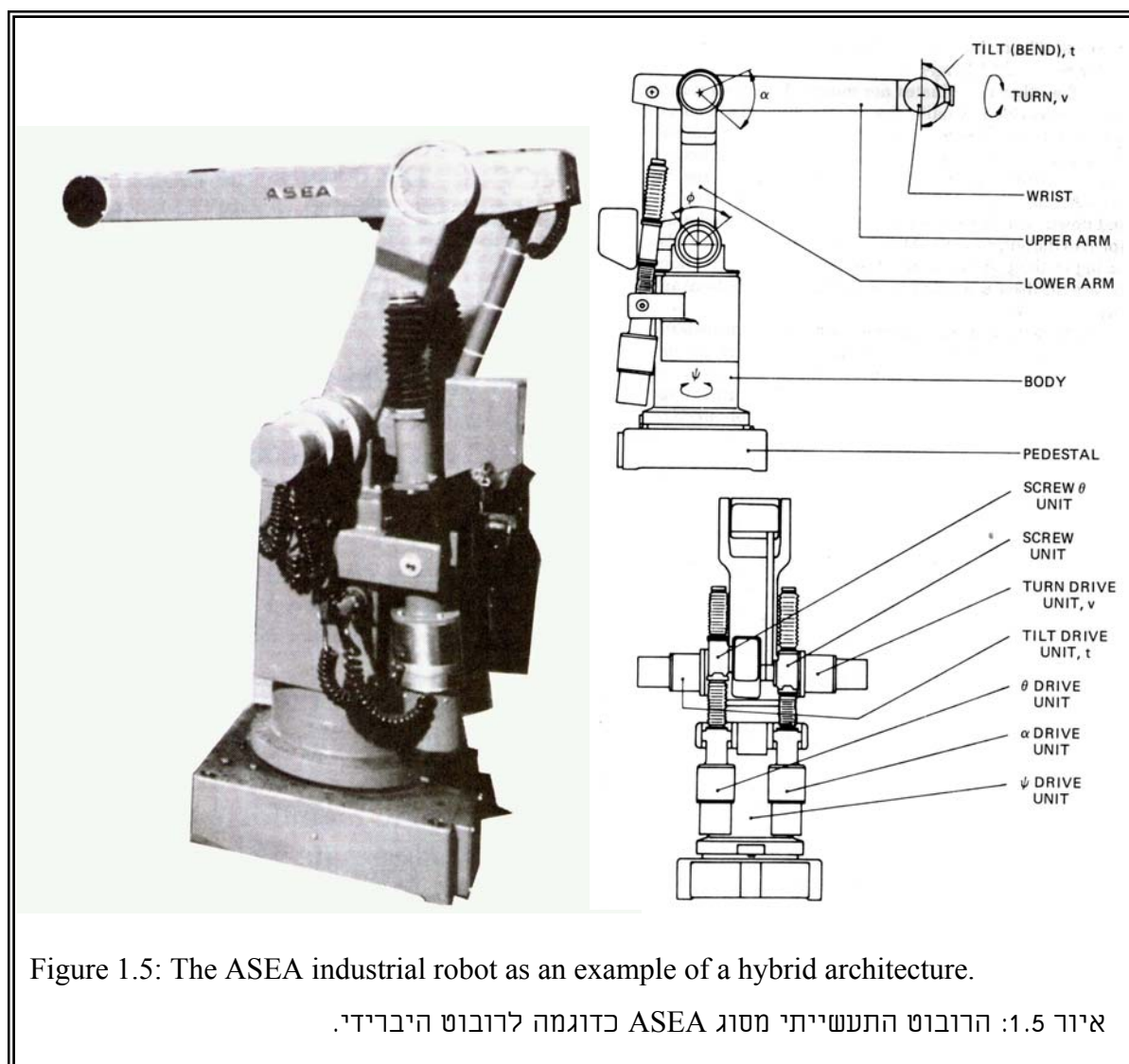
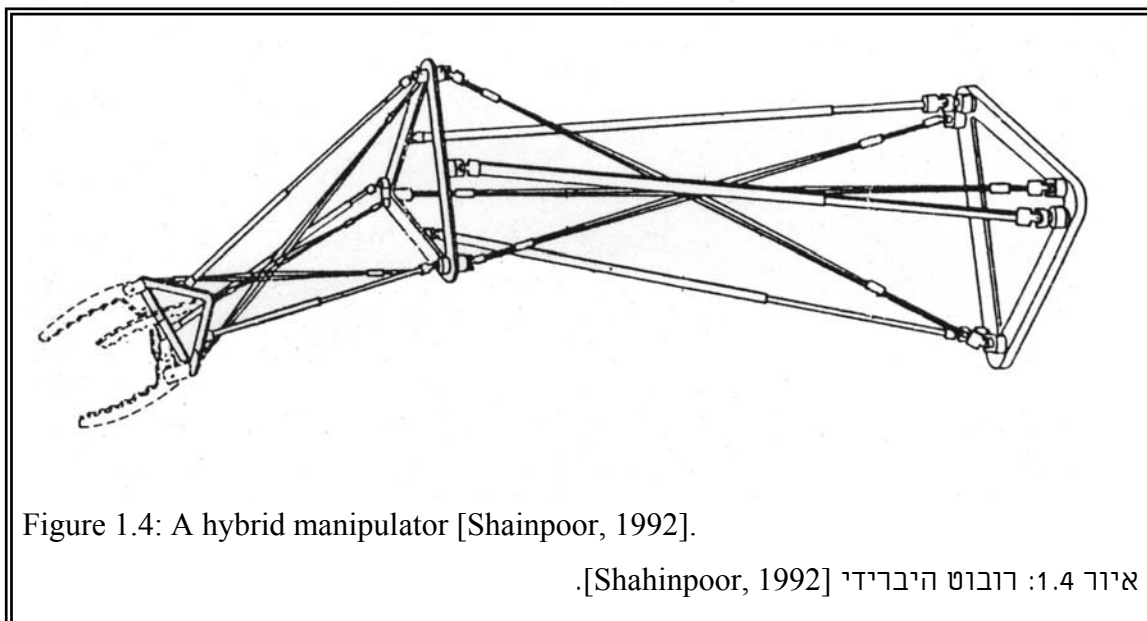


Fig. 1.4 presents a hybrid manipulator with six degrees of freedom [Shahinpoor, 1992]. The parallel sub-manipulators are connected in series. The manipulator is actuated by six extensible links. Fig 1.5 presents the 5 DOF ASEA industrial robot, which uses both open and closed kinematic chains. The main closed kinematic chain is a two DOF five-bar linkage, which moves the center of the wrist in a vertical plane relative to the ground. Tilt and turn motions of the wrist are achieved by two closed loop parallelogram linkages that transmit the motion from the motors located on the base to the wrist. The use of these linkages allowed the designers of this robot to locate the motors on the base.



1.2 Fully parallel and non-fully parallel manipulators

There are two major categories of parallel robots. These categories are the fully parallel robots, and the non-fully parallel robots. The distinction between these categories is based on the following definition. This definition is the same as the one presented in [Chablat and Wenger, 1998].

Definition: Fully parallel manipulator

A fully parallel manipulator is a parallel mechanism satisfying the following conditions:

- 1) The number of elementary kinematic chains equals the relative mobility (connectivity) between the base and the moving platform.
- 2) Every kinematic chain possesses only one active joint.
- 3) All the links in the kinematic chains are binary links, i.e. no segment of an elementary kinematic chain can be linked to more than two bodies.

Based on the solution multiplicity of the inverse kinematics problem this limiting definition can be summarized as follows. A fully parallel manipulator has one and only one solution to the inverse kinematics problem. Any parallel manipulator with multiple solutions for the inverse kinematics problem is a non-fully parallel manipulator. This will be shown mathematically in chapters 7 and 10 in terms of Jacobian matrix formulation and in terms of loss or gain of freedom in singular configurations.

Table 1.1 specifies the physical characteristics of serial and parallel manipulators. The table also briefly presents the differences between fully parallel and non-fully parallel manipulators.

Table 1.1: Comparison between Serial and Parallel manipulators.			
טבלה 1.1: השוואה בין מניפולטורים סטוריים ומקביליים.			
Property	Serial manipulator	Parallel manipulators	
		Fully parallel	Non-fully parallel
Type of Kinematic chains	Open kinematic chain	Closed kinematic chains	

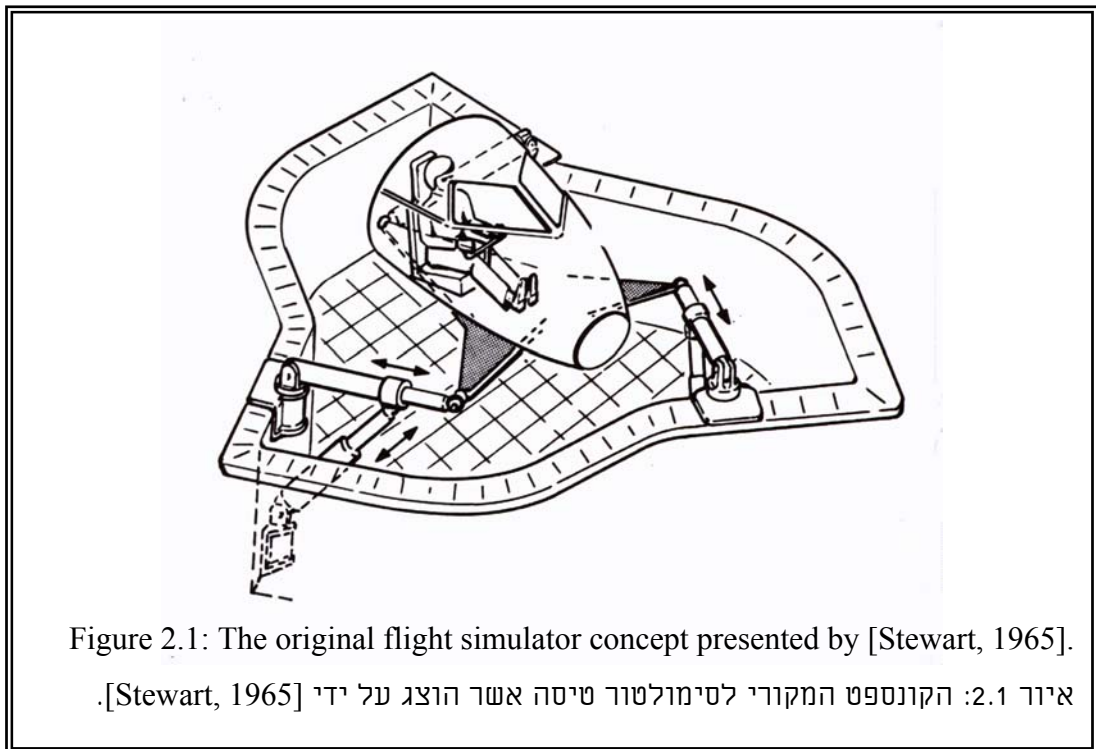
Table 1.1: Comparison between Serial and Parallel manipulators – continued.			
טבלה 1.1: השוואה בין מניפולטורים סדריים ומקביליים – המשך.			
Property	Serial manipulator	Parallel manipulators	
		Fully parallel	Non-fully parallel
Type of Joints Used	Active joints	Active and Passive Joints	
The role of active joints	Twist applicators	Wrench applicators	
Direct kinematics problem	Simple and single-valued solution	Complicated with up to 40 solutions	Complicated, but with less solutions
Inverse kinematics problem	Complicated with multiple solutions	Simple and single-valued solution	Simple with multiple solutions
Joint errors	Cumulative	Non-cumulative	
Positional accuracy	Poor	Average	
Payload-to-weight ratio	Low	Very high	
Singularity	Loss of freedoms	Gain of freedoms	Gain and loss of freedoms
Singularity domain	On the envelope of the workspace	Both inside and on the envelope of the workspace.	
Jacobian mapping	Maps joint speeds to end effector linear/angular velocity	Maps the end effector linear/angular velocity to active joints' speeds	
Work volume	Large	Small	
Inertia of moving parts	High	Low	

Chapter 2

Parallel Robots in Research and Industry: A Brief Review of the Literature

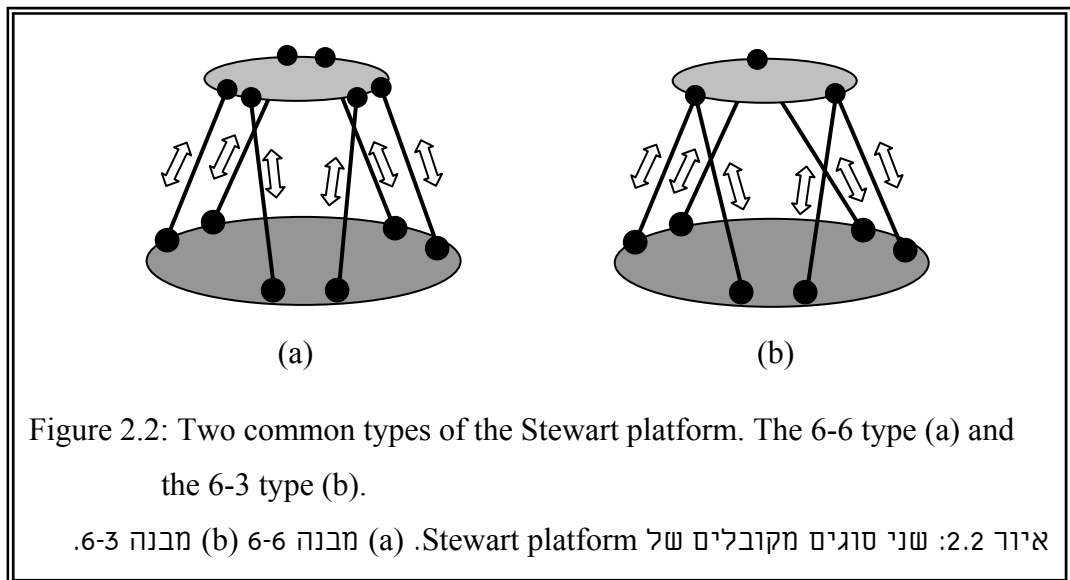
This chapter presents a brief summary of the implementation of parallel robots. The review of the literature in this chapter is limited to presenting examples of parallel robots in industry and research. A more detailed literature review is given at the beginning of the following chapters.

The first implementation of a parallel architecture by [Gough and Whitehall, 1962] presented a six degrees of freedom tire test machine with base and moving platforms interconnected by six extensible screw jacks. In 1965, Stewart presented a parallel robot for a six-degrees of freedom flight simulator [Stewart, 1965], Fig. 2.1. This robot was composed of a base and a triangular moving platform with three extensible links connecting the moving platform to the base. These three extensible links were connected to the base platform by Hooke's joints with one actuated axis. Rotations of the active axes of the Hooke's joints were achieved by additional three extensible links. Later, all platform-based manipulators were called Stewart-Gough platforms or, in short mistakenly, Stewart platforms.



It is possible to construct many Stewart platforms by altering the number of the connecting points on the moving and the base platforms. Therefore, a widely accepted coding system for sorting different Stewart platforms is the M-m code, which distinguishes between different Stewart platforms by the number of connecting points on the base and the moving platforms. Since this coding system does not fully define the topology of the parallel manipulator, Innocenti and Parenti-Castelli [1994] suggested an unambiguous coding system for distinguishing between topologically distinct Stewart platforms. Using this unambiguous coding system, they identified 17 topologically different Stewart platforms with single and/or double spherical pairs and four Stewart platforms with one triple spherical pair.

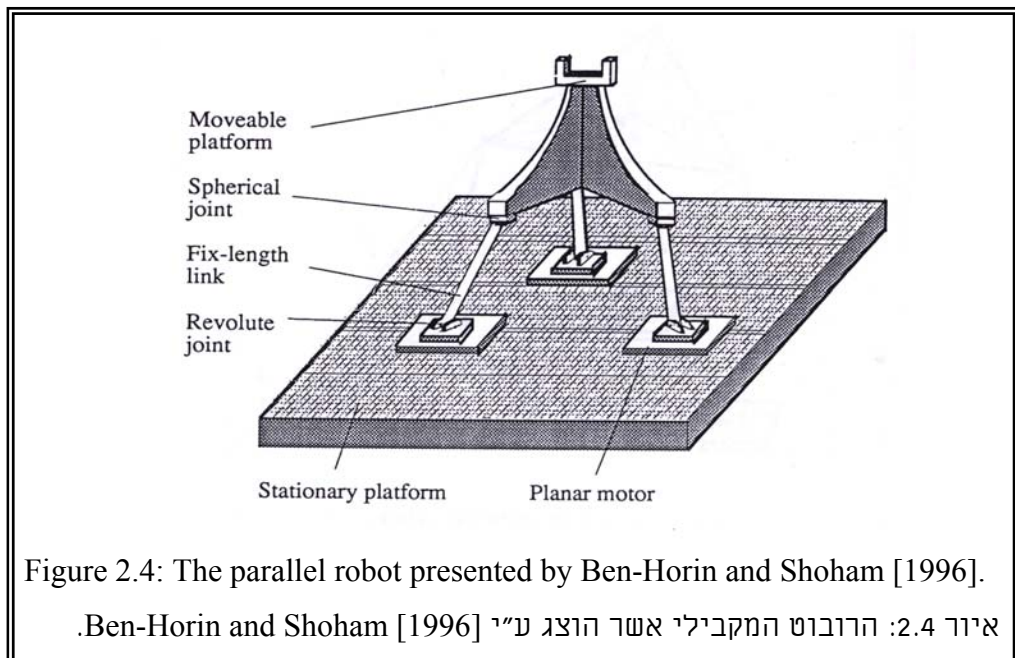
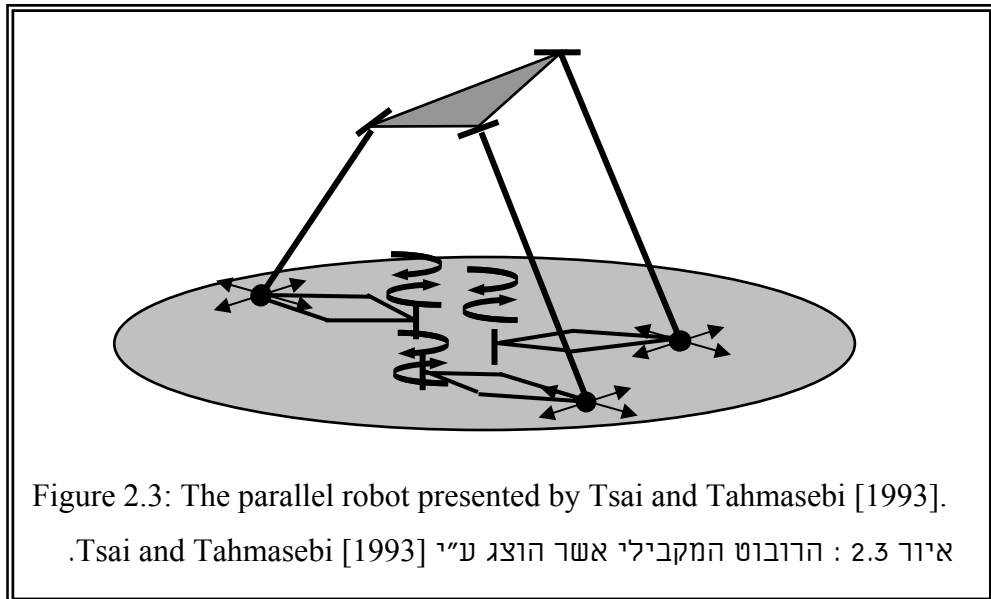
For instance, the Stewart platform of type 6-6 is a fully parallel robot with a moving platform connected to the base by six extensible links connected at six distinct points, both on the moving and the base platforms Fig. 2.2 (a). The Stewart 6-3 is a robot with six connecting points on the base and three connecting points on the moving platform, Fig. 2.2 (b).



Based on the definition of a fully parallel manipulator [Chablat and Wenger, 1998] one concludes that all the Stewart platforms are fully parallel manipulators. This fact indicates that these manipulators have a single solution to the inverse kinematics problem, but a rather limited workspace.

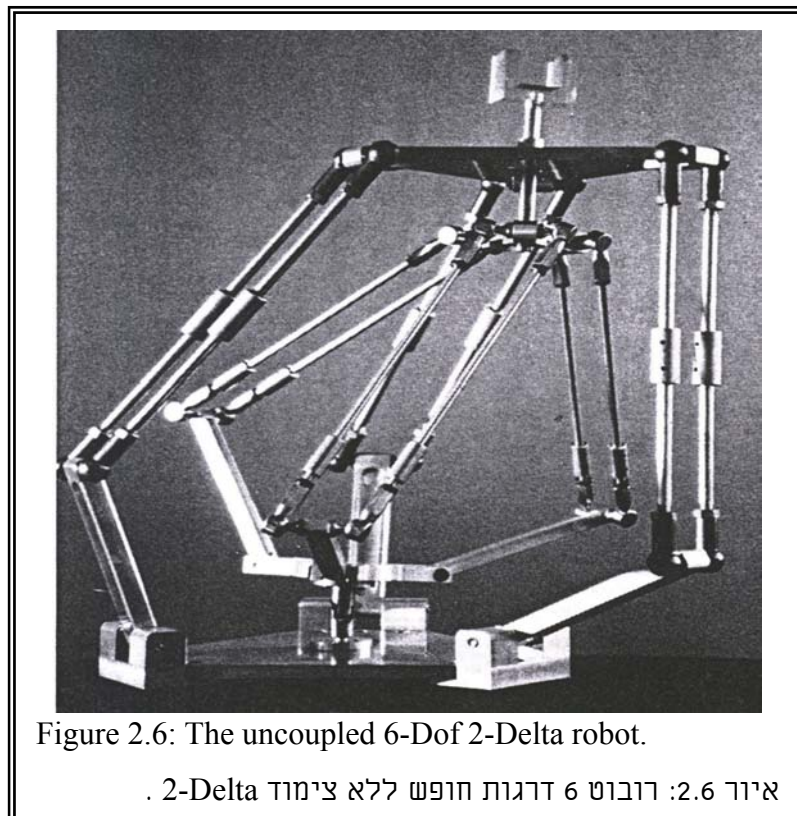
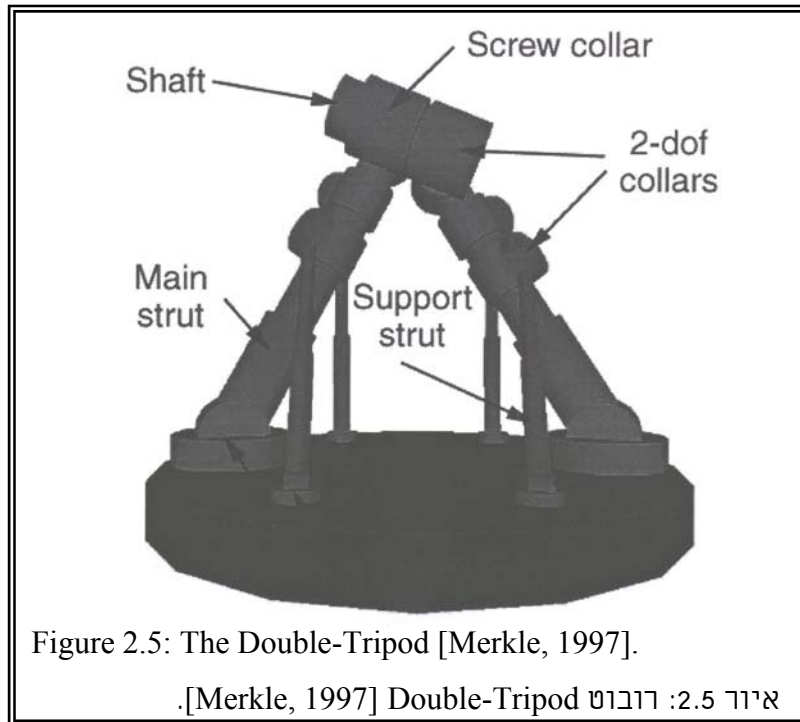
Fichter [Fichter, 1986] investigated the 6-3 Stewart parallel architecture, performed analysis of the workspace, and revealed two singular configurations of this structure. Innocenti and Parenti-Castelli [1994] performed an exhaustive enumeration of Stewart platforms and provided a listing of known Stewart platforms and their corresponding number of solutions for the direct kinematics problem. Later, many researchers investigated new parallel structures and did not limit their search for only fully parallel manipulators. Among

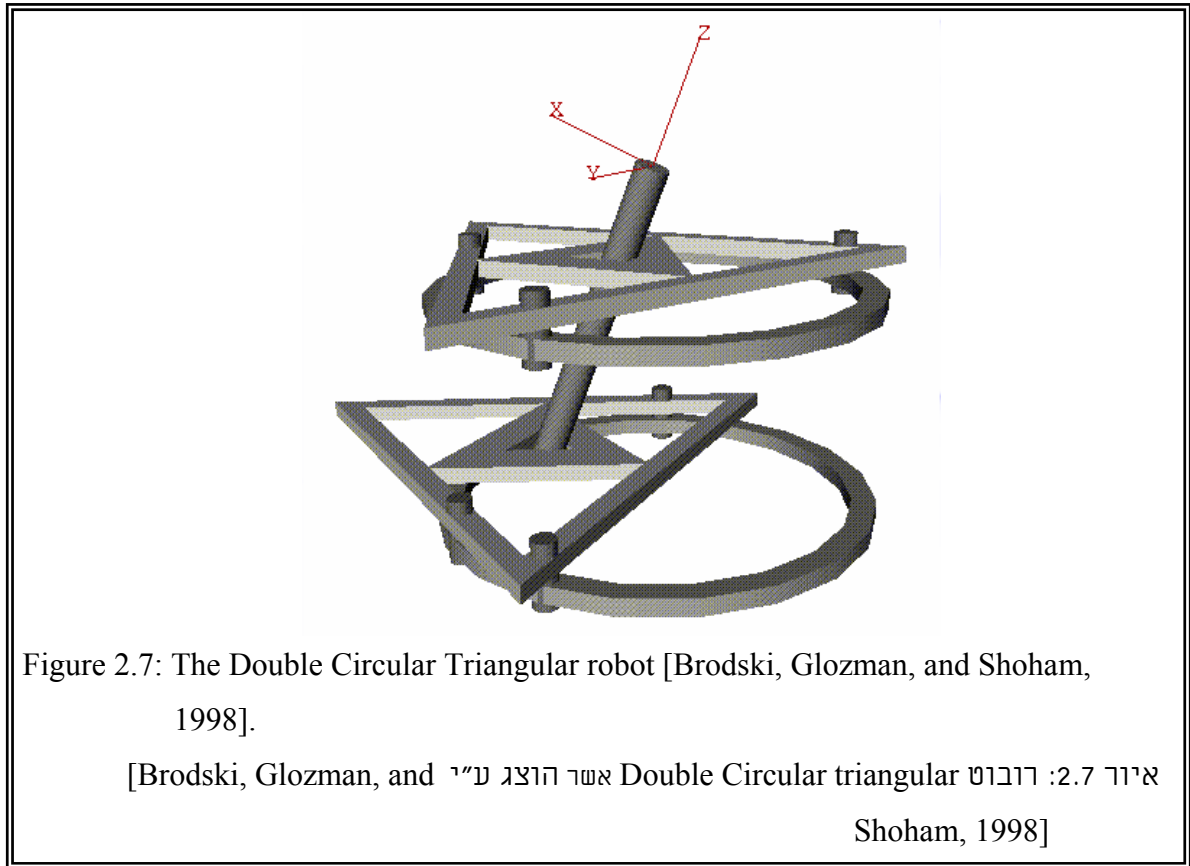
these researchers, Tsai and Tahmasebi [1993] and Ben-Horin and Shoham [1996] presented parallel robots featuring three kinematic chains with rigid links, Fig. 2.3 and 2.4 respectively. The lower extremities of the rigid links move in the plane of the base platform by planar motors or equivalent mechanisms. These robots feature large workspace because of the motion on the base plane. Merkle, of Xerox corporation, presented a parallel manipulator utilizing two tripods manipulating an output link and providing larger work volume than the Stewart platform [Merkle, 1997], Fig. 2.5.



Several researchers employ two parallel sub-mechanisms to achieve uncoupled rotation and translation movements of the moving platform [Lallemand et al., 1997; Lee, 1995], but this leads to a rather mechanically complicated architectures incorporating many

moving parts. Fig. 2.6 presents the 2-Delta uncoupled robot [Lallemand et al., 1997]. Simaan, Glozman, and Soham [1998], and Brodski, Glozman, and Shoham [1998] were inspired by the planar mechanism presented by Daniali, Zsombar-Murray, and Angeles [1993] and presented a six degrees of freedom parallel robot that incorporates two identical planar sub-mechanisms, Fig. 2.7.





Few works present innovative architectures providing simple closed form solution to the direct kinematics problem [Daniali, Zsombor-Murray, and Angeles, 1993; Brodski, Glozman, and Shoham 1998; Ceccarelli 1996; Ceccarelli 1997; Soreli, et al., 1997; Byun and Cho, 1997]. All these works implement passive sliders in the kinematic chains of each suggested robot, thus simplifying the direct kinematics problem.

Several researchers investigated parallel mechanisms with only rotational active joints in order to simplify actuation [Simaan, Glozman and Shoham, 1998; Cleary and Uebel, 1994; Zanganeh, Sinatra, and Angeles, 1997].

The implementations of parallel robots for industrial use developed during the last few years. The possible benefit from the structural rigidity and dynamical agility of parallel architectures motivated the development of grinding machines based on parallel architectures. The three examples for grinding machines are the six axis machine tool by Giddings-Lewis Corporation [Sheldon, 1995], the Hexaglide milling machine [Honegger, et al., 1997] and the octahedral machine by Ingersoll-Rand Corporation [Lindem, 1995]. Another study for a novel grinding machine featuring uncoupled motion was presented in [Lee, 1995].

There are other applications that benefit from the high motion agility of parallel architectures and employ this feature, for example, in flight simulation [Stewart, 1965]. Kawasaki Heavy Industries Ltd. presented a six degrees of freedom flight simulator based on the 6-6 Stewart platform architecture with hydraulic actuation [Nakashima, 1994]. Dunlop in [Dunlop, Jones, and Lintott, 1994; Dunlop and Jones, 1997] presented a 3 DOF Parallel manipulator based on the double tripod mechanism, which was presented by Hunt as a constant velocity joint [Hunt, 1978]. A 2 DOF version based on this mechanism was used for satellite tracking in order to overcome the tracking keyhole problem that arises when using conventional active Hooke's joint. Toyota R. & D. labs presented a 6-DOF Parallel mechanism for evaluating human motion sensation based on three five-bar mechanisms [Mimura and Funahashi, 1995].

The field of tele-operation takes advantage of the parallel architectures for developing six DOF master that provides effective force feedback in a compact form [Slutski, 1998]. Using this advantage, Collins and Long [1995(a)] presented a hand controller (master) for force reflection, which had a parallel architecture utilizing three pantograph mechanisms.

Finally, we refer the reader to Merlet's web page [Merlet, web page], which includes a comprehensive list of parallel robots and related bibliography. In this web page, the different robots are categorized based on their number of degrees of freedom and based on the type of kinematic chains.

Chapter 3

Robots for Medical Applications

3.1 Medical robots and parallel robots in medical applications

Robotic-assisted surgery is a new trend in medicine, which aims to help the surgeon by taking advantage of robots' high accuracy and accessibility. Introducing a robotic assistant as an integral part of the surgical tool array provides the surgeon with several advantages. These advantages include off-loading of the routine tasks and reduction of the number of human assistants in the operating room. In addition, by using the capabilities of the robot, the surgeon can complement his own skills with the accuracy, motion steadiness, and repeatability of the robot. The experimental comparison, presented in [Kavoussi, et al., 1996], compared the performance of a human assistant and a robotic assistant in manipulating a laparoscope. The results of this comparison emphasized the superiority of the robot in terms of motion steadiness. Another work [Kazanzides, et al., 1995] presented experimental results comparing the cross sections of a manually broached implant cavities and cross sections of robot milled cavities for hip replacement surgery. The comparison resulted in clear preeminence of the robot in performing accurate milling of the implant cavities. Noticing these features of the robot, several researchers invested efforts in assimilating the robot in the surgical arena [Taylor, et al., 1995; Ho, et al., 1995; Kienzle, et al., 1995; Harris, et al., 1997; Jensen, et al., 1994].

The approaches to robot assisted surgery divide into three main approaches. These approaches are the active execution approach, the semi-active approach, and the passive approach. In the active execution approach, the robot actively performs surgical procedures such as bone cutting and milling as in the works presented by [Kazanzides, et al., 1995; Brandt, et al., 1997]. In the first example, a serial robot performed milling of the femur bone to suite the implant in a knee surgery, and in the second one, a Stewart platform robot is used for hip surgery. In the semi-active execution approach, the robot is used as an aiding tool during surgery for tasks such as precise guidance of the surgical cuts without actually performing them. In this mode of operation, the robot holds the surgical tool while the surgeon moves the tool. The task of the robot is to prevent the surgeon from moving the tool out of the desired regions. Examples for this semi-active approach were presented in [Harris, et al., 1997; Ho, et al., 1995; Kienzel, et al., 1996] in total knee replacement surgery. Other works present systems that support both active and semi-active approaches, for example

[Brandt, et al., 1997]. In the third approach, the passive approach, the robot is merely a tool moved directly by the surgeon in remote manipulation mode as in [Grace, et al., 1993; Jensen, et al., 1994] that used a parallel six degrees of freedom robot in the field of ophthalmic surgery.

Most of the works listed above use serial robots. Some use special purpose serial robots like in [Taylor, et al., 1995]. Other works use industrial serial robots [Kienzle, et al., 1995; Kazanzides, et al., 1995]. These robots suffer from all the disadvantages of the serial architectures; thus, these designs result in large and heavy robots. The drawbacks of these serial robots motivate the research in the field of robot assisted surgery for a continuous search of task oriented robot architectures that best fit a specific group of medical applications. Among the vast array of robotic structures, the parallel structure seems promising because of its advantages that fit medical applications. Therefore, some investigators focused on exploring the capabilities of parallel robots in medical applications [Grace, et al., 1993; Brandt, et al., 1995]. The main advantages of the parallel architecture point toward it as being a better candidate than the serial one for use in surgery. Before listing those advantages we will first formulate the requirements from a medical robot and compare the parallel architecture with the serial one in terms of adequacy for medical applications.

3.2 The fundamental requirements from a medical robot

The following discussion is limited to formulating the fundamental requirements from the robotic architecture only. This section disregards the requirements from the data acquisition and registration systems or the pre-operative computer-based system. Some of the requirements were presented in [Khodabandehloo, et al., 1996] and implied in [Brandt, et al., 1997].

In order to insure the success of a medical robot, four fundamental requirements must be fulfilled. The first and most crucial requirement is safety. The following seven criteria constitute the safety requirement.

- 1) Effective control: The robot must allow, in all configurations, effective control of the tool with both speed and force control schemes implemented.
- 2) Limited Workspace: The robot must have limited workspace in order to prevent hazardous collisions between its moving parts and the medical staff or the patient.
- 3) Limited Forces or Force feedback: In applications where the robot is active in performing surgical procedures that include tactile tasks, the force applied by the

tool must be limited. Alternatively, in applications where the robot acts as a slave, the robot must convey a maximum amount of data to the surgeon about the forces exerted on the tool. This requirement is essential in the process of bone cutting where different levels of force are required during different stages of the cut [Harris, et al., 1997].

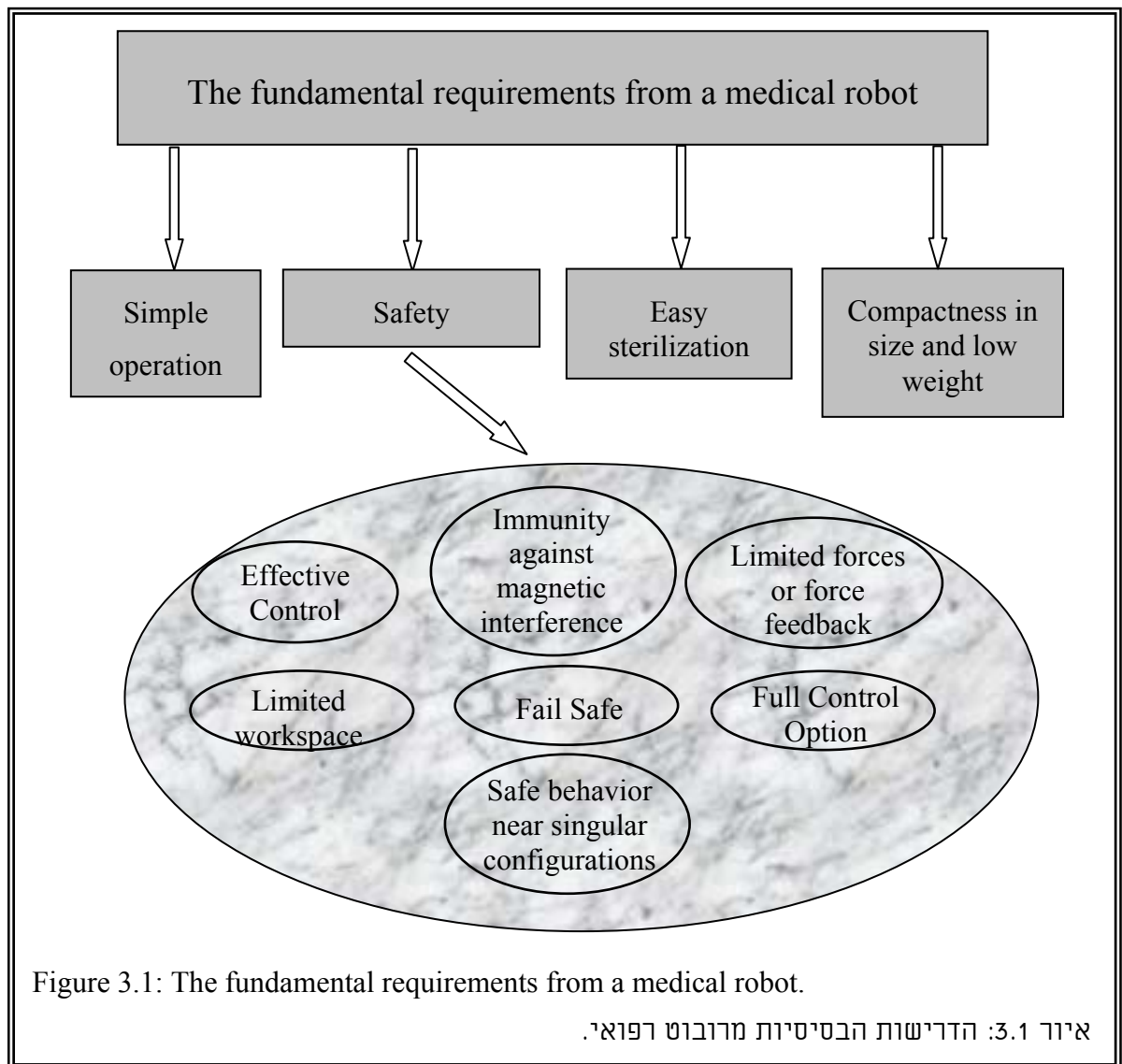
- 4) Immunity against magnetic interference of other surgical tools.
- 5) Full control option: In applications where the robot performs automated tasks, the control program must allow the surgeon, in any stage in the task, to interrupt the automatic execution process and take over the control to his hands.
- 6) Fail safe features: The most reliable systems will inevitably fail in some stage of their service. Based on this premise the robot must support a fail-safe mode. This includes keeping the position of the tool when the power supply is lost, electrical limiting of the end effector's speed and force even when the control program fails.
- 7) Safe behavior near singular configurations: The path planing of the robot should avoid passing near singular configurations. However, in the cases where the robot acts as a slave, the surgeon might manipulate it into singular configurations. Therefore, the architecture of the robot must provide signals for the surgeon that warn him from approaching singularity.

The second requirement from a medical robot is compactness in size and lightness. This ensures that the robot does not consume a large amount of essential space in the operating room and facilitates the relocation of the robot in different positions for different tasks. The third requirement is simple operation in order to improve the learning curve of new surgeons. The last, but not least important, requirement is the requirement for easy sterilization. This requirement is critical since any tool in the operating room must either be sterilized or covered with sterile drapes in order to prevent infections. To summarize the fundamental requirements of a medical robot we present figure 3.1.

3.3 Advantages of parallel robots in medical applications

From the two robot architectures, i.e., the serial and parallel ones, the one most compliant with the fundamental requirements is the parallel architecture. In contrast with the bulky serial architecture, the compact and lightweight parallel architectures simplify the relocation of the robot in the operating room, save necessary space, and allow easy sterilization by covering the robot with a closed drape. The relatively small work volume of

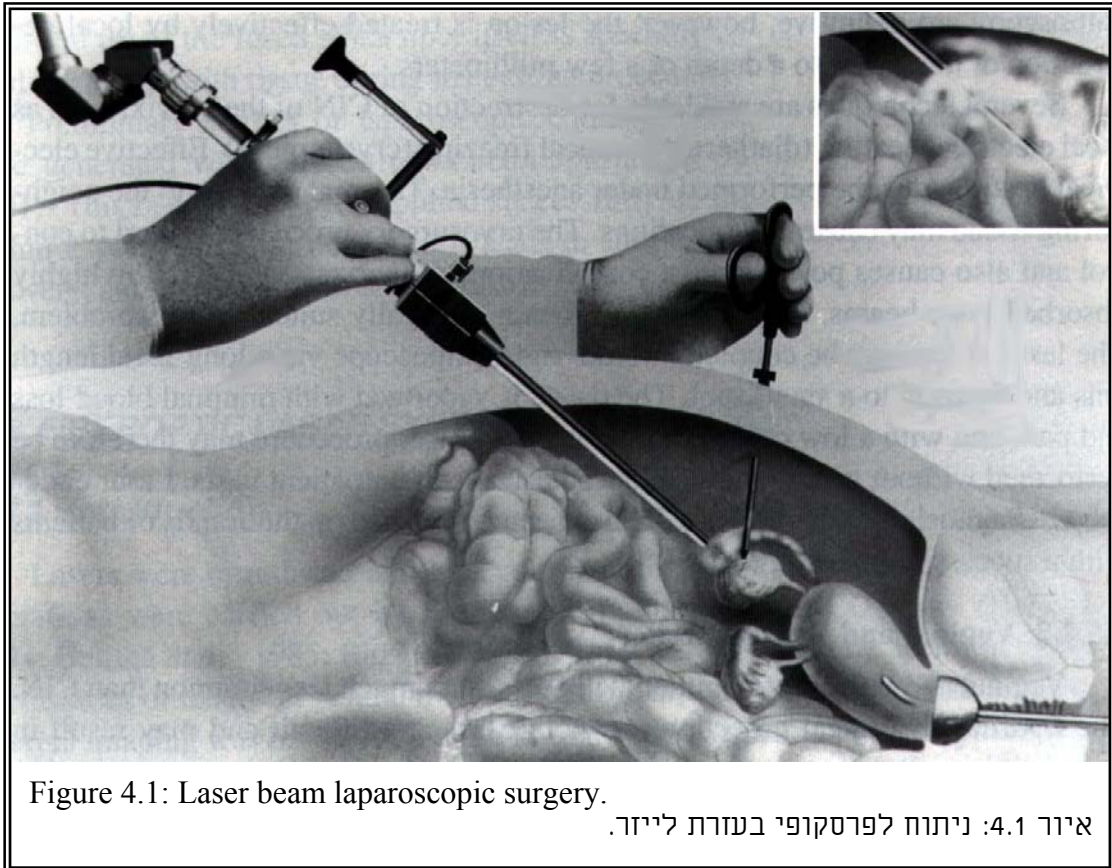
the parallel robots, if correctly designed, can introduce an important safety feature. In addition, parallel robots behave safely near singularity. When the robot traces a path towards a singular configuration, the required forces from the actuators reach high values. Consequently, monitoring the electrical current of the actuator motors gives a reliable warning against approaching singular configurations. In serial robots, singular configurations are associated with very high values of joint velocities and this introduces a hazardous element. The parallel robots provide accuracy with lower price when compared to similar serial robots with the same accuracy level. Some accuracy levels may not be achieved with serial robots. These high levels of accuracy are important for eye surgery [Jensen, et al., 1994]. Based on the above arguments, we may conclude that the parallel architecture is better than the serial one for medical applications that require a suitable workspace for reasonable robot design.



Chapter 4

Formulation of the Design Problem

This chapter presents the design requirements from a medical robot aimed for use in minimally invasive laparoscopic surgery. Minimally invasive surgery aims to overcome the disadvantages of open surgery by minimizing the number of openings performed during surgery; thus, reducing the patient's pain, shortening the recovery time and minimizing the esthetic damage to the patient's body. Laparoscopic surgery is an important procedure in minimally invasive surgery, in which, the surgeon performs several incisions in the abdominal wall and introduces the necessary surgical tools through these incisions. In the common mode of operation in laparoscopic surgery, the surgeon holds in his right hand the laparoscope and in his left hand the surgical tool, Fig. 4.1. In some cases, the surgeon works with a human



assistant who holds the laparoscopic camera in a desired orientation. This arrangement is far from being satisfactory because of the fact that one of the surgeon's hands is occupied in manipulating the laparoscope. In addition, the requirement for steadily holding the laparoscope for long time is physically demanding, thus, consuming unnecessary effort from the surgeon.

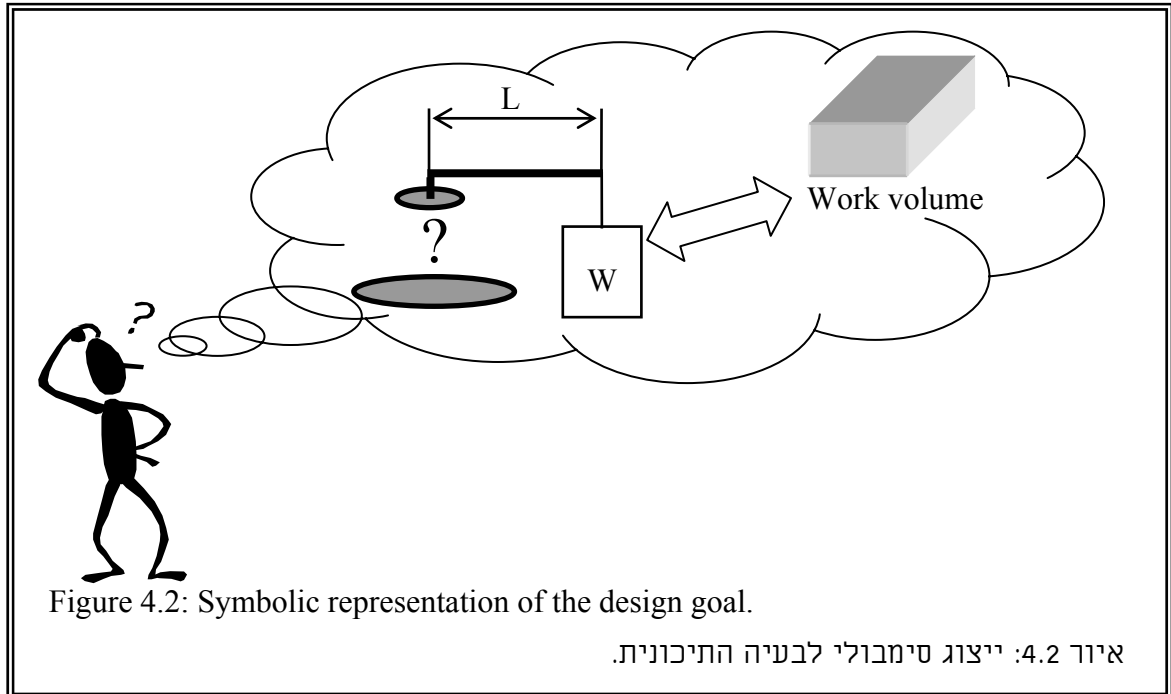
The motivation behind this work stems from the fact that in a laparoscopic surgery the robot can effectively play the role of a human assistant by manipulating the camera during the surgery. This allows the assistant to attend to other tasks, promises better stability of the camera, and bears possible future implementation in laser endoscopic surgery. The comparison between a human assistant manipulating a camera during a laparoscopic surgery and a robot performing the same task was presented in [Kavoussi, et al., 1996]. This experimental work resulted in a conclusion that a robot holds the camera significantly more steady without adversely affecting the total time of the surgical procedure. [Faraz and Payandeh, 1998] addressed the problem of laparoscopic surgery by searching for a suitable mechanism to serve as a passive stand that allows keeping the orientation of the camera even when the surgeon does not hold the laparoscope.

There are many methods for manipulating the laparoscopic camera by a robotic assistant. These methods are categorized into three main approaches. The first approach uses control signals initiated by the surgeon using a remote controller. The second approach uses automatic guidance of the laparoscopic camera, and the third method is the direct method, in which, the surgeon manipulates the laparoscopic camera directly by using force compliance control. Remote controllers take many forms such as hand controllers, leg actuated pedals, or systems that interpret the motions of the surgeon's head [Finlay and Ornstien, 1995]. Wei et al. [1997] presented a system for automatic laparoscopic camera guidance by tracking the laparoscopic instruments using color coding of the instruments.

In addition to all the fundamental requirements in Chapter 3, this chapter is devoted to formulating the design requirements in terms of required workspace and required force exertion capability from the medical robot presented in this thesis. The design problem is visualized in Fig. 4.2. The cube in Fig. 4.2 represents the required workspace for the specific medical application and the weight W represents the required load to be supported by the robot.

The explicit statement of the design problem is as follows. The design problem is to synthesize a robot that supports a load W and manipulates this load in a required workspace. Based on the conclusion of the previous chapter we choose to synthesize a mini parallel robot for this task. The synthesis includes both type and dimensional phases. The emphasis is on the fact that the robotic architecture is unknown and the research aims at comparing several architectures for the same task and choosing the best concept. One of the goals of the comparisons between several architectures is finding the smallest possible parallel robot

featuring a mechanically feasible design and presenting better characteristics than the other architectures. The details of the synthesis and comparison are presented in the following chapters.



The required load W and the desired workspace were defined based on physical estimate for the surgical laparoscopic procedures. The desired workspace is a 40x40x20-mm cube and the robot is required to reach every point within this cube while maintaining a rotation of 20° about the $[1,1,0]$ axis. This axis is described in a platform-attached coordinate system. The required external forces are equivalent to supporting a weight of $W=1.2$ kg with a lever of $L = 0.1$ [m]. The speed of the laparoscope tip should vary between 2.5 to 25 [mm/sec]. Based on these design requirements other possible implementations for the robot would be in knee arthroscopy and total knee replacement surgery using the semi active approach.

The design requirements listed above are used in the following chapters in the stage of dimensional synthesis of the robots. The following chapter presents the type synthesis for parallel robots.

Chapter 5

Type Synthesis

5.1 Introduction

Type synthesis deals with the construction of new mechanisms to fulfill a desired task by considering various arrangements of links and joints. In type synthesis, emphasis is placed on the type of joints and links rather than on the dimensional or geometric properties of the mechanism. Many researchers tried to systemize the invention process of new mechanisms. Among these researchers the following works focused on the synthesis of parallel manipulators [Hunt, 1983; Earl and Rooney, 1983; Malik and Kerr, 1992; Shoham and Roth, 1997]. These works were based on Grubler's equation for general mobility in mechanisms, which is the fundamental formula for type synthesis.

In order to clearly continue this chapter we wish to present the reader with the following definitions based on the material presented in [Hunt, 1978] and in [Phillips (a), 1984].

General Mobility: The general mobility of a mechanism is the required number of independently controlled joint variables in order to specify the location of the links relative to one another.

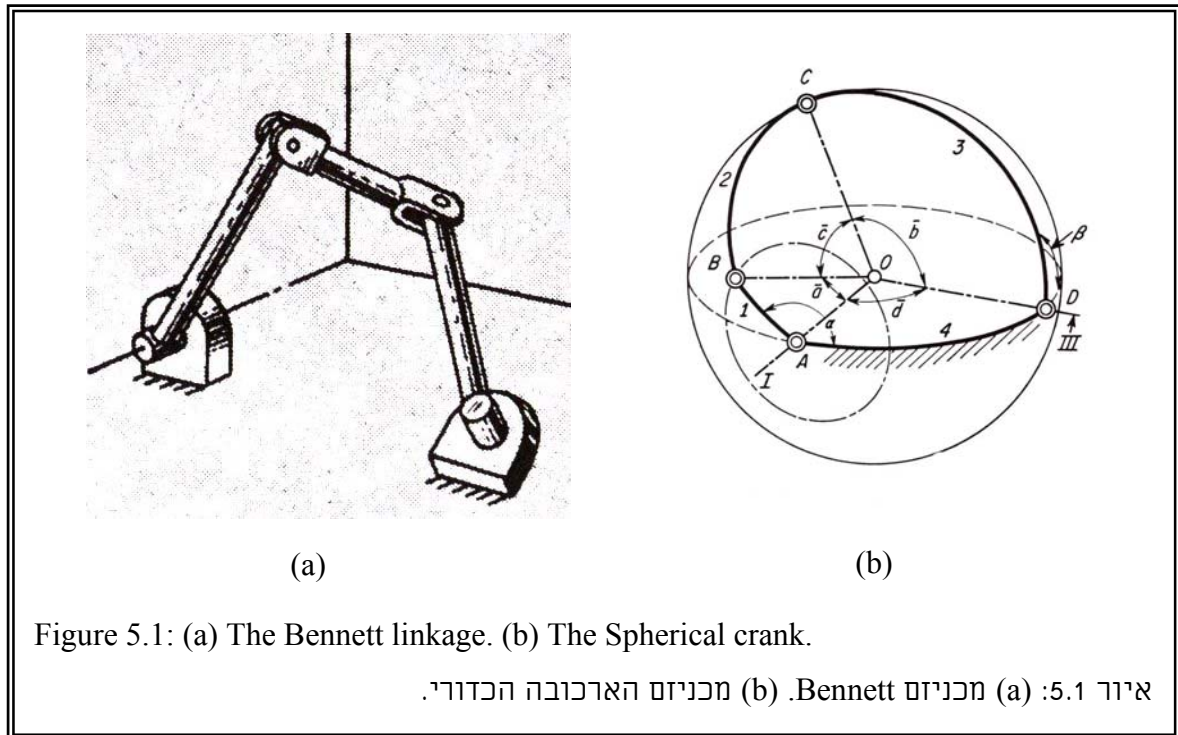
Connectivity: The relative degrees of freedom between two links in a mechanism.

The Grubler-Kutzbach equation for the general mobility in a mechanism is presented in Eq. (5.1).

$$M = d(n - g - 1) + \sum f_i \quad (5.1)$$

Where $d = 6$ for spatial mechanisms, $d = 3$ for planar and spherical mechanisms, and $d = 2$ for planar prismatic mechanisms. For the interpretation of all the cases $2 \leq d \leq 6$ see [Hunt, 1983]. n is the number of links in the mechanism including the ground link, g is the total number of joints in the mechanism, and $\sum f_i$ is the sum of the degrees of freedom in the mechanism. The general mobility equation disregards the geometric properties of the mechanism; therefore, it fails to describe mechanisms in singular configurations in which the mobility is a result of specific geometrical relations between the joints' axes. The parameter d in equation 5.1 is taken as 3 for spherical mechanisms or planar mechanisms because these mechanisms fulfill geometrical conditions that provide dependence of constraints regardless of the configuration of the mechanism. For example, Fig. 5.1 presents two such mechanisms. Fig. 5.1(a) presents

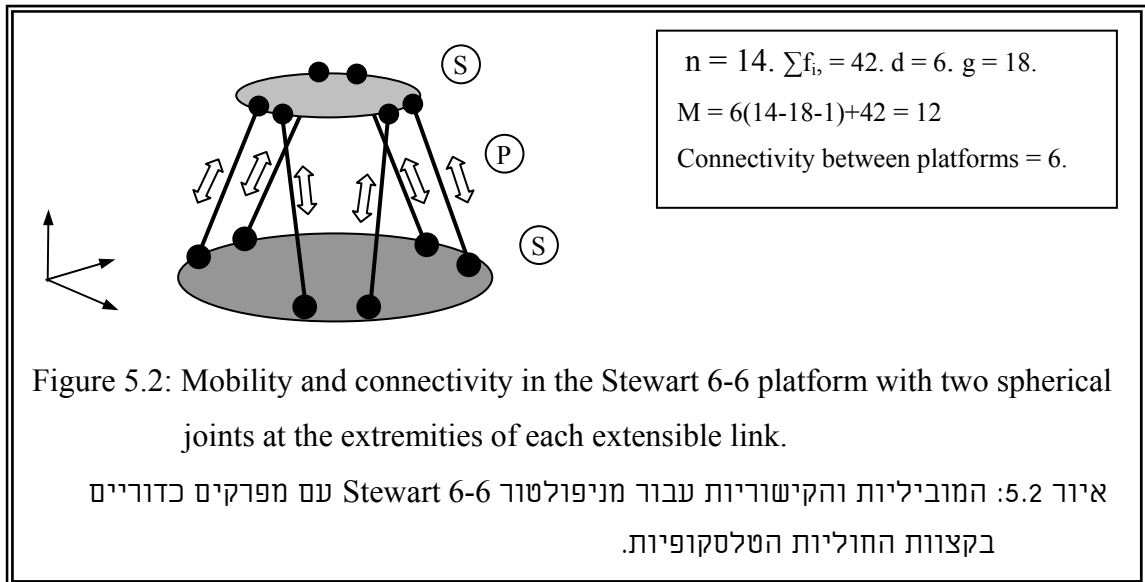
the famous spatial four-bar mechanism usually referred to as Bennett's linkage. Fig. 5.1(b) presents the spherical crank. For the analysis of Bennett's linkage refer to [Hon-Chung, 1981]. Both these linkages have mobility $M=1$ while Eq. (5.1) indicates zero mobility. A zero general mobility indicates that the analyzed combination of joints and links represents a statically determinate structure. Negative general mobility indicates a statically indeterminate (over-constrained) structure.



Many researchers addressed the problem of type synthesis for parallel spatial mechanisms. The synthesis of parallel manipulators was described using the screw theory and based on Grubler's equation in [Hunt, 1983]. This work presented criteria for avoiding undesirable robot arms that are prone to jamming and presented suggestions for six DOF parallel manipulators. Shoham and Roth implemented the graph theory in order to determine linkages, which have connectivity of six between at least two of the links. The work suggested a method for modifying the graph representation of mechanisms in order to facilitate computing the connectivity between every link pair in the mechanism. Malik and Kerr addressed the problem of type synthesis of in parallel mechanisms based on Grubler's equation and discussed all the possible mechanisms with mobility ranging from three to six. The work presented 14 distinct possible configurations with varying number of in-parallel kinematic chains.

In manipulator design, emphasis should be placed on the distinction between the general mobility and the connectivity. A six degrees-of-freedom manipulator is a mechanism

with a connectivity of order six between the ground link and the output link. Therefore, the connectivity and not the general mobility are important in manipulator synthesis [Shoham and Roth, 1997]. An example for this statement regarding mobility and connectivity is presented in Fig. 5.2. This figure presents the 6-6 Stewart platform with a moving and a base platform interconnected by six extensible links via spherical joints. The total number of links, n , in this mechanism is 14, the number of joints, g , is 18, and the sum of degrees of freedom, $\sum f_i$, is 42. Therefore, the General mobility when using Eq. 5.1 with $d = 6$ is 12. This result means that we need twelve geometric parameters to fully describe the geometry of the mechanism. The result is misleading since it includes the passive rotations of the extensible links around their respective axes of rotation. These rotations do not affect the fact that the moving platform



retains six degrees of freedom relative to the base platform.

5.2 Synthesis of a class of parallel manipulators

In this section, we present the type synthesis of parallel manipulators with identical kinematic chains. The focus on manipulators with similar and symmetrical distribution of the actuators stems from the need for even load distribution between the kinematic chains and design simplicity. The requirements for simplicity and structural rigidity guided us toward investigating mechanisms with minimal number of in-parallel kinematic chains and, in particular, kinematic chains that end with revolute joints connecting the kinematic chains' extremities with the moving platform. This architecture diminishes the problem of collisions between the adjacent kinematic chains and, as will be shown in chapter 8, this architecture has advantages in terms of structural rigidity and lower actuator forces.

We define the following quantities for the similar in-parallel kinematic chains. m_l represents the connectivity between the moving and the base platforms along each one of the identical kinematic chains. n_l represents the number of links including the moving and base platforms, g_l denotes the number of joints, and $\sum f_l$ is the sum of degrees of freedoms in the kinematic chains. Accordingly, every kinematic chain fulfills Eq. (5.2):

$$m_l = 6(n_l - g_l - 1) + \sum f_l \quad (5.2)$$

Furthermore, we denote the number of in parallel kinematic chains by the letter L . The total sum of degrees of freedom in the mechanism, $\sum f_i$, is given by Eq. (5.3).

$$\sum f_i = L \sum f_l \quad (5.3)$$

The total number of links in the mechanism and the total number of joints are given in Eq. (5.4) and Eq. (5.5), respectively.

$$n = (n_l - 2)L + 2 \quad (5.4)$$

$$g = L g_l \quad (5.5)$$

By substituting equations (5.3), (5.4), and (5.5) in Grubler's equation for the general mobility and substituting Eq. (5.2) for the connectivity along an in parallel kinematic chain we obtain the following result presented in Eq. (5.6).

$$M = L m_l - 6(L - 1) \quad (5.6)$$

Since we are interested in non-redundant manipulators with identical kinematic chains the number of active joints in a kinematic chain, g_{al} , in each kinematic chain is defined by Eq. (5.7).

$$g_{al} = M/L \quad (5.7)$$

Where the number of kinematic chains, L , ranges between unity for serial manipulators and $L = M$ for fully parallel manipulators. $1 \leq L \leq M$.

In order to avoid redundancy or unwanted freedoms, as the ones presented in the case of the Stewart platform example, the connectivity between the moving and base platforms along each kinematic chain must be six at most. However, the connectivity must be greater or equal to the general mobility of the mechanism, therefore, $6 \geq m_l \geq M$. Based on these results Eq. (5.6) becomes a simple tool for listing parallel manipulators with identical in-parallel kinematic chains. The equation yields the required connectivity, m_l , for a desired general mobility and a given number of kinematic chains, L . We note that Eq. (5.6) is fulfilled for any number of kinematic chains, L , if all the kinematic chains allow connectivity equal to six between the base and the moving platforms. Table 5.1 presents all the possible combinations for parallel robots with identical kinematic chains. The table presents six possible

manipulators. The work presented in [Malik and Kerr, 1992] considered the cases with $M \geq L \geq 3$. By using similar reasoning based on Grubler's mobility equation they presented 14 different combinations for parallel manipulators with different kinematic chains and non-uniformly distributed actuation joints.

Table 5.1: The possible parallel manipulators with identical kinematic chains. טבלה 5.1: הרובוטסים המקביליים האפשריים בעלי שרשראות קינמטיות זהות.			
General Mobility M	Number of kinematic chains L	required kinematic chain connectivity m_l	Active joints per kinematic chain g_{al}
2	2	4	1
3	2	-----	-----
	3	5	1
4	2	5	2
	3	-----	-----
	4	-----	-----
5	No solution available		
6	2	6	3
	3	6	2
	4, 5	-----	-----
	6	6	1

5.3 Selecting architectures based on design guidelines

According to table 5.1, there are three general architectures for obtaining six degrees of freedom parallel manipulators with identical kinematic chains. These three architectures differ one from another in the number of kinematic chains. The three general architectures can be achieved by many combinations of links and joints. Therefore, we must follow some design guidelines that take into account the practicality of the different manipulators.

We consider the practical joints of types R, P, S, U, and C. Where R stands for revolute joint, P for prismatic, S for spherical, U for Hooke's, and C for cylindrical joint. We

begin by first ruling out the helical joint because of its unnecessary complication. In the next step, we look for manipulators with simple kinematic chains. This requirement for simplicity highlights the essential use of coalescence of joint axes. For example, a spherical joint is preferable on its equivalent 3R kinematic chain in terms of simplicity. The importance of utilizing joint coalescence for simplifying the kinematic chains was highlighted in [Hunt, 1983].

For parallel manipulators with identical kinematic chains, there are two practical solutions with three or six kinematic chains. The case with $L=2$, i.e. two kinematic chains is ruled out because of the complexity of activating three joints in a kinematic chain. Table 5.2 presents the known six DOF parallel manipulators with three kinematic chains. The table specifies the kinematic chains in a customary way, in which, the kinematic chains are identified by the types of joints when traversing the chains from the base to the moving platform. The active joints in each kinematic chain are identified by bold font setting. Some works utilize four-bar, five-bar or other complex planar sub-mechanism for actuation; therefore, these planar mechanisms are equivalent to planar kinematic pairs. We refer to a planar kinematic pair by the letter E and we present the kinematic equivalence of the complex kinematic chains. Figures 5.3 to 5.15 present the schematic representations of the robots in table 5.2.

Table 5.2: Listing of known parallel manipulators with three kinematic chains. טבלה 5.2: רשימת המניפולטורים המקביליים הידועים עם שלוש שרשראות קינמטיות.		
Related work	Type of the kinematic chains	Figure
[Behi, 1988]	PRPS	Fig. 5.3
[Kholi, et al., 1988]	PRRS	Fig. 5.4
[Romiti and Soreli, 1990]	Two actuated parallelograms in series, P, S. Equivalent to EPS Kinematic chains.	Fig. 5.5
[Soreli, et al., 1997]	Double parallelogram actuation, P, S. Equivalent to EPS kinematic chain.	Fig. 5.6
[Zlatanov, et al., 1992]	Planar kinematic chains with asymmetrical distribution of actuation between the kinematic chains and planar sub-mechanisms. RRPS, RRPS, RRPS	Fig. 5.7

Table 5.2: Listing of known parallel manipulators with three kinematic chains – continued.		
טבלה 5.2: רשימת המניפולטורים המקביליים הידועים עם שלוש שרשראות קינמטיות – המושך.		
Related work	The kinematic chain	Figure
[Tsai and Tahmasebi, 1993]	A family of three legged manipulators with non-extensible rigid links and planar actuation by five bar linkages, pantographs or planar motors. Equivalent to ESR kinematic chain.	Fig. 2.3
[Ben-Horin and Shoham, 1996]	Planar motors, R, S. Equivalent to ERS kinematic chain.	Fig. 2.4
[Alizade, Tagiyev, and Duffy, 1994]	RRPS kinematic chains.	Fig 5.8
[Collins and Long, 1995(a)]	R, pantograph actuation, S. Equivalent to RES kinematic chain.	Fig 5.9
[Mimura and Funahashi, 1995]	R, Five bar mechanism actuation, S. Equivalent to RES kinematic chain.	Fig. 5.10
[Ebert and Gosselin, 1998]	Three Five-bar parallelogram linkages with actuation of both sides of each parallelogram in each kinematic chain. Equivalent to RES .	Fig. 5.11
[Byun and Cho, 1997]	PPSP Equivalent to ESP kinematic chain.	Fig. 5.12
[Cleary and Uebel, 1994]	URS kinematic chain with the U joints controlling the pitch and roll of the lower rotating links.	Fig. 5.13

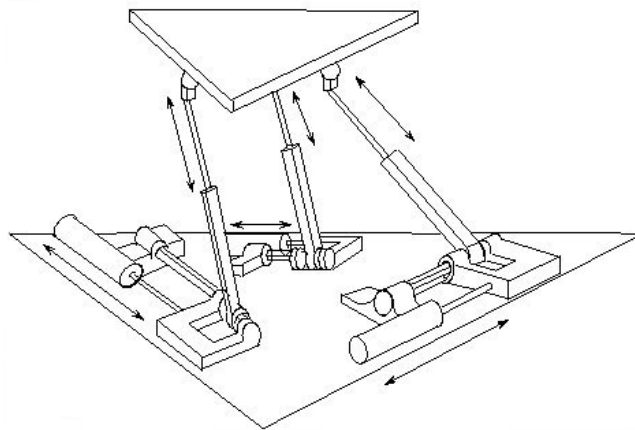


Figure 5.3: The robot presented by Behi [1988].

איור 5.3: הרובוט המקבילי של Behi [1988].

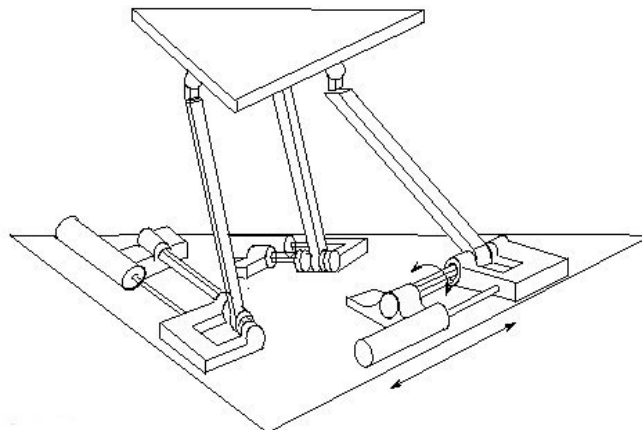


Figure 5.4: The robot presented by Kholi et al. [1988].

איור 5.4: הרובוט המקבילי של Kholi et al. [1988].

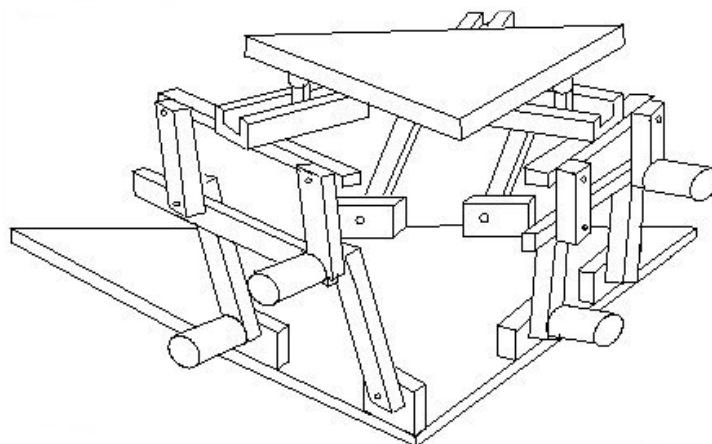


Figure 5.5: The robot presented by Romiti and Soreli [1990].

איור 5.5: הרובוט המקבילי של Romiti and Soreli [1990].

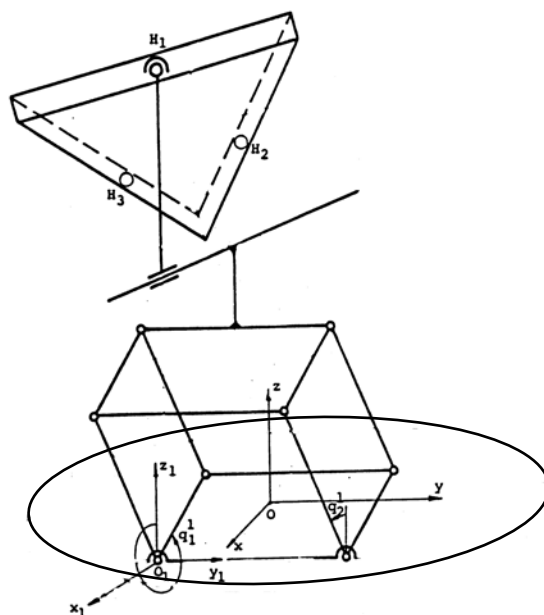


Figure 5.6: The kinematic chain of the robot presented by Soreli, et al. [1997].

איור 5.6: השרשרת הקינמטית של הרובוט המקבילי של Soreli, et al. [1997].

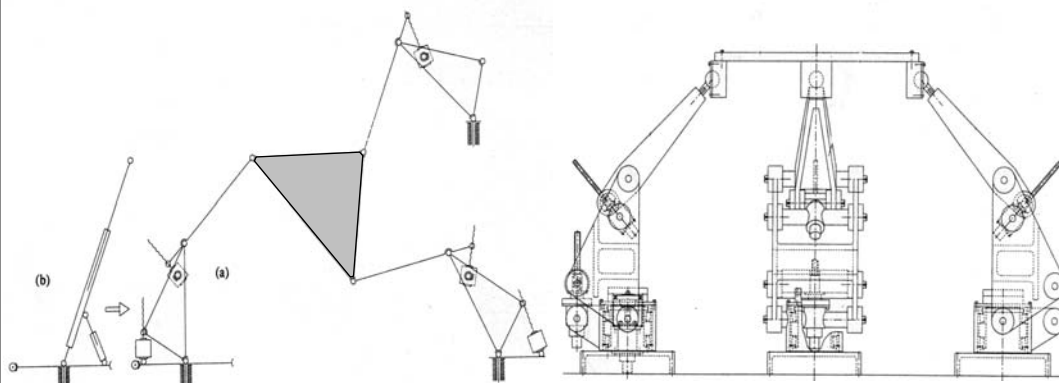


Figure 5.7: The robot presented by Zlatanov, et al. [1992].

איור 5.7: הרובוט המקבילי של Zlatanov, et al. [1992].

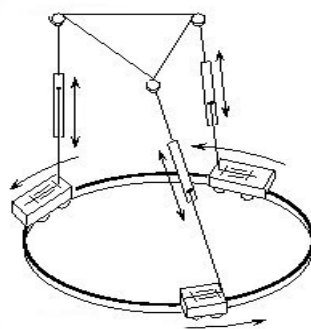
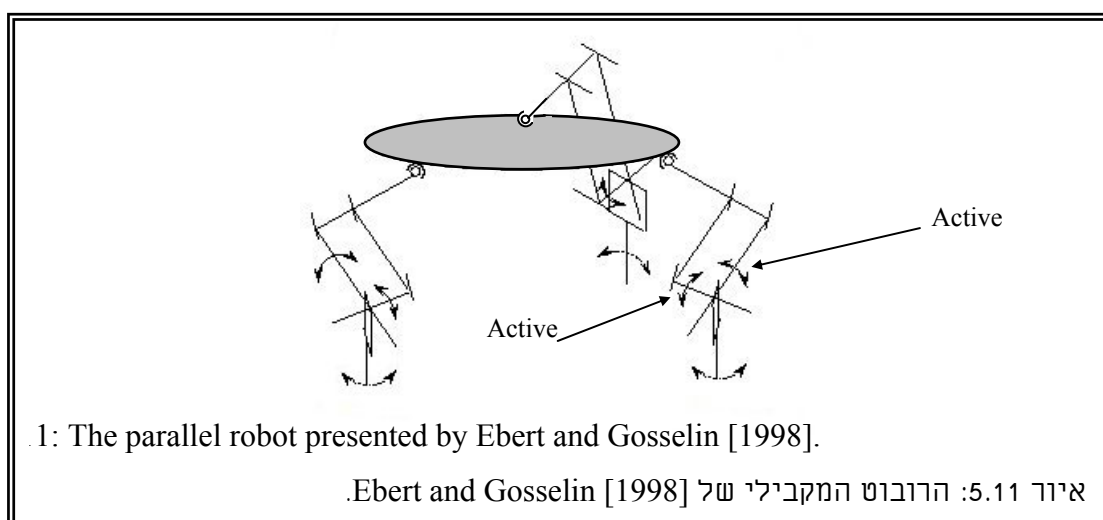
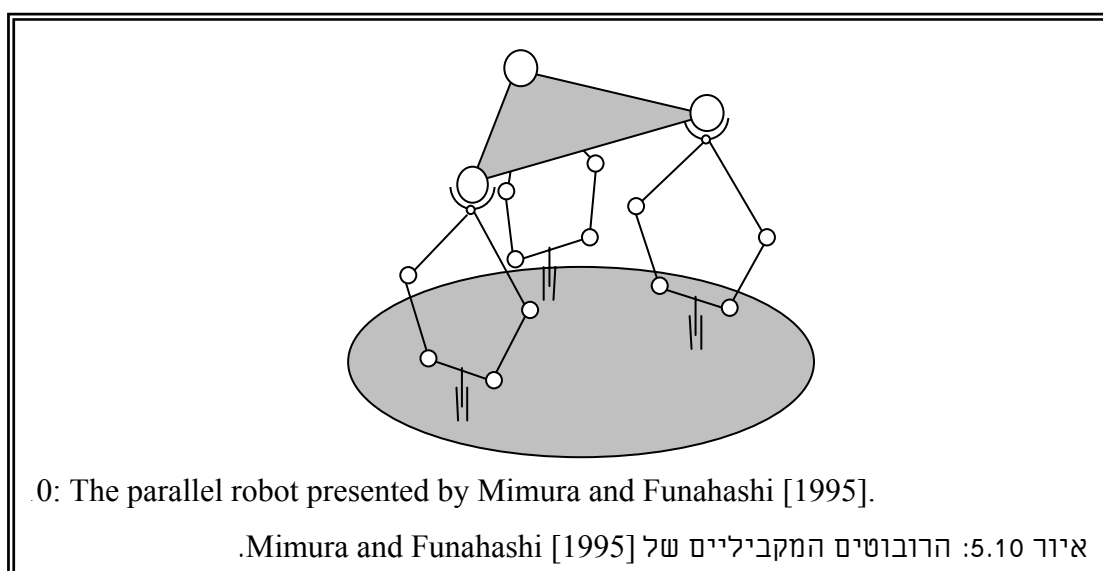
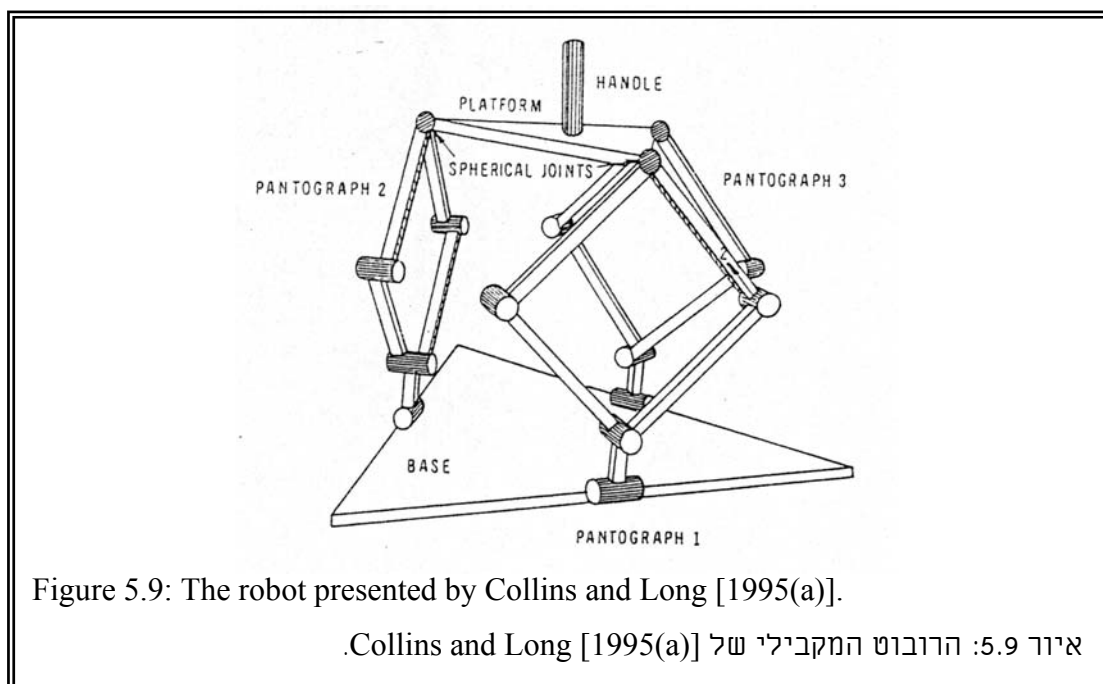
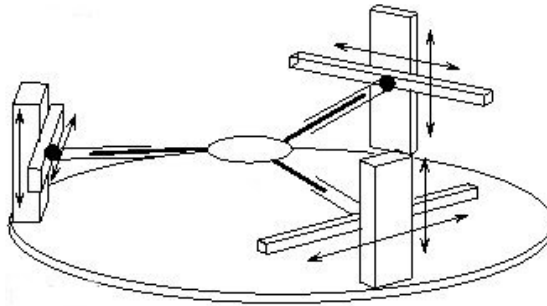


Figure 5.8: The robot presented by Alizade, Tagiyev, and Duffy [1994].

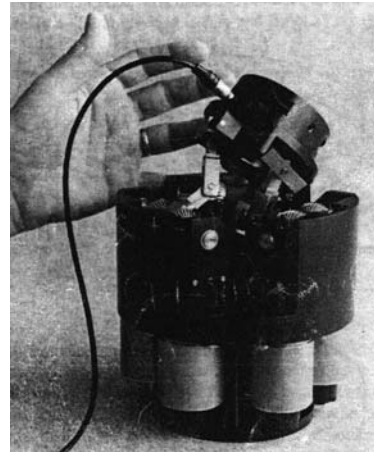
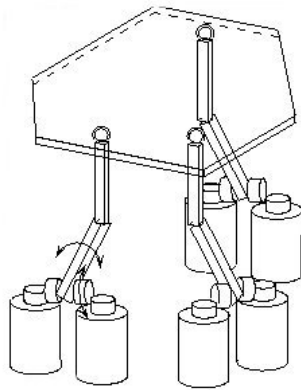
איור 5.8: הרובוט המקבילי של Alizade, Tagiyev, and Duffy [1994].





2: The parallel robot presented by Byun and Cho [1997].

איור 5.12: הרובוט המקבילי של Byun and Cho [1997].



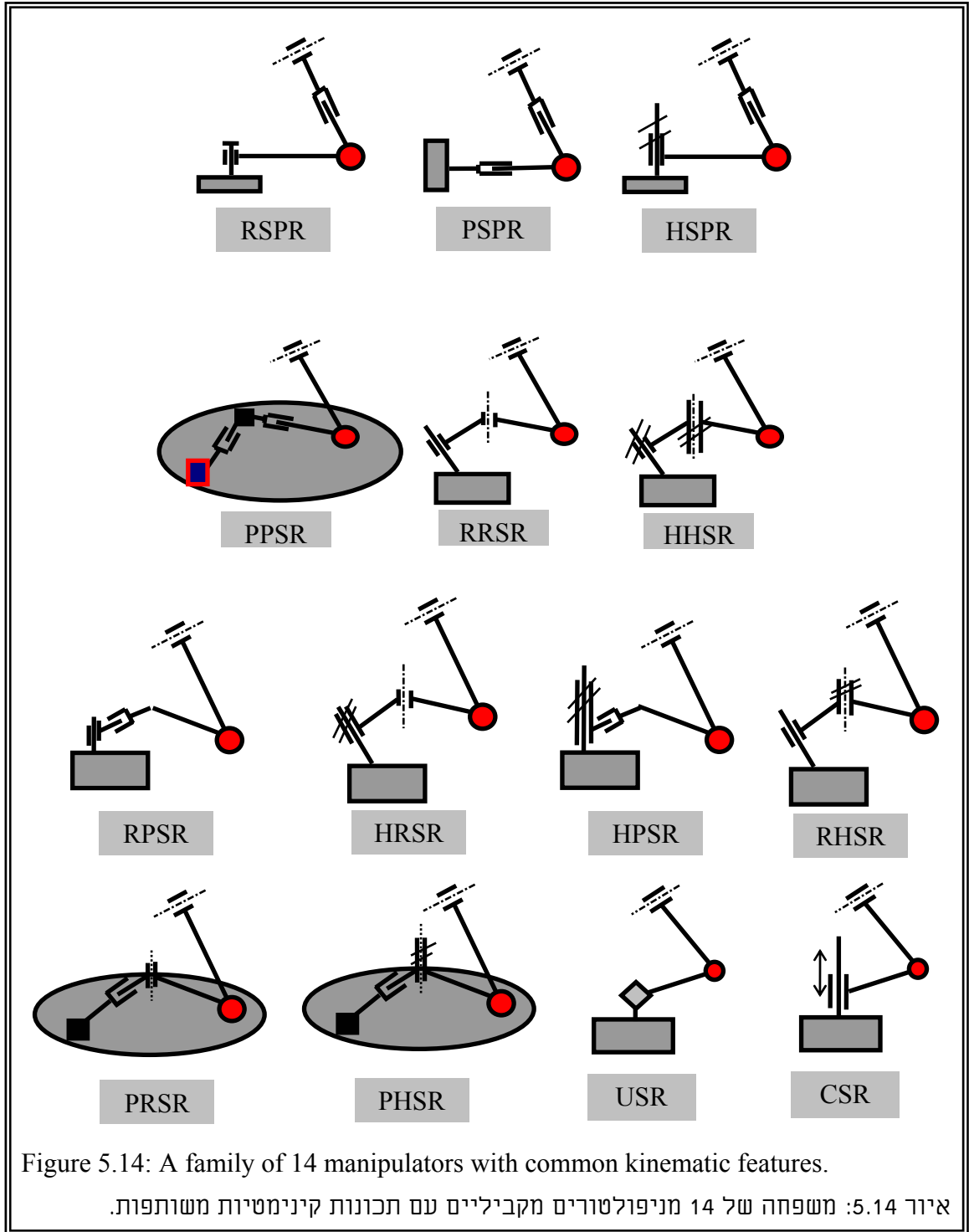
3: The parallel robot presented by Cleary and Uebel [1994].

איור 5.13: הרובוט המקבילי של Cleary and Uebel [1994].

5.4 A family of parallel manipulators

All the manipulators in table 5.2, except for the robot suggested by [Tsai and Tahmasebi, 1993], use kinematic chains that end with spherical joints to connect the kinematic chains with the moving platform. In this section, we present a family of parallel manipulators that includes fourteen distinct manipulators. All the manipulators in this family have three identical kinematic chains connected to the moving platform by revolute joints. In addition, all these manipulators have the same reactions acting on the moving platform. In chapter 7, we will show that these manipulators share the same instantaneous direct kinematics matrix, and in chapter 10, we will analyze the parallel singularities of this family of manipulators.

Figure 5.14 presents all the fourteen kinematic chains that belong to this family of manipulators. The last links in all the kinematic chains are connected to the moving platform



by revolute joints and apply on the moving platform the kinematic constraints of revolute-spherical (RS) dyads. The figure includes the PPSR kinematic chain, which is the same as the one presented by [Tsai and Tahmasebi, 1993]. Among all the fourteen kinematic chains in the figure, we chose two candidate manipulators for the task that was presented in chapter 4. The

two candidate manipulators are the RSPR and the USR manipulators. All the kinematic chains with helical (H) pairs were excluded because of the kinematic complexity introduced by these pairs. In the following section, we present in detail the kinematic parameters of the two suggested manipulators.

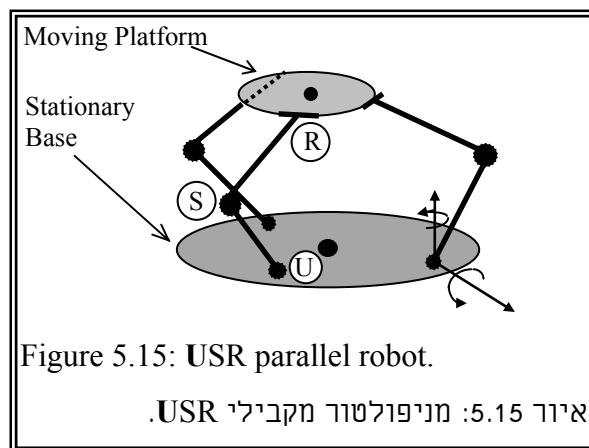
5.5 The RSPR and the USR manipulators

The USR and the RSPR manipulators are presented in Fig. 5.15 and 5.16. All the joints are indicated by encircled letters denoting the type of the joints. These manipulators were first presented in [Simaan, Glozman, and Shoham, 1998].

5.5.1 The USR manipulator

The USR robot consists of three identical kinematic chains connecting the base and the moving platform. Each kinematic chain is composed of two links. One link is connected to the base platform by a active universal (U) joint, the other link is connected to the moving platform by an R joint, and the two links are connected in between by a spherical (S) joint. The lower link of each kinematic chain is oriented in space by a differential drive, controlling its yaw and pitch angles relative to the base platform, Fig. 5.15.

Using the mobility equation shows that this manipulator has a mobility $m = 6$. The number of rigid links, n_l , in each kinematic is 4, the number of joints in each chain, g_l , is 3, and the sum of the joint freedoms in each kinematic chain, $\sum f_l$, is 6. Therefore, the connectivity between the moving and base platform is 6.



This structure is a variation of the structure described by [Cleary and Uebel, 1994] which uses URS joint combination for each kinematical chain, controlling the pitch and roll of the lower links. The structure that we suggest has, however, a different order of joints - a revolute joint connecting the links to the moving platform, and a spherical joint between the

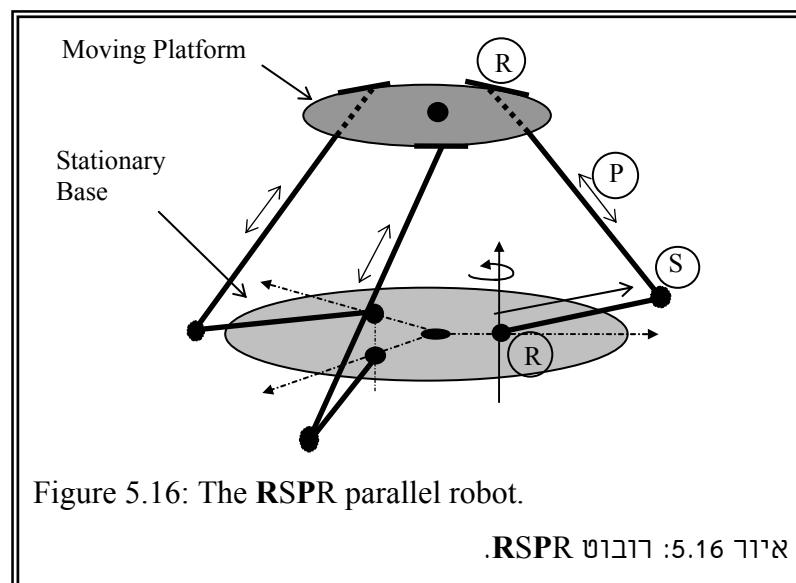
links. This modification prevents collision between links and eliminates some of the singular configurations in the **URS** manipulator.

5.5.2 The **RSPR** manipulator

This manipulator consists of three identical kinematic chains connecting the base and the moving platform. Each chain contains a lower link rotating around a pivot perpendicular to the base platform and offset-placed from the center of the base. At the other end of the lower link, a prismatic actuator is attached by a spherical joint. The upper end of the prismatic actuator is connected to the moving platform by a revolute joint. The axes of the revolute joints constitute an equilateral triangle in the plane of the moving platform, Fig. 5.16.

The mobility equation indicates that this manipulator has a mobility $m = 6$. The number of rigid links, n_l , in each kinematic is 5, the number of joints in each chain, g_l , is 4, and the sum of the joint freedoms in each kinematic chain, Σf_l , is 6. Therefore, the connectivity between the moving and base platform is 6.

This manipulator is distinguished by the location of the lower links revolute axes being placed offset from the center of the base platform. Alizade, Tagiyev, and Duffy [1994] presented a robot with **RRPS** kinematic chains. We will show in chapter 8 that the **RSPR** robot requires less actuator effort for the same task. In chapter 10 we will show that this robot eliminates some of the singular configurations that are present in the **RRPS** robot. However, using the swept volume analysis, which was presented in Zhiming, [1994], reveals that when eccentricity is eliminated in **RSPR** robot then both **RSPR** and **RRPS** have the same swept volume of the kinematic chains' upper extremities. Since **RSPR** robot has an **R** joint at the



end of each kinematic chain, which imposes additional perpendicularity constraints, it results in a smaller vertex space and work volume than RRPS robot. We will show in chapter 10 that, unlike the robot by Alizade, Tagiyev, and Duffy [1994], the eccentricity of the lower revolute joints eliminates singular configuration of the robot.

Chapter 6

Kinematics of the USR and the RSPR Robots

6.1 Introduction

The kinematics of a robot deals with finding the analytical relations between its input variables (the values of the active joints) and output variables (the position and orientation of the gripper). The equations that connect between the input and the output variables of a mechanism are called the kinematic equations of the mechanism. The equations that connect between input and output velocities in a mechanism are called the instantaneous kinematic equations of the mechanism. The direct kinematics problem deals with finding the output variables of the robot, i.e. the position and orientation of the gripper, for a given set of input variables, namely, the active joints' variables. The inverse kinematics problem deals with finding the required input variables (active joints' values) that correspond to a given set of output variables (position and orientation of the gripper).

The inverse kinematics problem of the Stewart-Gough manipulators is trivial with single solution, but when the number of kinematic chains is reduced, the number of solutions of the inverse kinematics problem increases and the problem becomes more challenging. The direct kinematics problem of parallel manipulators is by far more challenging than the inverse kinematics problem since it requires solving a set of polynomial equations in the output variables. While the inverse kinematics problem for a general Stewart-Gough manipulator has only one solution, the direct kinematic problem has up to 40 real solutions [Lazard, 1993]. Recently, Deitmaier [1998] systematically changed the geometric properties of a general Stewart-Gough manipulator and, for the first time, gave an example of a manipulator with 40 real solutions to the direct kinematics problem.

In this chapter, we will show that the USR and the RSPR robots have eight solutions for the inverse kinematics problem. These inverse kinematics solutions for the USR and the RSPR robots are used in the simulations for evaluation of the workspace of both manipulators. The direct kinematics problem for a tripod mechanism such as the upper tripods of the USR and the RSPR robots was solved in [Tahmasebi and Tsai, 1994(a)]. Tahmasebi and Tsai [1994(a)] showed that there are 16 solutions for the direct kinematics problem of the tripod mechanism with pairs of solutions that are the mirror images of one another with respect to the plane that passes through the spherical joints. Based on the solution in [Tahmasebi and Tsai, 1994(a)], the direct kinematics problem of the RSPR and the USR

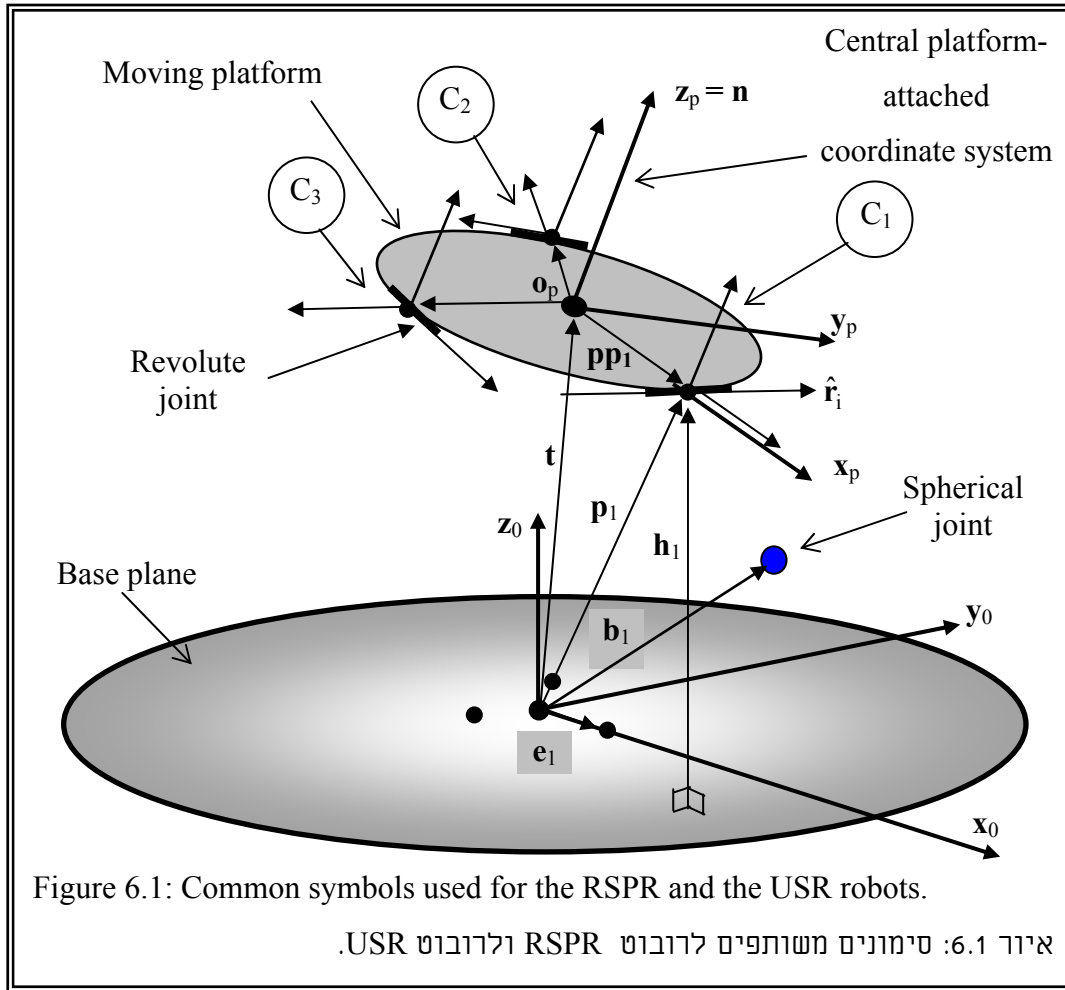
robots becomes simple. This is because the only required additional step is finding the positions of the spherical joints and defining the transformation matrices from the planes through the spherical joints' centers and the base planes of the robots. For parallel robots, only the Inverse kinematic solution is needed for control purposes; therefore, we do not need to solve the direct kinematics problem and we limit this chapter to presenting the inverse kinematic solutions of the USR and the RSPR robots.

Without loss of generality, the following analysis assumes symmetrical robots, but the same analysis presented here can be adapted for any non-symmetrical geometry of the manipulators. We refer to the plane, which is defined by the three lower extremities of the kinematic chains as the base plane. We assume that the lower extremities of the kinematic chains define an equilateral triangle in the base plane. The incenter of this triangle is called the center point of the base platform and we fix the origin of the world coordinate system at this point. The world coordinate system is defined such that its x-axis points from the center point to the lower extremity of the first kinematic chain. The z-axis points upward from the base plane and the y-axis completes the right-handed coordinate system. We also assume that the upper extremities of the kinematic chains connect to the moving platform at three distinct points such that these points define an equilateral triangle in the plane of the moving platform. The incenter of this triangle is called the center point of the moving platform and we attach a coordinate system having its origin coincident with this point. This coordinate system is referred to as the central platform-attached coordinate system. The x-axis, of this coordinate system, points from the center point of the moving platform to the upper extremity of the first kinematic chain. The z-axis is normal to the moving platform and the y-axis completes the system to a right-handed coordinate system, Fig. 6.1. In addition to the central platform-attached system, we define three platform-attached coordinate systems called C_1 , C_2 , and C_3 , Fig. 6.1. These coordinate systems are right-handed and rotated about the z-axis of the central platform-attached coordinate system. The y-axis of the i 'th coordinate system, C_i , is parallel to the axis of the upper revolute joint of the i 'th kinematic chain. The origin of the C_i coordinate systems is located at the upper extremity of the i 'th kinematic chain.

In order to facilitate the formulation of the inverse kinematics problems for the USR and the RSPR robots we introduce the following symbols that will be used for both manipulators. Fig. 6.1 presents these common symbols without showing the details of the kinematic chains.

i : an index indicating a specific kinematic chain $i = 1, 2, 3$.

\mathbf{o}_p : center point of the moving platform.



r_p : the radius of the moving platform.

t : position vector of the center of the moving platform.

p_i : position vector of the upper extremity of the i 'th kinematic chain.

pp_i : position vector of the upper extremity of the i 'th kinematic chain in the central platform-attached coordinate system.

ξ_{pi} : an angle measured from the x -axis of the central platform-attached coordinate system, x_p , to pp_i according to the right-hand rule about z_p .

e_i : position vector of the lower extremity of the i 'th kinematic chain.

e : the eccentricity measure (equal to the Euclidean norm of e_i).

ξ_{bi} : an angle measured from the x -axis of the world coordinate system, x_0 , to e_i according to the right-hand rule about z_0 .

b_i : position vector of the spherical joint of the i 'th kinematic chain.

n : a unit vector normal to the moving platform.

\hat{r}_i : a unit vector along the axis of the upper revolute joint in the i 'th kinematic chain.

\mathbf{h}_i : A vector specifying the height of the i 'th kinematic chain upper extremity relative to the base plane.

${}^w\mathbf{R}_p$: rotation matrix transforming vectors from the central platform-attached coordinate system to world coordinate system.

${}^p\mathbf{R}_{C_i}$: rotation matrix form the C_i coordinate system to the central platform-attached coordinate system.

Note: all the vectors, unless otherwise noted, are expressed in the world coordinate system.

Equations (6.1) and (6.2) give the expressions of the vectors describing the location of the connection points of the kinematic chains to the platforms, \mathbf{pp}_i and \mathbf{e}_i .

$$\mathbf{pp}_i = [r_p \cos(\xi_{pi}), r_p \sin(\xi_{pi}), 0]^t \quad (6.1)$$

$$\mathbf{e}_i = [e \cos(\xi_{bi}), e \sin(\xi_{bi}), 0]^t \quad (6.2)$$

Where the angles ξ_{pi} and ξ_{bi} are equal and have the values given by Eq. (6.3).

$$\xi_{pi} = \xi_{bi} = \frac{2(i-1)}{3}\pi \quad (6.3)$$

Eq. (6.4) gives the expression for the unit vectors $\hat{\mathbf{r}}_i$.

$$\hat{\mathbf{r}}_i = [\cos(\xi_{pi} + \pi/2), \sin(\xi_{pi} + \pi/2), 0]^t \quad (6.4)$$

The columns of the rotation matrices ${}^p\mathbf{R}_{C_i}$ are the unit vectors along \mathbf{pp}_i , $\hat{\mathbf{r}}_i$, and \mathbf{n} expressed in the central platform-attached coordinate system; therefore, Eq. (6.5) has the following form.

$${}^p\mathbf{R}_{C_i} = \begin{bmatrix} \cos(\xi_{pi}) & -\sin(\xi_{pi}) & 0 \\ \sin(\xi_{pi}) & \cos(\xi_{pi}) & 0 \\ 0 & 0 & 1 \end{bmatrix} \quad (6.5)$$

6.2 Inverse kinematics of the RSPR robot

Figure 6.2 presents the kinematic model of RSPR robot with additional symbols that are defined herein.

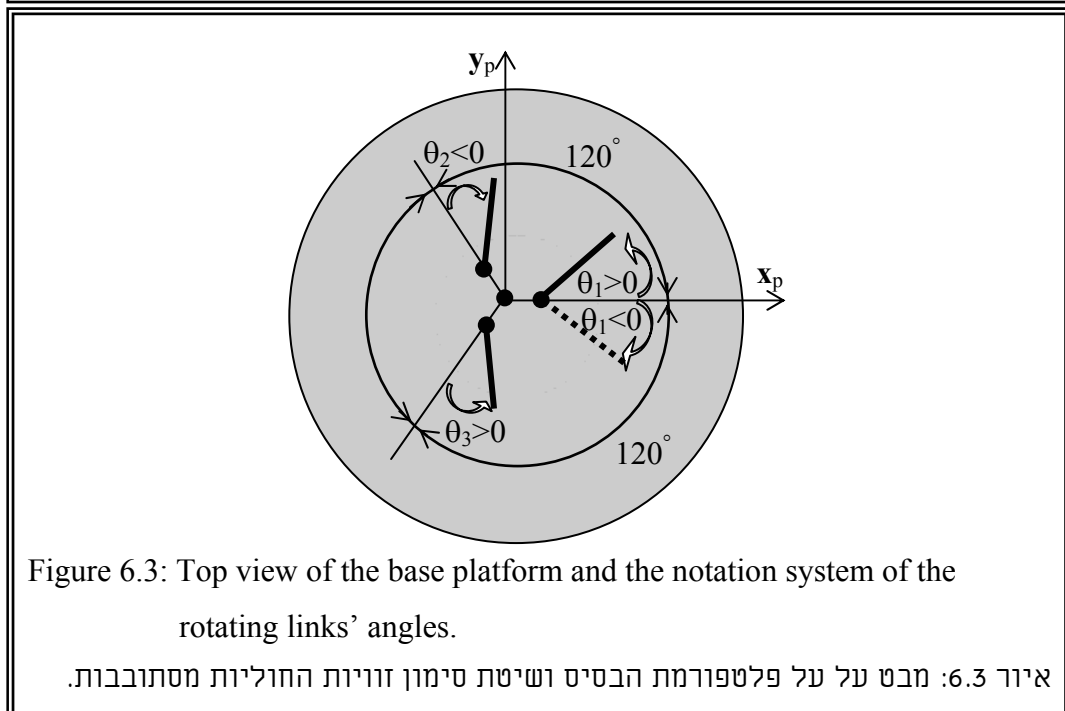
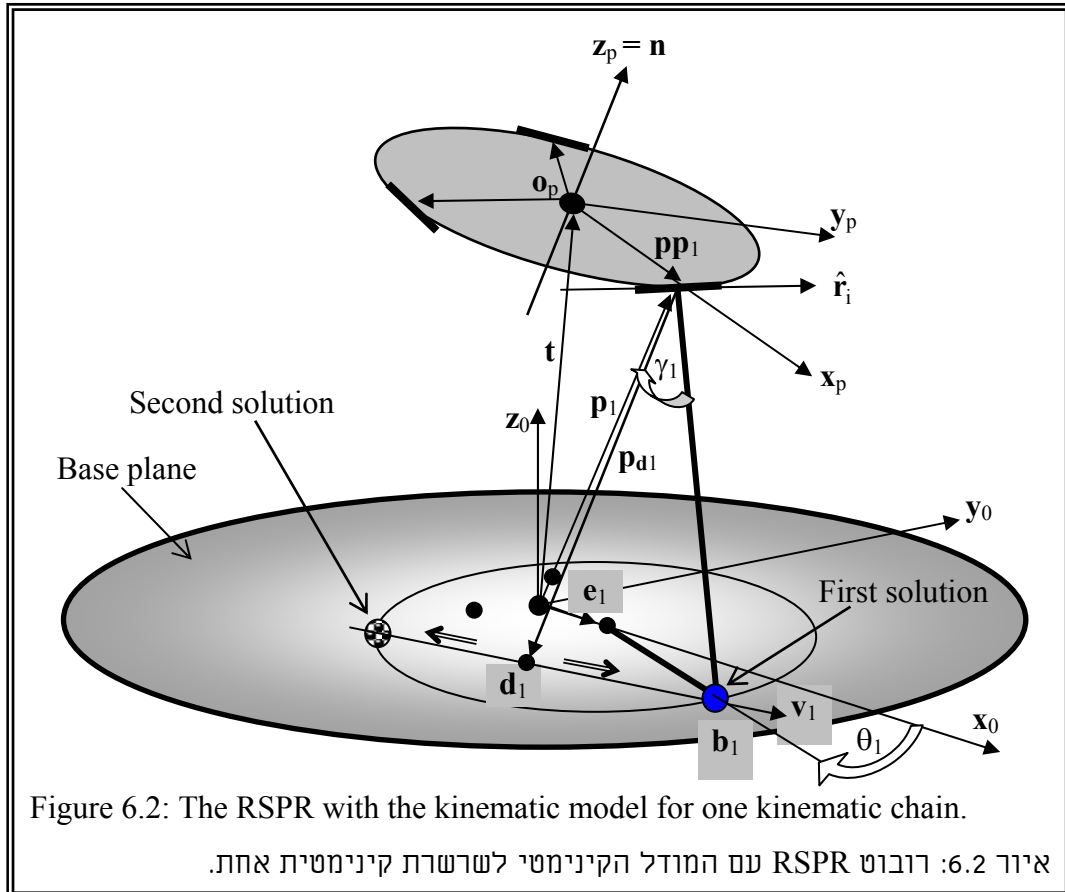
r_b : the length of the rotating links.

γ_i : the angle between the normal, \mathbf{n} , and the normal to the base plane.

P_i : the plane in which the i 'th extensible link rotates about the revolute joint, $\hat{\mathbf{r}}_i$.

\mathbf{v}_i : the line of intersection between the plane P_i and the base plane.

In addition to these symbols, we define the active joints' variables that control the movement of the moving platform. Figure 6.3 presents a top view of the base platform. The rotation of the i 'th rotating link is measured as indicated in the figure and is denoted by θ_i . The length of the i 'th extensible link is indicated by the symbol l_i .



The locus of the spherical joint of the i 'th kinematic chain is a circle with a radius equal to the length of the rotating links, r_b . The center of the spherical joint, \mathbf{u}_i , is defined by the intersection of the plane P_i with the circle of the rotating link. This indicates that when the position and orientation of the moving platform is given then there are two possible solutions for each rotating link as demonstrated in Fig. 6.2. Since every rotating link has two possible values for θ , the whole manipulator has eight solutions for the inverse kinematics problem.

The solution presented here allows careful selection of the desired inverse kinematics solutions for every kinematic chain. This is important in order to maintain consistency of the solution during the simulations for workspace evaluation.

The unit vector normal to the moving platform is given by the third column of the rotation matrix ${}^w\mathbf{R}_p$ as expressed in Eq. (6.6).

$$\mathbf{n} = {}^w\mathbf{R}_p * [0,0,1]^t \quad (6.6)$$

The position of the kinematic chain upper extremity is given by:

$$\mathbf{p}_i = \mathbf{t} + {}^w\mathbf{R}_p * \mathbf{pp}_i \quad (6.7)$$

We define a point \mathbf{d}_i as the point, in which, a line parallel to the normal, \mathbf{n} , and passing through \mathbf{p}_i pierces the base plane. We also define the vector \mathbf{pd}_i as the vector from point \mathbf{p}_i to \mathbf{d}_i .

$$|\mathbf{pd}_i| = \frac{|\mathbf{h}_i|}{\cos(\gamma_i)} \quad (6.8)$$

Where the symbol $|\mathbf{pd}_i|$ indicates the magnitude of the vector \mathbf{pd}_i .

Using the scalar product definition between the vector $-\mathbf{n}$ and \mathbf{h}_i and substituting it in Eq. (6.8) yields:

$$|\mathbf{pd}_i| = \frac{-|\mathbf{h}_i|^2}{\mathbf{n}^t \mathbf{h}_i} \quad (6.9)$$

The point \mathbf{d}_i is obtained by Eq. (6.10).

$$\mathbf{pd}_i = \mathbf{p}_i + \mathbf{pd}_i = \mathbf{p}_i - |\mathbf{pd}_i| * \mathbf{n} \quad (6.10)$$

Point \mathbf{d}_i belongs to the plane P_i ; therefore, it is possible to obtain the two solutions of the inverse kinematics problem by tracing along \mathbf{v}_i in two directions as shown in Fig. 6.2. Any point (x, y) on \mathbf{v}_i is define by the parametric equation in Eq. (6.11).

$$\begin{aligned} x &= d_{ix} + t * v_x \\ y &= d_{iy} + t * v_y \end{aligned} \quad t \in [-\infty, \infty] \quad (6.11)$$

We define a point \mathbf{t}_p along the normal \mathbf{n} such that

$$\mathbf{t}_p = \mathbf{t} + r_p \mathbf{n} \quad (6.12)$$

The equation of the plane P_i is given by the determinant of the matrix \mathbf{M} expressed in Eq. (6.13).

$$M = \det \begin{bmatrix} x - x_1 & y - y_1 & z - z_1 \\ x - x_2 & y - y_2 & z - z_2 \\ x - x_3 & y - y_3 & z - z_3 \end{bmatrix} \quad (6.13)$$

Where (x_1, y_1, z_1) , (x_2, y_2, z_2) , and (x_3, y_3, z_3) are the Cartesian coordinates of the points \mathbf{t}_p , \mathbf{t} , and \mathbf{p}_i , respectively. Equation (6.14) for the line \mathbf{v}_i , is obtained by substituting $z = 0$ in Eq. (6.13) and expanding the determinant.

$$A_x x + A_y y + C = 0 \quad (6.14)$$

Where A_x , A_y , and C are given by:

$$A_x = (-z_3 y_1 + z_3 y_2 - z_2 y_3 + z_1 y_3 + z_2 y_1 - z_1 y_2) \quad (6.15)$$

$$A_y = (-x_1 z_2 - x_2 z_3 + x_1 z_3 - x_3 z_1 + x_3 z_2 + x_2 z_1) \quad (6.16)$$

$$C = x_1 z_2 y_3 - x_3 z_2 y_1 - x_1 z_3 y_2 + x_2 z_3 y_1 - x_2 z_1 y_3 + x_3 z_1 y_2 \quad (6.17)$$

We use the letter m to refer to the slope of the line \mathbf{v}_i . The unit vector along this line is given by Eq. (6.18).

$$\mathbf{v}_i = \text{sgn} \left(\left({}^w \mathbf{R}_p \mathbf{p}_i \right)^t \begin{bmatrix} 1 \\ \frac{m}{\sqrt{1+m^2}} \\ 0 \end{bmatrix} \right) * \begin{bmatrix} 1 \\ \frac{m}{\sqrt{1+m^2}} \\ 0 \end{bmatrix}^t \quad (6.18)$$

The sign term in Eq. (6.18) ensures that the unit vector \mathbf{v}_i points in the same direction as the projection of the vector \mathbf{p}_i on the base, Fig. 6.2. The sign of the parameter t distinguishes between the two solutions of the inverse kinematics for one kinematic chain. This method for identifying the solutions holds for all the cases, except for the case when the vector \mathbf{p}_i is perpendicular to the base plane. This occurs when the platform is perpendicular relative to the base plane and this configuration is outside the desired rotational capability of the manipulator.

The parameter t is found by the intersection of the line \mathbf{v}_i with the circle of the lower rotating link. The equation of the circle is given by Eq. (6.19).

$$(x - e_x)^2 + (y - e_y)^2 = r_b^2 \quad (6.19)$$

By substituting Eq. (6.11) in Eq. (6.19), we obtain a quadratic equation with the unknown parameter t .

$$at^2 + bt + c = 0 \quad (6.20)$$

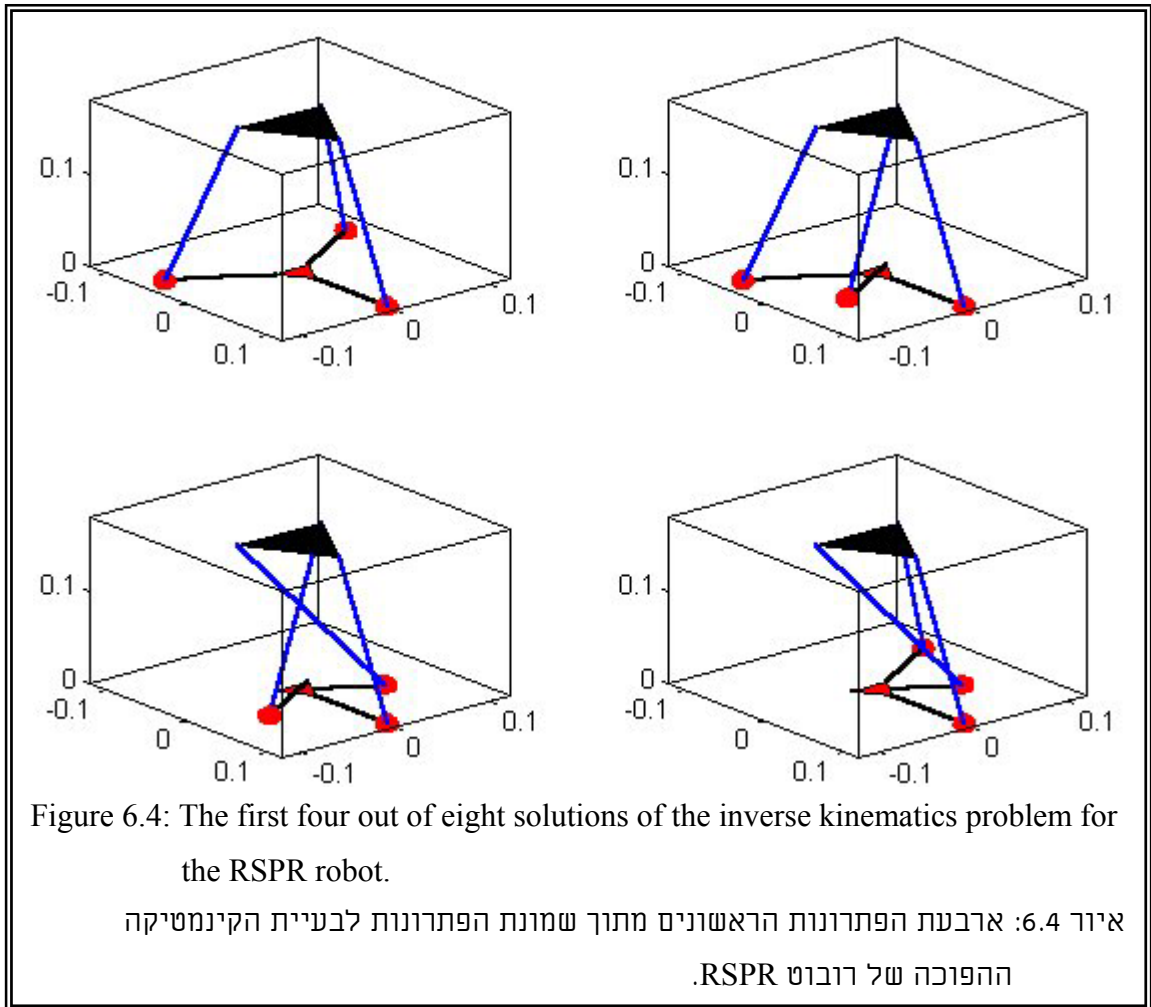
Where a , b , and c are given by:

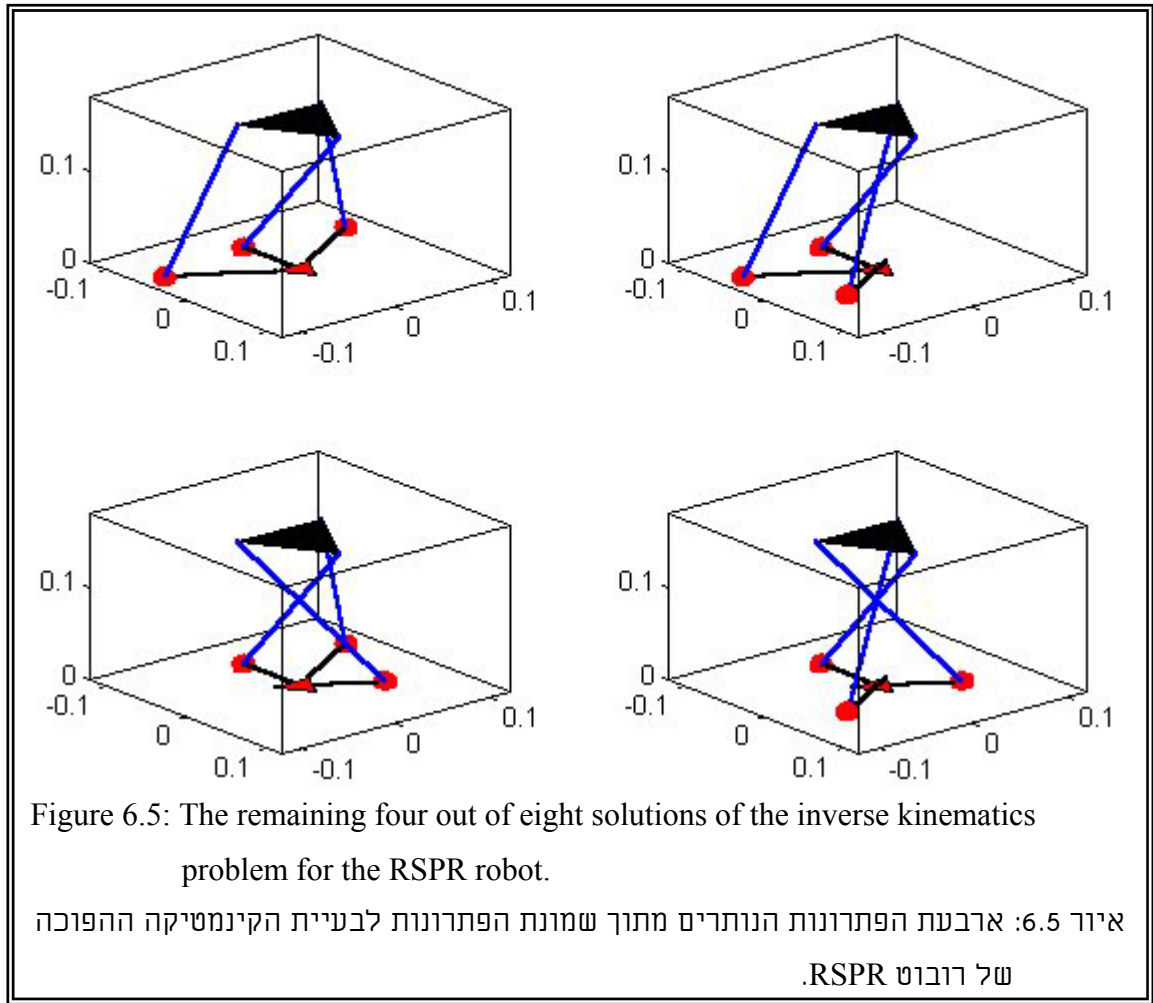
$$a = \mathbf{v}_i^t \mathbf{v}_i, \quad b = 2(\mathbf{d}_i - \mathbf{e}_i)^t \mathbf{v}_i, \quad c = \mathbf{d}_i^t \mathbf{d}_i + \mathbf{e}_i^t \mathbf{e}_i - 2\mathbf{d}_i^t \mathbf{e}_i - r_b^2. \quad (6.21)$$

The solution for t is given by Eq. (6.22).

$$t = \frac{-b \pm \sqrt{b^2 - 4ac}}{2a} \quad (6.22)$$

The solution with the plus sign corresponds to the solution shown in Figure 6.1 and labeled as the first solution. The solution with the minus sign corresponds to the second solution shown in Fig. 6.2. Figures 6.4 and 6.5 present the eight inverse kinematics solutions for the RSPR robot with the moving platform parallel and right above the base platform.





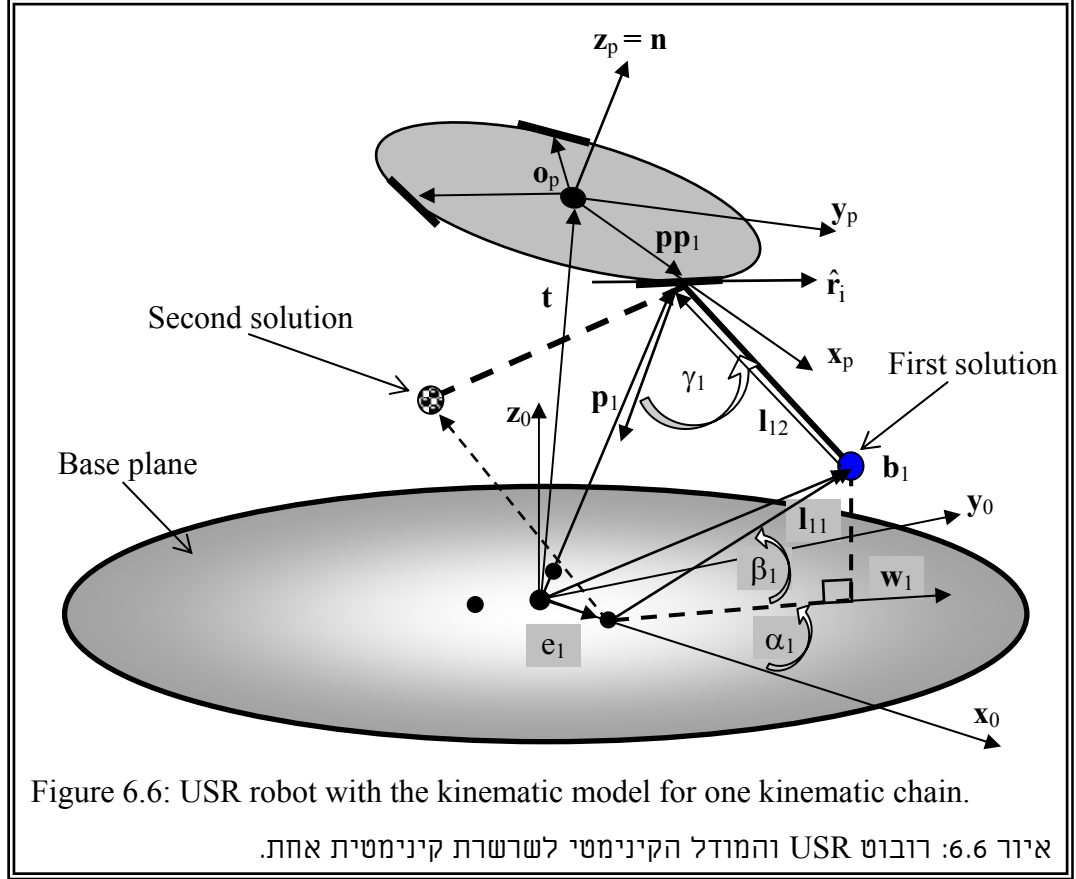
6.3 Inverse kinematics of the USR robot

The USR robot, like the RSPR robot, has eight possible solutions for the inverse kinematics problem. The yaw and the pitch angles of the lower rotating links are the unknown parameters of the inverse kinematics problem.

Figure 6.6 presents the USR robot with the relevant symbols. We use the following symbols in addition to the symbols and geometrical assumptions that were presented in section 6.1.

- α_i : the yaw angle of the lower rotating link. α_i is measured in the same way like θ_i for the RSPR robot. Figure 6.3 applies for the USR robot with the replacement of θ_i with α_i .
- β_i : the pitch angle of the lower rotating link. β_i is measured relative to the base plane as shown in Fig. 6.6.

- l_{i1} : a vector pointing from the center of the active Hook's joint to the center of the spherical joint.
- l_{i2} : a vector pointing from the center of the spherical joint to the upper extremity of the kinematic chain.
- l_1 : the length of the lower rigid links in the kinematic chains.
- l_2 : the length of the upper rigid links in the kinematic chains.



The rotation of upper rigid link about the axis of the revolute joint defines a circle with a radius l_1 . This circle is the locus of the spherical joint in the platform-attached coordinate system. The lower link defines a sphere, with a radius l_1 . All the points on this sphere are the locus of the spherical joint in the world coordinate system. The solution of the inverse kinematics problem of one kinematic chain is obtained by finding the intersection points between the circle and the sphere associated with the kinematic chain. Consequently, there are two solutions for every kinematic chain and, in total, there are eight solutions for the whole manipulator.

The position of the center of the spherical joint in a kinematic chain is given by Eq. (6.23).

$$\mathbf{b}_i = \mathbf{p}_i - \mathbf{l}_{i2} \quad (6.23)$$

Where \mathbf{p}_i is given by Eq. (6.7) and \mathbf{l}_{i2} is expressed in world coordinate system by Eq. (6.24).

$$\mathbf{l}_{i2} = {}^w\mathbf{R}_p {}^p\mathbf{R}_{C_i} [-l_2 \sin(\gamma_i), 0, l_2 \cos(\gamma_i)]^t \quad (6.24)$$

Substituting Eq. (6.24) and Eq. (6.7) in Eq. (6.23) results in:

$$\mathbf{b}_i = \mathbf{t} + {}^w\mathbf{R}_p (\mathbf{p}\mathbf{p}_i + {}^p\mathbf{R}_{C_i} * [l_2 \sin(\gamma_i), 0, -l_2 \cos(\gamma_i)]^t) \quad (6.25)$$

The vector along the lower rotating link, \mathbf{l}_{i1} , is given by Eq. (6.26).

$$\mathbf{l}_{i1} = \mathbf{b}_i - \mathbf{e}_i \quad (6.26)$$

The rotating link has a constant length l_1 , therefore, we obtain one constraint equation, Eq. (6.27).

$$|\mathbf{t} + {}^w\mathbf{R}_p * (\mathbf{p}\mathbf{p}_i + {}^p\mathbf{R}_{C_i} [l_2 \sin(\gamma_i), 0, -l_2 \cos(\gamma_i)]^t) - \mathbf{e}_i| = l_1 \quad (6.27)$$

Raising Eq. (6.27) to the power of two results in an equation with one unknown parameter γ_i .

$$a \cos(\gamma_i) + b \sin(\gamma_i) = c \quad (6.28)$$

Where a, b, and c are given by:

$$a = 2l_2([\mathbf{e}_i - \mathbf{p}_i]^t \mathbf{n}) \quad (6.29)$$

$$b = \frac{-2l_2}{r_p} ([\mathbf{e}_i - \mathbf{p}_i]^t {}^w\mathbf{R}_p \mathbf{p}\mathbf{p}_i) \quad (6.30)$$

$$c = l_1^2 - l_2^2 - |\mathbf{p}_i|^2 - \mathbf{e}^2 + 2\mathbf{p}_i^t \mathbf{e}_i \quad (6.31)$$

Equation 6.28 has two solutions [Lipkin and Duffy, 1985]:

$$\gamma_i = \text{Atan2}\left(\frac{b}{a}\right) + \text{Atan2}\left(\frac{\pm \sqrt{a^2 + b^2 - c^2}}{c}\right) \quad (6.32)$$

These solutions are demonstrated in Fig. 6.6. The solution with the minus sign corresponds to the first solution in Fig. 6.6 and it is characterized by positive γ_i . The solution with the plus sign corresponds to the second solution in Fig. 6.6 and it is characterized by negative γ_i .

After selecting the desired solution we substitute γ_i in Eq. (6.26) and we obtain the vector \mathbf{l}_{i1} . We use the symbol \mathbf{w}_i to refer to the unit vector along the perpendicular projection line of \mathbf{l}_{i1} on the base plane. \mathbf{w}_i is given by Eq 6.34.

$$\mathbf{w}_i = \frac{1}{\sqrt{l_{i1_x}^2 + l_{i1_y}^2}} * \begin{bmatrix} l_{i1_x} & l_{i1_y} & 0 \end{bmatrix}^t \quad (6.34)$$

Where l_{i1_x} and l_{i1_y} are the first two direction numbers of \mathbf{l}_{i1} . We compute the required yaw angle, α_i , by utilizing the expression for dot and cross products between \mathbf{w}_i and a unit vector along \mathbf{e}_i .

$$\cos(\alpha_i) = \left(\frac{\mathbf{e}_i^t \mathbf{w}_i}{e} \right) \quad (6.35)$$

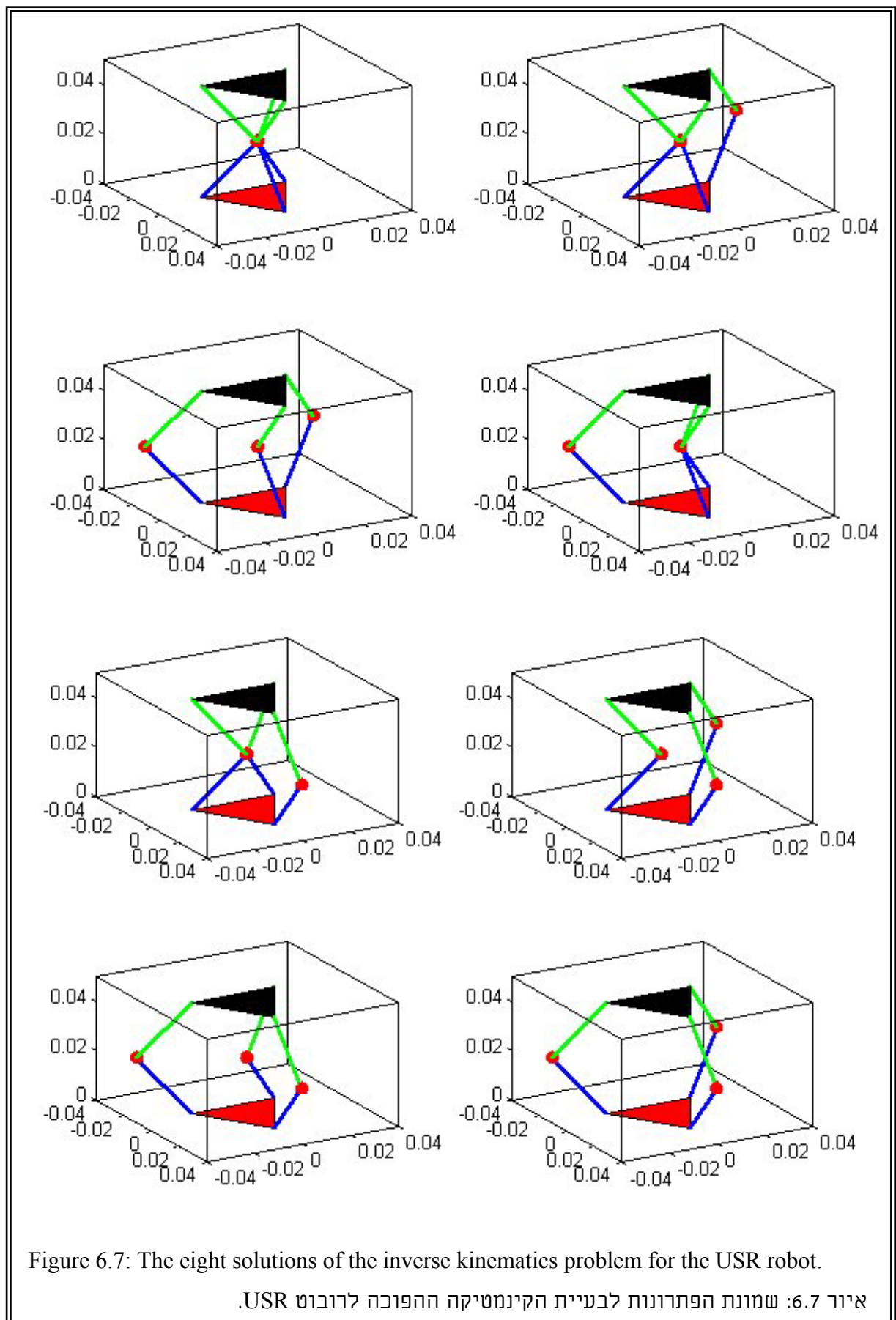
$$\sin(\alpha_i) = \frac{[\mathbf{e}_i \times \mathbf{w}_i]^t \mathbf{z}_0}{e} \quad (6.36)$$

$$\alpha_i = A \tan 2 \left(\frac{\sin(\alpha_i)}{\cos(\alpha_i)} \right) \quad (6.37)$$

The pitch angle, β_i , is limited in the range $\beta_i \in [0, \pi]$; therefore, computing the scalar product between the unit vectors along \mathbf{l}_{i1} and \mathbf{w}_i is sufficient for explicit computation of β_i .

$$\beta_i = \cos^{-1} \left(\frac{\mathbf{w}_i^t \mathbf{l}_{i1}}{l_1} \right) \quad (6.38)$$

Equations (6.37) and (6.38) give the desired yaw and pitch angles for every active universal joint in the manipulator, hence, the solution of the inverse kinematics problem is complete. Figures 6.7 display the eight solutions of the inverse kinematics problem with the moving platform parallel and right above the base platform.



Chapter 7

Jacobian Formulation of A Class of Parallel Robots

7.1 Introduction

This chapter presents the Jacobian formulation of a class of parallel manipulators that was introduced in section 5.4 Fig. 5.14. The robots in this class of manipulators share a common tripod mechanism, which constitutes of a moving platform and three links connected to it by revolute joints. These links transmit to the moving platform the same constraints as the constraints associated with a spherical-revolute (SR) dyad. This fact allows unifying the Jacobian formulation for this class of manipulators.

Various Jacobian formulation methods for parallel robots can be found in the literature. The methods are based on velocity equations [Tahmasebi and Tsai, 1992], static equilibrium [Cleary and Uebel, 1994, Simaan, Glozman, and Shoham, 1998] and screw theory [Waldron and Hunt, 1991]. Collins and Long [1995(b)] formulated the Jacobian matrices for fully parallel and serial manipulators based on reciprocal screws. More recently, [Tsai, 1998] used similar method to the one presented in [Collins and Long, 1995(b)] and utilized reciprocal screws to formulate the Jacobian matrix of the PPSR parallel-chain robot, which was presented in [Tsai and Tahmasebi, 1993]. This formulation of the Jacobian matrix, though mathematically simple, lacks the geometrical view that allows simpler derivation of the Jacobian matrix. The formulation presented in the sequel divides a typical manipulator of Fig. 5.14 into a parallel part and a serial part. This overcomes the problem of obtaining a line-based Jacobian formulation [Hao and McCarthy, 1998] for the class of manipulators of Fig. 5.14 and unifies the singularity analysis of this class of manipulators. The method enables interpreting the singular configurations in terms of the geometry of the robot.

7.2 The Jacobian matrix for parallel manipulators

The Jacobian matrix for parallel manipulators relates the instantaneous twist motion of the moving platform with the corresponding required speeds of the active joints. This definition is dual to the definition of the Jacobian matrix for serial manipulators where the Jacobian matrix relates the speeds of the active joints with the corresponding instantaneous twist motion of the moving platform. This duality was presented in [Waldron and Hunt, 1991] and later in [Collins and Long, 1995(b)]. The duality of the Jacobian definitions for Serial and Parallel manipulators stems from the duality between wrenches and twists. For serial

manipulators, the twist of the end effector is a linear combination of the motion screws associated with the active joints. For parallel manipulators, the resultant wrench acting on the moving platform is a linear combination of the active joints' action screws. Equation (7.1) is the general form of the input-output velocity relation of a general non-redundant manipulator [Gosselin and Angeles, 1990].

$$\mathbf{A}\dot{\mathbf{x}} = \mathbf{B}\dot{\mathbf{q}} \quad (7.1)$$

Where \mathbf{x} denotes the vector of the output link's position and orientation variables, $\dot{\mathbf{x}}$ denotes twist rates of the output link, \mathbf{q} denotes the vector of the active joints values, and $\dot{\mathbf{q}}$ denotes the speeds of the active joints.

For open-chain manipulators, the direct kinematics is trivial; therefore, there exists an explicit relation in the form of Eq. (7.2).

$$\mathbf{x} = \mathbf{f}(\mathbf{q}) \quad (7.2)$$

Taking the time derivative of Eq. (7.2) yields a relation in the general form of Eq. (7.1) with the matrix \mathbf{A} being the identity matrix. Therefore, the definition of the Jacobian matrix for serial manipulators is according to Eq. (7.3).

$$\dot{\mathbf{x}} = \mathbf{J}\dot{\mathbf{q}} \quad (7.3)$$

The matrix \mathbf{J} is the Jacobian matrix for serial manipulators and it is defined by the partial derivatives of the direct kinematics relations.

$$J_{ij} = \frac{\partial x_i}{\partial q_j} \quad (7.4)$$

The direct kinematics of closed-chain manipulators does not have simple explicit form and the inverse kinematics problem has explicit and relatively trivial form. Therefore, a relation in the form of Eq. (7.5) is always attainable. Alternatively, loop closure equations may be used for the Jacobian formulation [Basu and Ghosal, 1996].

$$\mathbf{q} = \mathbf{f}(\mathbf{x}) \quad (7.5)$$

Taking the derivative of Eq. (7.5) with respect to time yields a relation in the form of Eq. (7.1). For a fully-parallel manipulator, the matrix \mathbf{B} is a diagonal matrix and it is easy to invert it. Therefore, the definition of the Jacobian matrix and the input/output velocity relation for parallel manipulators is given by Eq. (7.6). This definition assures that for a fully-parallel manipulator the Jacobian matrix exists for all configurations [Ma and Angeles, 1992].

$$\dot{\mathbf{q}} = \mathbf{J}\dot{\mathbf{x}} \quad (7.6)$$

Equation (7.7) gives the expression for the Jacobian matrix cells. Moreover, the Jacobian matrix, \mathbf{J} , is the product of multiplying two matrices according to Eq. (7.8), [Gosselin and Angeles, 1990].

$$J_{ij} = \frac{\partial q_i}{\partial x_j} \quad (7.7) \quad \mathbf{J} = \mathbf{B}^{-1} \mathbf{A} \quad (7.8)$$

The matrices, \mathbf{A} and \mathbf{B} , are called the instantaneous direct kinematics matrix and the instantaneous inverse kinematics matrix, respectively. These matrices are used for determining the singularity conditions regarding loss or gain of degrees of freedom [Gosselin and Angeles, 1990] and will be used in the singularity analysis presented in chapter 10.

By assuming no power loss in the manipulator, we obtain the input/output static forces relation. For serial manipulators, the Jacobian relates between the wrench applied by the output link on the environment and the corresponding forces of the active joints, Eq (7.9).

$$\boldsymbol{\tau} = \mathbf{J}^t \mathbf{f} \quad (7.9)$$

Where $\boldsymbol{\tau}$ is the vector of active joints' forces and \mathbf{f} is the wrench applied on the environment by the output link. For parallel manipulators, the Jacobian matrix relates between the force/torque intensities of the active joints and the resultant wrench on the output link according to Eq. (7.10).

$$\boldsymbol{\tau} = \mathbf{J}^{t^{-1}} \mathbf{f} \quad (7.10)$$

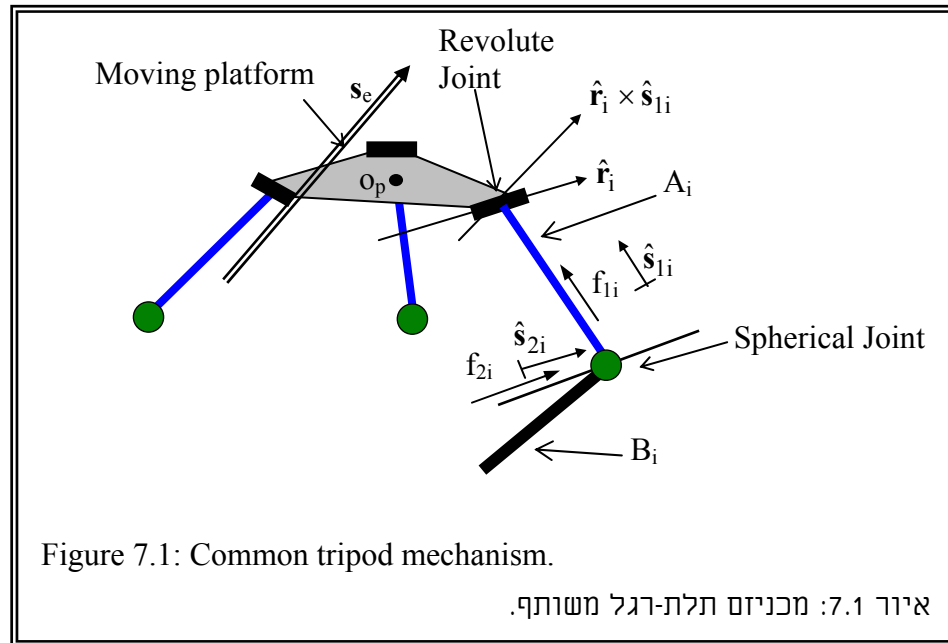
Table 7.1 summarizes the input/output velocity and static forces relations for parallel and serial manipulators.

Table 7.1: Jacobian definition for Parallel and Serial manipulators. טבלה 7.1: הגדרת היעקוביאן לרובוטים מקביליים ולרובוטים סוריים.		
General input/output velocity relation: $\mathbf{A}\dot{\mathbf{x}} = \mathbf{B}\dot{\mathbf{q}}$		
Property	Parallel manipulators	Serial manipulators
Explicit kinematic relation	$\mathbf{q} = \mathbf{f}(\mathbf{x})$	$\mathbf{x} = \mathbf{f}(\mathbf{q})$
Instantaneous relation	$\dot{\mathbf{q}} = \mathbf{J}\dot{\mathbf{x}}$	$\dot{\mathbf{x}} = \mathbf{J}\dot{\mathbf{q}}$
Jacobian definition	$J_{ij} = \frac{\partial q_i}{\partial x_j} \quad \mathbf{J} = \mathbf{B}^{-1} \mathbf{A}$	$J_{ij} = \frac{\partial x_i}{\partial q_j} \quad \mathbf{J} = \mathbf{B}$
Static forces relation	$\boldsymbol{\tau} = \mathbf{J}^{t^{-1}} \mathbf{f}$	$\boldsymbol{\tau} = \mathbf{J}^t \mathbf{f}$

In chapter 1 we gave the definition of a fully-parallel manipulator. This definition results in parallel robots with diagonal and non-singular instantaneous inverse kinematics matrices. Therefore, we refer to every manipulator that has a non-diagonal instantaneous inverse kinematics matrix as a non-fully-parallel manipulator.

7.3 Jacobian formulation of a class of parallel robots

All the manipulators in Fig. 5.14 share the same tripod mechanism shown in Fig. 7.1. Accordingly, we first develop the Jacobian matrix of this tripod mechanism and we use this Jacobian matrix to develop the Jacobian matrix of a complete manipulator that belongs to the aforementioned class of manipulators. We then concentrate in particular on the USR and the RSPR robots and we derive the Jacobian matrices for these robots. We will use force decomposition method to formulate the Jacobian of the tripod mechanism and the RSPR robot. We will also formulate the Jacobian matrix for the USR robot and demonstrate the velocity-based method. The formulation of the Jacobian matrices for the USR, RSPR, and the Double Circular Triangular (Fig. 2.7) robots was presented in [Simaan, Glozman, and Shoham, 1998] based on the force decomposition method.



7.3.1 Jacobian of the tripod mechanism

The tripod in Fig. 7.1 includes a moving platform and three links, A_i . The links, A_i , are connected to the moving platform by revolute joints and to the previous links in the kinematic chains, B_i , by spherical joints. The spherical joint simplifies the force decomposition since it

transmits forces only [Cleary and Uebel, 1994]; therefore, we will use this method to formulate the Jacobian.

We will use the following symbols in agreement with and in addition to the symbols presented in chapter 6:

i : an index referring to a specific kinematic chain. $i=1,2,3$.

\mathbf{o}_p : the center point of the moving platform.

$\hat{\mathbf{r}}_i$: a unit vector along the axis of the upper revolute joint in the i 'th kinematic chain.

${}^w\mathbf{R}_p$: rotation matrix transforming vectors from the central platform-attached coordinate system to world coordinate system.

$\hat{\mathbf{s}}_{1i}$: a unit vector along the i 'th tripod link, A_i .

\mathbf{s}_{1i} : a vector from the spherical joint center to the upper extremity of the i 'th kinematic chain.

$\hat{\mathbf{s}}_{2i}$: a unit vector through the center of the spherical joint of the i 'th kinematic chain and parallel to the axis of the upper revolute joint $\hat{\mathbf{r}}_i$.

f_{1i} : the magnitude of the force transmitted along link A_i .

f_{2i} : the magnitude of force acting on the tripod link, A_i , along $\hat{\mathbf{s}}_{2i}$.

\mathbf{f}_1 : three-dimensional vector of the force intensities f_{1i} .

\mathbf{f}_2 : three-dimensional vector of the force intensities f_{2i} .

\mathbf{s}_e : the external wrench applied by the moving platform on its environment. The external wrench is a six-dimensional vector specifying in its upper three elements the resultant external force \mathbf{f}_e , and in its last three elements the resultant moment \mathbf{t}_e , i.e., $\mathbf{s}_e = [\mathbf{f}_e, \mathbf{t}_e]$.

Link A_i is connected to the moving platform and to link B_i by a revolute joint and a spherical joint, respectively. Consequently, in static analysis it is capable of exerting on the platform a force in a direction spanned by the flat pencil of $\hat{\mathbf{s}}_{1i}$ and $\hat{\mathbf{r}}_i$, and a moment in the direction of $\hat{\mathbf{r}}_i \times \hat{\mathbf{s}}_{1i}$ as illustrated in Fig. 7.2. Link B_i can exert on link A_i through the center of the spherical joint, a force in a direction defined by the flat pencil of $\hat{\mathbf{s}}_{1i}$ and $\hat{\mathbf{s}}_{2i}$, Fig. 7.2. Therefore, we decompose the force transmitted from link B_i to A_i into two components. The first component is of magnitude f_{1i} and in the direction of $\hat{\mathbf{s}}_{1i}$ and the second component is of magnitude f_{2i} and in the direction of $\hat{\mathbf{s}}_{2i}$.

Equations (7.11) and (7.12) result from static equilibrium of forces and moments about the center point of the moving platform, respectively.

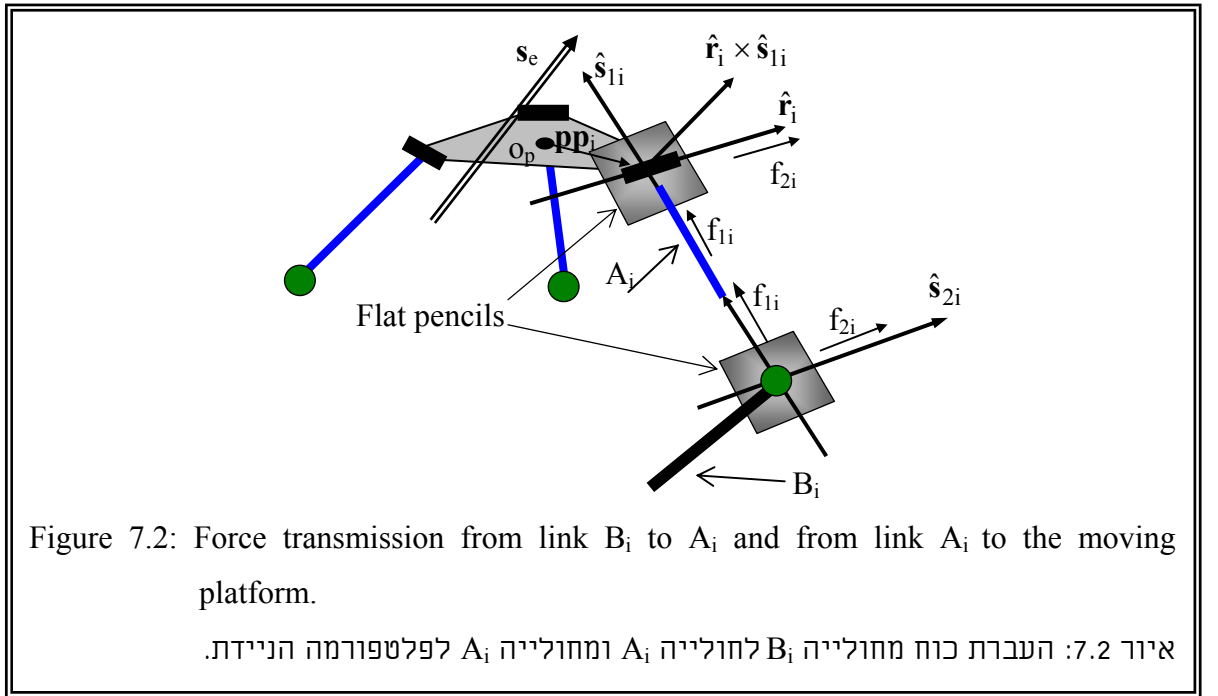
$$\sum_{i=1}^3 f_{1i} \hat{s}_{1i} + \sum_{i=1}^3 f_{2i} \hat{s}_{2i} - \mathbf{f}_e = \mathbf{0} \quad (7.11)$$

$$\sum_{i=1}^3 {}^w \mathbf{R}_{p\mathbf{pp}_i} \times \mathbf{f}_{1i} \hat{s}_{1i} + \sum_{i=1}^3 {}^w \mathbf{R}_{p\mathbf{pp}_i} \times \mathbf{f}_{2i} \hat{s}_{2i} + \sum_{i=1}^3 -\mathbf{s}_{1i} \times \mathbf{f}_{2i} \hat{s}_{2i} - \mathbf{t}_e = \mathbf{0} \quad (7.12)$$

Where the expression $\sum_{i=1}^3 -\hat{s}_{1i} \times \mathbf{f}_{2i} \hat{s}_{2i}$ represents the moments of the forces $\mathbf{f}_{2i} \hat{s}_{2i}$ along the axes $\hat{\mathbf{r}}_i \times \hat{s}_{1i}$, Fig. 7.2.

Writing Equations (7.11) and (7.12) in a matrix form yields:

$$\begin{bmatrix} \hat{s}_{1i} & \hat{s}_{2i} \\ {}^w \mathbf{R}_{p\mathbf{pp}_i} \times \hat{s}_{1i} & ({}^w \mathbf{R}_{p\mathbf{pp}_i} - \mathbf{s}_{1i}) \times \hat{s}_{2i} \end{bmatrix} \begin{bmatrix} \mathbf{f}_1 \\ \mathbf{f}_2 \end{bmatrix} = \begin{bmatrix} \mathbf{f}_e \\ \mathbf{t}_e \end{bmatrix} \quad (7.13)$$



Equation (7.13), when compared to Eq. (7.10), yields the Jacobian matrix of the tripod mechanism, which will be referred to by the symbol $\tilde{\mathbf{J}}$.

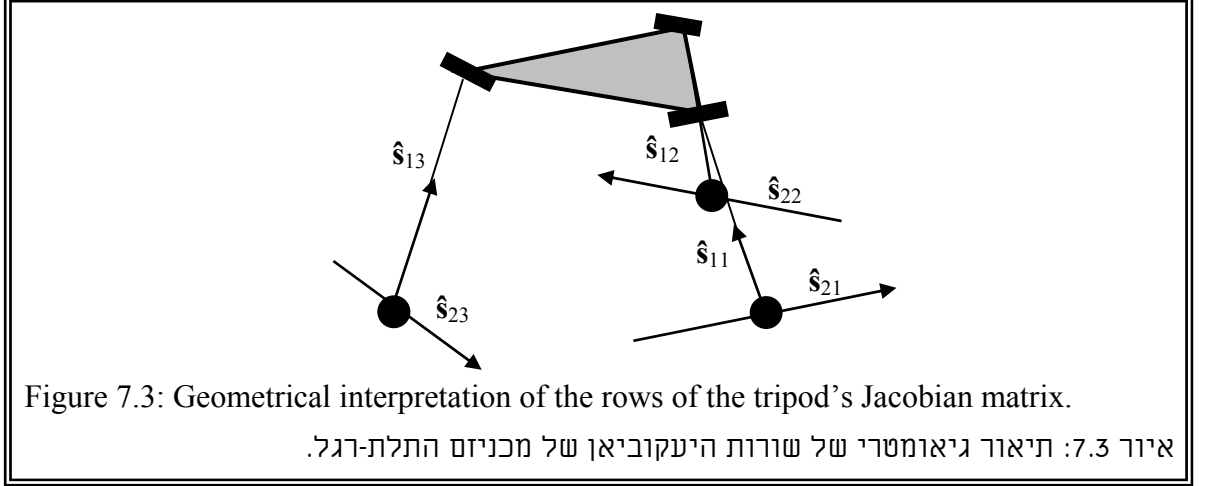
$$\tilde{\mathbf{J}} = \begin{bmatrix} \hat{s}_{1i} & \hat{s}_{2i} \\ {}^w \mathbf{R}_{p\mathbf{pp}_i} \times \hat{s}_{1i} & ({}^w \mathbf{R}_{p\mathbf{pp}_i} - \mathbf{s}_{1i}) \times \hat{s}_{2i} \end{bmatrix}^t \quad (7.14)$$

The forces at the spherical joints are given by:

$$\begin{bmatrix} \mathbf{f}_1 \\ \mathbf{f}_2 \end{bmatrix} = \tilde{\mathbf{J}}^t{}^{-1} \begin{bmatrix} \mathbf{f}_e \\ \mathbf{t}_e \end{bmatrix} \quad (7.15)$$

The rows of the Jacobian matrix of the tripod, $\tilde{\mathbf{J}}$, are the Plücker line coordinates of the lines along the links, \hat{s}_{1i} , and the lines \hat{s}_{2i} . This geometric interpretation of the Jacobian matrix, $\tilde{\mathbf{J}}$, is presented in Fig. 7.3.

Unlike the result obtained by [Tsai, 1998], The formulation of $\tilde{\mathbf{J}}$ presents a matrix which is constructed from lines that are easy to determine since it describes a typical subassembly of a class of manipulators. The geometrical interpretation of the rows of $\tilde{\mathbf{J}}$ is important for the singularity analysis, which is based on line geometry. The geometry of the lines of the Jacobian $\tilde{\mathbf{J}}$ is easily determined in a platform-attached coordinate system.



The group of manipulators in Fig. 5.14 shares the same tripod mechanism. The complete Jacobian matrix of a manipulator in this group is easily obtained by taking into account the equilibrium of forces at the spherical joints. It is possible to obtain a relation between the forces f_{1i} and f_{2i} and the active joints forces by treating the remainder of the kinematic chains as a serial chain and applying the reactions on link B_i . The relation between the actuators' force intensities and the forces at the spherical joints is given in Eq. (7.16) where \mathbf{J}_s denotes the Jacobian matrix of the serial chains.

$$\tau = \mathbf{J}_s^t \begin{bmatrix} \mathbf{f}_1 \\ \mathbf{f}_2 \end{bmatrix} \quad (7.16)$$

Substituting the expression for the forces at the spherical joints according to Eq. (7.15) in Eq. (7.16) results in:

$$\tau = \mathbf{J}_s^t \begin{bmatrix} \mathbf{f}_1 \\ \mathbf{f}_2 \end{bmatrix} = \mathbf{J}_s^t \tilde{\mathbf{J}}^t \mathbf{s}_e \quad (7.17)$$

Equation (7.17) and Eq. (7.10) have the same form, therefore, by using the definition of the Jacobian matrix we conclude that the Jacobian of a complete manipulator is given by Eq. (7.18).

$$\mathbf{J} = \mathbf{J}_s^{-1} \tilde{\mathbf{J}} \quad (7.18)$$

Therefore, the instantaneous direct kinematics matrix, \mathbf{A} , is the Jacobian matrix of the tripod mechanism and it is common for all the manipulators in Fig. 5.14. The instantaneous inverse kinematics matrix, \mathbf{B} , is the Jacobian matrix of the serial part of the kinematic chains and every manipulator of Fig. 5.14 has a different matrix.

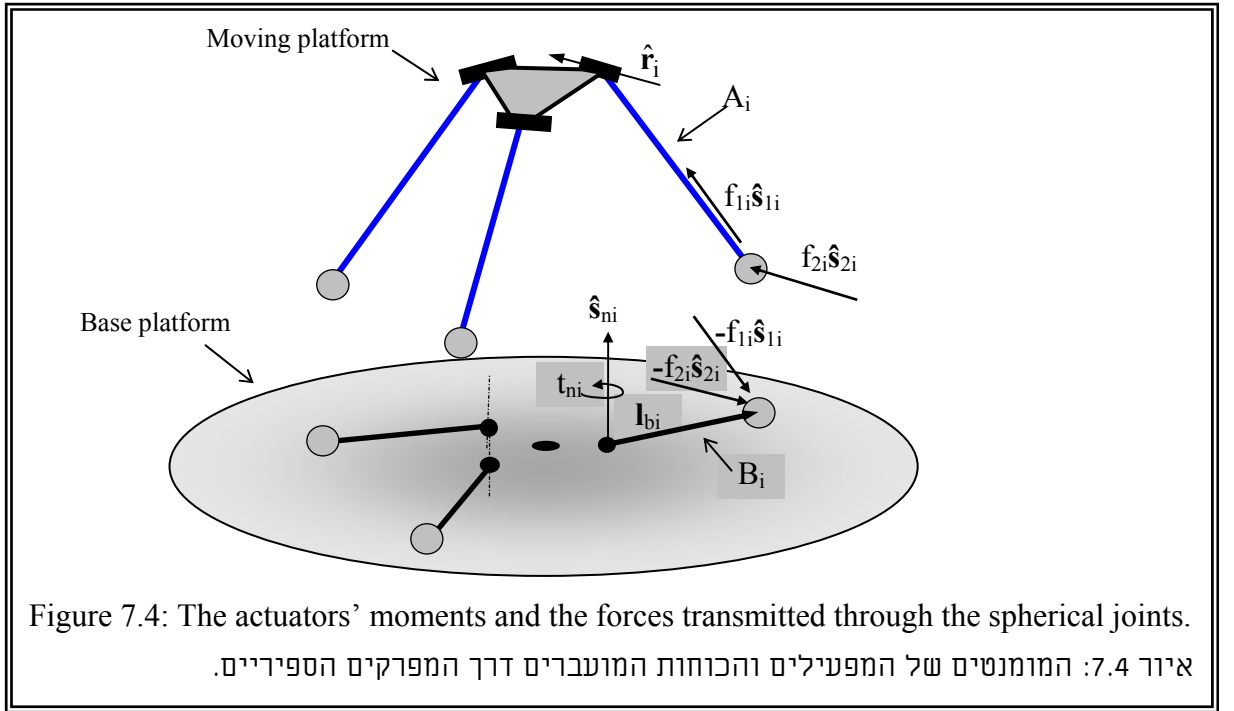
7.3.2 Jacobian matrix of the RSPR robot

The Jacobian matrix of the RSPR robot can be easily obtained by using the method described in the previous section. Figure 7.4 presents the lower part of the manipulator separated from the tripod mechanism.

We use these additional symbols For the RSPR robot:

\mathbf{l}_{bi} : the vector from the center of rotation of link B_i to the center of the i 'th spherical joint.

$\hat{\mathbf{s}}_{ni}$: a unit vector along the axis of rotation of link B_i .



The torque required from a rotational actuator balances the moment of the forces acting on link B_i through the spherical joint. Therefore, the expression for the required torque intensity, t_{ni} , after performing algebraic manipulations is:

$$t_{ni} = \left[(\hat{\mathbf{s}}_{1i} \times \hat{\mathbf{s}}_{ni})^t \mathbf{l}_{bi} \right] f_{1i} + \left[(\hat{\mathbf{s}}_{2i} \times \hat{\mathbf{s}}_{ni})^t \mathbf{l}_{bi} \right] f_{2i} = Cn_{1i} f_{1i} + Cn_{2i} f_{2i} \quad (7.19)$$

Where Cn_{1i} and Cn_{2i} are the coefficients of f_{1i} and f_{2i} in Eq. (7.19), respectively.

We define the active joints force/torque intensities vector, $\boldsymbol{\tau}$, as the linear actuator forces and the rotating link's torques; therefore, by substituting Eq. (7.19) and Eq. (7.15) we obtain the Jacobian matrix of the whole manipulator.

$$\boldsymbol{\tau} = \begin{bmatrix} \mathbf{f}_1 \\ \mathbf{t}_n \end{bmatrix} = \begin{bmatrix} \mathbf{I} & \mathbf{0} \\ \mathbf{Cn}_1 & \mathbf{Cn}_2 \end{bmatrix} \begin{bmatrix} \mathbf{f}_1 \\ \mathbf{f}_2 \end{bmatrix} = \begin{bmatrix} \mathbf{I} & \mathbf{0} \\ \mathbf{Cn}_1 & \mathbf{Cn}_2 \end{bmatrix} \tilde{\mathbf{J}}^t \mathbf{s}_e \quad (7.20)$$

Where \mathbf{t}_n is a three-dimensional vector of rotating link's torque intensities, \mathbf{Cn}_1 and \mathbf{Cn}_2 are 3 by 3 diagonal matrices having Cn_{1i} and Cn_{2i} on their main diagonals, respectively. According to Eq. (7.20) and Eq. (7.17) the instantaneous inverse kinematics matrix, \mathbf{J}_s is:

$$\mathbf{J}_s = \begin{bmatrix} \mathbf{I} & \mathbf{Cn}_1 \\ \mathbf{0} & \mathbf{Cn}_2 \end{bmatrix} \quad (7.21)$$

The Jacobian matrix of the whole manipulator is given by Eq. (7.22).

$$\mathbf{J} = \mathbf{J}_s^{-1} \tilde{\mathbf{J}} = \begin{bmatrix} \mathbf{I} & \mathbf{Cn}_1 \\ \mathbf{0} & \mathbf{Cn}_2 \end{bmatrix}^{-1} \begin{bmatrix} \hat{\mathbf{s}}_{1i} & \hat{\mathbf{s}}_{2i} \\ {}^w \mathbf{R}_p \mathbf{pp}_i \times \hat{\mathbf{s}}_{1i} & ({}^w \mathbf{R}_p \mathbf{pp}_i - \mathbf{s}_{1i}) \times \hat{\mathbf{s}}_{2i} \end{bmatrix}^t \quad (7.22)$$

We note that the Jacobian matrix is defined in all the configurations in which the inverse kinematics matrix \mathbf{J}_s is non-singular. We will deal with the physical interpretation of this phenomenon in chapter 10, where we present the singularity analysis.

7.3.3 Jacobian matrix of the USR robot

It is possible to use the same method that was used for the RSPR robot to formulate the Jacobian matrix of the USR robot. However, to demonstrate the loop closure method we will formulate the Jacobian matrix of the USR robot based on this method.

We will use the following additional symbols for the USR robot.

θ_{ni} : the yaw angle of the i 'th link B_i .

θ_{ri} : the pitch angle of the i 'th link B_i .

$\boldsymbol{\theta}_n$: three-dimensional vector of the yaw angles θ_{ni} .

$\boldsymbol{\theta}_r$: three-dimensional vector of the pitch angles θ_{ri} .

${}^w \boldsymbol{\omega}^{B_i}$: the angular velocity of the i 'th link B_i relative to world coordinate system.

${}^w \boldsymbol{\omega}^p$: the angular velocity of the moving platform relative to world coordinate system.

$\hat{\mathbf{s}}_{ni}$: a unit vector along the yaw axis of the universal joint.

$\hat{\mathbf{s}}_{ri}$: a unit vector along the pitch axis of the universal joint.

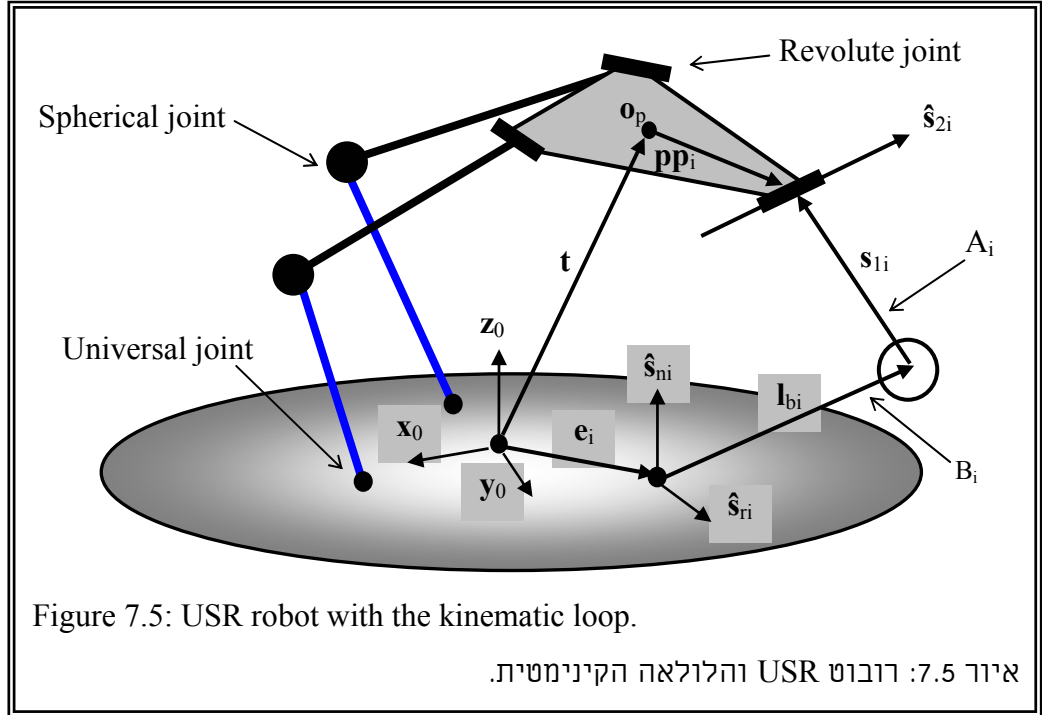
Figure 7.5 depicts the kinematic loops of the USR robot. There are three independent loops that lead to the closure equation in Eq. (7.23). In addition, the perpendicularity of A_i relative to the revolute joint axes is expressed in Eq. (7.24).

$$\mathbf{s}_{1i} = \mathbf{t}^w \mathbf{R}_p \mathbf{p} \mathbf{p}_i - \mathbf{l}_{bi} - \mathbf{e}_i \quad (7.23)$$

$$\mathbf{s}_{1i}^t \hat{\mathbf{s}}_{2i} = 0 \quad (7.24)$$

The time derivative of Eq. (7.23) and (7.24) is given in the following equations.

$$\dot{\mathbf{s}}_{1i} = \dot{\mathbf{t}}^w \boldsymbol{\omega}^p \times^w \mathbf{R}_p \mathbf{p} \mathbf{p}_i - {}^w \boldsymbol{\omega}^{B_i} \times \mathbf{l}_{bi} \quad (7.25)$$



$$\dot{\mathbf{s}}_{1i}^t \hat{\mathbf{s}}_{2i} + \mathbf{s}_{1i}^t \dot{\hat{\mathbf{s}}}_{2i} = 0 \quad (7.26)$$

The lower link is actuated by controlling its pitch and yaw angles, therefore, the expression for ${}^w \boldsymbol{\omega}^{B_i}$ is:

$${}^w \boldsymbol{\omega}^{B_i} = \dot{\theta}_{ni} \hat{\mathbf{s}}_{ni} + \dot{\theta}_{ri} \hat{\mathbf{s}}_{ri} \quad (7.27)$$

In addition, the upper link A_i is rigid, therefore, the following condition is fulfilled.

$$\dot{\mathbf{s}}_{1i}^t \hat{\mathbf{s}}_{1i} = 0 \quad (7.28)$$

By substituting equations (7.25) and (7.27) in Eq. (7.26) and performing mathematical manipulations, we obtain the following result.

$$\hat{\mathbf{s}}_{2i}^t \dot{\mathbf{t}} + \left[\left({}^w \mathbf{R}_p \mathbf{p} \mathbf{p}_i - \mathbf{s}_{1i} \right) \times \hat{\mathbf{s}}_{2i} \right]^t {}^w \boldsymbol{\omega}^p = (\hat{\mathbf{s}}_{2i} \times \hat{\mathbf{s}}_{ni})^t \mathbf{l}_{bi} \dot{\theta}_{ni} + (\hat{\mathbf{s}}_{2i} \times \hat{\mathbf{s}}_{ri})^t \mathbf{l}_{bi} \dot{\theta}_{ri} \quad (7.29)$$

We also substitute equations (7.25) and (7.27) in equation (7.28) and we obtain the following result.

$$\hat{\mathbf{s}}_{1i}^t \dot{\mathbf{t}} + \left({}^w \mathbf{R}_p \mathbf{p} \mathbf{p}_i \times \hat{\mathbf{s}}_{1i} \right)^t {}^w \boldsymbol{\omega}^p = (\hat{\mathbf{s}}_{1i} \times \hat{\mathbf{s}}_{ni})^t \mathbf{I}_{bi} \dot{\boldsymbol{\theta}}_{ni} + (\hat{\mathbf{s}}_{1i} \times \hat{\mathbf{s}}_{ri})^t \mathbf{I}_{bi} \dot{\boldsymbol{\theta}}_{ri} \quad (7.30)$$

Writing equations (7.29) and (7.30) in a matrix results in a matrix equation in the form of Eq. (7.1).

$$\begin{bmatrix} \hat{\mathbf{s}}_{1i} & \hat{\mathbf{s}}_{2i} \\ {}^w \mathbf{R}_p \mathbf{p} \mathbf{p}_i \times \hat{\mathbf{s}}_{1i} & ({}^w \mathbf{R}_p \mathbf{p} \mathbf{p}_i - \mathbf{s}_{1i}) \times \hat{\mathbf{s}}_{2i} \end{bmatrix}^t \begin{bmatrix} \dot{\mathbf{t}} \\ {}^w \boldsymbol{\omega}^p \end{bmatrix} = \begin{bmatrix} \mathbf{Cn}_1 & \mathbf{Cr}_1 \\ \mathbf{Cn}_2 & \mathbf{Cr}_2 \end{bmatrix} \begin{bmatrix} \dot{\boldsymbol{\theta}}_n \\ \dot{\boldsymbol{\theta}}_r \end{bmatrix} \quad (7.31)$$

Where \mathbf{Cn}_1 , \mathbf{Cn}_2 , \mathbf{Cr}_1 , and \mathbf{Cr}_2 are 3 by 3 diagonal matrices with the following elements on the main diagonal.

$$\mathbf{Cn}_{1i} = (\hat{\mathbf{s}}_{1i} \times \hat{\mathbf{s}}_{ni})^t \mathbf{I}_{bi} \quad \mathbf{Cn}_{2i} = (\hat{\mathbf{s}}_{2i} \times \hat{\mathbf{s}}_{ni})^t \mathbf{I}_{bi} \quad (7.32)$$

$$\mathbf{Cr}_{1i} = (\hat{\mathbf{s}}_{1i} \times \hat{\mathbf{s}}_{ri})^t \mathbf{I}_{bi} \quad \mathbf{Cr}_{2i} = (\hat{\mathbf{s}}_{2i} \times \hat{\mathbf{s}}_{ri})^t \mathbf{I}_{bi} \quad (7.33)$$

The instantaneous direct and inverse kinematics matrices are directly obtained by equating Eq. (7.31) with Eq. (7.1) and the Jacobian matrix of the USR robot is given by Eq. (7.8).

$$\mathbf{J} = \begin{bmatrix} \mathbf{Cn}_1 & \mathbf{Cr}_1 \\ \mathbf{Cn}_2 & \mathbf{Cr}_2 \end{bmatrix}^{-1} \begin{bmatrix} \hat{\mathbf{s}}_{1i} & \hat{\mathbf{s}}_{2i} \\ {}^w \mathbf{R}_p \mathbf{p} \mathbf{p}_i \times \hat{\mathbf{s}}_{1i} & ({}^w \mathbf{R}_p \mathbf{p} \mathbf{p}_i - \mathbf{s}_{1i}) \times \hat{\mathbf{s}}_{2i} \end{bmatrix}^t \quad (7.34)$$

7.4 Conclusions

We showed that the Jacobian formulation for all the robots of Fig. 5.14 has the same instantaneous direct kinematics matrix \mathbf{A} , which is determined solely by the upper tripod mechanism. However, these robots differ in the instantaneous inverse kinematics matrix, \mathbf{B} , which is determined by the serial part of the kinematic chains.

Additionally, the rows of the instantaneous direct kinematics matrix were shown to be the Plücker line coordinates of the lines that govern the kinematics of the tripod mechanism. The formulation of the Jacobian matrix, when compared to other methods such as the formulation which was suggested by [Tsai, 1998] using reciprocal screws, yields a direct geometrical interpretation regarding the lines that govern the kinematics of the system.

The Jacobian formulation in this chapter serves as a mathematical background for the singularity analysis of the family of manipulators presented in Fig. 5.14. This method is simpler for mechanisms with spherical joints because of the easy decomposition of the forces transmitted through the spherical joint.

Chapter 8

Dimensional Synthesis of the USR and the RSPR Robots and Performance-Based Comparison

8.1 Introduction

This chapter presents the dimensional synthesis of the USR and RSPR robots to fulfill the task assigned for in chapter 4. The details of this work were presented in [Simaan, Glozman, and Shoham, 1998] where, in addition to the USR and the RSPR robots, we included in the comparison the Double Circular Triangular robot and the RRPS parallel robot.

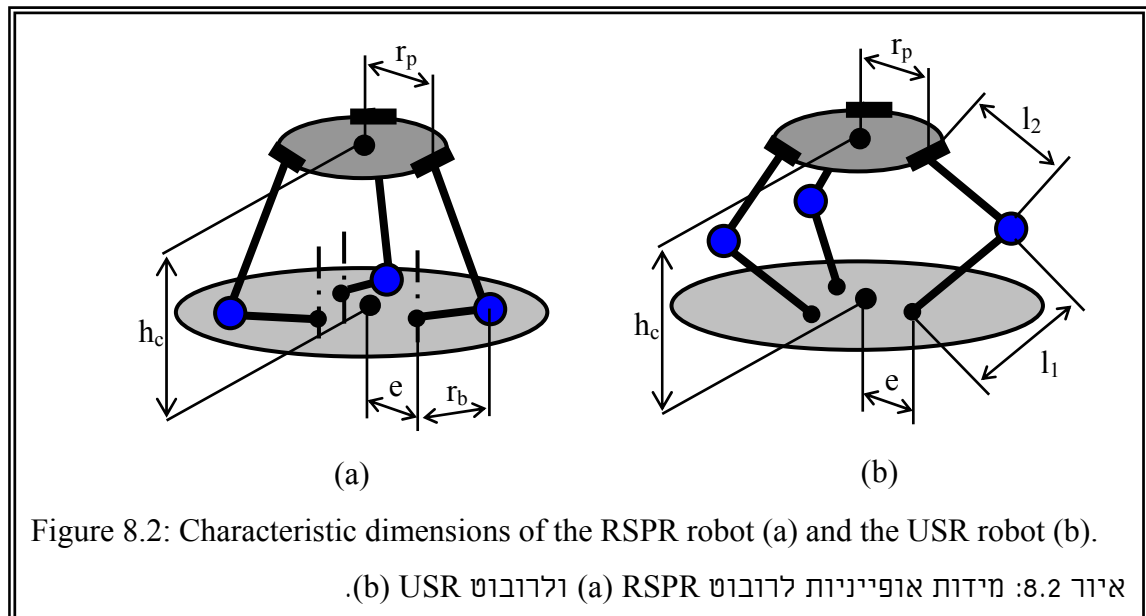
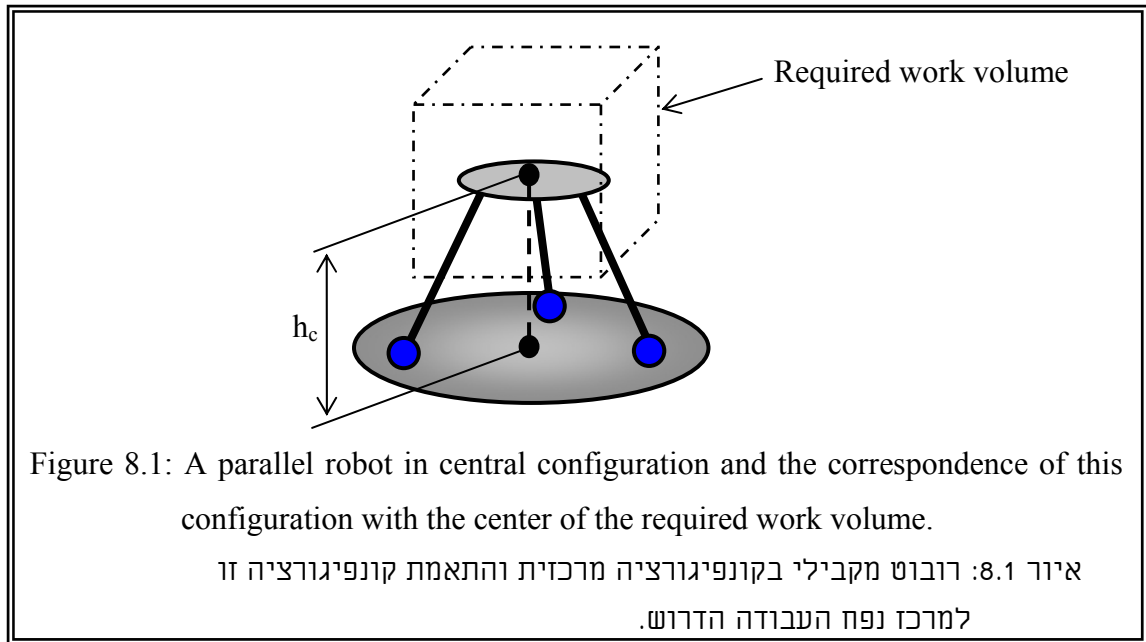
The aim of the synthesis process is to find the minimal dimensions of the robots that provide the required work volume and end effector forces (refer to chapter 4 for details). The synthesis process is based on computer simulations that use the inverse kinematics and the Jacobian formulations of the robots in order to evaluate the required actuator forces/ranges and spherical joint limits. The synthesis of the robots also included ruling out robots that exhibit singular configurations in the required work volume.

8.2 Dimensional synthesis

The dimensional synthesis presented in this chapter is based on computer simulations. In the simulations, we scan a vast range of robots with different characteristic dimensions and we select the robot with the minimal dimensions that satisfies the desired work volume with minimal actuator forces.

In addition to the symbols presented in chapters 6 and 7, we introduce the terms central configuration and initial height of a robot. In a central configuration, the moving platform is parallel to the base platform and its center is located right above the center of the base platform and displaced from the base platform by an amount equal to the initial height parameter. We will use the symbol h_c to refer to the initial height parameter. The central configuration of a robot corresponds with the center point of the required work volume cube, Fig. 8.1.

The characteristic dimensions of the RSPR robot are the radius of the moving platform, r_p ; the radius of the lower rotating links, r_b ; the eccentricity amount, e ; and the initial height h_c , Fig 8.2(a). The characteristic dimensions of the USR robot are the radius of the moving platform, r_p ; the length of the lower and upper rotating links, l_1 and l_2 respectively; the eccentricity amount, e ; and the initial height, h_c , Fig. 8.2(b).



The computer simulations aim to determine all the admissible robots that fulfill the desired task (presented in chapter 4) and additional design requirements. The design requirements included feasible actuator forces and spherical joint tilting ranges.

The characteristic dimensions of the USR and the RSPR robots were altered during the simulations and a vast array of robots was examined. Table 8.1 presents the scanned range of the characteristic dimensions for the USR and the RSPR robots in the final simulations. Prior to these final simulations, we carried out initial simulations, in which we scanned a larger array of characteristic dimensions and we induced an evaluation of the minimal required actuator forces/ranges. In addition, the final simulations took into account the requirement for reasonable actuator forces. This was accomplished by determining upper bounds for the

actuator forces based on evaluation of what is achievable from reasonable rotary/linear actuators. This also insures that the robots do not acquire singularities inside the desired work volume. For the RSPR robot, we set the upper bounds for the linear actuator forces and the rotating links' moments at 30[N] and 1.0 [Nm], respectively. For the USR robot, we set the bound for the universal joint moments at 2.0 [Nm].

The solutions for the RSPR robot were limited by the minimal length and stroke of the linear actuators. This requirement of actuator length stemmed from the initial simulation set. The minimal length of the linear actuators was evaluated from design requirements of the linear actuators and this evaluation of the minimal length and stroke of the linear actuators was stipulated as a design requirement in the final simulation. Table 8.2 presents all the twenty-two RSPR robots that fulfill the desired work volume, the desired actuator dimensions, and upper the bounds of actuator forces/moments. Figure 8.3 explains all the symbols presented in Table 8.2.

Table 8.1: The scanned range of characteristic dimensions of the RSPR and USR robots. טבלה 8.1: תחום המידות האופייניות לרובוטים RSPR ו USR אשר נסקרו בסימולציות.			
Property	Symbol	RSPR	USR
Platform radius	r_p	30: 10: 100	20: 10: 60
Rotating link length	r_b	30: 10: 100	-----
Initial height	h_c	40: 10: 200	50: 10: 120
Eccentricity	e	20: 10: 80	20: 10: 60
Lower link length	l_1	-----	20: 10: 80
Upper link length	l_2	-----	20: 10: 80
Number of scanned robots		7616	9800
Number of admissible robots		22	95
Note: All dimensions are in millimeters.			

Table 8.3 presents forty out of ninety-five USR robots that fulfill the design requirements. In addition, the table presents additional motion limits. These motion limits inhibit inverse kinematic singularity by limiting the angle between the upper and the lower links.

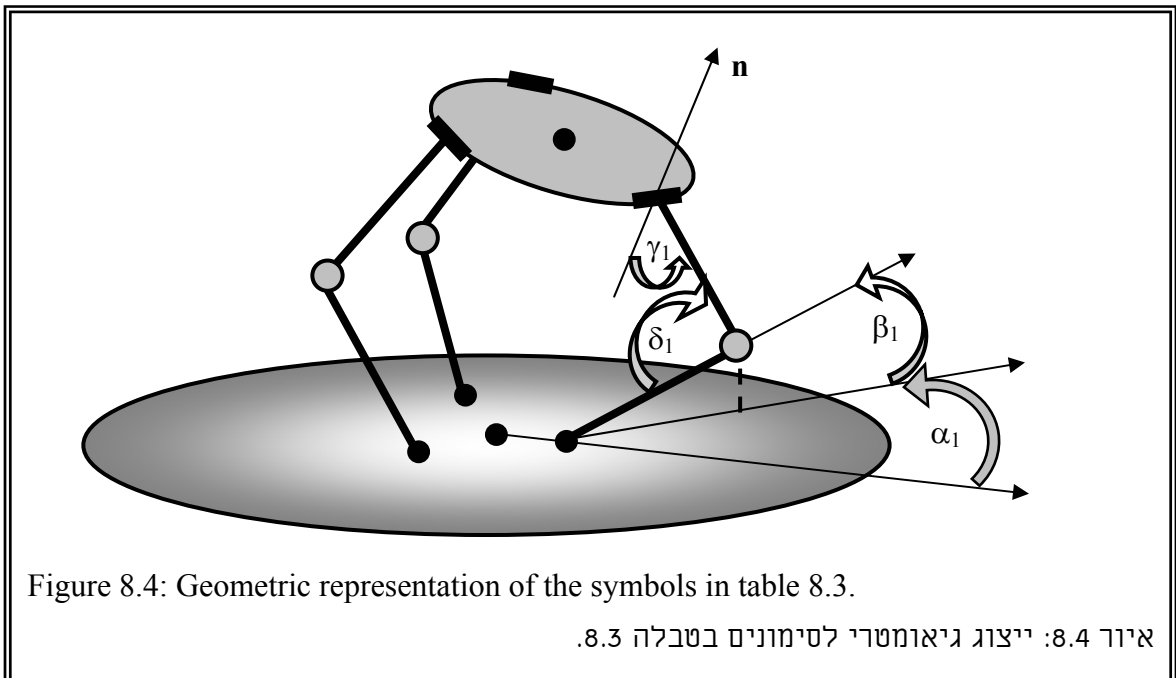
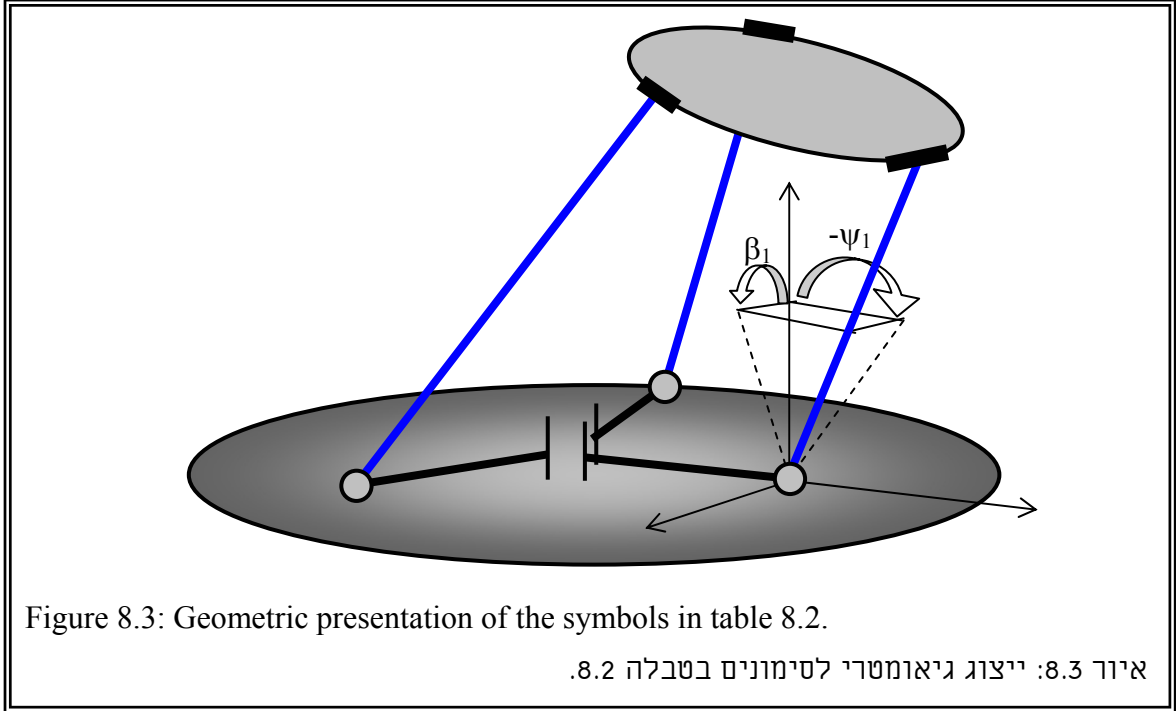


Table 8.2: Simulation results for the RSPR robot.

טבלה 8.2: תוצאות סימולציה עבור רובוט RSPR.

Actuator limits: $L_{\min}=138.00$ [mm], $L_{\max}=208.00$ [mm]

r_p	r_b	h_c	e	L_{\min}	ΔL	θ_{\min}	θ_{\max}	$\Delta\theta$	ψ_{\min}	ψ_{\max}	$\Delta\psi$	β_{\min}	β_{\max}	$\Delta\beta$	T_{\min}	T_{\max}	f_{\min}	f_{\max}
3	8	13	6	13.83	6.65	-69	40	110	20	43	23	-16	15	31	-0.30	0.52	-8	9
3	8	14	5	14.12	6.46	-80	43	123	15	39	24	-12	10	22	-0.25	0.51	-9	10
3	9	10	8	13.96	6.79	-45	29	73	37	57	20	-24	27	51	-0.56	0.73	-9	9
3	9	11	7	13.86	6.70	-48	31	79	32	52	20	-20	22	42	-0.47	0.66	-8	8
3	9	12	6	13.82	6.65	-52	33	85	27	48	21	-16	17	33	-0.40	0.62	-8	8
3	9	13	5	13.94	6.54	-56	35	91	23	43	21	-13	12	25	-0.33	0.59	-8	9
3	9	14	4	14.23	6.35	-61	37	98	18	39	20	-9	7	17	-0.27	0.58	-8	10
3	9	15	2	14.34	5.90	-66	40	106	11	32	21	-6	3	10	-0.16	0.61	-10	12
3	9	15	3	14.68	6.11	-66	40	106	14	34	20	-6	4	10	-0.21	0.58	-9	11
3	10	10	7	14.02	6.73	-39	26	65	37	57	20	-21	23	44	-0.62	0.81	-9	9
3	10	11	6	13.94	6.63	-42	27	69	32	52	20	-17	18	35	-0.51	0.74	-8	8
3	10	12	5	13.90	6.57	-45	29	74	27	48	20	-13	14	27	-0.43	0.69	-8	8
3	10	13	4	14.03	6.46	-48	31	79	23	43	21	-10	9	19	-0.36	0.66	-8	9
3	10	14	2	13.86	6.11	-52	33	85	15	37	21	-7	4	11	-0.25	0.67	-9	10
3	10	14	3	14.31	6.28	-51	33	84	18	39	20	-7	5	11	-0.29	0.65	-8	9
3	10	15	2	14.75	6.04	-55	35	90	14	35	20	-6	3	9	-0.22	0.64	-9	11
4	9	15	2	13.84	6.19	-66	40	106	8	30	22	-7	4	11	-0.11	0.62	-9	12
4	9	15	3	14.12	6.43	-66	40	106	11	32	21	-6	3	10	-0.16	0.59	-9	11
4	10	13	5	13.85	6.92	-48	31	79	22	44	21	-10	9	20	-0.35	0.64	-8	8
4	10	15	2	14.18	6.36	-55	35	90	11	32	21	-7	4	11	-0.17	0.66	-9	11
5	9	16	2	14.37	6.39	-73	42	115	5	26	21	-7	4	12	-0.11	0.62	-9	14
6	9	16	2	14.01	6.67	-73	42	115	2	23	22	-9	5	14	-0.20	0.64	-9	14

L = linear actuator length. f = Linear actuator force. T = Rotary actuator torque.

Units: r_p , r_b , h_c , e , L_{\min} , ΔL = [cm]. θ_{\min} , θ_{\max} , $\Delta\theta$, ψ_{\min} , ψ_{\max} , $\Delta\psi$, β_{\min} , β_{\max} , $\Delta\beta$ = [Degrees]. T_{\min} , T_{\max} = [Nm]. f_{\min} , f_{\max} = [N].

Note: The row with the dark background indicates the chosen candidate robot.

Table 8.3: Simulation results for the USR robot- The first
20 robots out of 95 admissible robots.

טבלה 8.3: תוצאות סימולציה עבור רובוט USR – 20 הרובוטים
הראשונים מתוך רשימת 95 רובוטים קבילים.

Design requirements: $-90 < \alpha < 90$, $0 < \gamma < 90$, $0 < \delta < 180$, $ T_n < 2$ [Nm], $ T_r < 2$ [Nm].																							
$T_{r_{max}}$	$T_{r_{min}}$		$T_{n_{max}}$	$T_{n_{min}}$	e	r_p	h_c	l_1	l_2	α_{min}	α_{max}	$\Delta\alpha$	β_{min}	β_{max}	$\Delta\beta$	γ_{min}	γ_{max}	$\Delta\gamma$	δ_{min}	δ_{max}	$\Delta\delta$		
2	2	6	6	8	-73	50	123	-32	44	75	2	87	85	34	70	36	-0.41	0.75	-0.72	0.87			
2	2	7	6	7	-57	41	98	-7	58	65	4	89	85	49	89	40	-0.58	0.85	-1.01	1.02			
2	2	7	6	8	-59	43	102	-19	48	68	3	83	79	44	80	37	-0.41	0.74	-0.81	0.91			
2	2	8	6	7	-65	46	112	3	63	60	0	83	82	60	102	42	-0.50	0.79	-1.05	1.02			
2	2	8	6	8	-64	41	106	-8	54	62	1	78	77	53	91	38	-0.39	0.71	-0.89	0.94			
2	2	8	7	8	-48	35	83	-2	54	56	8	87	79	51	84	33	-0.63	0.90	-1.08	1.08			
2	2	9	7	6	-63	52	115	24	76	51	1	89	88	70	116	46	-0.76	1.00	-1.90	1.40			
2	2	9	7	7	-57	43	100	15	67	52	4	85	81	65	104	39	-0.65	0.91	-1.43	1.23			
2	2	9	7	8	-54	38	92	6	59	52	5	82	76	60	95	35	-0.54	0.84	-1.11	1.08			
2	2	10	7	8	-62	43	106	14	64	50	1	76	75	69	106	38	-0.46	0.77	-1.15	1.08			
2	2	10	8	7	-52	42	94	25	70	45	7	87	80	69	106	38	-0.79	1.04	-1.95	1.47			
2	2	10	8	8	-49	36	85	17	62	45	9	84	75	64	97	33	-0.69	0.95	-1.47	1.29			
2	2	11	8	7	-63	49	112	30	75	45	1	80	79	78	120	42	-0.60	0.91	-1.66	1.37			
2	2	11	8	8	-56	41	98	23	67	44	4	78	74	73	109	36	-0.56	0.86	-1.38	1.25			
2	3	6	7	8	-46	39	85	-28	41	69	4	89	85	32	71	39	-0.49	0.82	-0.71	0.88			
2	3	7	7	8	-46	35	81	-17	45	62	3	85	81	41	80	40	-0.48	0.81	-0.79	0.91			
2	3	8	7	7	-48	37	85	2	57	56	1	87	86	53	99	46	-0.59	0.87	-1.05	1.02			
2	3	8	7	8	-49	34	83	-8	49	57	1	81	79	49	90	41	-0.46	0.78	-0.86	0.92			
2	3	9	8	8	-43	32	74	5	54	50	6	85	79	54	93	39	-0.63	0.91	-1.09	1.08			
2	3	10	8	8	-47	35	82	11	58	47	2	80	78	62	103	41	-0.53	0.84	-1.12	1.07			
Units: r_p , e , h_c , l_1 , l_2 =[cm]. α , β , γ , δ =[Degrees]. T_n , T_r = [Nm].																							

Units: r_p , e , h_c , l_1 , l_2 =[cm]. α , β , γ , δ =[Degrees]. T_n , T_r = [Nm].

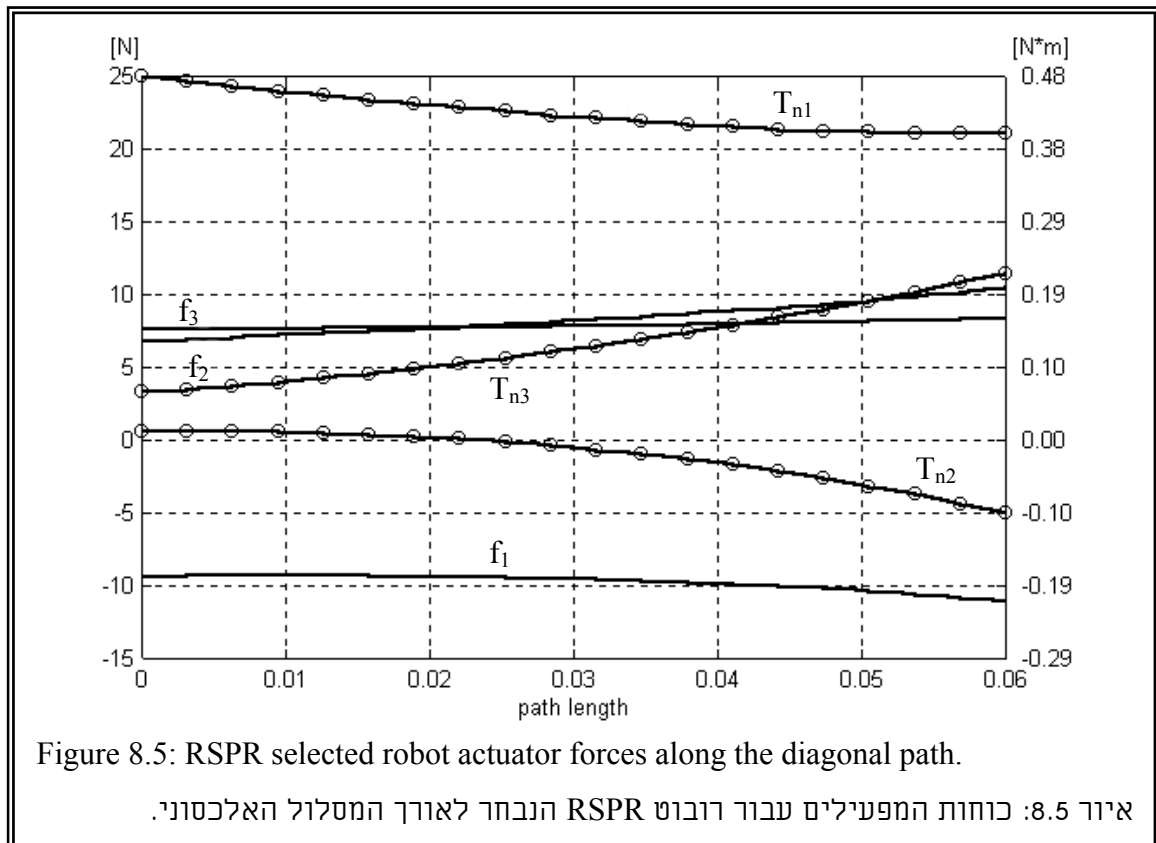
<div> <div>טבלה 8.3: תוצאות סימולציה עבור רובוט USR – 20 הרובוטים השניים מתוך רשימת 95 רובוטים קבילים.</div> <div>Table 8.3: Simulation results for the USR robot - the robots out of 95 admissible robots.</div> </div>																							
Design requirements: $-90 < \alpha < 90$, $0 < \gamma < 90$, $0 < \delta < 180$, $ T_n < 2$ [Nm], $ T_r < 2$ [Nm].																							
$T_{r_{max}}$	$T_{r_{min}}$	$T_{n_{max}}$	$T_{n_{min}}$	e	r_p	h_c	l_1	l_2	α_{min}	α_{max}	$\Delta\alpha$	β_{min}	β_{max}	$\Delta\beta$	γ_{min}	γ_{max}	$\Delta\gamma$	δ_{min}	δ_{max}	$\Delta\delta$			
2	4	7	8	8	-38	30	68	-17	42	58	4	87	83	37	81	44	-0.56	0.88	-0.77	0.92			
2	4	8	8	8	-40	29	69	-8	46	54	1	83	81	44	90	45	-0.52	0.85	-0.84	0.92			
3	2	8	6	7	-67	51	118	9	71	63	7	89	82	60	106	47	-0.63	0.87	-1.29	1.07			
3	2	8	6	8	-64	44	108	-3	62	65	8	85	77	53	95	42	-0.51	0.77	-0.93	0.92			
3	2	9	6	8	-77	51	128	6	68	61	4	80	76	63	108	45	-0.43	0.70	-0.95	0.92			
3	2	9	7	8	-55	42	97	12	65	54	11	88	76	60	98	39	-0.67	0.91	-1.38	1.16			
3	2	10	7	7	-73	58	132	27	80	52	4	83	79	75	123	48	-0.59	0.85	-1.53	1.24			
3	2	10	7	8	-65	48	112	18	71	52	7	81	74	69	110	41	-0.54	0.81	-1.25	1.12			
3	2	10	8	8	-50	40	90	22	68	46	14	89	75	64	101	36	-0.83	1.05	-1.97	1.41			
3	2	11	7	8	-84	58	142	25	77	52	1	76	74	78	124	46	-0.42	0.73	-1.19	1.08			
3	2	11	8	7	-67	56	124	35	81	46	6	84	78	78	124	46	-0.68	0.94	-1.95	1.44			
3	2	11	8	8	-59	46	105	27	73	45	9	83	73	73	112	39	-0.64	0.90	-1.62	1.31			
3	2	12	8	8	-73	55	128	33	78	46	3	77	73	82	125	43	-0.49	0.79	-1.45	1.23			
3	3	7	6	8	-59	44	103	-22	51	73	3	84	81	41	84	43	-0.38	0.70	-0.70	0.79			
3	3	8	6	8	-64	43	107	-11	56	67	1	79	79	51	95	44	-0.36	0.67	-0.77	0.79			
3	3	8	7	8	-48	36	84	-4	56	60	8	89	81	49	88	39	-0.58	0.85	-0.95	0.94			
3	3	9	7	7	-56	46	102	14	69	55	3	87	85	63	109	46	-0.60	0.85	-1.28	1.06			
3	3	9	7	8	-54	40	93	4	61	56	4	83	79	58	99	41	-0.50	0.78	-0.98	0.94			
3	3	10	8	7	-52	44	95	24	72	48	6	89	84	67	111	44	-0.74	0.96	-1.78	1.27			
3	3	10	8	8	-48	38	86	16	64	48	8	86	78	62	101	39	-0.64	0.89	-1.32	1.14			
Units: r_p , e , h_c , l_1 , l_2 =[cm]. α , β , γ , δ =[Degrees]. T_n , T_r = [Nm]. Note: The row with the dark background indicates the chosen candidate robot.																							

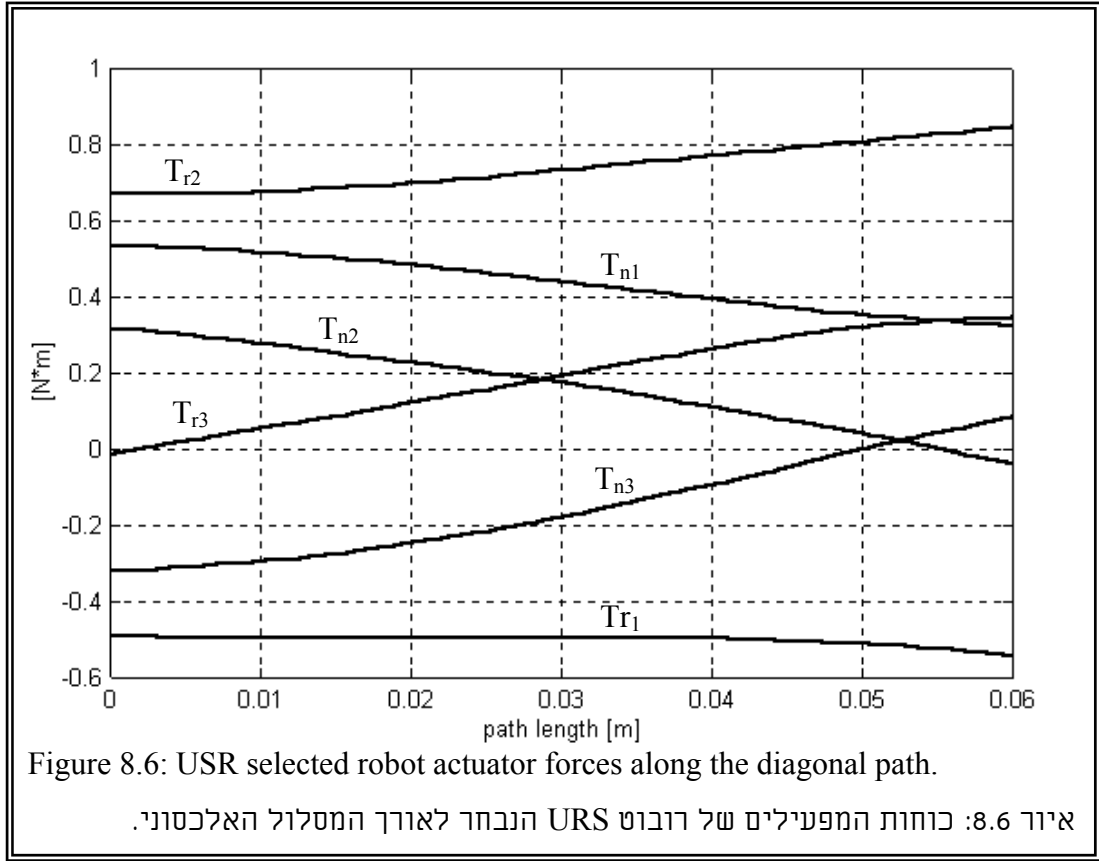
8.3 Selecting a prototype candidate

Based on the simulation results in tables 8.2 and 8.3 we chose one robot from the admissible RSPR robots and one robot from the admissible USR robots. These robots are identified in tables 8.2 and 8.3 by their dark background data rows. Theoretically, we should select the smallest robots in tables 8.1 and 8.2; however, we chose mechanically feasible robots. This requirement stems from the fact that we intend to locate the motors between the base and the moving platforms of the RSPR robot. Also for the USR robot we selected a robot with dimensions that allow locating three active Hooke's joints in the base platform.

Tables 8.2 and 8.3 show that the rotary actuators in the RSPR robot are required to provide smaller moments than the rotary actuators for the USR robot. The required spherical joint tilting range for the selected RSPR robot is smaller than the one for the selected USR robot.

In addition to the above simulations, we compared the selected USR and the RSPR robots by plotting the required actuator forces along a diagonal path from the lower corner of the workspace cube (point $[-20, -20, -10]$ mm) to the upper corner of the cube (point $[20, 20, 10]$ mm), while keeping the moving platform with an orientation of 20 about the $[1, 1, 1]$ axis. The results shown in Fig. 8.5 and Fig. 8.6 correspond to a $[7, 7, 7]$ [N], $[0.7, 0.7, 0.7]$ [Nm]] wrench applied by the moving platform on its environment.





The results in Fig. 8.5 and 8.6 show that the required actuator moments of the selected RSPR robot are smaller than the ones required from the actuators of the selected USR robot. In addition, the USR robot suffers from mechanically complicated design because of the usage of the three active Hooke's joints. We will show in chapter 10 that the use of these active Hooke's joints introduces undesirable singularities. Based on these results and on the design advantages of the RSPR robot we chose the RSPR robot as the best solution to our design problem because of its relatively small size, small required actuator forces and achievable spherical joint tilting ranges. Therefore, the prototype, which is presented in chapter 11, is based on the selected RSPR robot.

8.4 Work volume of the selected RSPR robot

This section analyses the workspace the RSPR robot. The algorithm for workspace evaluation starts from an initial position with a valid inverse kinematics solution. We use cylindrical coordinate system $[\rho, \phi, z]$ to evaluate the work volume. For every constant z section, we move the platform in radial directions for a varying angular coordinate, ϕ , and we register the maximal radial distances ρ_{\max} that correspond to a valid solution. All the workspace figures in this section give the workspace in a $[x', y', z']$ coordinate system

parallel to the base-platform-attached coordinate system $[x_0, y_0, z_0]$ with an origin fixed at the initial position. Therefore in these figures $z = 0$ denotes the workspace section in which the robot maintains a height equal to its height in the initial position, Fig. 8.7.

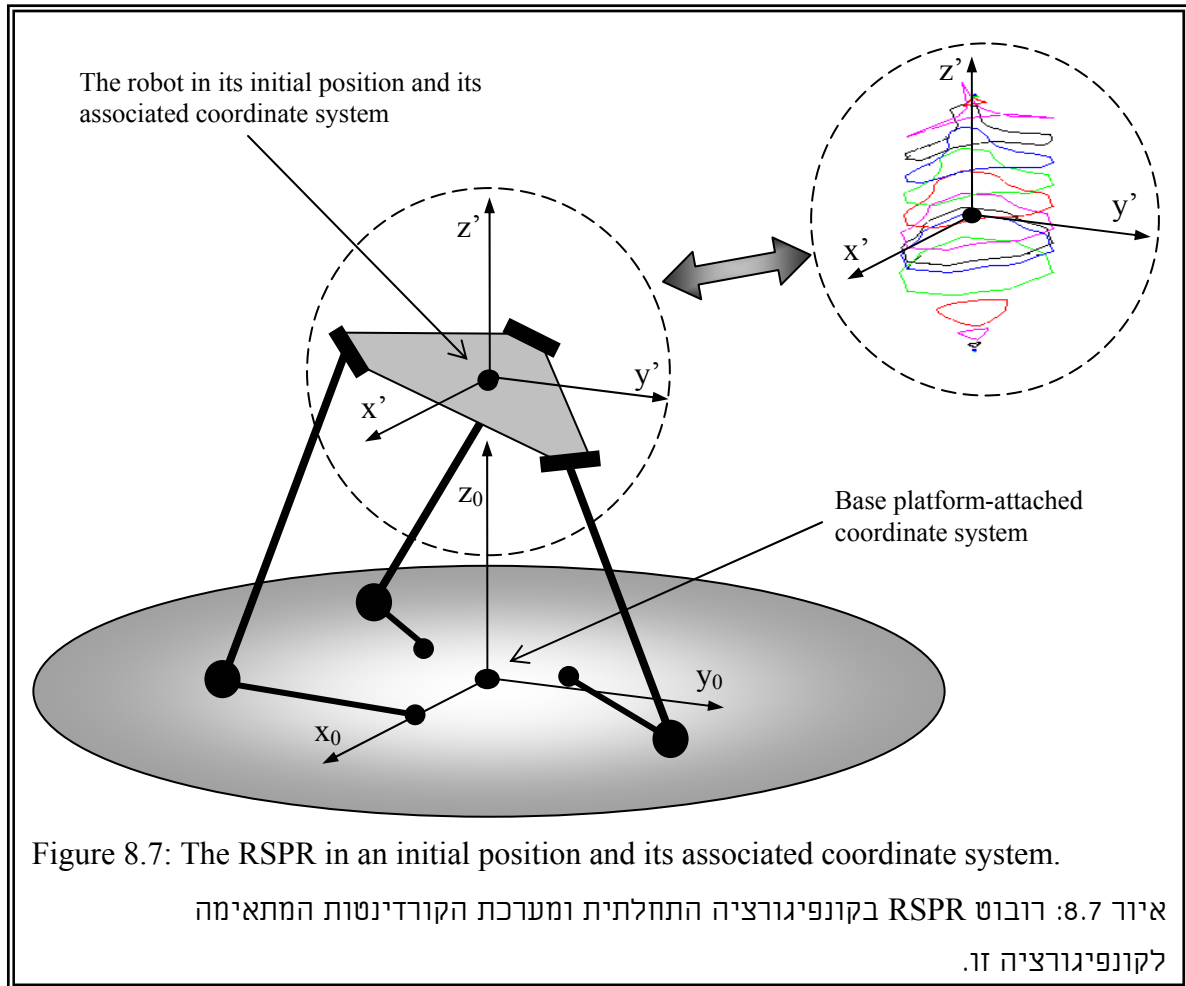
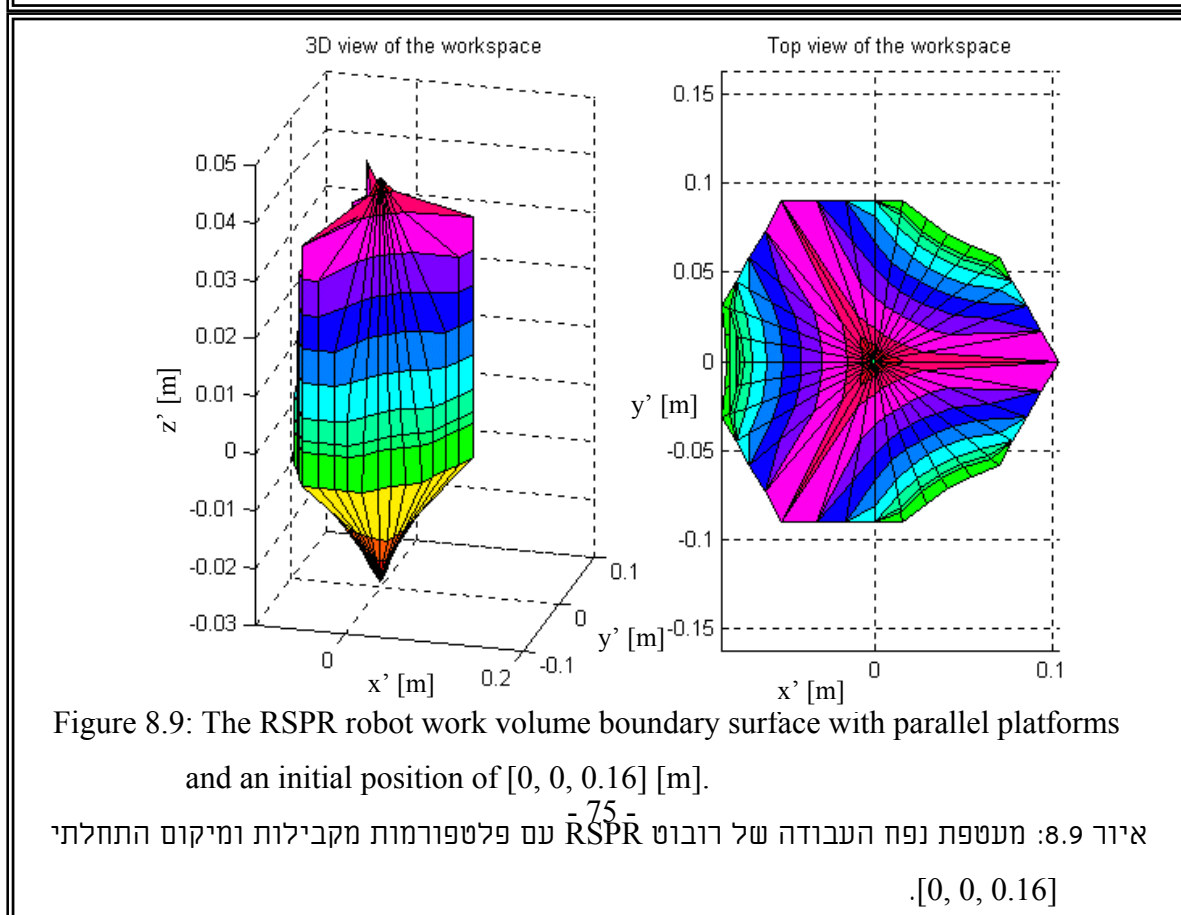
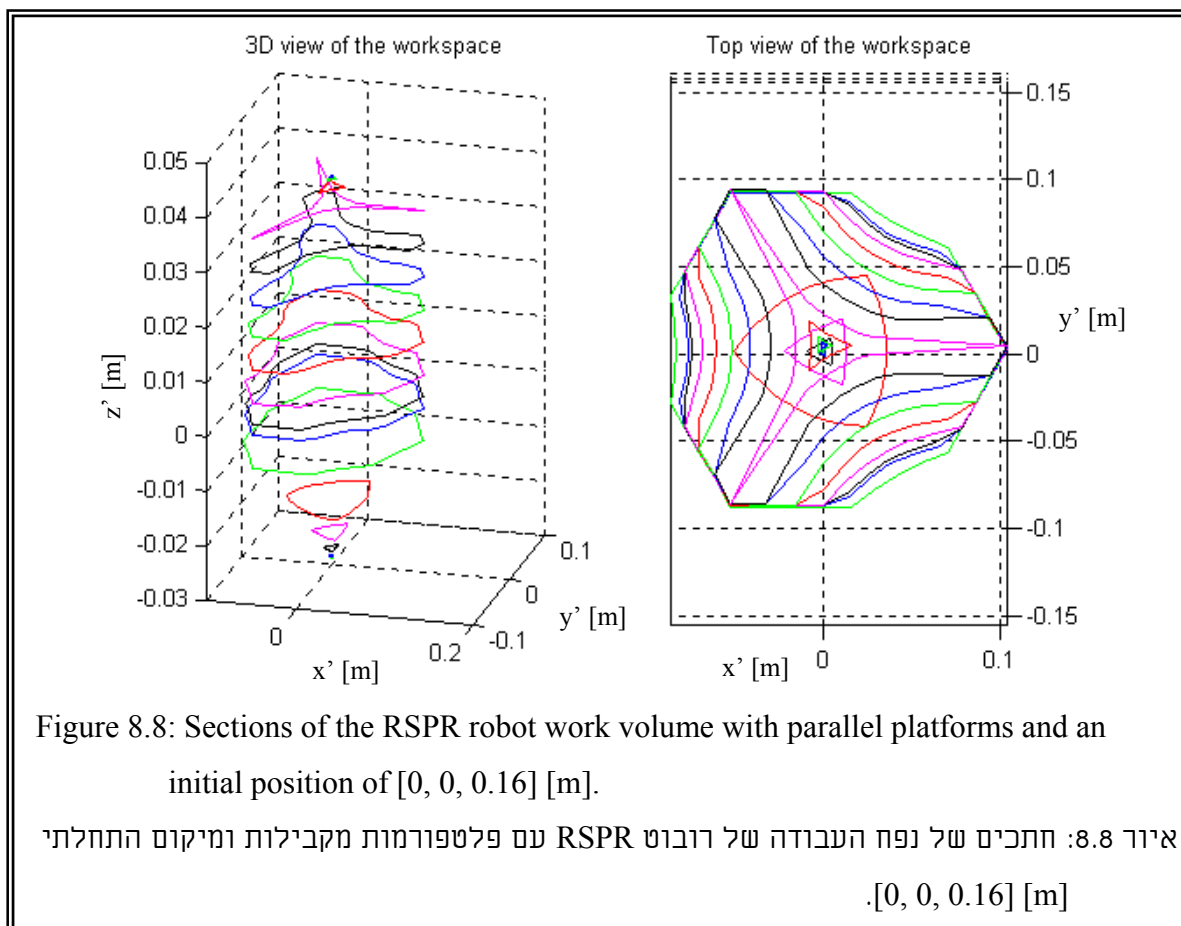
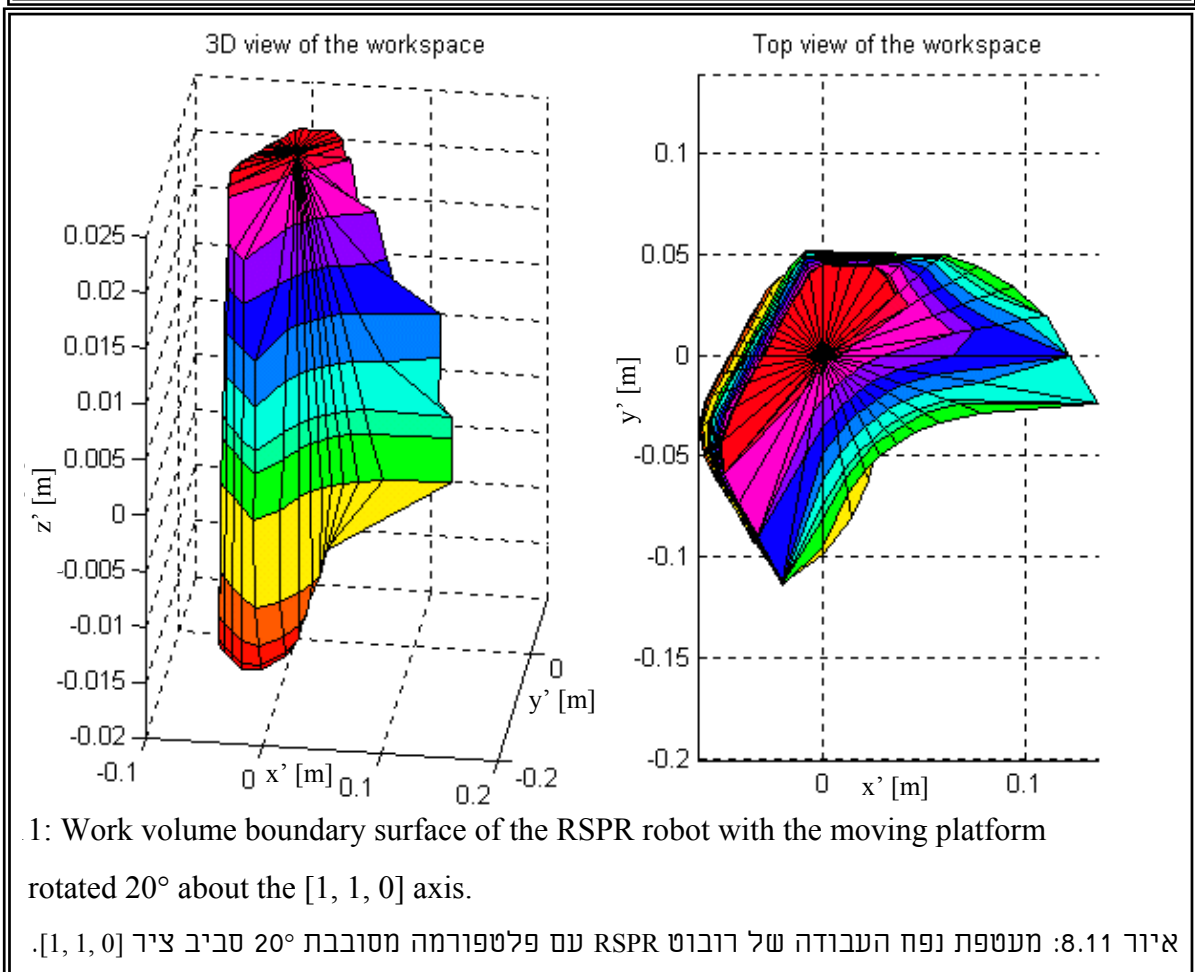
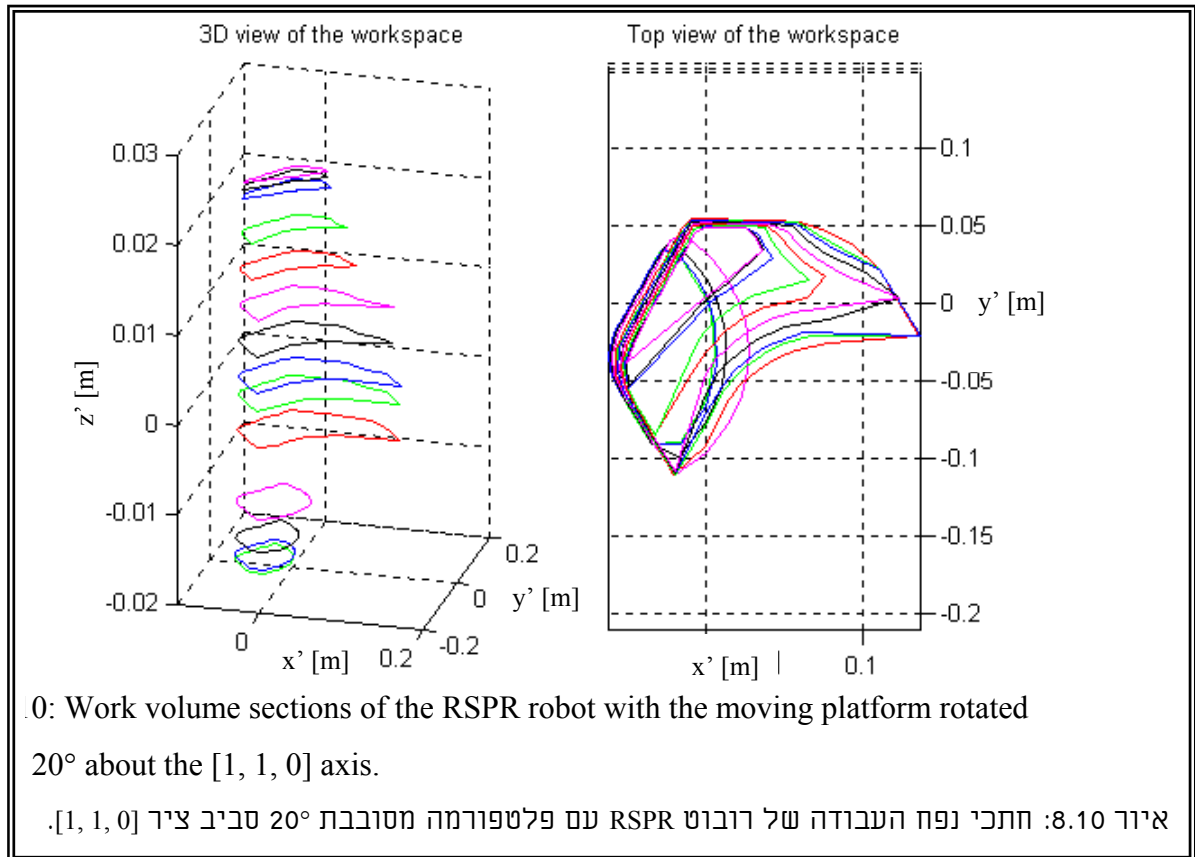


Fig. 8.8 presents constant height sections of the workspace of the RSPR robot. Fig 8.9 depicts the 3-D work volume boundary surface of the RSPR robot. Both these figures represent the workspace of the RSPR robot with a moving platform parallel to the base platform and with an initial position $[0, 0, 0.16]$ [m] with respect to the base platform attached coordinate system.

Figures 8.10 and 8.11 depict the workspace of the RSPR robot with a moving platform oriented 20° about the $[1, 1, 0]$ axis. From these figures, it is clear that the desired $40 \times 40 \times 20$ -mm work volume cube is within the workspace of the moving platform and it is obvious that the work volume of the RSPR robot is markedly affected by the orientation of the moving platform. However, even with 20° rotation of the moving platform about the $[1, 1, 0]$ axis we still fulfill the desired workspace cube.





8.5 Conclusion

Based on the design objectives set forth in chapter 4 we performed dimensional synthesis of the USR and the RSPR robots. The comparison of the RSPR robot with the USR robot, the Double circular triangular robot, and the RRPS robot indicated that the RSPR robot is better than the others in terms of smaller required actuator forces and smaller spherical joint tilting range. The synthesis process resulted in 22 admissible RSPR robots and 95 possible USR robots with different characteristic dimensions. Based on design guidelines we chose one USR robot and one RSPR robot as candidate robots for our design task. We performed comparison between the two selected robots and we showed that the candidate RSPR robot is better than the candidate USR robot in terms of mechanical simplicity and smaller actuator forces. Therefore, we chose the RSPR candidate robot as the preferable solution to our design problem. Chapter 11 will present prototype of the RSPR robot, which has the characteristic dimensions of the candidate RSPR robot described in this chapter. The following chapters present additional advantages of the RSPR robot over the USR robot in terms of less singular configurations.

Chapter 9

Introduction to Line Geometry

9.1 Introduction

This chapter serves as a humble introduction to the subject of line geometry in space. The objective of this chapter is to lay the logical foundations for the singularity analysis presented in the next chapter.

Line geometry deals with defining the elementary geometrical forms in space and determining the conditions for linear dependence between points, planes and lines. The material in this chapter is mainly based on [Veblen and Young, 1910; Graustein, 1930; Sommerville, 1934; Hunt, 1978]. Other good references, for the reader who is interested in a summary of the subject, are [Ben Horin, 1997] and [Dandurand, 1984].

9.2 Homogeneous coordinates of points, planes and lines in space

Every point in space is ordinarily defined by the set of three Cartesian coordinates $[x, y, z]$. This representation lacks the capability of treating points, lines, and planes at infinity. The definition of homogeneous coordinates allows overcoming this obstacle and leads to homogeneous equations for planes, thus, facilitating the analysis of linear dependence between planes and transforming it into a problem of solving a set of homogeneous equations. The use of lines at infinity is important in kinematics since, for example, it allows describing the motion of a prismatic joint and linear motion in plane by using screw motion about a line at infinity with zero pitch. Furthermore, the homogeneous coordinates have no metric basis and serve as a tool for projective geometry.

9.2.1 Homogeneous coordinates of a point in space

Let a point in space be represented by the non-homogenous Cartesian coordinates $[x, y, z]$. The *Homogeneous coordinates* of this point are defined by Eq. (9.1) Where the entire coordinate sets $[x_1, x_2, x_3, x_4]$ and $k[x_1, x_2, x_3, x_4]$, with $x_4 \neq 0$, represent the same point $[x, y, z]$.

$$\frac{x_1}{x_4} = x \quad \frac{x_2}{x_4} = y \quad \frac{x_3}{x_4} = z \quad (9.1)$$

Additionally, the coordinate set $[l, m, n, 0]$ represents a point located at an infinite distance along all rays having the direction numbers l, m, n . This is proved by writing the

parametric representation of the Cartesian coordinates of the points located along a ray with l, m, n direction numbers. The Cartesian coordinates, written in a homogeneous form, of these points are $[x_0 + lt, y_0 + mt, z_0 + nt, 1]$. Where x_0, y_0 , and z_0 are the Cartesian coordinates of a point on the ray. By dividing by the parameter t and considering the case where t approaches infinity, we obtain $[l, m, n, 0]$.

9.2.2 Homogeneous coordinates of a plane in space

The equation of a plane in Cartesian coordinates, $[x, y, z]$, is given by

$$ax + by + cz + d = 0 \quad (9.2)$$

By using the definition of homogeneous coordinates, one obtains the *homogeneous equation of a plane* as presented in Eq. (9.3).

$$a_1x_1 + a_2x_2 + a_3x_3 + a_4x_4 = 0 \quad (9.3)$$

Thus, the *homogeneous coordinates of a plane* are the ordered set $[a_1, a_2, a_3, a_4]$. We note that since $[l, m, n, 0]$ represents a point at infinity along a ray with l, m, n direction numbers, then the equation $x_4 = 0$ represents the plane at infinity.

If we refer to the plane having the homogeneous plane coordinates $[a_1, a_2, a_3, a_4]$ as **a**, and to the point having the homogeneous coordinates $[x_1, x_2, x_3, x_4]$ as **x**, then we can interpret Eq. (9.3) in two dual forms. Eq. (9.3) represents all the planes, **a**, passing through a given point, **x**, and in a dual form, it represents all the points, **x**, lying on a given plane, **a**. This brings us to the following duality principle in projective geometry.

9.2.3 The principle of duality

The principle of duality states that the basic elements in space, the plane and the point, are dual. Duality stems from the fact that points and planes have the same four-dimensional form of homogeneous coordinates. This duality is used in [Veblen, 1910] and [Graustein, 1930] where all the theorems regarding points appear in pairs with all the theorems regarding planes by interchanging the words point and plane. In plane geometry, the line and the point are the dual of each other. To summarize, table 9.1 lists the dualities in space and plane geometry.

Table 9.1: Duality of geometric basic elements		
טבלה 9.1: דואליות של אלמנטים גיאומטריים בסיסיים.		
Dimension	Homogeneous equation	Duality
Space geometry:	$a_1x_1 + a_2x_2 + a_3x_3 + a_4x_4 = 0$	Point \Leftrightarrow Plane.
Plane geometry:	$a_1x_1 + a_2x_2 + a_3x_3 = 0$	Point \Leftrightarrow Line.

9.2.4 Homogeneous coordinates of a line

Either two distinct points or two planes define a line in space. Based on this fact, Julius Plucker introduced the homogeneous coordinates of a line, \mathbf{l} , as the ordered six coordinates defined by Eq. (9.4)

$$\mathbf{l} = [p_{41}, p_{42}, p_{43}, p_{23}, p_{31}, p_{12}] \quad (9.4)$$

Where p_{jk} is defined by Eq. (9.5).

$$p_{jk} = x_j y_k - x_k y_j \quad j, k = 1, 2, 3, 4. \quad j \neq k. \quad (9.5)$$

One can notice that Eq. (9.5) defines twelve entities, which only six of them are linearly independent. This is due to the fact that $p_{ij} = -p_{ji}$. If \mathbf{x} and \mathbf{y} represent homogeneous coordinates of two distinct points, then Eq. (9.4) is referred to as the Plucker homogeneous ray coordinates of a line. If \mathbf{x} and \mathbf{y} represent homogeneous coordinates of two distinct planes then Eq. (9.4) is referred to as the Plucker axis coordinates of a line.

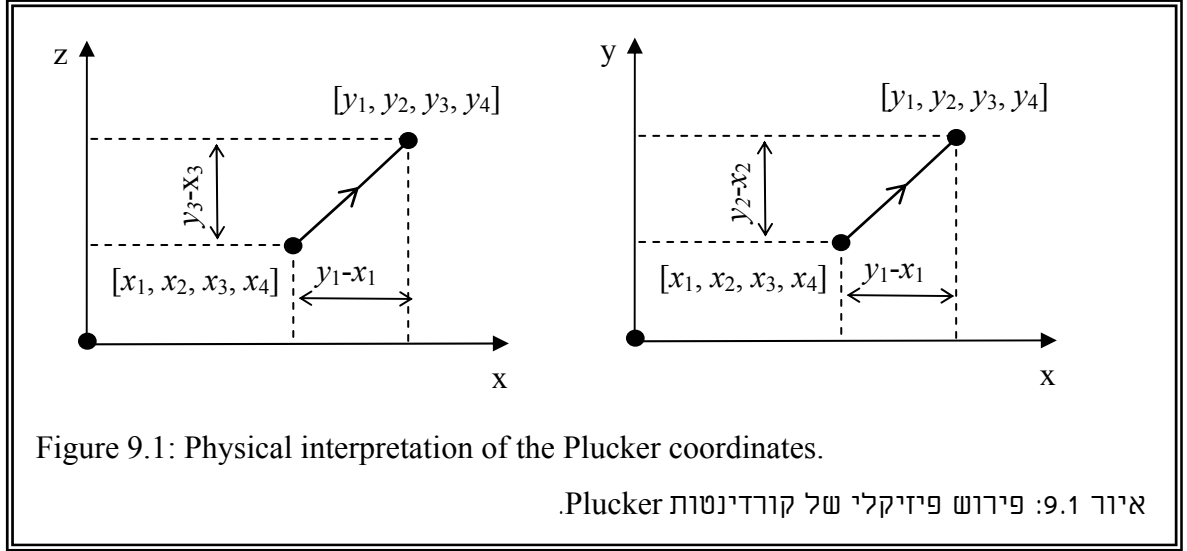
The Plucker coordinates of a line can be represented in a compact form by using the homogeneous coordinates of two points, \mathbf{x} and \mathbf{y} , located on it. Eq. (9.6) presents a 2×4 matrix used to compute the p_{jk} Plucker coordinate by computing the determinant of a 2×2 matrix constructed from the j and the k columns.

$$\begin{bmatrix} x_1 & x_2 & x_3 & x_4 \\ y_1 & y_2 & y_3 & y_4 \end{bmatrix} \quad (9.6)$$

Let \mathbf{l} be a line defined by the points $\mathbf{x} = [x_1, x_2, x_3, x_4]$ and $\mathbf{y} = [y_1, y_2, y_3, y_4]$. If we associate with this line an intensity of force acting along it, then the first three ray coordinates of line \mathbf{l} represent the vector of the force and the last three coordinates represent the moment of the force about the origin. For instance, the Plucker coordinate p_{12} represents the intensity of the moment of a force along line \mathbf{l} about the z -axis, Fig 9.1. The expression for p_{12} in Eq. (9.5) is manipulated to have the following form in Eq. (9.7).

$$p_{12} = x_1 y_2 - x_2 y_1 = x_1(y_2 - x_2) - x_2(y_1 - x_1) \quad (9.7)$$

If we draw the line, \mathbf{l} , in scale as in Fig. 9.1, then its length is proportional to its intensity. Therefore, Eq. (9.7) gives the moment of a force along line \mathbf{l} about the z -axis. Similarly p_{23} and p_{31} represent the intensity of the moment of a force along line \mathbf{l} about the x and y axes, respectively. The first three Plucker line coordinates p_{41} , p_{42} , and p_{43} are the direction numbers of the force vector along line \mathbf{l} .



Based on the above explanation, the Plucker coordinate set $[0, 0, 0, p_{23}, p_{31}, p_{12}]$ represents a line on the plane at infinity, which is perpendicular to a line with the direction numbers $[p_{23}, p_{31}, p_{12}]$. This result is obtained by substituting two point coordinates \mathbf{x} and \mathbf{y} in Eq. (9.5) with $x_4 = 0$ and $y_4 = 0$. For example, A line with the Plucker line coordinates $[0, 0, 0, 1, 0, 0]$ is located in a plane at infinity, which is perpendicular to the x axis and has only a moment about the x axis. This reasoning, presented in [Hunt, 1978], helps to understand the following relation between the Plucker coordinates of a line:

$$p_{12}p_{43} + p_{31}p_{42} + p_{41}p_{23} = 0 \quad (9.8)$$

Eq. (9.8) represents the perpendicularity between the moment of a line about the origin and the line itself. This equation is a quadric surface in a five dimensional space and every point on it represents a sextuple $[a_1, a_2, a_3, a_4, a_5, a_6]$ which satisfies the condition for being a legal set of homogeneous line coordinates [Graustein, 1930]. Therefore, every point on this quadric is a line in the 3-dimensional space. This equation is referred to as the *Grassmannian* or the *Plucker quadric* [Merlet, 1989].

9.3 The basic geometric forms

This section deals with the questions related to the minimal number of points/planes/lines required to define the space.

Two distinct points, \mathbf{x} and \mathbf{y} , define a *range of points* such that all the points, \mathbf{z} , belonging to this range of points, fulfill the following equation.

$$\mathbf{z} = a\mathbf{x} + b\mathbf{y} \quad (9.9)$$

All these points, i.e., the points that fulfill Eq. (9.9), are collinear with \mathbf{x} and \mathbf{y} .

Three points, \mathbf{x} , \mathbf{y} and \mathbf{z} , can either be collinear, or not. If the three points are collinear they belong to the same range of points. If they are non-collinear they define a *plane of points*. All the points lying on this plane, \mathbf{w} , are linear combination of the three points.

$$\mathbf{w} = a\mathbf{x} + b\mathbf{y} + c\mathbf{z} \quad (9.10)$$

Four distinct points \mathbf{u} , \mathbf{v} , \mathbf{w} , \mathbf{z} may either be collinear, coplanar, or non-coplanar. If the four points are collinear they obey Eq. (9.9) and, therefore, they are linearly dependent. If the four points are coplanar then they are linearly dependent and fulfill Eq. (9.10). If the four points are non-coplanar, then they define all the points in space, \mathbf{s} , as a linear combination:

$$\mathbf{s} = a\mathbf{u} + b\mathbf{v} + c\mathbf{w} + d\mathbf{z} \quad (9.11)$$

Based on these facts, any group of more than four points is linearly dependent.

To summarize, points define three basic geometric forms, i.e., the range of points (or pencil of points), the plane of points, and the space.

We can now consider planes and use the point-plane dualities to deduce the following results: Two planes having the homogeneous plane coordinates, $\mathbf{x} = [x_1, x_2, x_3, x_4]$, and $\mathbf{y} = [y_1, y_2, y_3, y_4]$, define a *pencil of planes* such that every plane, \mathbf{z} , fulfills Eq. (9.9), where \mathbf{x} and \mathbf{y} in this equation are plane coordinates. Three copunctal planes define a *plane sheaf*, or in other words, a *bundle of planes*. All the planes, \mathbf{w} , in this bundle of planes, fulfill Eq. (9.9), where \mathbf{x} , \mathbf{y} , \mathbf{z} , are plane coordinates. Four non-copunctal planes define the totality of planes in space, such that every plane in the space, \mathbf{s} , fulfills the plane version of Eq. (9.11). Therefore, by using the duality principle, we concluded that the plane defines three basic geometric forms, namely, the pencil of planes, the bundle of planes, and the space.

Two distinct lines, \mathbf{l} and \mathbf{m} , may be either skew or copunctal. If the lines are copunctal then the two pairs of points $[\mathbf{x}_1, \mathbf{x}_2] \in \mathbf{l}$ and $[\mathbf{y}_1, \mathbf{y}_2] \in \mathbf{m}$ are coplanar; thus, they are linearly dependent, i.e., $|\mathbf{x}_1 \ \mathbf{x}_2 \ \mathbf{y}_1 \ \mathbf{y}_2| = 0$, or by implementing the definition of Plucker line coordinates $(\mathbf{l}, \mathbf{m}) = 0$. Where the operator (\mathbf{l}, \mathbf{m}) is defined for six-dimensional vectors $\mathbf{l} = [l_1, l_2, l_3, l_4, l_5, l_6]$ and $\mathbf{m} = [m_1, m_2, m_3, m_4, m_5, m_6]$ according to Eq. (9.12).

$$(\mathbf{l}, \mathbf{m}) \equiv l_1 m_4 + l_2 m_5 + l_3 m_6 + l_4 m_1 + l_5 m_2 + l_6 m_3 \quad (9.12)$$

If \mathbf{l} and \mathbf{m} are two Plucker coordinate vectors of two lines, then writing Eq. (9.12) in terms of the Plucker ray coordinates of the lines results in:

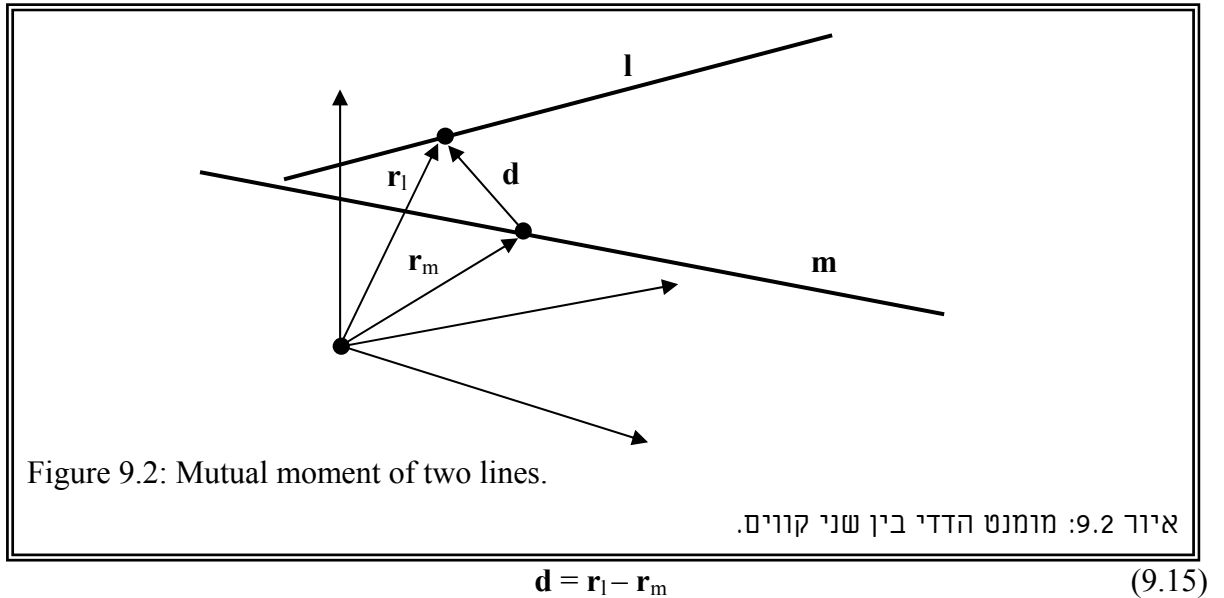
$$(\mathbf{l}, \mathbf{m}) = l_{41} m_{23} + l_{42} m_{31} + l_{43} m_{12} + l_{23} m_{41} + l_{31} m_{42} + l_{12} m_{43} \quad (9.13)$$

The equation $(\mathbf{a}, \mathbf{a}) = 0$, when \mathbf{a} is a Plucker ray coordinate vector, is the same as the expression for the Grassmannian in Eq. (9.8). Therefore, the equation $(\mathbf{a}, \mathbf{a}) = 0$ is the necessary condition for a given six-dimensional vector, \mathbf{a} , to be an admissible ray coordinate vector. Furthermore, we will show that the operator (\mathbf{l}, \mathbf{m}) based on Eq. (9.13) for two lines, \mathbf{l} and \mathbf{m} , represents the mutual moment of the lines.

To explain Eq. (9.13) we consider two lines \mathbf{l} and \mathbf{m} having Plucker ray coordinates $\mathbf{l} = [\mathbf{l}_v, \mathbf{l}_0]^t$ and $\mathbf{m} = [\mathbf{m}_v, \mathbf{m}_0]^t$. Where \mathbf{l}_v and \mathbf{m}_v are the unit vectors of lines \mathbf{l} and \mathbf{m} and \mathbf{l}_0 , \mathbf{m}_0 are the moment vectors of lines \mathbf{l} and \mathbf{m} about the origin, respectively. The expression for the moment intensity, Q , of a unit force acting along the line \mathbf{l} about the line \mathbf{m} is given by Eq. (9.14).

$$Q = (\mathbf{d} \times \mathbf{l}_v)^t \mathbf{m}_v \quad (9.14)$$

The vector \mathbf{d} is a vector from a point on line \mathbf{m} to a point on line \mathbf{l} , Fig 9.2. Let \mathbf{r}_l and \mathbf{r}_m represent two vectors from the origin to an arbitrary point on lines \mathbf{l} and \mathbf{m} , respectively. The vector \mathbf{d} is given by Eq. (9.15)



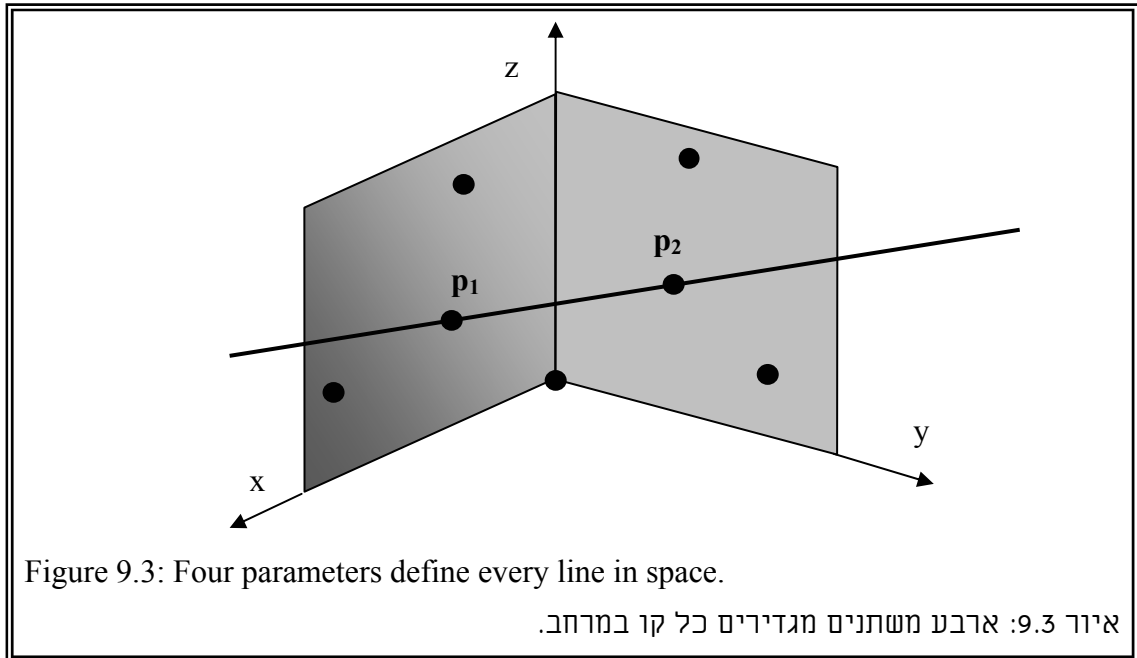
Substituting Eq. (9.15) in Eq. (9.14) and performing some algebraic manipulation leads to the result in Eq. (9.16).

$$Q = (\mathbf{d} \times \mathbf{l}_v)^t \mathbf{m}_v = (\mathbf{r}_l \times \mathbf{l}_v)^t \mathbf{m}_v + \mathbf{l}_v^t (\mathbf{r}_m \times \mathbf{m}_v) \quad (9.16)$$

The expressions $(\mathbf{r}_l \times \mathbf{l}_v)$ and $(\mathbf{r}_m \times \mathbf{m}_v)$ are the moment vectors of lines \mathbf{l} and \mathbf{m} about the origin, respectively. Therefore, we showed that the result in Eq. (9.16) is the same as the one in Eq. (9.13).

Two intersecting lines, \mathbf{x} and \mathbf{y} , define a pencil of lines, such that every line in this pencil of lines, \mathbf{z} , fulfills the line version of Eq. (9.9). Three copunctal, but non-coplanar, lines define a *bundle of lines*, such that every line in this bundle, \mathbf{w} , fulfills Eq. (9.10). Three coplanar, but non-copunctal, lines define a *plane of lines* and every line in this plane obeys the line version of Eq. (9.10).

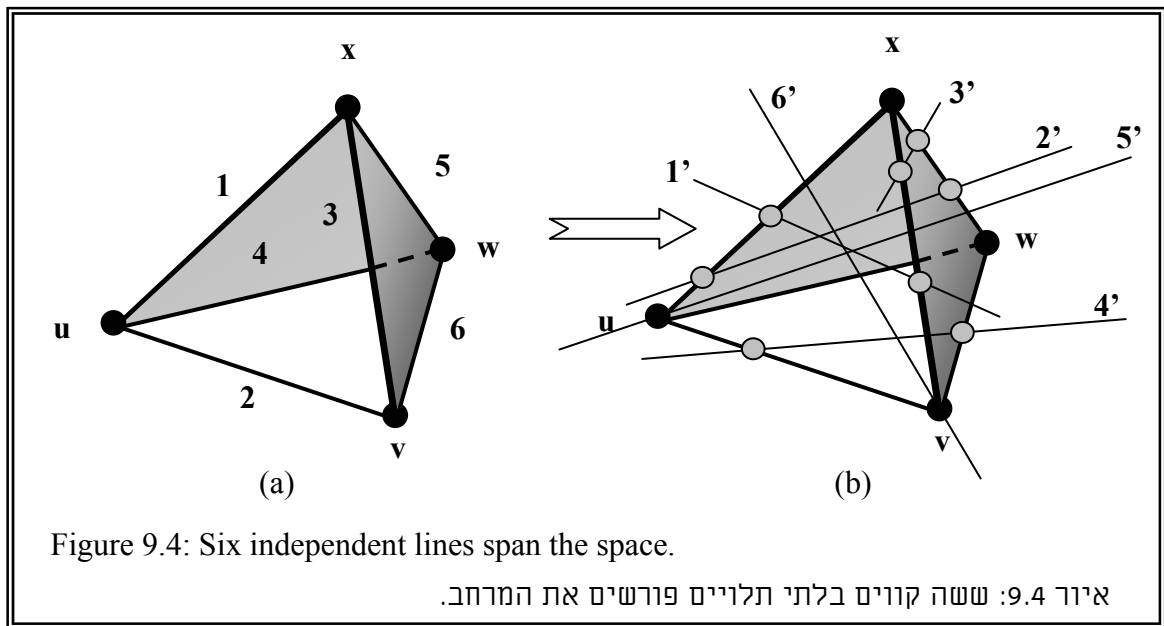
Consider the two planes x-z and y-z of a Cartesian coordinate system. Each of these two planes is defined by the point of origin and another two points on each plane, Fig 9.3. Therefore, every point on each of these planes fulfills Eq. (9.10) with only two independent variables. Consequently, every line in space is defined by four independent variables that correspond with the two pairs of variables that define its piercing points, \mathbf{p}_1 and \mathbf{p}_2 , with planes x-z and y-z. Hence, there are ∞^4 lines in space. Based on this fact lines are equivalently defined by the slope-intersect method, which depends on only four parameters of the slope and intersect variables of two of its projected lines on planes x-y and x-z [Roth, 1984].



We now come to answering the question: how many lines define the space? This question is legal since we know that the six Plucker coordinates of a line are connected by the Grassmannian and the norm of a unit vector along the line. Since a line in space is dependent only on four parameters, one might think that four lines are sufficient to define all the lines in

space. However, since the two relations of the direction numbers with the Grassmannian and the norm of a unit vector along a line are nonlinear equations, then all the six Plucker coordinates are **linearly** independent. Therefore, six independent lines define all the lines in space. Another synthetic method to prove this, which was not presented in any of the above-mentioned references, is presented hereafter.

The proof relies on the previous conclusions regarding the number of points and planes to define the space. Fig. 9.4 (a) presents the complete quadrangle, which is defined by four non-coplanar points \mathbf{x} , \mathbf{u} , \mathbf{v} , \mathbf{w} . Since these four points are non-coplanar, they are linearly independent and they span the space. Similarly, these points define four non-copunctal planes, therefore, these planes are independent and span the whole planes in the space. We note that every three lines that correspond to the edges of a facet define every facet plane of the quadrangle. Therefore, every three adjacent lines, along the edges of a tetrahedron facet, span all the lines in the plane of the facet. Accordingly, the required number of lines to span all the lines in space is six.



In the general case, it is possible to find six independent skew lines $1', 2', 3', 4', 5', 6'$ that span the space. We use the notations $\mathbf{l} \in \text{Plane}(\mathbf{x}, \mathbf{y}, \mathbf{z})$ and $\mathbf{l} \in \text{Bundle}(\mathbf{x}, \mathbf{y}, \mathbf{z})$ to indicate the fact that a line, \mathbf{l} , belongs to a plane of lines or a bundle of lines that are defined by lines \mathbf{x} , \mathbf{y} , and \mathbf{z} , according to Eq. (9.10), respectively. Fig. 9.4 (b) shows six independent lines $1', 2', 3', 4', 5'$, and $6'$. These lines depend on the edges of the quadrangle in Fig. 9.4 (a) as indicated in table 9.2.

Table 9.2: Linear dependence relations between the lines in Fig. 9.4 (a) and the lines in Fig. 9.4 (b).

טבלה 9.2: קשרים של תלות ליניארית בין הקווים באיור 9.4 (a) והקווים בציור 9.4 (b).

$1' \in \text{Plane}(1, 2, 3).$	$2' \in \text{Plane}(1, 4, 5).$	$3' \in \text{Plane}(3, 5, 6).$
$4' \in \text{Plane}(2, 4, 6).$	$5' \in \text{Bundle}(1, 2, 4).$	$6' \in \text{Bundle}(2, 3, 6).$

Writing Eq. (9.10) six times according to the relations in table 9.2 results in six linear equations represented in matrix form in Eq. (9.17).

$$[1, 2, 3, 4, 5, 6] \mathbf{B} = [1', 2', 3', 4', 5', 6'] \quad (9.17)$$

Where \mathbf{B} is a 6x6 matrix, in which, every column includes the coefficients of the equation in the form of Eq. (9.10) that corresponds to line $1'$, through $6'$. Based on Eq. (9.17), If matrix \mathbf{B} is non-singular then the lines $1', 2', 3', 4', 5', 6'$ are linearly independent and they span all the lines in space. The objective of the following section is to determine the necessary geometric conditions that render a group of six lines to be linearly independent.

9.4 Line families and linear dependence of lines

In general, there are ∞^4 lines in space. If we impose on the homogeneous coordinates of a line, \mathbf{p} , a set of homogeneous linear constraints in the form of Eq. (9.18), then we define families of lines.

$$(\mathbf{a}, \mathbf{p}) = 0 \quad (9.18)$$

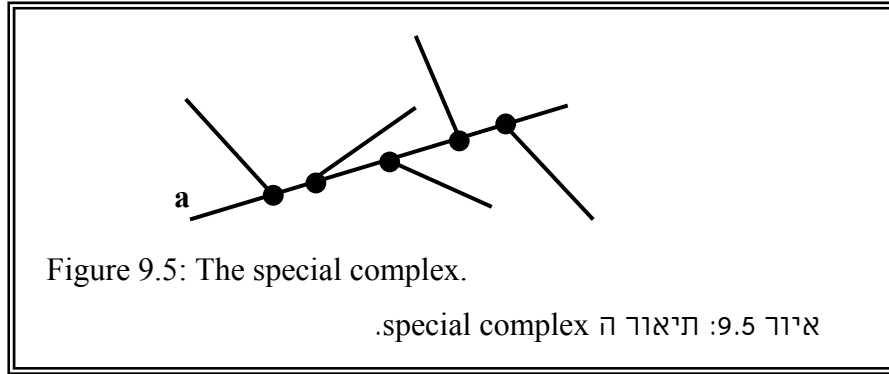
Every family of lines includes all the lines that satisfy a given set of constraints. Imposing one linear equation as a constraint creates a family of ∞^3 lines. This family is called the *linear complex*. Similarly, imposing two constraints defines a family of ∞^2 lines, which is called the *linear congruence*. Three constraints define a third family of lines, which is referred to as the *reguli*. Four constraints define a finite number of lines in space.

9.4.1 The linear complex

We know that the condition for a given sextuple, \mathbf{a} , for being a legal set of line coordinates is given by $(\mathbf{a}, \mathbf{a}) = 0$. Accordingly, we consider two cases, the first is when $(\mathbf{a}, \mathbf{a}) = 0$, and the second when $(\mathbf{a}, \mathbf{a}) \neq 0$.

The special complex

If $(\mathbf{a}, \mathbf{a}) = 0$, then \mathbf{a} represents a line and \mathbf{p} in Eq. (9.18) represents all the lines that intersect the line \mathbf{a} . This is due to the fact that all such lines, \mathbf{p} , have zero moment intensity about line \mathbf{a} , Fig. 9.5. Therefore, the lines of the complex are all the lines which intersect a given line, including the given line itself. The family of these lines is referred to as the *special complex*. All the lines in space that intersect the axis of the special complex, \mathbf{a} , are linearly dependent on any five lines of the special complex.



The general complex

If $(\mathbf{a}, \mathbf{a}) \neq 0$, then the number sextuple in \mathbf{a} does not represent Plucker coordinates of a line and Eq. (9.18) is interpreted according to the definition in Eq. (9.12). We first substitute the definition of the Plucker coordinates of line \mathbf{p} , based on two points, \mathbf{x} and \mathbf{y} , as given in Eq. (9.5). The resulting equation is Eq. (9.19). Therefore, Eq. (9.18) can now be interpreted in the following way.

$$\sum_{(n,j,k) \in [(1,2,3), (2,3,1), (3,1,2), (4,4,1), (5,4,2), (6,4,3)]} a_n (x_j y_k - x_k y_j) = 0 \quad (9.19)$$

This equation, i.e., Eq. (9.19), is linear and homogeneous in the coordinates of point \mathbf{x} ; therefore, it represents the equation of a plane on which point \mathbf{x} moves. This means that all the lines of the linear complex pass through a given point, \mathbf{y} , and another point, \mathbf{x} , which moves in a plane. Consequently, all the lines of the complex form a flat pencil of lines through \mathbf{y} . A linear complex of this kind is called a *general linear complex* or *non-special complex*. The above analysis of a general linear complex is presented in the following theorem.

Theorem 1: A general linear complex has a pencil of lines in every plane and a pencil of lines through every point in space. [Graustein, 1930].

Based on theorem 1, we deduce that every flat pencil through any point in space defines a sub-group of a general linear complex, which is associated with it. Therefore, every

line that depends on the generators of the flat pencil depends also on the generators of the associated general complex.

Another theorem regarding the general linear complex was presented in [Veblen and Young, 1910]. This theorem states the following.

Theorem 2: A linear complex consists of all lines linearly dependent on the edges of a simple skew pentagon. The proof for this theorem is presented in detail in [Veblen and Young, 1910].

9.4.2 The linear congruence

Two equations in the form of Eq. (9.18) define two linear complexes. The linear congruence is a family of lines with ∞^2 lines that belong to two complexes. Eq. (9.20) represents the homogeneous linear equations associated with the linear congruence, where \mathbf{a} and \mathbf{b} are sextuples of constants not all zero, and \mathbf{p} is the Plucker coordinate vector of a line in the linear congruence.

$$(\mathbf{a}, \mathbf{p}) = 0 \quad (\mathbf{b}, \mathbf{p}) = 0 \quad (9.20)$$

Eq. (9.20) states that the congruence is the intersection of two complexes. Any line, \mathbf{p} , which belongs to the linear congruence, fulfills Eq. (9.15), where k and l are arbitrary constants. Equation (9.21) represents a flat pencil of linear complexes.

$$k(\mathbf{a}, \mathbf{p}) + l(\mathbf{b}, \mathbf{p}) = 0 \quad (9.21)$$

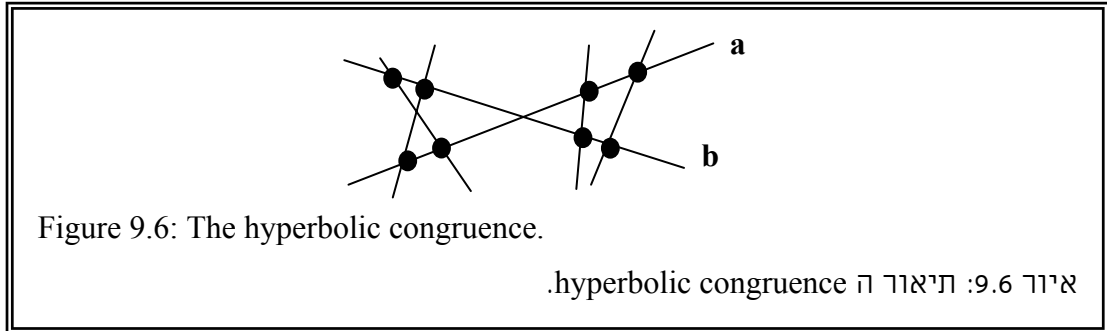
The flat pencil of complexes, in Eq. (9.21), includes special complexes and the lines of the congruence intersect the axes of all the special linear complexes that are defined by this equation. The axes of these special complexes are called the *directrices* of the congruence. All the lines in a linear congruence intersect all the directrices of the congruence.

The condition for a complex, defined by Eq. (9.21), to be a special complex is given by Eq. (9.22).

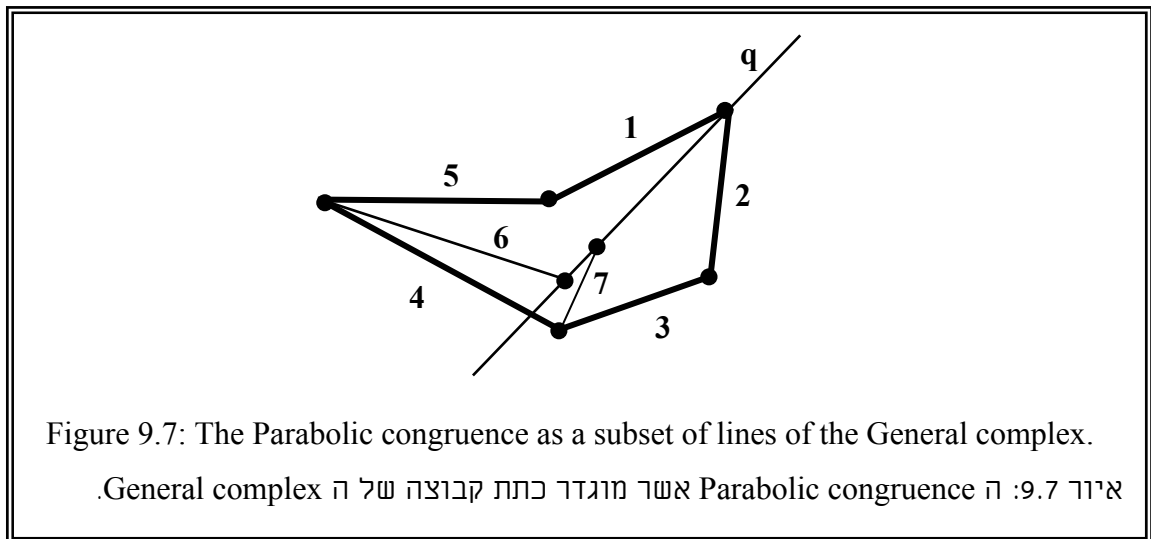
$$(k\mathbf{a} + l\mathbf{b}, k\mathbf{a} + l\mathbf{b}) = 0 \Rightarrow k^2(\mathbf{a}, \mathbf{a}) + kl(\mathbf{a}, \mathbf{b}) + l^2(\mathbf{b}, \mathbf{b}) = 0 \quad (9.22)$$

If we suppose that the complexes defined by \mathbf{a} and \mathbf{b} are special, then $(\mathbf{b}, \mathbf{b}) = 0$ and $(\mathbf{a}, \mathbf{a}) = 0$, but $(\mathbf{a}, \mathbf{b}) \neq 0$ because \mathbf{a} and \mathbf{b} are not allowed to intersect. Consequently, the two directrices of the general linear congruence are two skew lines. A linear congruence, with two skew directrices, is called a *non-parabolic congruence* [Graustein, 1930] or a *hyperbolic congruence* [Veblen and Young, 1910].

The hyperbolic congruence is defined by four lines concurrent with two skew directrices. These four lines are called the generators of the hyperbolic congruence. Any line that is also concurrent with the directrices belongs to the congruence and linearly depends on the four generators of the congruence.



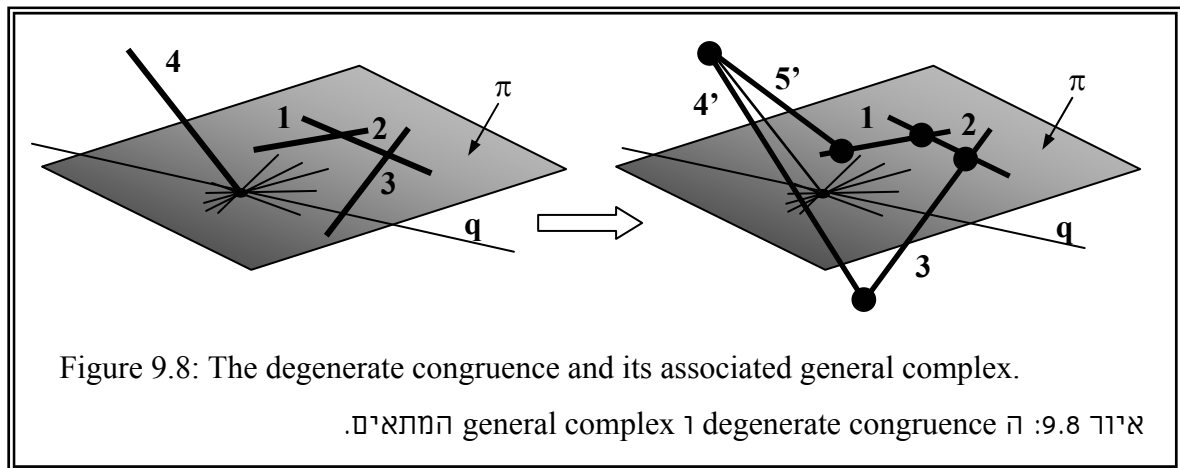
If the directrices of the linear complex, in Eq. (9.21), are concurrent, then it has one (doubly counting) directrix, q , and this directrix is a line in a flat pencil of a general complex. In this case the linear complexes defined by a and b are identical and general; therefore, there is only one directrix. This directrix is a line of one of the flat pencils of the general pentagon defining the linear complex. Figure 9.7 shows a simple spatial pentagon defining a linear complex.



If we consider a directrix, q , which belongs to the flat pencil defined by lines 1 and 2 , then the flat pencil $[4,5]$ has a line 6 , which intersects the directrix. Similarly, the flat pencil $[3,4]$ has a line 7 that intersects the directrix. Hence, all the lines defined by the three flat pencils $[6,q]$ $[7,q]$ and $[2,q]$ belong to the linear complex and constitute a linear congruence. This type of linear congruence is called a *parabolic congruence*. All the lines, which belong to one of the three flat pencils of the parabolic congruence, linearly depend on the lines q , 2 ,

6, and 7.

If there is a group of four lines, with three coplanar lines **1**, **2**, **3**, defining a plane π , and a fourth line, **4**, piercing π , then a *Degenerate congruence* [Veblen and Young, 1910] or a *special congruence* [Graustein, 1930] forms. The three coplanar lines define all the lines in π ; therefore, they define a flat pencil of lines with a center at the point in which line **4** pierces π . Any line, **q**, in this flat pencil is a directrix of the degenerate congruence. Figure 9.8 presents the simple pentagon associated with the degenerate congruence. Obviously, all the lines of the degenerate congruence belong to its associated general complex, which is defined by the simple pentagon **1**, **2**, **3**, **4'**, **5'**. The lines that linearly depend on lines **1**, **2**, **3**, and **4** are all the



lines in the plane π and all the lines through the center of the flat pencil of directrices.

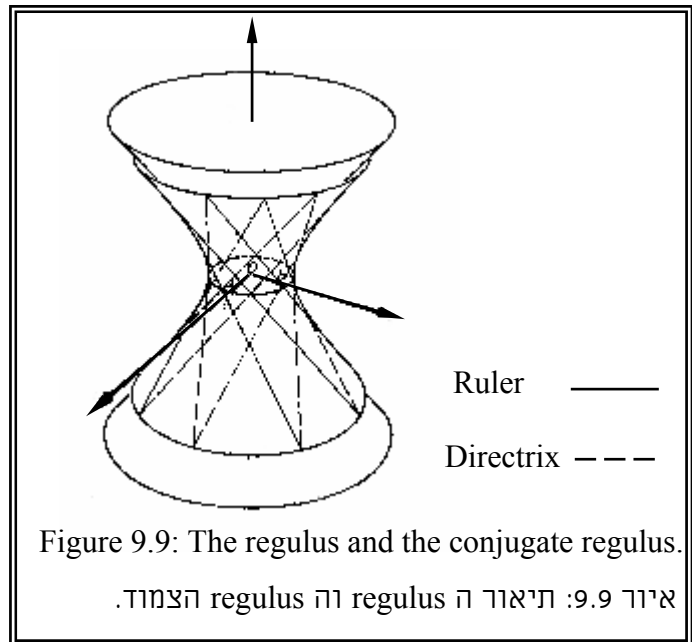
The *elliptic congruence* has imaginary directrices and it is constituted from four mutually skew and linearly independent lines. A line quadruple contains three line triplets. If all the lines in a line quadruple are mutually skew, then every line triplet defines a ruled surface called a *regulus*. The lines that depend on the four generators of the elliptic congruence are the lines that depend on each one of the three reguli.

9.4.3 The reguli

This family of lines has ∞^1 lines that belong to three linear complexes. There are four types of reguli, the first is called the regulus and the other three are called degenerate reguli. The regulus is formed by three mutually skew directrices **a**, **b**, and **c**, and it is defined by all the lines that intersect these three directrices. The lines that intersect all the directrices are called the rulers of the regulus, for they define the ruled surface of the regulus. The points of the regulus lie on a single sheet hyperboloid. The totality of the ruling lines of this ruled

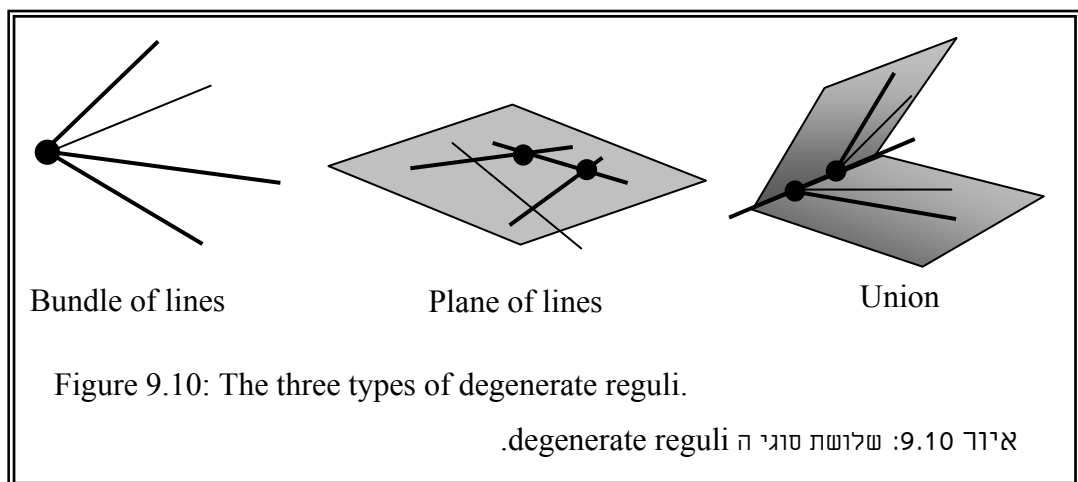
surface is called a *regulus*. No pair of the regulus rulers is allowed to intersect, for if two rulers intersect, then two of the directrices are coplanar. Fig. 9.9 presents the regulus.

The rulers of a given regulus intersect its three directrices. Similarly, the directrices of the regulus are the rulers of a *conjugate regulus* and any three rulers of the regulus are the directrices of the conjugate regulus. Hence, the regulus is a doubly ruled surface for both the regulus and the conjugate regulus define the same ruled surface. All the lines that belong to a regulus linearly depend on any three of its rulers.



The other three degenerate reguli, in Fig. 9.10, are the bundle of lines, the plane of lines, and the *union*. The first two degenerate reguli, i.e., the bundle of lines and the plane of lines are two basic geometric forms, which we already presented. The union is defined by two distinct flat pencils having one line in common.

All the lines that pass through the center of the bundle of lines linearly depend on any three lines of the bundle. All the coplanar lines linearly depend on any three distinct and non-copunctal lines in this plane. All the lines that belong to any of the two flat pencils of the union linearly depend on the three generators of the union. In Fig. 9.10 the thick lines indicate the independent lines and the thin lines indicate a linearly dependent line.



9.5 Line varieties

A set of lines is a variety if all the lines in the set linearly depend on the base of the set and no line outside the set linearly depends on the base of the set. Six line varieties are defined based on the dimension of the base of the variety. All the lines in space depend on a six-dimensional base of six independent lines; thus, all the lines in the space belong to the most general *space* variety. The set of lines that linearly depend on five-dimensional base is the lines of the linear complex; therefore, the line variety of rank five is the linear complex variety. The variety of rank four is the linear congruence. The variety of rank three is the *planes* variety. The variety of rank two is the *lines* variety. Finally, the variety of rank one is the *point* variety.

The point variety includes only one line in space, the line in the base of this variety. The lines variety has a two dimensional base. If the lines of the base are skew then these lines are the only lines of the variety, i.e., no other lines in space depend upon these lines. If the lines of the base intersect, then the variety includes all the lines in the flat pencil of the base.

Tables 9.3, 9.4, and 9.5 are reproduced from [Dandurand, 1984]. These tables are synthetic tables, i.e., they provide a logical tool for determining the geometric conditions for linear dependence between lines. The tables are a summary of the subject of linear dependence of lines and do not present the mathematical background of the subject. Therefore, we wrote this chapter in order to present the mathematical background of the subject.

Table 9.3 presents the line varieties and each variety is divided into several cases. Each case is indicated by a number denoting the rank of the variety, and a letter specifying the specific case in the variety. This method of indicating a specific case of a variety is common among the researchers in the field of line geometry. Table 9.4 presents the result of adding lines one by one starting with single line and ending with a six-dimensional base of the space variety. Table 9.5 shows equivalent cases, which are combinatorially distinct figures of lines, and belong to one of the cases presented in table 9.3.

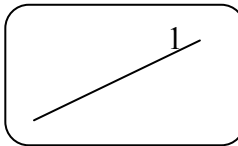
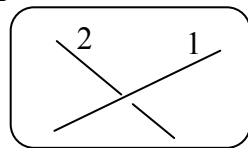
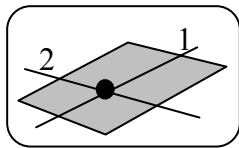
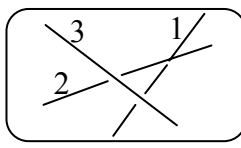
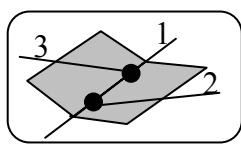
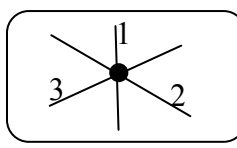
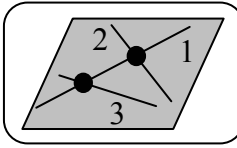
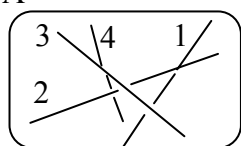
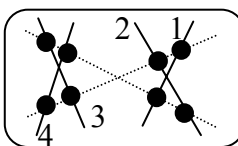
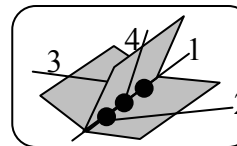
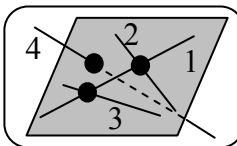
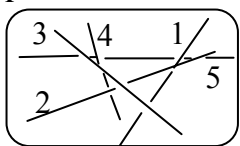
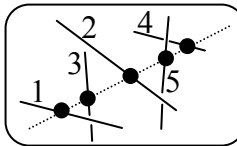
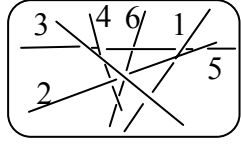
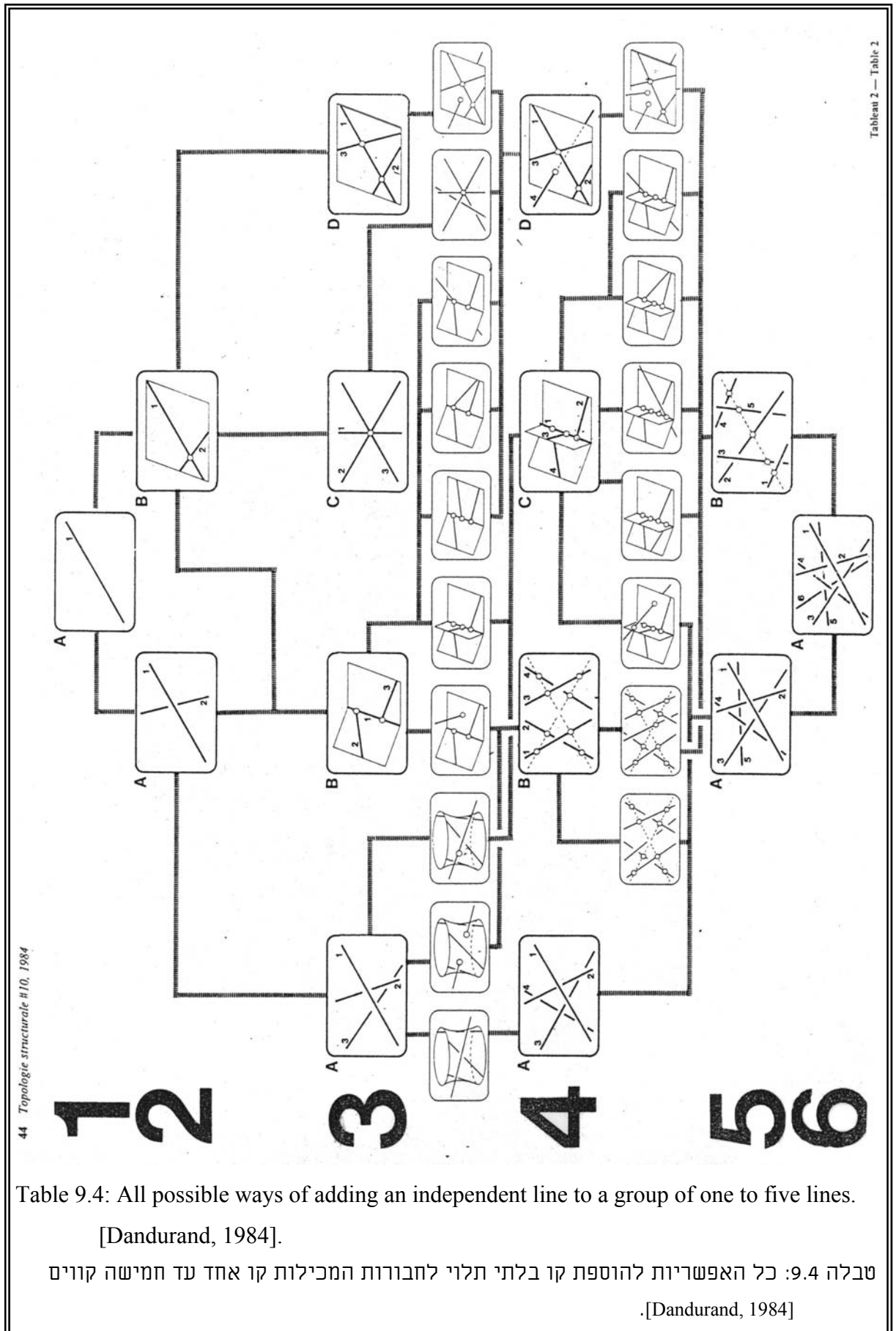
1	A 			
2	A 		B 	
3	A 	B 	C 	D 
4	A 	B 	C 	D 
5	A 		B 	
6	A 			

Table 9.3: Synthetic representation of the six line varieties reproduced from [Dandurand, 1984].

טבלה 9.3: ששת ה line varieties בייצוג סינתטי על פי [Dandurand, 1984].



--	--	--	--	--	--	--	--	--	--	--	--	--	--	--	--	--	--	--	--	--	--	--	--	--

Table 9.5: Combinatorially equivalent cases. [Dandurand, 1984].

טבלא 9.5: מקרים אקוויולנטיים על פי [Dandurand, 1984].

Chapter 10

Singularity Analysis

10.1 Introduction

Singularity analysis of parallel robots is a subject of extreme importance for control and synthesis of robot mechanisms. Many researchers, [Merlet, 1989; Gosselin and Angeles, 1990; Ma and Angeles, 1992; Hunt, Samuel, and McAre, 1991; Zlatanov et al., 1995; Basu and Ghosal, 1996; Xu, Kholi, and Weng, 1992; Ben Horin, 1997], invested immense efforts in solving this problem.

A general non-redundant mechanism can be considered as an input-output device, with the input variables being the generalized coordinates variables, and the output variables being the posture variables of the output link. The term posture refers to the six variables, position and orientation, required to fully describe the location and orientation of a rigid body in space.

Singular configurations are defined as configurations, in which, the relation between the input variables and the output variables is not fully defined. For serial mechanisms, with n degrees of freedom, a configuration is regarded singular when the instantaneous input-output map $\dot{\mathbf{x}} = \mathbf{J}\dot{\mathbf{q}}$ is singular. Where $\dot{\mathbf{x}}$ denotes an $n \times 1$ vector of the output link linear/angular velocities, $\dot{\mathbf{q}}$ denotes an $n \times 1$ actuator velocities vector, and the matrix \mathbf{J} is the system Jacobian. Unlike with serial mechanisms, for parallel mechanisms a configuration, \mathbf{q} , is regarded singular when the input-output map $\dot{\mathbf{q}} = \mathbf{J}\dot{\mathbf{x}}$ is singular [Zlatanov, et al., 1995].

For a general mechanism, with n degrees of freedom, the relation between the input output variables takes the form:

$$\mathbf{A}\dot{\mathbf{x}} = \mathbf{B}\dot{\mathbf{q}} \quad (10.1)$$

Where \mathbf{A} and \mathbf{B} are $n \times n$ matrices. This relation stems from differentiating all the loop closure equations and the kinematic constrain equations in each loop with respect to time. For fully parallel manipulators the matrix \mathbf{B} is diagonal and its inversion is always possible [Ma and Angeles, 1992]. Therefore, the common definition for the Jacobian matrix for parallel manipulators takes the form $\mathbf{J} = \mathbf{B}^{-1} \mathbf{A}$ and the instantaneous inverse kinematics problem is define by $\dot{\mathbf{q}} = \mathbf{J}\dot{\mathbf{x}}$. The matrices \mathbf{A} and \mathbf{B} are referred to as the direct kinematics and the inverse kinematics matrices, respectively [Chablat and Wenger 1998]. This notation stems from the facts that singularity of the matrix \mathbf{A} leads to an undefined forward instantaneous kinematics problem and singularity of the matrix \mathbf{B} leads to undefined inverse instantaneous kinematics problem. Based on rank-deficiency of the matrices \mathbf{A} and \mathbf{B} Gosselin and Angeles

[1990] divided the singular configurations into three cases: the first, when only \mathbf{A} is singular; the second one, when only \mathbf{B} is singular; and the third, when both \mathbf{A} and \mathbf{B} are singular. We adopt the terminology in [Chablat and Wenger 1998] and refer to the singular configurations associated with singularities of the direct kinematics matrix, \mathbf{A} , and the inverse kinematics matrix, \mathbf{B} , as parallel singularities and serial singularities, respectively.

Hunt, Samuel, and McAree [1991] discussed the singular configurations in serial, parallel, and composite serial and in-parallel robots, by using motion and action screws. The main observation of this work is presented in the statement that in a serial manipulator the actuators are twist applicators, and in a fully parallel robot the actuators are wrench applicators. Moreover, the authors use the reciprocity principle to deduce results from the space of constraints and interpret them in the space of freedoms. The reciprocity principle states that any screw taken from the space of freedom, i.e., motion screw is reciprocal to any screw taken from the space of constraint, i.e., action screw. The authors proved that a work-piece grasped by a serial chain can only loose degrees of freedom (or reciprocally, gain constraint); while a work-piece grasped by fully in parallel manipulator can only gain degrees of freedom (or reciprocally, lose constraint) in configurations inside its workspace domain. A non-fully parallel manipulator can either loose or gain degrees of freedom.

This result, regarding loss or gain of freedoms, can be explained by inspecting Eq. (10.1) as follows: if the direct kinematics matrix is singular (parallel singularity), then the linear equation system $\mathbf{B}^{-1} \mathbf{A} \dot{\mathbf{x}} = \dot{\mathbf{q}}$ has a non-trivial solution $\dot{\mathbf{x}} \neq \mathbf{0}$ for $\dot{\mathbf{q}} = \mathbf{0}$. Therefore, the moving platform gains degrees of freedom and performs movements in the direction of $\dot{\mathbf{x}}$ that belong to the nullspace of the Jacobian matrix \mathbf{J} . If a serial singularity occurs, i.e., \mathbf{B} is singular, then the linear system of equations $\dot{\mathbf{x}} = \mathbf{A}^{-1} \mathbf{B} \dot{\mathbf{q}}$ has a non-trivial solution $\dot{\mathbf{q}} \neq \mathbf{0}$ for $\dot{\mathbf{x}} = \mathbf{0}$. Therefore, the moving platform loses degrees of freedom.

While serial singularities occur on the boundary of the workspace of a parallel manipulator, parallel singularities may occur inside the workspace of the manipulator. Serial singularities are associated with sets of configurations where different branches of the inverse kinematic problem meet, and parallel singularities are associated with sets of configurations where different branches of the direct kinematic problem meet [Gosselin and Angeles, 1990].

In both cases, i.e. serial and parallel singularities, control of the robot is lost. In serial singularities, the actuated joints velocities reach extreme values, and in parallel singularities, the moving platform loses one or more constraints and falls along a path of singular configurations. Parallel singularities are hazardous to the mechanical assembly of the robot

and may lead to mechanical failure. The relation between the actuator forces vector and the wrench acting on the moving platform is given in equation (10.2):

$$\mathbf{B}^{t^{-1}} \boldsymbol{\tau} = \mathbf{A}^{t^{-1}} \mathbf{f} \quad (10.2)$$

Where $\mathbf{B}^{t^{-1}}$ and $\mathbf{A}^{t^{-1}}$ are the inverse transpose of \mathbf{B} and \mathbf{A} .

In parallel singularities \mathbf{A} is singular and the system of equations in Eq. (10.2) has a non-trivial solution $\boldsymbol{\tau} \neq \mathbf{0}$ for $\mathbf{f} = \mathbf{0}$. Thus, near singularity the actuators forces reach extreme values and the joints undergo high stresses, especially if the kinematic chains include passive revolute joints transmitting moments. In serial singularities, the system of equations in Eq. (10.2) has a non-trivial solution $\mathbf{f} \neq \mathbf{0}$ for zero actuator forces $\boldsymbol{\tau} = \mathbf{0}$. Consequently, in serial singular configurations, the wrench acting on the moving platform does not affect one or more actuator forces.

Zlatanov, et al. [1995] proposed a general velocity equation for interpreting the singularities of a general manipulator by considering the singularities of the instantaneous direct and inverse kinematics matrices and the matrix defining the relation between the actuated joint velocities and the passive joint velocities. Based on singularity of these matrices, this method allows physical interpretation of the singular configurations.

Ma and Angeles [1992] proposed classifying the singularities of parallel manipulators into three categories. The first category is called architecture singularities, the second category is called configuration singularities, and the third category is the formulation singularities. Architecture singularities are singularities that depend on the architecture of the robot. Such singularities exist for all configurations inside a considerable part of, or the entire workspace of the manipulator. Configuration singularity is caused by a particular configuration of the manipulator. Formulation singularity is a singularity caused by the mathematical model due to failure in representing the system at a particular configuration. Burton [1979] referred to architecture singularities as permanent critical forms, and to configuration singularities as instantaneous critical forms. Architecture singularities are of particular importance in stages of conceptual design of new parallel manipulators since the designer must assure that the suggested architecture is not architecturally singular. Ma and Angeles [1992] proved, by analyzing the rank of the Jacobian matrix, that a 6-6 Stewart platform is architecture singular if the moving and the base platform are similar polygons. In addition, they proved that if the moving and base platforms are similar irregular polygons, then the manipulator is singular throughout a considerable part of its workspace. Karger

[1998] investigated the spatial architectures for parallel robots which are architecture singular, and presented a list of all degenerated parallel manipulators.

Dandurand [1984] addressed the problem of rigidity conditions of compound spatial grids by using line geometry. Parallel singularities were solved by line geometry by Merlet [1989] for a 3-6 Stewart platform. Ben-Horin [1997] implemented the method of line geometry for many fully-parallel manipulators. He showed that for fully-parallel manipulator the Jacobian matrix consists of Plucker coordinates of the lines along the prismatic actuators. Therefore, he based the singularity analysis on finding geometrical conditions for linear dependence between these lines. Collins and Long [1995(a)] used the line geometry method for analyzing the singularities of the hand controller in Fig. 5.9. Notash [1998] used line geometry to investigate redundant three-branch platform manipulators and their preferable actuation distribution in order to eliminate singularities. Hao and McCarthy [1998] discussed the conditions on the joint arrangements that ensure line-based singularities in platform manipulators. They showed that in order to have line-based singularities the platform must connect to the kinematic chains by spherical joints or equivalent joint arrangements. In our work, the USR and the RSPR robots do not fulfill this requirement, but thanks to the use of the instantaneous direct and inverse kinematics matrices, we overcome this obstacle.

A fully parallel manipulator has only one solution for the inverse kinematics problem; therefore, the associated inverse instantaneous kinematics matrix, \mathbf{B} , is diagonal and non-singular for all the cases where the linear actuator's lengths is not zero. In contrast with fully-parallel manipulators, non-fully parallel manipulators use compound kinematic chains that allow more than one solution for the inverse kinematic problem. Consequently, for non-fully parallel manipulators, singularity of both matrices \mathbf{A} and \mathbf{B} should be considered for complete analysis of singular configurations. Singularity of the matrix \mathbf{B} indicates a loss of degrees of freedom in one of the kinematic chains.

Based on the singularities of matrices \mathbf{A} and \mathbf{B} we divide the singularity analysis into two stages. In section 10.2, we analyze parallel singularities by using line geometry method. This provides the analysis of parallel singularities for a class of non-fully parallel manipulators that share the same direct instantaneous kinematics matrix \mathbf{A} . This class of non-fully parallel manipulators includes 14 different architectures already listed in Fig. 5.14. In section 10.3, we inspect the matrix \mathbf{B} for serial singularities and we apply the analysis for the RSPR and the USR robots shown in Fig. 5.16 and 5.15.

10.2 Analysis of Parallel singularities for a class of non-fully parallel manipulators

10.2.1 The method of analysis

This section presents configuration singularity analysis of the tripod part of the RSPR and USR robots. The Jacobian matrix $\tilde{\mathbf{J}}$ presented in Eq. (7.14) corresponds to this tripod mechanism. Furthermore, the Jacobian matrix, $\tilde{\mathbf{J}}$, is common for a class of non-fully parallel manipulators that share an identical tripod mechanism to the one appearing in the RSPR and the USR robots. This class of manipulators was presented in Fig. 5.14. In Chapter 7, we showed that the Jacobian matrix $\tilde{\mathbf{J}}$ of the tripod mechanism in Fig. 7.1 is the direct kinematics matrix of a complete parallel manipulator with such tripod mechanism. Therefore, the singularity analysis of $\tilde{\mathbf{J}}$ reveals all the parallel singularities associated with the aforementioned class of non-fully parallel manipulators in Fig. 5.14 (including the RSPR and USR robots).

The method of analysis is based on line geometry and synthetic proofs. The emphasis is placed on the geometric interpretation of each singular configuration rather than on developing the determinants describing the singularity from algebraic point of view. The analysis starts with low-rank line varieties and ends with the linear complex variety. For each case in Fig. 9.3, we inspect the conditions for having $n+1$ lines belonging to a variety of rank n , $n=1..6$. In cases where we consider singularity of flat pencils, we assume that the tested line triplet forms such a flat pencil and we write the geometric conditions for such singularity.

10.2.2 Preliminary definitions

When utilizing line geometry method in singularity analysis, it is a preliminary task to notice all the relations between lines, planes, and locus of points. First, we begin by setting up the relevant nomenclature for this section. Then we register a list of useful geometric relations upon which we will base all following geometrical proofs.

Fig. 10.1 presents a geometric interpretation of the Jacobian matrix $\tilde{\mathbf{J}}$ associated with the tripod part of the RSPR robot. In chapter 7 we showed that the rows of the Jacobian matrix $\tilde{\mathbf{J}}$ are the Plucker ray coordinates of the lines in Fig. 7.3. We will use the symbols \mathbf{l}_k $k=1..6$ to refer to row number k in the tripod's Jacobian matrix $\tilde{\mathbf{J}}$. Hence, the Plucker ray coordinates of lines \mathbf{l}_1 , \mathbf{l}_2 , \mathbf{l}_3 , \mathbf{l}_4 , \mathbf{l}_5 , and \mathbf{l}_6 in Fig. 10.1 are the rows of the tripod Jacobian matrix

$\tilde{\mathbf{J}}$. Singularity of $\tilde{\mathbf{J}}$ stems from linear dependence of its rows $\mathbf{l}_1, \mathbf{l}_2, \mathbf{l}_3, \mathbf{l}_4, \mathbf{l}_5$, and \mathbf{l}_6 ; therefore, we use line geometry to find all the configurations in which these lines are linearly dependent.

Nomenclature:

The following symbols facilitate the formulation of the geometrical proofs in this chapter. All the symbols are explained herein and shown in Fig. 10.1.

\mathbf{p}_i : center points of the revolute joints on the moving platform. $i=1,2,3$.

\mathbf{r}_i : vectors of the revolute joints' axes on the moving platform. $i=1,2,3$.

\mathbf{b}_i : Center points of the spherical joints. $i=1,2,3$.

\mathbf{o}_p : The center point of the moving platform.

\mathbf{n} : Normal to the moving platform that passes through \mathbf{o}_p .

P_i : The plane defined by \mathbf{n} and a point \mathbf{p}_i , $i=1,2,3$.

P_0 : The plane defined by points \mathbf{p}_i , $i=1,2,3$.

B_0 : The plane defined by points \mathbf{b}_i , $i=1,2,3$. This plane is hereafter referred to as the tripod base plane.

jk : A flat pencil generated by lines \mathbf{l}_j and \mathbf{l}_k . $k, j \in \{1,2,3,4,5,6\}$, $k \neq j$.

X_{jk} : A flat pencil generated by lines \mathbf{l}_j and \mathbf{l}_k that belongs to category of flat pencils X . The expression X_{jk} represents the same flat pencil as X_{kj} ($X_{jk} = X_{kj}$).

$^p X_{jk}$: The plane associated with flat pencil X_{jk} .

$^c X_{jk}$: The center point of flat pencil X_{jk} .

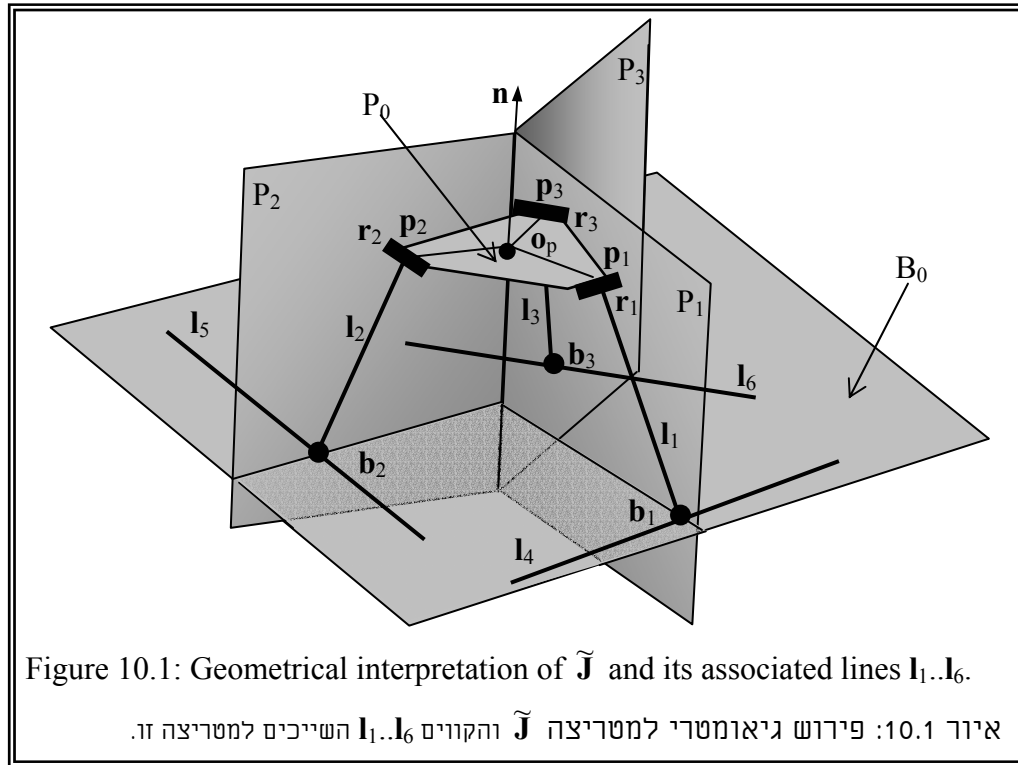
$\mathbf{p}_j \mathbf{p}_k$: the line defined by points \mathbf{p}_j and \mathbf{p}_k .

Γ : the complete group of the Jacobian lines. $\Gamma = \{\mathbf{l}_1, \mathbf{l}_2, \mathbf{l}_3, \mathbf{l}_4, \mathbf{l}_5, \mathbf{l}_6\}$.

C_{jk} : the group of Jacobian lines other than the Jacobian lines \mathbf{l}_j and \mathbf{l}_k .

$$C_{jk} = \{\mathbf{l}_n: \mathbf{l}_n \in \Gamma, n \neq j, n \neq k\}.$$

We regard lines and planes as sets of points. Therefore, the symbols \cap and \in have the same interpretation for groups of points. Accordingly, the expression $\mathbf{a} \cap \mathbf{b}$ indicates the intersection of two lines, \mathbf{a} and \mathbf{b} , in a common point, or the intersection of two planes, \mathbf{a} and \mathbf{b} , along a common intersection line, or a line \mathbf{a} piercing a plane \mathbf{b} . The expression $\mathbf{a} \in \mathbf{b}$ indicates that a point, \mathbf{a} , is on the line/plane, \mathbf{b} ; or that a line, \mathbf{a} , lies in the plane \mathbf{b} .



Geometric relations:

The tripod mechanism in Fig. 10.1 determines the following geometric relations. These geometric relations are self-evident and stem directly from the architecture of the tripod in Fig 10.1.

Geometric relation A1: Points \mathbf{p}_i are not collinear. $i=1,2,3$.

Geometric relation A2: $\mathbf{b}_1 \in P1, \mathbf{b}_2 \in P2, \mathbf{b}_3 \in P3$.

Geometric relation A3: $\mathbf{r}_1 \in P_0, \mathbf{r}_2 \in P_0, \mathbf{r}_3 \in P_0$.

Geometric relation A4: $\mathbf{l}_4 \parallel \mathbf{r}_1, \mathbf{l}_5 \parallel \mathbf{r}_2, \mathbf{l}_6 \parallel \mathbf{r}_3$.

Geometric relation A5: $\mathbf{r}_1 \perp \mathbf{P1}$, $\mathbf{r}_2 \perp \mathbf{P2}$, $\mathbf{r}_3 \perp \mathbf{P3}$.

Geometric relation A6: $\mathbf{p}_i \notin \mathbf{r}_j$, $i, j=1,2,3$, $i \neq j$.

Corollaries:

The following corollaries result from geometric relations A1..A5. Each corollary is followed by brackets enclosing a list of the geometric relations used to prove it.

Corollary Cr1 [A2]: $\mathbf{l}_1 \in P1, \mathbf{l}_2 \in P2, \mathbf{l}_3 \in P3$.

Corollary Cr2 [A3, A4]: $I_4 \parallel P_0, I_5 \parallel P_0, I_6 \parallel P_0$.

Corollary Cr3 [A4, A5]: $\mathbf{l}_4 \perp \mathbf{P1}$, $\mathbf{l}_5 \perp \mathbf{P2}$, $\mathbf{l}_6 \perp \mathbf{P3}$.

Corollary Cr4 [A2, A4, A5]: $\mathbf{l}_4 \perp \mathbf{l}_1, \mathbf{l}_5 \perp \mathbf{l}_2, \mathbf{l}_6 \perp \mathbf{l}_3$.

Next, the singularity of the tripod mechanism is presented. We refer to each case in the line varieties according to the nomenclature in Fig. 9.3.

10.2.3 Point singularities (1a)

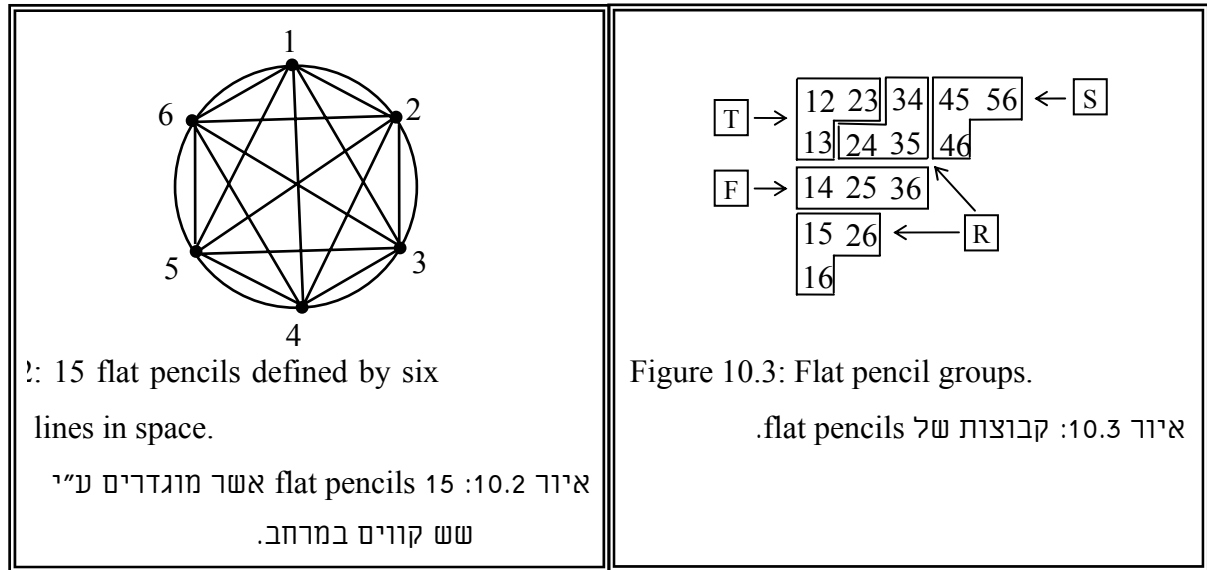
Singularity of the point variety in which two lines are coincident is not possible. This is because lines \mathbf{l}_1 , \mathbf{l}_2 , and \mathbf{l}_3 belong to three distinct planes P_1 , P_2 , and P_3 , respectively. They also pass through three distinct points \mathbf{p}_1 , \mathbf{p}_2 , and \mathbf{p}_3 , therefore no couple from these lines can be simultaneously concurrent with the intersection line of the three planes P_1 , P_2 , and P_3 . Lines \mathbf{l}_4 , \mathbf{l}_5 , \mathbf{l}_6 move such that each one is perpendicular to the planes P_1 , P_2 , P_3 , respectively. Therefore, concurrence of a couple of lines from this group is not possible.

10.2.4 Flat pencil singularities (2b)

We seek to find singularities which stem from subsets of lines $\mathbf{l}_1.. \mathbf{l}_6$ that include more than two lines in one common flat pencil, therefore, we inspect all the cases with three lines in one flat pencil.

A group of n lines in space can form $n(n-1)/2$ different flat pencils. Fig. 10.2 registers all possible flat pencils for the case $n=6$. Each point on the circle circumference represents a line and each line connecting two points on the circumference of the circle represents a flat pencil. For example, the point 1 on the circumference of the circle represents line \mathbf{l}_1 and the line connecting between point 1 and point 2 on the circumference of the circle represents the flat pencil defined by lines \mathbf{l}_1 and \mathbf{l}_2 .

Figure 10.3 lists all 15 distinct flat pencils formed by lines $\mathbf{l}_1.. \mathbf{l}_6$. Each two-digit number, jk , in the diagram represents a flat pencil formed by lines \mathbf{l}_j and \mathbf{l}_k . The figure presents four different categories of flat pencils: T, R, S, and F categories. Each category includes three or six flat pencils. Flat pencils in each category are similar in a sense that it is sufficient to analyze the singularity of one category member and to apply a similar analysis to all other members of the same category. This process of flat pencil grouping is possible due to similarity of all the kinematic chains of the tripod. The kinematic chain similarity induces cyclic analogy between flat pencil category members; for example T_{12} , T_{23} , and T_{31} are analogous because each one is formed by adjacent prismatic actuator axes. We refer to a category member that is subjected to our singularity analysis as a category representing flat pencil.



We distinguish between constant flat pencils and temporary flat pencils. While a temporary flat pencil is a configuration-dependent flat pencil, i.e., it forms under certain conditions on the configuration variables; a constant flat pencil is configuration independent or, in other words, it is architecture dependent. Hence, we refer to constant flat pencils as architectural flat pencils.

We notice that the F category includes architectural flat pencils and the remaining categories include temporary flat pencils only.

The four categories of flat pencils are:

The T category: $T = \{T_{12}, T_{23}, T_{13}\}$.

The F category: $F = \{F_{14}, F_{25}, F_{36}\}$.

The S category: $S = \{S_{45}, S_{46}, S_{56}\}$.

The R category: $R = \{R_{15}, R_{16}, R_{24}, R_{25}, R_{34}, R_{35}\}$.

The flat pencils are divided into four categories. These categories are tested for singularities by testing a category representing flat pencil and considering the geometrical conditions that lead to singularity. There are four cases; each case corresponds to a different category.

In the following sections, we consider a category representing flat pencil in each category. For every category representing flat pencil defined by lines \mathbf{l}_j and \mathbf{l}_k ($\mathbf{l}_j, \mathbf{l}_k \in \Gamma$) we test all the lines in the complementary group C_{jk} . For every line \mathbf{l}_n in the complementary group ($\mathbf{l}_n \in C_{jk}$) we determine the geometric relations that render or prohibit it from belonging to the flat pencil of lines \mathbf{l}_j and \mathbf{l}_k .

Case 1 line $\mathbf{l}_n \in T_{jk}$, $j, k = 1, 2, 3$, $j \neq k$, $\mathbf{l}_n \in C_{jk}$:

Let T_{12} be a category representing flat pencil. We inspect all cases where T_{12} spans a line $\mathbf{l}_n \in C_{12}$. Based on the symmetry of the tripod, there are three distinct cases: $\mathbf{l}_n = \mathbf{l}_3$, $\mathbf{l}_n = \mathbf{l}_4$, and $\mathbf{l}_n = \mathbf{l}_6$. The case $\mathbf{l}_n = \mathbf{l}_5$ is equivalent to case $\mathbf{l}_n = \mathbf{l}_4$ due to symmetry considerations.

Case 1.1 $\mathbf{l}_n = \mathbf{l}_3$:

The following proof shows that $\mathbf{l}_3 \in T_{12}$ only if the tripod reduces to the planar case, i.e., the moving platform lies in the tripod base plane B_0 .

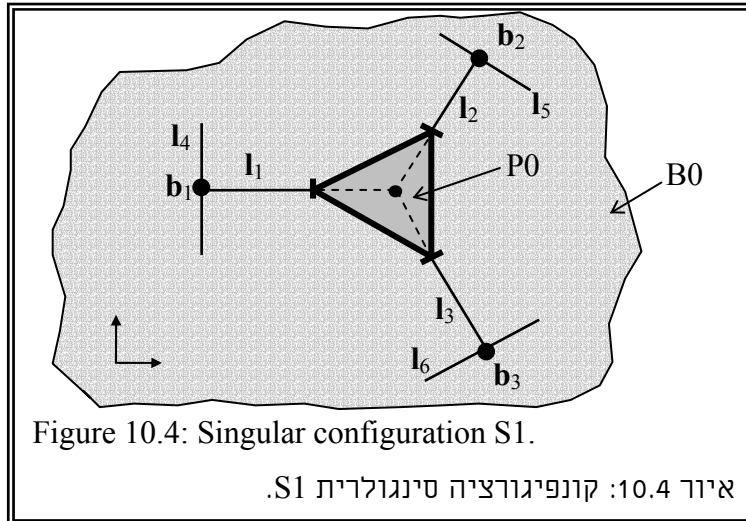
Proof:

- 1) Points \mathbf{p}_i and \mathbf{b}_i define line \mathbf{l}_i , $i=1, 2, 3$.
- 2) Points \mathbf{p}_i define the moving platform plane, P_0 .
- 3) Points \mathbf{b}_i define the base plane B_0 .
- 4) In the case where line $\mathbf{l}_3 \in T_{12}$ all the points \mathbf{p}_i and \mathbf{b}_i ($i = 1, 2, 3$) belong to the same plane, i.e., $\mathbf{p}_i \in {}^P T_{12}$, $\mathbf{b}_i \in {}^P T_{12}$. Therefore, the moving platform lies in the base plane $P_0 = B_0 = {}^P T_{12}$.

This case is shown in Fig 10.4. We refer to this singular configuration as singular configuration S1. The geometric conditions of this singular configuration are:

Singular configuration S1: $B_0 = P_0 \Rightarrow \mathbf{l}_n \in T_{jk}$.

$j, k, n = 1, 2, 3. j \neq k \neq n.$



Since we showed that the configuration in Fig 10.4 is singular, we will henceforth exclude the possibility that the moving platform lies in the tripod base plane.

Case 1.2 $\mathbf{l}_n = \mathbf{l}_4$ (equivalent to $\mathbf{l}_n = \mathbf{l}_5$):

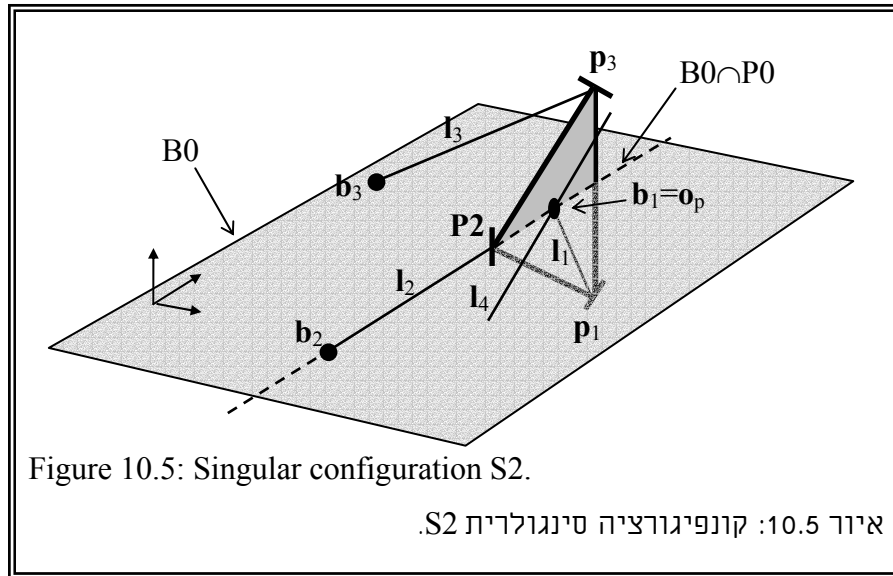
This case leads to a singular configuration S2.

Proof:

- 1) Line \mathbf{l}_4 passes through point \mathbf{b}_1 ($\mathbf{b}_1 \in \mathbf{l}_4$).
- 2) $\mathbf{l}_1 \in P1$, $\mathbf{l}_2 \in P2$ and \mathbf{n} is the intersection line of P1 with P2; therefore, ${}^cT_{12}$ is located along \mathbf{n} .
- 3) In a singular configuration, line \mathbf{l}_4 passes through ${}^cT_{12}$. Point \mathbf{b}_1 fulfills $\mathbf{b}_1 \in P1$, $\mathbf{b}_1 \in B0$ and line \mathbf{l}_4 is perpendicular to P1 ($4 \perp P1$). Hence, line \mathbf{l}_4 intersects \mathbf{n} only when point \mathbf{b}_1 coincides with the piercing point of \mathbf{n} with plane B0, i.e., $\mathbf{b}_1 = \mathbf{n} \cap B0$.
- 4) Lines \mathbf{l}_1 and \mathbf{l}_4 define F_{14} and lines \mathbf{l}_1 and \mathbf{l}_2 define T_{12} such that line \mathbf{l}_1 is the intersection line of the two planes ($\mathbf{l}_1 = {}^pT_{12} \cap {}^pF_{14}$).
- 5) In a singular configuration, line \mathbf{l}_4 lies in ${}^pT_{12}$. Since line \mathbf{l}_4 is not the intersection line of ${}^pF_{14}$ with ${}^pT_{12}$ it lies in ${}^pT_{12}$ only if ${}^pT_{12} = {}^pF_{14}$.
- 6) Points \mathbf{b}_1 , \mathbf{p}_1 , and \mathbf{p}_2 define ${}^pT_{12}$. Line \mathbf{r}_1 and point \mathbf{b}_1 define ${}^pF_{14}$. Since points $\mathbf{b}_1 \in \mathbf{l}_1$, $\mathbf{p}_1 \in \mathbf{l}_1$ and $\mathbf{l}_1 \in {}^pT_{12} \Rightarrow \mathbf{b}_1 \in {}^pT_{12}$ and $\mathbf{p}_1 \in {}^pT_{12}$; therefore, the only condition for fulfilling ${}^pT_{12} = {}^pF_{14}$ is $\mathbf{p}_2 \in {}^pF_{14}$.
- 7) Based on geometric relation A6, line \mathbf{r}_1 and point \mathbf{p}_2 define the plane of the moving platform P0.
- 8) Line \mathbf{r}_1 is the intersection line of the planes P0 and ${}^pF_{14}$. Since point \mathbf{p}_2 is not on \mathbf{r}_1 ($\mathbf{p}_2 \notin \mathbf{r}_1$) then $\mathbf{p}_2 \in {}^pF_{14}$ is fulfilled only when ${}^pF_{14} = P0$, i.e., in this configuration ${}^pT_{12} = {}^pF_{14} = P0$.
- 9) $\mathbf{b}_1 = \mathbf{n} \cap B0$ and $\mathbf{b}_1 \in P0$; therefore, point \mathbf{b}_1 is the center point of the moving platform \mathbf{o}_p , ($\mathbf{b}_1 = \mathbf{o}_p$).
- 10) Singular Configuration S2 is defined such that ${}^pT_{12} = P0$ and $\mathbf{b}_1 = \mathbf{o}_p$. This singular configuration is shown in Fig. 10.5.

Singular configuration S2: ${}^pT_{jk} = P0$, $\mathbf{b}_j = \mathbf{o}_p \Rightarrow \mathbf{l}_n \in T_{jk}$

$$(j, k, n) \in \{(1, 2, 4), (2, 1, 5), (2, 3, 5), (3, 2, 6), (3, 1, 6), (1, 3, 4)\}.$$



Case 1.3 $\mathbf{l}_n = \mathbf{l}_6$:

This case leads to two singular configurations S3 and S4. In these singular configurations, line \mathbf{l}_6 belongs to T_{12} .

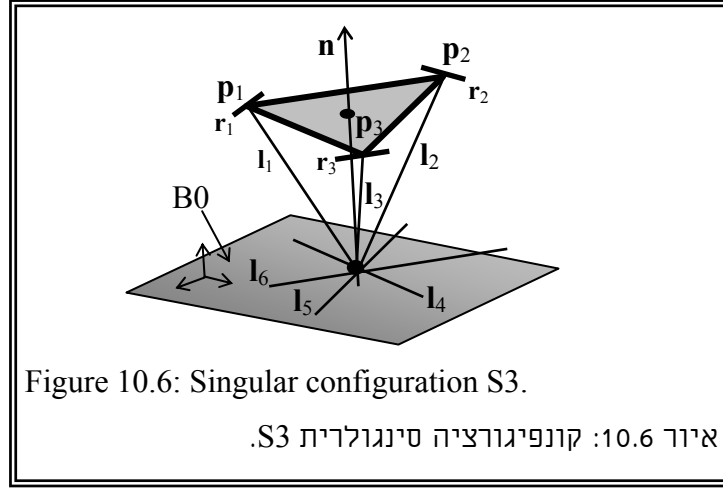
Proof:

- 1) Line \mathbf{l}_6 passes through \mathbf{b}_3 ($\mathbf{b}_3 \in \mathbf{B}$).
- 2) Line \mathbf{l}_6 fulfills $\mathbf{l}_6 \parallel \mathbf{r}_3$.
- 3) If the geometry of the moving platform fulfills $\mathbf{r}_3 \parallel \mathbf{p}_1 \mathbf{p}_2$, then $\mathbf{l}_6 \parallel \mathbf{p}_1 \mathbf{p}_2$.
- 4) $\mathbf{p}_1 \in \mathbf{l}_1, \mathbf{p}_2 \in \mathbf{l}_2 \Rightarrow \mathbf{p}_1 \mathbf{p}_2 \in {}^P T_{12}$.
- 5) $\mathbf{l}_6 \parallel \mathbf{p}_1 \mathbf{p}_2, \mathbf{p}_1 \mathbf{p}_2 \in {}^P T_{12} \Rightarrow \mathbf{l}_6 \parallel {}^P T_{12}$
- 6) In a singular configuration, line \mathbf{l}_6 fulfills $\mathbf{l}_6 \in T_{12}$. Since $\mathbf{l}_6 \parallel {}^P T_{12}$ the condition $\mathbf{b}_3 \in {}^P T_{12}$ is a sufficient condition to fulfill $\mathbf{l}_6 \in {}^P T_{12}$.
- 7) $\mathbf{l}_1 \in P1, \mathbf{l}_2 \in P2$ and \mathbf{n} is the intersection line of P1 with P2; therefore, the center of T_{12} , i.e. ${}^c T_{12}$, is located along \mathbf{n} .
- 8) In a singular configuration, line \mathbf{l}_6 passes through the center of T_{12} . Point \mathbf{b}_3 fulfills $\mathbf{b}_3 \in P3, \mathbf{b}_3 \in B0$ and line \mathbf{l}_6 is perpendicular to P3 ($\mathbf{l}_6 \perp P3$). Hence, line \mathbf{l}_6 intersects \mathbf{n} only when point \mathbf{b}_3 coincides with the piercing point of \mathbf{n} with plane B0, i.e., $\mathbf{b}_3 = \mathbf{n} \cap B0$.
- 9) There are two cases: in the first, ${}^c T_{12}$ is located along \mathbf{n} above the moving platform, and in the second, ${}^c T_{12}$ is located along \mathbf{n} beneath the moving platform.

Singular configuration S3 (${}^cT_{12}$ located beneath the moving platform): Since $\mathbf{b}_3 \in B0$, then singular case S3 occurs when point ${}^cT_{12} \in B0$ and \mathbf{b}_3 is concurrent with it. Therefore, In a singular configuration $\mathbf{b}_3 = \mathbf{n} \cap B0 = {}^cT_{12}$. In this singular configuration points \mathbf{b}_1 , \mathbf{b}_2 , and \mathbf{b}_3 are copunctal. Fig. 10.6 illustrates this singular configuration. The geometric conditions of this singular configuration are:

Singular configuration S3: $\mathbf{b}_1 = \mathbf{b}_2 = \mathbf{b}_3$. $\mathbf{r}_i \parallel \mathbf{p}_j \mathbf{p}_k \Rightarrow \mathbf{l}_n \in T_{jk}$.

$$(j, k, n) \in \{(1, 2, 6), (2, 3, 4), (3, 1, 5)\}. i, j, k = 1, 2, 3. i \neq j \neq k.$$



Singular configuration S4 (${}^cT_{12}$ located above the moving platform): In this singular configuration $\mathbf{b}_3 = {}^cT_{12} \in B0$, $\mathbf{l}_1 \in T_{12}$, $\mathbf{l}_2 \in T_{12}$, $\mathbf{b}_1 \in T_{12}$, $\mathbf{b}_2 \in T_{12}$; therefore ${}^pT_{12} = B0$. This singular configuration is illustrated in Fig. 10.7.

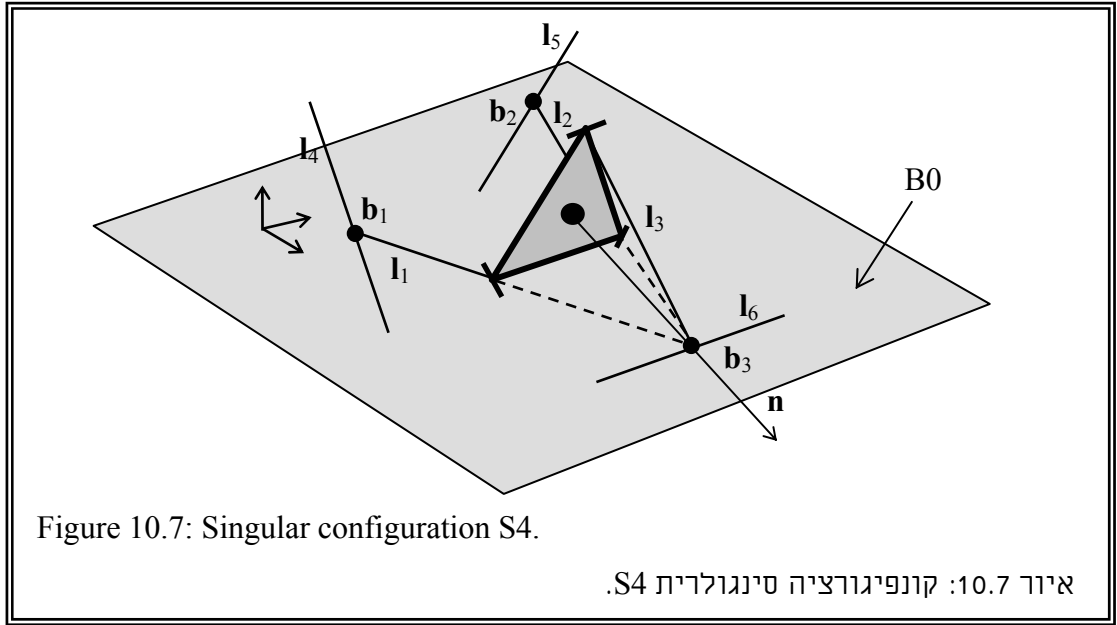
Singular configuration S4: ${}^pT_{jk} = B0$. $\mathbf{r}_i \parallel \mathbf{p}_j \mathbf{p}_k$. $\mathbf{b}_i = {}^cT_{jk} \Rightarrow \mathbf{l}_n \in T_{jk}$.

$$(j, k, n) \in \{(1, 2, 6), (2, 3, 4), (3, 1, 5)\}. i, j, k = 1, 2, 3. i \neq j \neq k.$$

Case 2 line $\mathbf{l}_n \in F_{jk}$. $(j, k) \in \{(1, 4), (2, 5), (3, 6)\}$. $\mathbf{l}_n \in C_{jk}$:

Let F_{14} be a category representing flat pencil. We look for a line $\mathbf{l}_n \in C_{14}$, which is linearly dependent with the generators of F_{14} . Based on the symmetry of the tripod, we consider only two cases: $\mathbf{l}_n = \mathbf{l}_2$ (equivalent to $\mathbf{l}_n = \mathbf{l}_3$), and $\mathbf{l}_n = \mathbf{l}_5$ (equivalent to $\mathbf{l}_n = \mathbf{l}_6$).

Case 2.1 $\mathbf{l}_n = \mathbf{l}_2$ (equivalent to $\mathbf{l}_n = \mathbf{l}_3$): This case is identical to case 1.2 $\mathbf{l}_n = \mathbf{l}_4$.



Case 2.2 $l_n = l_5$ (equivalent to $l_n = l_6$):

This case leads to a new singular configuration S5. In a singular configuration line l_5 belongs to flat pencil F_{14} therefore, the flat pencil S_{45} also exists.

Proof:

- 1) $l_4 \parallel P0$, $l_5 \parallel P0$ [corollary Cr2] ; therefore ${}^pS_{45} \parallel P0$.
- 2) If ${}^pS_{45} \neq {}^pF_{14}$, then l_4 is the intersection line of ${}^pS_{45}$ with ${}^pF_{14}$.
- 3) If ${}^pS_{45} \neq {}^pF_{14}$, then l_5 can not simultaneously fulfill $l_5 \in {}^pS_{45}$ and $l_5 \in {}^pF_{14}$; consequently, both conditions are simultaneously fulfilled only if ${}^pS_{45} = {}^pF_{14}$. Thus, in a singular configuration, $l_5 \in {}^pS_{45}$ and $l_5 \in {}^pF_{14}$; Thus, ${}^pS_{45} = {}^pF_{14}$.
- 4) If ${}^pS_{45} = {}^pF_{14}$, then ${}^pF_{14} \parallel P0$, but since $p_1 \in {}^pF_{14}$ and $p_1 \in P0$ we conclude that in a singular configuration ${}^pS_{45} = {}^pF_{14} = P0$.
- 5) Point b_2 is on line l_5 ($b_2 \in l_5$). Point b_1 is the center of F_{14} ($b_1 = {}^cF_{14}$).
- 6) In a singular configuration $l_5 \in F_{14}$; hence, $b_1 \in l_5$.
- 7) $b_1 \in B0$, $b_2 \in B0 \Rightarrow l_5 \in B0$.
- 8) $r_2 \parallel l_5$ and in a singular configuration $l_5 \in B0$, therefore, $r_2 \parallel B0$.

The singular configuration S5 is illustrated in Fig. 10.8 and Fig. 10.9. This singular configuration is defined as follows:

Singular Configuration S5:

First set: ${}^P F_{jk} = P0, \mathbf{b}_{j+1} \in P0 \Rightarrow \mathbf{l}_n \in F_{jk}.$

$(j, k, n) \in \{(1, 4, 5), (2, 5, 6), (3, 6, 4)\}.$

Second set: ${}^P F_{jk} = P0, \mathbf{b}_{j-1} \in P0 \Rightarrow \mathbf{l}_n \in F_{jk}.$

$(j, k, n) \in \{(1, 4, 6), (2, 5, 4), (3, 6, 5)\}.$

Note: index j follows a cyclic order such that for $j = 3 \Rightarrow j+1 = 1$ and for $j = 1 \Rightarrow j-1 = 3$.

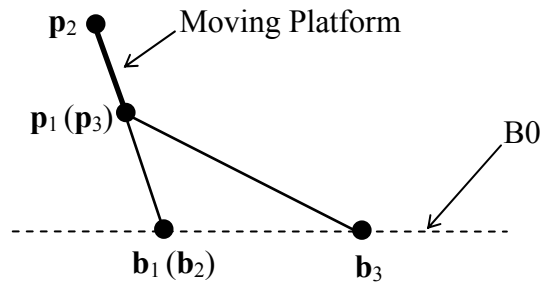


Figure 10.8: Side view of singular configuration S5.

איור 10.8: מבט צד לקונפיגורציה סינגולרית S5.

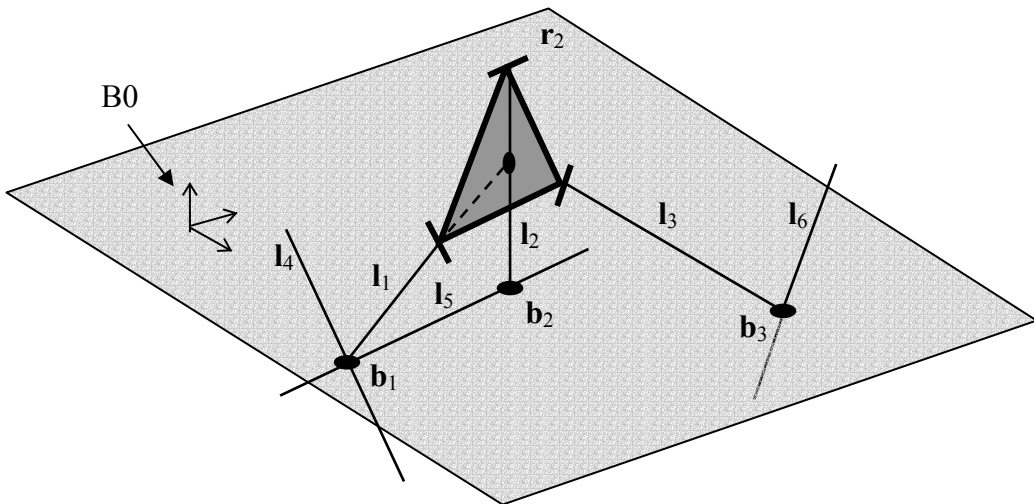


Figure 10.9: Singular configuration S5.

איור 10.9: קונפיגורציה סינגולרית S5.

Case 3 line $\mathbf{l}_n \in S_{jk}$. $(j, k) \in \{(4, 5), (4, 6), (5, 6)\}$. $\mathbf{l}_n \in C_{jk}$:

We choose S_{45} as a category representing flat pencil. In a singular configuration flat pencil S_{45} exists and it spans a line $\mathbf{l}_n \in C_{45}$. There are three distinct cases to be considered. The three cases are $\mathbf{l}_n = \mathbf{l}_1$ (analogous to $\mathbf{l}_n = \mathbf{l}_2$), $\mathbf{l}_n = \mathbf{l}_3$, and $\mathbf{l}_n = \mathbf{l}_6$.

Case 3.1 $\mathbf{l}_n = \mathbf{l}_1$ (equivalent to $\mathbf{l}_n = \mathbf{l}_2$):

This case is the same as case 2.2.

Case 3.2 $\mathbf{l}_n = \mathbf{l}_3$:

This case leads to a singular configuration, which is special case of architectural singular case S1.

Proof:

- 1) $\mathbf{l}_4 \parallel P0$ $\mathbf{l}_5 \parallel P0$ [corollary Cr2] therefore ${}^P S_{45} \parallel P0$.
- 2) Point \mathbf{p}_3 satisfies: $\mathbf{p}_3 \in P0$, $\mathbf{p}_3 \in \mathbf{l}_3$.
- 3) In a singular configuration $\mathbf{l}_3 \in {}^P S_{45}$, therefore, $\mathbf{p}_3 \in {}^P S_{45}$. Consequently, in a singular configuration ${}^P S_{45} = P0$.
- 4) Point \mathbf{b}_3 lies on \mathbf{l}_3 , i.e. $\mathbf{b}_3 \in \mathbf{l}_3$, and in a singular configuration $\mathbf{b}_3 \in {}^P S_{45}$.
- 5) Points \mathbf{b}_1 and \mathbf{b}_2 satisfy: $\mathbf{b}_1 \in \mathbf{l}_4$, $\mathbf{b}_2 \in \mathbf{l}_5$; hence $\mathbf{b}_1 \in {}^P S_{45}$ and $\mathbf{b}_2 \in {}^P S_{45}$.
- 6) We showed that \mathbf{b}_1 , \mathbf{b}_2 , and \mathbf{b}_3 belong to ${}^P S_{45}$; therefore, $B0 = {}^P S_{45} = P0$.

Case 3.3 $\mathbf{l}_n = \mathbf{l}_6$:

The following proof shows that this case leads to singular configurations S6 and S7. In these singular configurations the moving platform is parallel to the tripod base plane.

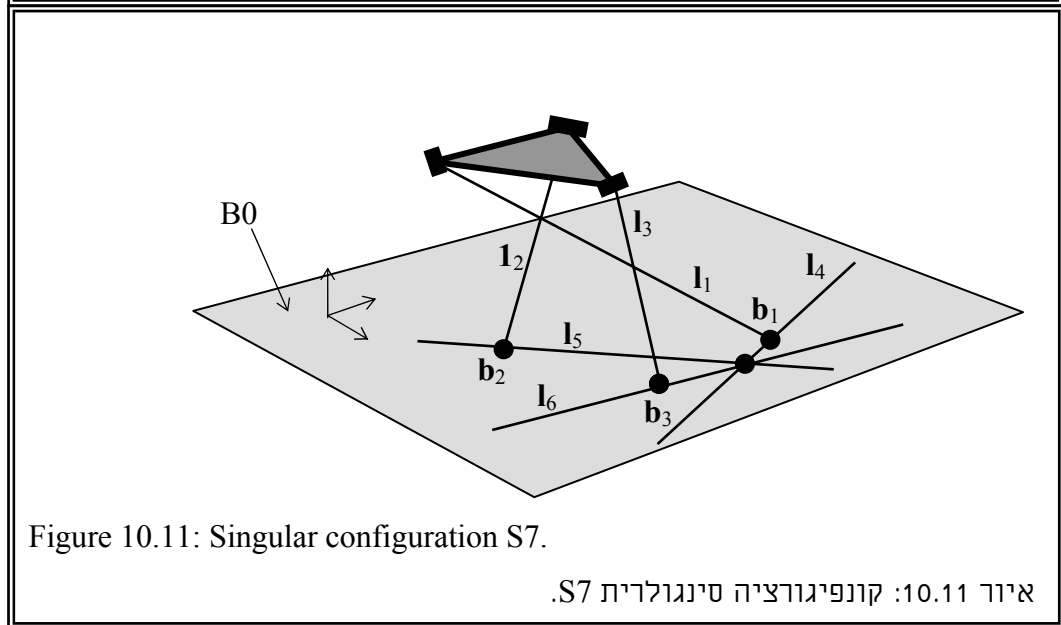
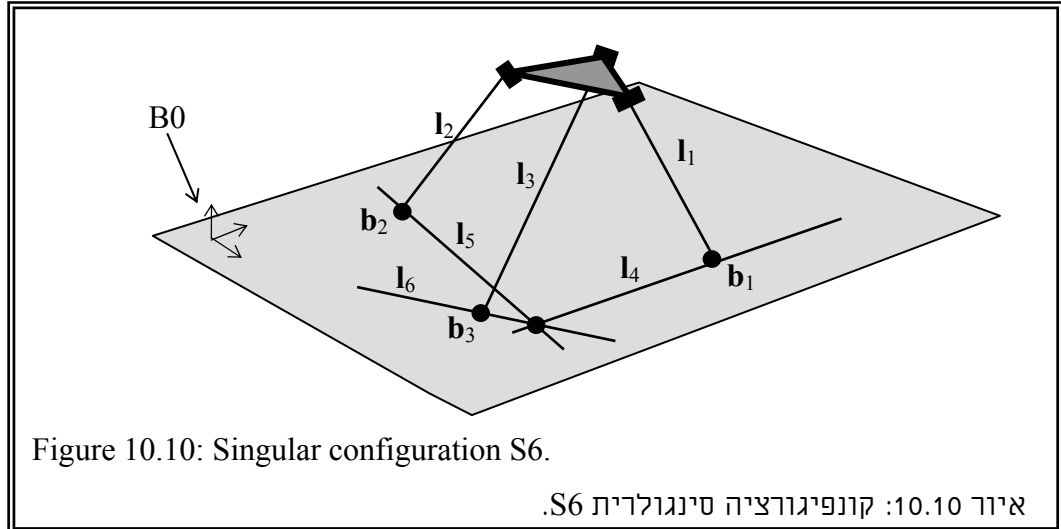
Proof:

- 1) $\mathbf{l}_4 \parallel P0$ $\mathbf{l}_5 \parallel P0$ [corollary Cr2] therefore ${}^P S_{45} \parallel P0$.
- 2) In a singular configuration $\mathbf{l}_6 \in {}^P S_{45}$ and ${}^C S_{45}$ lies on \mathbf{l}_6 .
- 3) $\mathbf{b}_1 \in \mathbf{l}_4$, $\mathbf{b}_2 \in \mathbf{l}_5$ and $\mathbf{b}_3 \in \mathbf{l}_6$; therefore $\mathbf{b}_1 \in {}^P S_{45}$, $\mathbf{b}_2 \in {}^P S_{45}$, $\mathbf{b}_3 \in {}^P S_{45}$ and $B0 = {}^P S_{45}$.

Therefore, $B0 \parallel P0$.

Singular configurations S6 and S7 are illustrated in Fig. 10.10 and Fig. 10.11.

Singular configurations S6, S7: $B0 \parallel P0$. $\mathbf{l}_n \in S_{jk}$.
 $j, k, n = 4, 5, 6$. $j \neq k \neq n$.



Case 4 $\mathbf{l}_n \in R_{jk}$. $(j, k) \in \{(1, 5), (1, 6), (2, 4), (2, 5), (3, 4), (3, 5)\}$. $\mathbf{l}_n \in C_{jk}$:

Let R_{15} be a category representing flat pencil. This case leads to for four cases that we already dealt with.

Case 4.1 $\mathbf{l}_n = \mathbf{l}_2$: This case is the same as case 1.2.

Case 4.2 $\mathbf{l}_n = \mathbf{l}_3$: This case is equivalent to case 1.3 and leads to similar singularity.

Case 4.3 $\mathbf{l}_n = \mathbf{l}_4$: This case is the same like case 2.2 and leads to same singular configurations.

Case 4.4 $\mathbf{l}_n = \mathbf{l}_6$: This case is equivalent to case 3.2 and leads to singular configuration S1.

10.2.5 Planes singularities

This section presents the singular configurations that belong to a rank three system. Therefore, we inspect all the cases, in which, four lines belong to the planes variety.

Regulus Singularities (3A):

The group of lines, $\Gamma = \{l_1..l_6\}$, includes three permanent flat pencils F_{14} , F_{25} , and F_{36} . Consequently, the maximum number of skew lines in Γ is three. We recall that all lines in the same regulus are skew and intersect all the lines in the conjugate regulus [Veblen, 1910]. Based on this fact, if we suppose that lines l_1 , l_2 , l_3 form a regulus, then lines l_4 , l_5 , and l_6 can not belong to this regulus because line l_4 intersects l_1 , l_5 intersects l_2 , and l_6 intersects l_3 . Therefore, no group of more than three lines can belong to the same regulus and singularity of type (3A) is not possible.

Union singularities (3B):

The lines that depend on the generators of a union are all the lines that depend on each of its two flat pencils. Therefore, we need not consider this case since we already considered all the singularities that stem from flat pencil singularities.

Bundle singularities (3C):

A singular bundle includes more than three lines intersecting in a common point. In order to find all singular bundles we register all possible line quadruplets in Γ and we divide them into four different line quadruplet groups.

Table 10.1 lists all the 15 line quadruplets. A singular bundle forms if all the lines in one of these line quadruplets are copunctal. The process of line quadruplet grouping is possible due to the kinematic chain symmetry of the tripod. This table also presents four different quadruplet groups, namely, groups Q1, Q2, Q3 and Q4.

Table 10.1: 15 line quadruplets and their separation into four categories. טבלה 10.1: 15 חבורות של ארבע קווים ופירוט חלוקתם לקבוצות.	
Physical meaning of quadruplet category	Quadruplet category members
Q1: All the quadruplets that include all prismatic actuator axes and one of the lines l_4 , l_5 , l_6 .	$Q1 = \{(l_1 l_2 l_3 l_4), (l_1 l_2 l_3 l_5), (l_1 l_2 l_3 l_6)\}$
Q2: All the quadruplets that include lines associated with adjacent kinematic chains.	$Q2 = \{(l_1 l_2 l_4 l_5), (l_1 l_3 l_4 l_6), (l_2 l_3 l_5 l_6)\}$

Table 10.1: 15 line quadruplets and their separation into four categories – continued. טבלה 10.1: 15 חבורות של ארבע קווים ופירוט חלוקתם לקבוצות – המשך.	
Q3: Any line quadruplet including two lines associated with a first kinematic chain, one prismatic actuator axis associated with a second kinematic chain, and one line from $\{l_4, l_5, l_6\}$ that belongs to a third kinematic chain.	$Q3 = \{(l_1 l_2 l_4 l_6), (l_1 l_3 l_4 l_5), (l_2 l_3 l_4 l_5), (l_1 l_2 l_5 l_6), (l_1 l_3 l_5 l_6), (l_2 l_3 l_4 l_6)\}.$
Q4: All line quadruplets including a constant flat pencil from one kinematic chain, and two other lines from l_4, l_5, l_6 such that each line belongs to either a second or a third kinematic chain.	$Q4 = \{(l_1 l_4 l_5 l_6), (l_2 l_5 l_4 l_6), (l_3 l_6 l_4 l_5)\}$

Case 1 Singularities of Q1 line quadruplets:

Let $(l_1 l_2 l_3 l_6)$ be a category representing line quadruplet. This case leads to singular configurations that are the general cases of singular configurations S3 and S4 in which the geometry of the moving platform does not fulfill $l_6 \parallel p_1 p_2$.

Proof:

- 1) Point b_3 fulfills $b_3 = l_3 \cap l_6$, i.e., $b_3 = {}^c F_{36}$.
- 2) In a singular configuration, lines l_1, l_2, l_3 , and l_6 intersect in one common point.
- 3) Since $b_3 = l_3 \cap l_6$ and $l_3 \neq l_6$ the only possible common point of intersection for lines l_1, l_2, l_3 , and l_6 is b_3 .
- 4) $b_3 \in l_3, l_3 \in P3, l_2 \in P2$, and $l_1 \in P1$; therefore, the intersection is possible only along $n = P1 \cap P2 \cap P3$, i.e., $b_3 \in n$.
- 5) $b_3 \in B0$ and in a singular configuration $b_3 \in n$; therefore $b_3 = n \cap B0$, namely, b_3 is the piercing point of n with the tripod base plane $B0$.
- 6) In a singular configuration ${}^c T_{12} = {}^c F_{36} = b_3$. Therefore, there are two possibilities.
The first is when ${}^c T_{12}$ is located above the moving platform, and the second is when ${}^c T_{12}$ is located beneath the moving platform.
- 7) If ${}^c T_{12}$ is beneath the moving platform it means that $b_1 = b_2 = b_3$; therefore, this is the singular configuration S3.

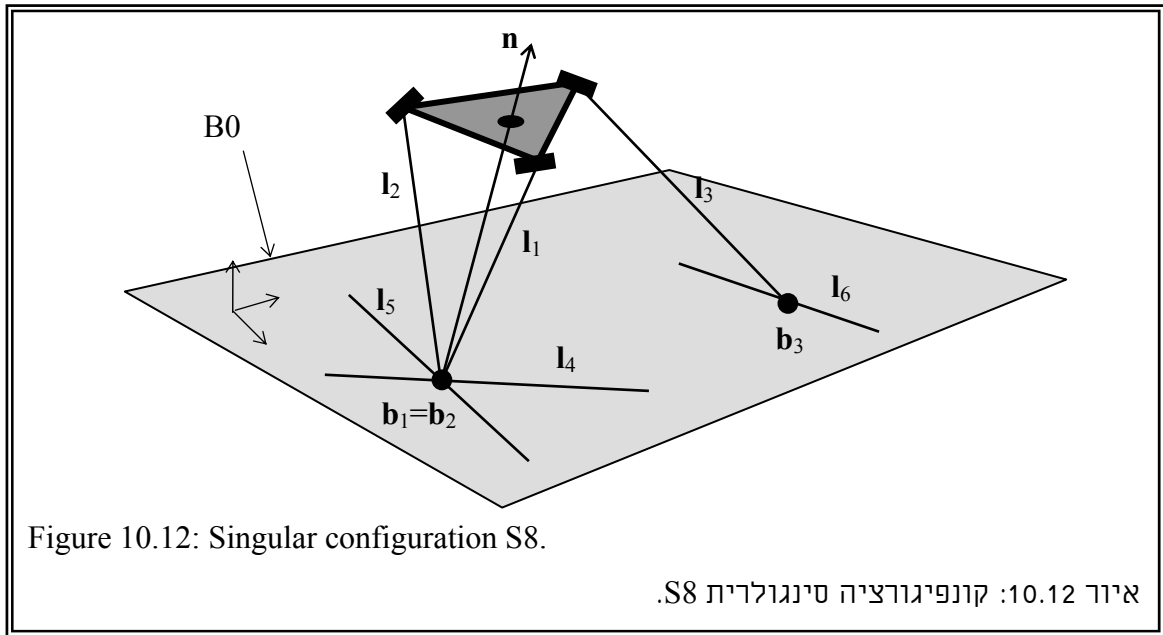
- 8) If ${}^cT_{12}$ is above the moving platform then in this configuration $\mathbf{l}_1 = \mathbf{b}_1\mathbf{b}_3$ and $\mathbf{l}_2 = \mathbf{b}_2\mathbf{b}_3$, therefore, $\mathbf{l}_1 \in B0$, $\mathbf{l}_2 \in B0$. This singular configuration was already presented in Fig. 10.7. This is the general case of singular configuration S4.

Case 2 Singularities of Q2 line quadruplets:

Let $(\mathbf{l}_1 \mathbf{l}_2 \mathbf{l}_4 \mathbf{l}_5)$ be a category representing line quadruplet. This line quadruplet forms a singular bundle if a pair of spherical joints coincides. We designate this singular configuration as S8. Fig. 10.12 illustrates this singular configuration.

Proof:

- 1) $\mathbf{b}_1 = \mathbf{l}_1 \cap \mathbf{l}_4$, $\mathbf{b}_2 = \mathbf{l}_2 \cap \mathbf{l}_5$; therefore the only possible intersection point for the four distinct lines is $\mathbf{b}_1 = \mathbf{b}_2$.
- 2) $\mathbf{b}_1 \in P1$, $\mathbf{b}_2 \in P2$; consequently, the intersection point $\mathbf{b}_1 = \mathbf{b}_2$ is located along $\mathbf{n} = P1 \cap P2$.
- 3) $\mathbf{b}_1 \in B0$, $\mathbf{b}_2 \in B0$; therefore, in a singular configuration $\mathbf{b}_1 = \mathbf{b}_2 = \mathbf{n} \cap B0$, i.e., the spherical joints coincide at the piercing point of \mathbf{n} with the tripod base plane, B0.



Singular configuration S8: $\mathbf{b}_j = \mathbf{b}_k$, $j, k=1,2,3$, $j \neq k$.

Case 3 Singularities of Q3 lines quadruplets:

All the line quadruplets in this category lead to singular configuration S8. We choose $(\mathbf{l}_1 \mathbf{l}_2 \mathbf{l}_4 \mathbf{l}_6)$ as a category representing quadruplet and present the following proof.

Proof:

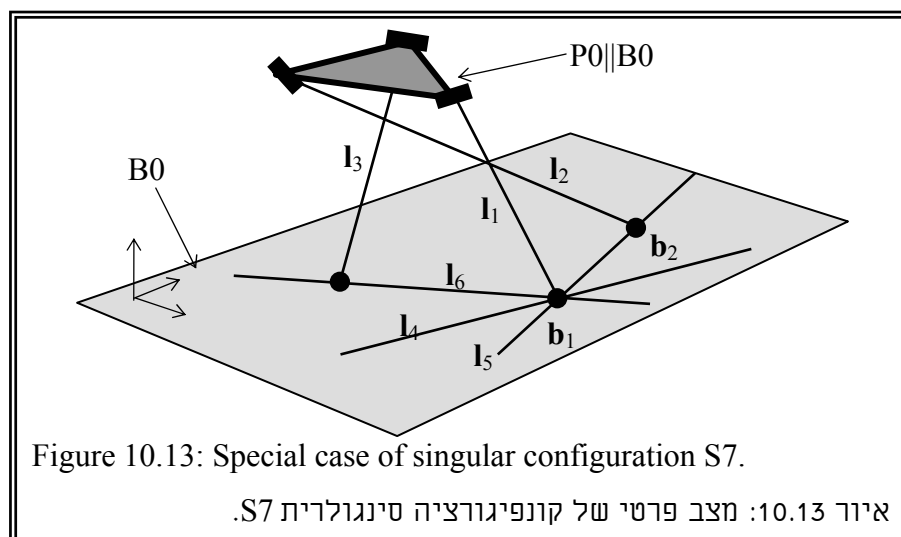
- 1) Point \mathbf{b}_1 fulfills $\mathbf{b}_1 \in B0$, $\mathbf{b}_1 = \mathbf{l}_1 \cap \mathbf{l}_4$; therefore, in a singular configuration all distinct lines \mathbf{l}_1 , \mathbf{l}_2 , \mathbf{l}_4 , and \mathbf{l}_6 intersect in point \mathbf{b}_1 .
- 2) $\mathbf{l}_1 \in P1$, $\mathbf{l}_2 \in P2$; thus, the intersection points of these lines is located along $\mathbf{n} = P1 \cap P2$.
- 3) In a singular configuration line \mathbf{l}_2 intersects \mathbf{l}_1 in point \mathbf{b}_1 . Therefore, $\mathbf{b}_1 = {}^cT_{12}$.
- 4) $\mathbf{b}_2 = \mathbf{l}_2 \cap B0$, i.e., \mathbf{b}_2 is the piercing point of \mathbf{l}_2 with the tripod base plane. This means that $\mathbf{b}_1 = \mathbf{b}_2 = {}^cT_{12}$. Consequently, this configuration is singular configuration S8 shown in Fig. 10.12.

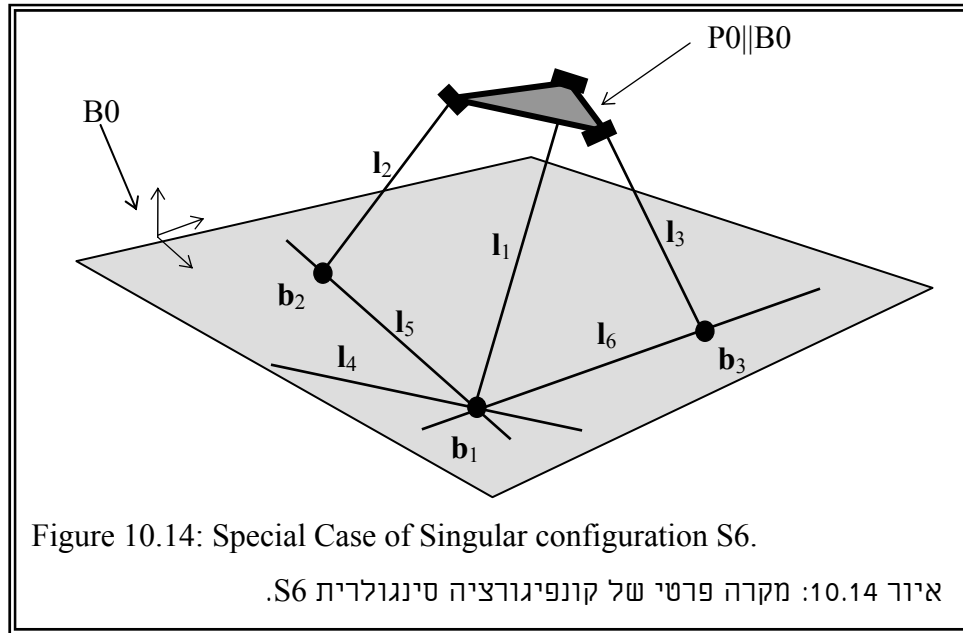
Case 4 Singularities of Q4 lines quadruplets:

This case leads to two singular configurations which are special cases of singular configurations S6 and S7. To prove this we select $(\mathbf{l}_1 \mathbf{l}_4 \mathbf{l}_5 \mathbf{l}_6)$ to be a category representing quadruplet.

Proof:

- 1) $\mathbf{b}_1 = \mathbf{l}_1 \cap \mathbf{l}_4$; therefore, in a singular configuration, \mathbf{b}_1 is the common intersection point of all lines in the quadruplet.
- 2) $\mathbf{l}_6 \parallel \mathbf{P0}$, $\mathbf{l}_5 \parallel \mathbf{P0}$ [corollary Cr2]; thus, ${}^P\mathbf{S}_{56} \parallel \mathbf{P0}$.
- 3) $\mathbf{b}_1 \in \mathbf{B0}$ and in a singular configuration $\mathbf{b}_1 = {}^c\mathbf{S}_{56}$; therefore ${}^c\mathbf{S}_{56} \in \mathbf{B0}$.
- 4) Points \mathbf{b}_2 , \mathbf{b}_3 and ${}^c\mathbf{S}_{56}$ define ${}^P\mathbf{S}_{56}$. Since all these points belong to $\mathbf{B0}$ we conclude that in a singular configuration $\mathbf{B0} \parallel \mathbf{P0}$, i.e., the tripod base plane and the moving platform are parallel. Fig. 10.13 and 10.14 present the two special cases of singular configurations S6 and S7.





Plane singularities (3D):

Singularities of type 3D are characterized by having more than three coplanar lines in the group $\Gamma = \{l_1, l_2, l_3, l_4, l_5, l_6\}$. Therefore, we inspect all the line quadruplets to determine the singularities that stem from this case.

There are four line quadruplet groups as we already presented in table 10.1. We consider the cases, in which, a category representing line quadruplet is coplanar.

Case 1 Q1 coplanar line quadruplet:

All lines in this category are coplanar only if the moving platform lies in the tripod base plane. We choose (l_1, l_2, l_3, l_4) as a category representing line quadruplet.

Proof:

- 1) Lines l_1, l_2 and l_3 pierce the plane of the moving platform, P_0 , in points p_1, p_2 , and p_3 respectively. Since these points are not collinear, [geometric relation A1], then these lines lie in one plane only if this plane is the plane of the moving platform P_0 .
- 2) Line l_4 is parallel to the moving platform; therefore, if lines l_1, l_2 , and l_3 lie in the plane of the moving platform, then also l_4 lies in this plane.
- 3) Points b_1, b_2 , and b_3 lie on lines $l_1, 2$, and 3 , respectively; therefore, they belong to P_0 and the moving platform lies in the tripod base plane.

Case 2 Q2 coplanar line quadruplet:

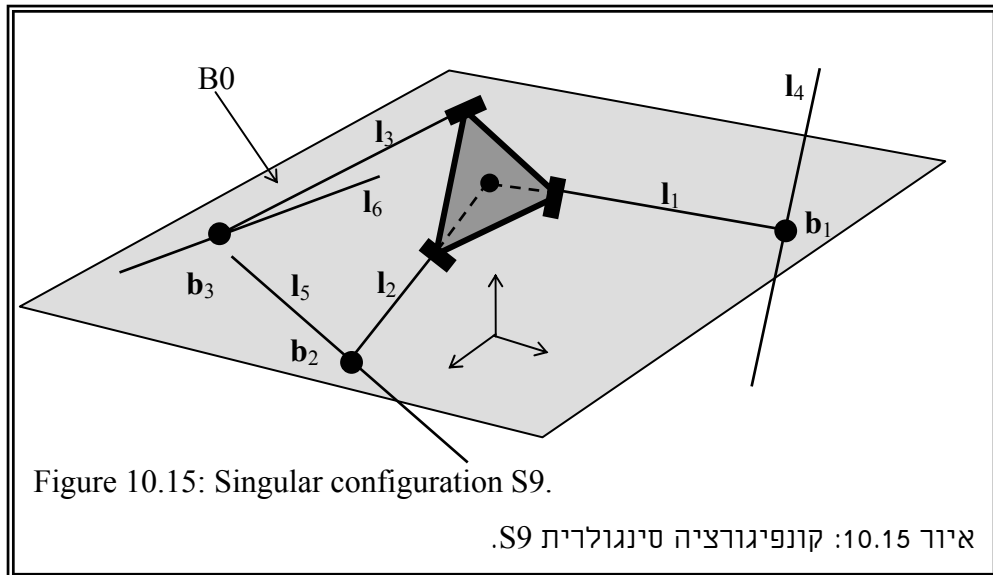
The quadruplets in Q2 lie in one plane if two of the prismatic actuator axes lie in the plane of the moving platform. We choose (l_1, l_2, l_4, l_5) as a category representing line quadruplet.

Proof:

- 1) Lines \mathbf{l}_4 and \mathbf{l}_5 are parallel to the moving platform. $\mathbf{l}_4 \parallel \mathbf{r}_1$, $\mathbf{l}_5 \parallel \mathbf{r}_2$, [geometric relation A4]. The plane they define, ${}^P S_{45}$, is parallel to P_0 .
- 2) Points \mathbf{b}_1 and \mathbf{b}_2 lie on both planes ${}^P S_{45}$ and ${}^P T_{12}$, therefore line $\mathbf{b}_1\mathbf{b}_2$ is the intersection line of these two planes.
- 3) Points \mathbf{b}_1 and \mathbf{p}_1 define line \mathbf{l}_1 . Similarly, points \mathbf{b}_2 and \mathbf{p}_2 define line \mathbf{l}_2 .
- 4) $\mathbf{p}_1 \in P_0$, $\mathbf{p}_2 \in P_0$. Points \mathbf{p}_1 and \mathbf{p}_2 lie on the plane ${}^P S_{45}$ only if ${}^P S_{45} = P_0$.

Figure 10.15 presents singular configuration S9. This singular configuration occurs when two lines out of $\mathbf{l}_1, \mathbf{l}_2, \mathbf{l}_3$ lie in the plane of the moving platform.

Singular configuration S9: $\mathbf{l}_j \in P_0, \mathbf{l}_k \in P_0, j, k = 1, 2, 3, j \neq k$.



Case 3 Q3 coplanar line quadruplet:

All line quadruplets in this category are coplanar only if the tripod reduces to the planar case. We choose $(\mathbf{l}_1 \mathbf{l}_2 \mathbf{l}_4 \mathbf{l}_6)$ as a category representing line quadruplet and present the following proof.

Proof:

- 1) Line \mathbf{r}_1 fulfills: $\mathbf{r}_1 \in P_0$, $\mathbf{r}_1 \parallel \mathbf{l}_4$; therefore \mathbf{r}_1 is the intersection line of plane P_0 and ${}^P F_{14}$, ($\mathbf{r}_1 = P_0 \cap {}^P F_{14}$).

- 2) Line \mathbf{l}_2 pierces P_0 in point \mathbf{p}_2 . In singular configuration line \mathbf{l}_2 lies in ${}^P F_{14}$; therefore, point \mathbf{p}_2 lies in the plane ${}^P F_{14}$.
- 3) Point \mathbf{p}_2 does not lie on \mathbf{r}_1 , ($\mathbf{p}_2 \notin \mathbf{r}_1$); therefore it lies in ${}^P F_{14}$ only if ${}^P F_{14} = P_0$. Therefore, Point \mathbf{b}_1 fulfills $\mathbf{b}_1 \in P_0$.
- 4) In this case Line \mathbf{l}_2 lies in P_0 if $\mathbf{b}_2 \in P_0$.
- 5) Line \mathbf{l}_6 is parallel to \mathbf{r}_3 and \mathbf{r}_3 lies in P_0 ; therefore, it is parallel to P_0 . $\mathbf{l}_6 \parallel P_0$.
- 6) $\mathbf{b}_3 \in \mathbf{l}_6$ and $\mathbf{l}_6 \parallel P_0$, thus, line \mathbf{l}_6 lies in P_0 only when point \mathbf{b}_3 lies in P_0 . Therefore, the moving platform lies in the tripod base plane.

Case 4 Q4 coplanar line quadruplet:

Let $(\mathbf{l}_1 \mathbf{l}_4 \mathbf{l}_5 \mathbf{l}_6)$ be a category-representing line quadruplet. The following proof shows that all line quadruplets in this category lie in one plane only if the moving platform lies in the tripod base plane.

Proof:

- 1) $\mathbf{b}_1 \in \mathbf{l}_4$, $\mathbf{b}_2 \in \mathbf{l}_5$, $\mathbf{b}_3 \in \mathbf{l}_6$.
- 2) $\mathbf{l}_4 \parallel \mathbf{r}_1$, $\mathbf{l}_5 \parallel \mathbf{r}_2$, $\mathbf{l}_6 \parallel \mathbf{r}_3$; therefore, in a singular configuration, these lines define a plane parallel to the plane P_0 and this plane is the tripod base plane, B_0 .
- 3) Line \mathbf{l}_1 pierces P_0 in point \mathbf{p}_1 . It also pierces the plane B_0 in point \mathbf{b}_1 ; therefore, line \mathbf{l}_1 lies in B_0 if point \mathbf{p}_1 lies in B_0 . Because $B_0 \parallel P_0$ then $\mathbf{p}_1 \in B_0$ only if $B_0 = P_0$.

10.2.6 Linear Congruence singularities

This section presents the singularities that stem from having five lines in one linear congruence.

Elliptic congruence (4A):

Four skew lines in space form three distinct reguli and a fifth line is linearly dependent with them if it belongs to one of these reguli. Elliptic congruence singularities are not possible in our case since there are no four lines in the same regulus (see case 3A).

Hyperbolic congruence (4B):

Four lines concurrent with two other skew lines form a hyperbolic congruence. Any fifth line concurrent with the same two skew lines is linearly dependent with the four lines.

A group of six lines contains six line quintuplets. These line quintuplets are $(l_1 l_2 l_3 l_4 l_5)$, $(l_1 l_2 l_3 l_4 l_6)$, $(l_1 l_2 l_3 l_5 l_6)$, $(l_1 l_2 l_4 l_5 l_6)$, $(l_1 l_3 l_4 l_5 l_6)$, and $(l_2 l_3 l_4 l_5 l_6)$. We notice that all these groups contain two constant flat pencils of type F. In a singular configuration all the lines in one of these groups are concurrent with two skew lines, l_a and l_b . Since each group has two constant flat pencils of type F the line l_a is defined by the centers of these flat pencils. We notice that there are two distinct categories of line quintuplets; therefore, we define F1 and F2 quintuplet categories as follows:

$$F1 = \{(l_1 l_2 l_3 l_4 l_5), (l_1 l_2 l_3 l_4 l_6), (l_1 l_2 l_3 l_5 l_6)\}.$$

$$F2 = \{(l_1 l_2 l_4 l_5 l_6), (l_1 l_3 l_4 l_5 l_6), (l_2 l_3 l_4 l_5 l_6)\}.$$

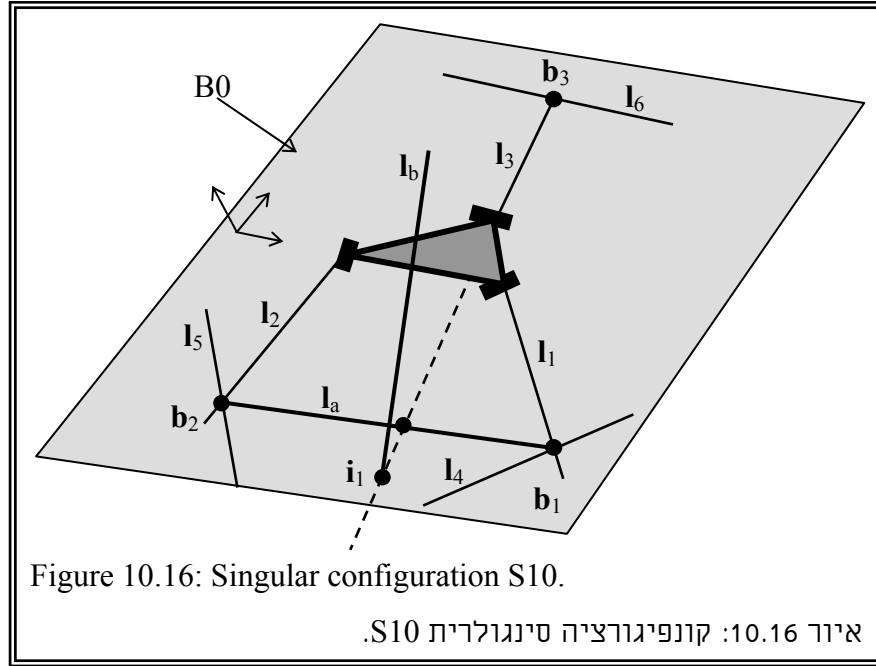
Case 1 F1 line quintuplets:

Let $(l_1 l_2 l_3 l_4 l_5)$ be a category-representing line quintuplet. This line quintuplet contains the architecture constant flat pencils F_{14} and F_{25} . Two skew lines l_a and l_b that intersect the lines l_1 , l_2 , l_4 , and l_5 are defined such that $l_a = {}^c F_{14} {}^c F_{25}$ and line l_b is the intersection line between the planes defined by these flat pencils, i.e., $l_b = {}^p F_{14} \cap {}^p F_{25}$. We look for a fifth line, l_3 , which intersects lines l_a and l_b . The following proof presents a new singular configuration S10.

Proof:

- 1) $l_a = {}^c F_{14} {}^c F_{25}$, $l_b = {}^p F_{14} \cap {}^p F_{25}$.
- 2) $b_1 = {}^c F_{14}$, $b_2 = {}^c F_{25}$; therefore $l_a \in B0$.
- 3) Line l_3 rotates in the plane $P3$, i.e., $l_3 \in P3$.
- 4) Let i_1 be the piercing point of line l_b with the plane $P3$, i.e., $i_1 = l_b \cap P3$. If line l_3 intersects l_a and passes through point i_1 , then a singular configuration of type 4B forms. In particular, if the intersection line l_b lies in plane $P3$, then line l_3 will always intersect it.
- 5) $b_3 \in B0$ and $l_a \in B0$. There are two possibilities for line l_3 to intersect l_a : in the first, line l_3 does not lie in the tripod base plane, therefore, it intersects l_a only if point b_3 lies on l_a . In this case, a singular special complex forms; therefore, this case will be presented under the special complex singularities. The second possibility is $l_3 \in B0$, i.e., line l_3 lies in the base plane; therefore, it intersects l_a .
- 6) If $l_3 \in B0$ then singularity occurs if point i_1 lies along line l_3 . Figure 10.16 presents this singular configuration.

Singular configuration S10: $\mathbf{l}_n \in B0$, ${}^pF_{j,j+3} \cap {}^pF_{k,k+3} \cap B0 \in \mathbf{l}_n$
 $j, k, n = 1, 2, 3. j \neq k \neq n.$



Case 2 F2 category:

Let $(\mathbf{l}_1 \mathbf{l}_2 \mathbf{l}_4 \mathbf{l}_5 \mathbf{l}_6)$ be a category-representing group. Like in case 1, \mathbf{l}_a and \mathbf{l}_b are defined such that $\mathbf{l}_a = {}^cF_{14} {}^cF_{25}$, $\mathbf{l}_b = {}^pF_{14} \cap {}^pF_{25}$. We define points \mathbf{i}_1 and \mathbf{i}_2 such that \mathbf{i}_1 is the intersection point of line \mathbf{l}_1 with ${}^pF_{25}$ and \mathbf{i}_2 the intersection point of \mathbf{l}_4 with ${}^pF_{25}$. Additionally, we define point \mathbf{i}_3 as the intersection point of \mathbf{l}_b with the base plane. This case introduces new singular configuration S11. In this singular configuration lines $\mathbf{l}_1, \mathbf{l}_2, \mathbf{l}_4, \mathbf{l}_5$, and \mathbf{l}_6 are concurrent with two skew lines \mathbf{l}_a and \mathbf{l}_b .

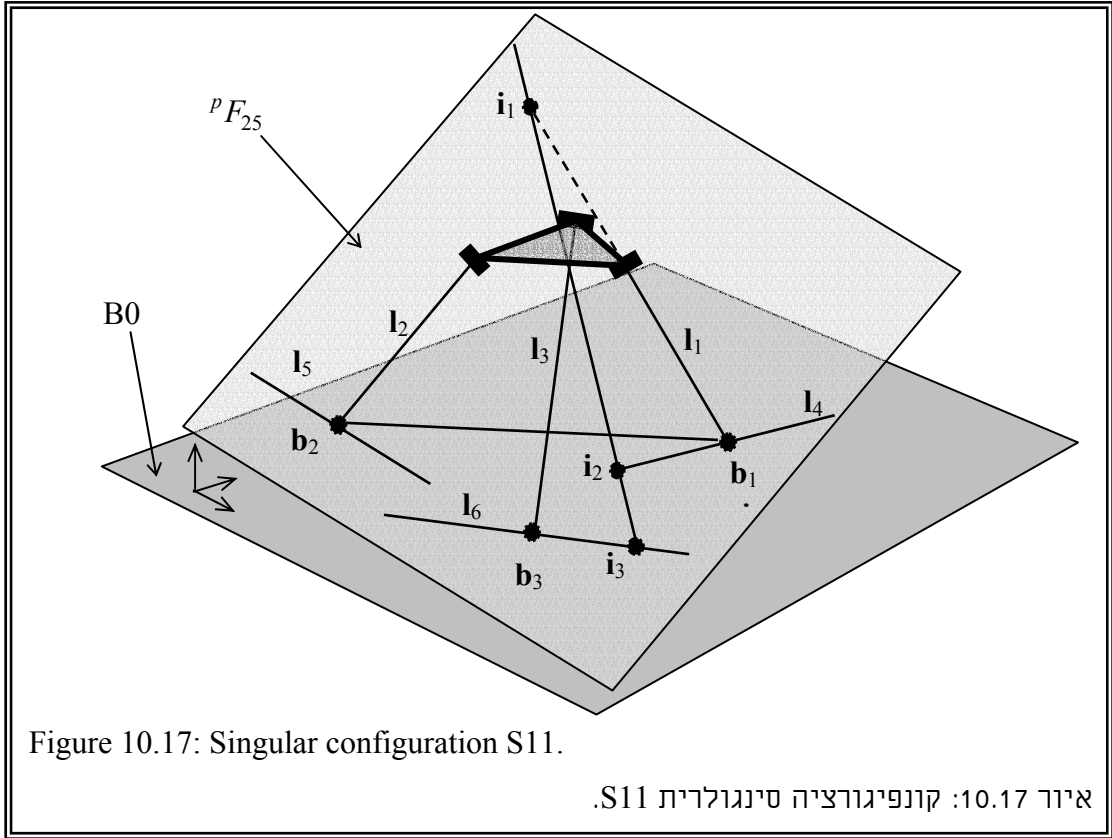
Proof:

- 1) $\mathbf{b}_3 \in B0$ and line \mathbf{l}_6 passes through \mathbf{b}_3 .
- 2) In a singular configuration, line \mathbf{l}_6 intersects \mathbf{l}_a .
- 3) $\mathbf{l}_a \in B0$, therefore, excluding the case where $\mathbf{b}_3 \in \mathbf{l}_a$, in a singular configuration line \mathbf{l}_6 lies in the tripod base plane.
- 4) line \mathbf{l}_b is defined by points \mathbf{i}_1 and \mathbf{i}_2 .
- 5) if \mathbf{l}_6 passes through point \mathbf{i}_3 , then all the five lines $\mathbf{l}_1, \mathbf{l}_2, \mathbf{l}_4, \mathbf{l}_5$, and \mathbf{l}_6 are concurrent with \mathbf{l}_a and \mathbf{l}_b .

Figure 10.17 presents singular configuration S11.

Singular configuration S11: $l_n \in B0$, ${}^pF_{j,j+3} \cap {}^pF_{k,k+3} \cap B0 \in l_n$.

$(j, k, n) \in \{(1, 2, 6), (2, 3, 4), (3, 1, 5)\}$.



Parabolic congruence (4C):

This case unifies all flat pencil singularities related with one or more flat pencils of the parabolic congruence, therefore, it does not add new singular configurations.

Degenerate congruence (4D):

The lines that dependent on the four generators of a degenerate congruence are the lines of a plane (3D) and the lines that pierce this plane in a common point. Accordingly, we have to inspect the case, in which there are two lines piercing in a common point the plane defined by the other three lines.

A group of six lines has 20 line triplets. Table 10.2 lists all these line triplets and presents six groups of them, U1..U6. We consider all the cases in which these line triplets are coplanar and two other lines intersect their plane in a common point.

Case 1 U1 line triplets:

This category includes only one line triplet. The lines in the triplet (l_1, l_2, l_3) are coplanar only when the moving platform lies in the tripod base plane. This was already proved in flat pencil singularities (2B) in case 1.1.

Table 10.2: Complete listing of all 20 line-triplets and their separation into six groups. טבלה 10.2: רישום כל 20 שלישיות הקווים וחלוקתם לשש קבוצות.
$U1 = \{(l_1 l_2 l_3)\}$
$U2 = \{(l_1 l_3 l_5), (l_2 l_3 l_4), (l_1 l_2 l_6)\}$
$U3 = \{(l_1 l_2 l_4), (l_1 l_2 l_5), (l_1 l_3 l_5), (l_1 l_3 l_6), (l_2 l_3 l_5), (l_2 l_3 l_6)\}$
$U4 = \{(l_1 l_4 l_5), (l_1 l_4 l_6), (l_2 l_5 l_6), (l_3 l_5 l_6), (l_3 l_4 l_6), (l_2 l_4 l_5)\}$
$U5 = \{(l_1 l_5 l_6), (l_2 l_4 l_6), (l_3 l_4 l_5)\}$
$U6 = \{(l_4 l_5 l_6)\}$

Case 2 U2 line triplets:

Let $(l_1 l_3 l_5)$ be a category-representing triplet. We assume that lines $(l_1 l_3 l_5)$ are coplanar. Therefore, lines l_1 and l_3 define the flat pencil ${}^pT_{13}$. There are two cases to be considered. In the first, lines l_4 and l_6 intersect ${}^pT_{13}$ in a single point, and in the second, lines l_2 and l_6 intersect ${}^pT_{13}$ in one point.

Case 2.1 lines l_4 and l_6 intersect ${}^pT_{13}$ in one point:

${}^pT_{13}$ is defined by lines l_1 and l_3 . Lines l_4 and l_6 pierce ${}^pT_{13}$ in points b_1 and b_3 , respectively. Therefore, these lines intersect ${}^pT_{13}$ in one point only if $b_1=b_3$. This is the singular case S8.

Case 2.2 lines l_2 and l_6 intersect ${}^pT_{13}$ in one point:

This case also leads to singular configuration S8.

Proof:

- 1) Line l_2 rotates in the plane $P2$, $l_2 \in P2$.
- 2) The center of T_{13} lies along the normal, ${}^cT_{13} \in n$.
- 3) b_3 is the intersection point of line l_6 with ${}^pT_{13}$, $b_3 = l_6 \cap {}^pT_{13}$.
- 4) If line l_2 and l_6 intersect ${}^pT_{13}$ in one point, then this point must be b_3 .
- 5) $b_3 \in P3$ and $l_2 \in P2$, therefore, line l_2 may pass through b_3 only if $b_3 \in n$.

6) If $\mathbf{b}_3 \in \mathbf{n}$ then since lines \mathbf{l}_1 and \mathbf{l}_3 define flat pencil T_{13} then $\mathbf{b}_3 = {}^c T_{13}$.

Therefore $\mathbf{b}_1 = \mathbf{b}_3 \in {}^p T_{13}$ and this is singular configuration S8.

Case 3 U3 line triplets:

All the line triplets in this category include one flat pencil of type F. Let $(\mathbf{l}_1 \mathbf{l}_2 \mathbf{l}_4)$ be a category-representing line triplet. Based on the proof in flat pencil singularity (2B) case 1.2, the lines in this line triplet are coplanar only if lines \mathbf{l}_1 and \mathbf{l}_2 lie in the moving platform plane, P_0 . In this case line \mathbf{l}_5 also lies in the moving platform plane, therefore this case leads to singular configuration S9 in Fig. 10.15.

Case 4 U4 line triplets:

We examine the line triplet $(\mathbf{l}_1, \mathbf{l}_4, \mathbf{l}_5)$ as a category representing one. In flat pencil singularity analysis, case 2.2, we proved that the lines of this triplet are coplanar only if they lie in the moving platform plane, P_0 . In this case also line \mathbf{l}_2 lies in P_0 since it is defined by point $\mathbf{b}_2 \in \mathbf{l}_5$ and $\mathbf{p}_2 \in P_0$. Therefore, this is singular configuration S9 in Fig. 10.15.

Case 5 U5 line triplets:

This case leads to singular configuration S1. We already proved in flat pencil singularity analysis, case 3.2, that the lines in the category representing line triplet $(\mathbf{l}_3, \mathbf{l}_4, \mathbf{l}_5)$ are coplanar only if the moving platform lies in the tripod base plane.

Case 6 U6 line triplets:

Based on flat pencil singularity analysis, case 3.3, the lines $(\mathbf{l}_4, \mathbf{l}_5, \mathbf{l}_6)$ are coplanar if the moving platform and the tripod base plane are parallel. Two lines from the group $(\mathbf{l}_1, \mathbf{l}_2, \mathbf{l}_3)$ intersect the tripod base plane in a common point only if two of the spherical joints coincide. This leads to a special case of singular configuration S8 in Fig. 10.12.

10.2.7 Linear complex singularities

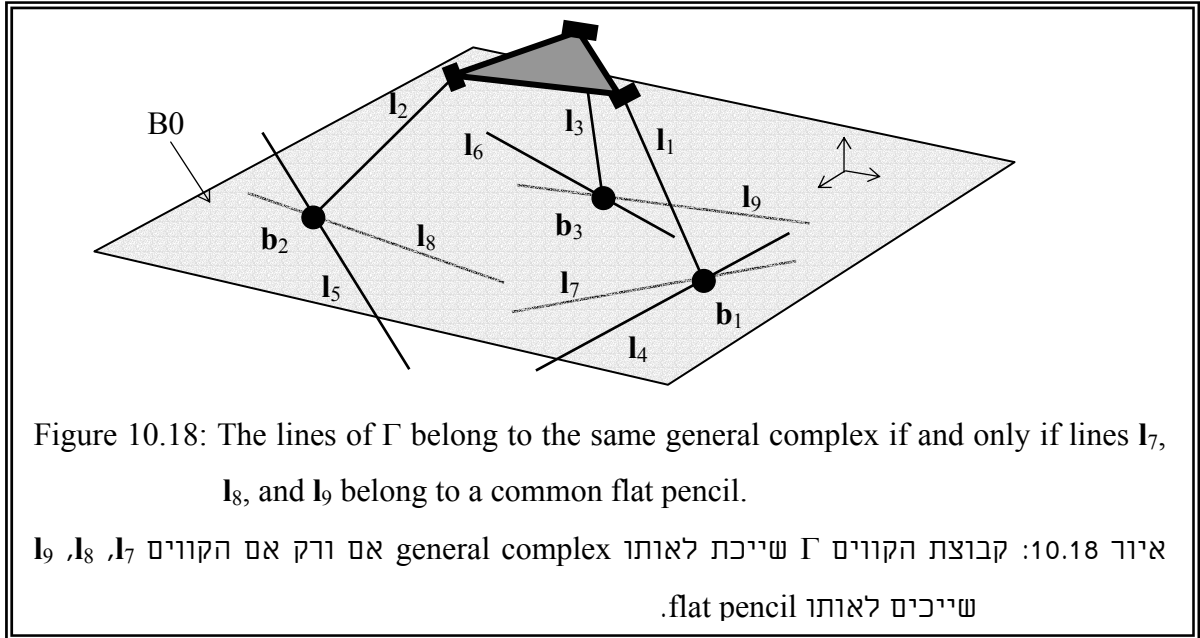
A group of six lines degenerates from the space variety to the linear complex variety in two ways. If all the six lines belong to a general spatial linear pentagon, then singularity of the general complex occurs. If all the six lines intersect one common line, then a singularity of the special complex occurs.

Case 1 Six lines in a general complex (5A):

Table 9.5 presents eight equivalent cases to the general complex. We note that all the line quintuplets include two architecture constant flat pencils. Therefore, the equivalent case in the table is the third case, i.e., case 5A-(3).

There are six line quintuplets in $\Gamma=\{l_1..l_6\}$. All these line quintuplets include two architecture constant flat pencils. We define lines l_7 , l_8 , and l_9 as the intersection lines of the flat pencils F_{14} , F_{25} , F_{36} with the base plane B_0 , respectively (Fig. 10.18).

$$l_7 = {}^pF_{14} \cap B_0 \quad l_8 = {}^pF_{25} \cap B_0 \quad l_9 = {}^pF_{36} \cap B_0$$



Lines l_7 , l_8 , and l_9 are linearly dependent with the flat pencil generators of F_{14} , F_{25} , F_{36} and, vice versa, lines l_1 , l_2 , and l_3 are linearly dependent with the flat pencils generated by the line pairs $(l_4 l_7)$, $(l_5 l_8)$, and $(l_6 l_9)$. Similarly, lines l_4 , l_5 and l_6 are linearly dependent with the flat pencils generated by the line pairs $(l_1 l_7)$, $(l_2 l_8)$, and $(l_3 l_9)$.

Based on theorem 1 of chapter 9 we prove that the condition for having all the six lines of Γ in one general complex is that lines l_7 , l_8 , and l_9 intersect in one common point and belong to the same flat pencil. For convenience, we recall theorem 1 of chapter 9:

Theorem 1: A general linear complex has a pencil of lines in every plane and a pencil of lines through every point in space. [Graustein, 1930].

Based on this theorem every plane is associated with a flat pencil. Accordingly, the tripod base plane, B_0 , is associated with a flat pencil of lines residing in it. To demonstrate the proof we consider the general complex of lines generated by the two architectural flat pencils F_{14} and F_{25} and either line l_3 or line l_6 . Lines l_7 and l_8 belong to this general complex because of their linear dependence with the generators of F_{14} and F_{25} . Lines l_7 and l_8 lie in the base plane B_0 and define a flat pencil of lines of the general complex. Therefore, if line l_9 is not in this flat pencil then the flat pencils defined by $(l_3 l_9)$ and $(l_6 l_9)$ do not belong to

this general complex and the possibility of having all six lines of Γ in this general complex is ruled out.

Consider the general complex defined by F_{14} , F_{25} and line l_3 . If line l_9 belongs to the flat pencil of lines l_7 and l_8 then the flat pencil $(l_3 l_9)$ belongs to this general complex and it follows that line l_6 also belongs to this general complex since it lies in the flat pencil $(l_3 l_9)$. In a similar way line l_3 belongs to the general complex defined by F_{14} , F_{25} and line l_6 only if line l_9 belongs to the flat pencil of lines l_7 and l_8 .

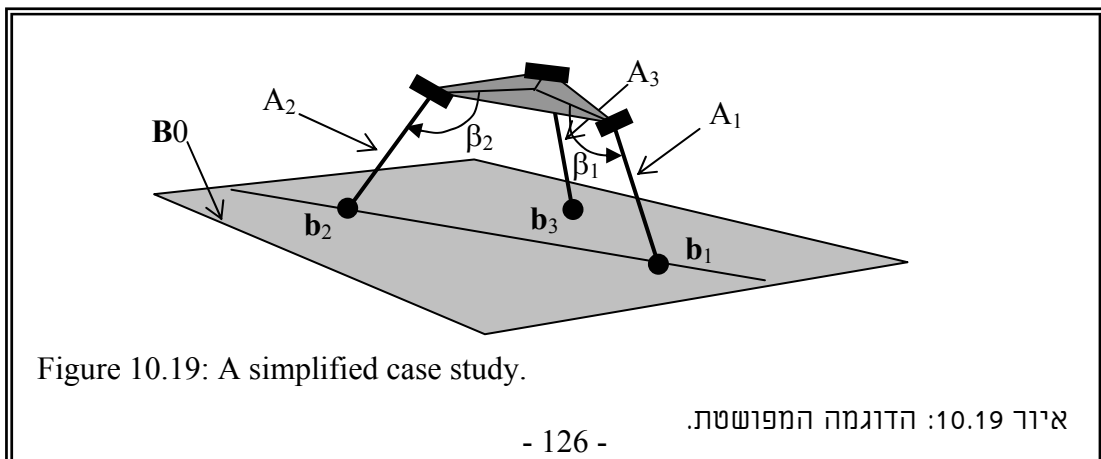
When lines l_7 , l_8 , and l_9 intersect in one point all the four planes ${}^pF_{14}$, ${}^pF_{25}$, ${}^pF_{36}$, and B_0 intersect in a common point. Therefore, the condition for this singularity is:

$$\text{Singular configuration S12: } {}^pF_{14} \cap {}^pF_{25} \cap {}^pF_{36} \cap B_0 \neq \emptyset$$

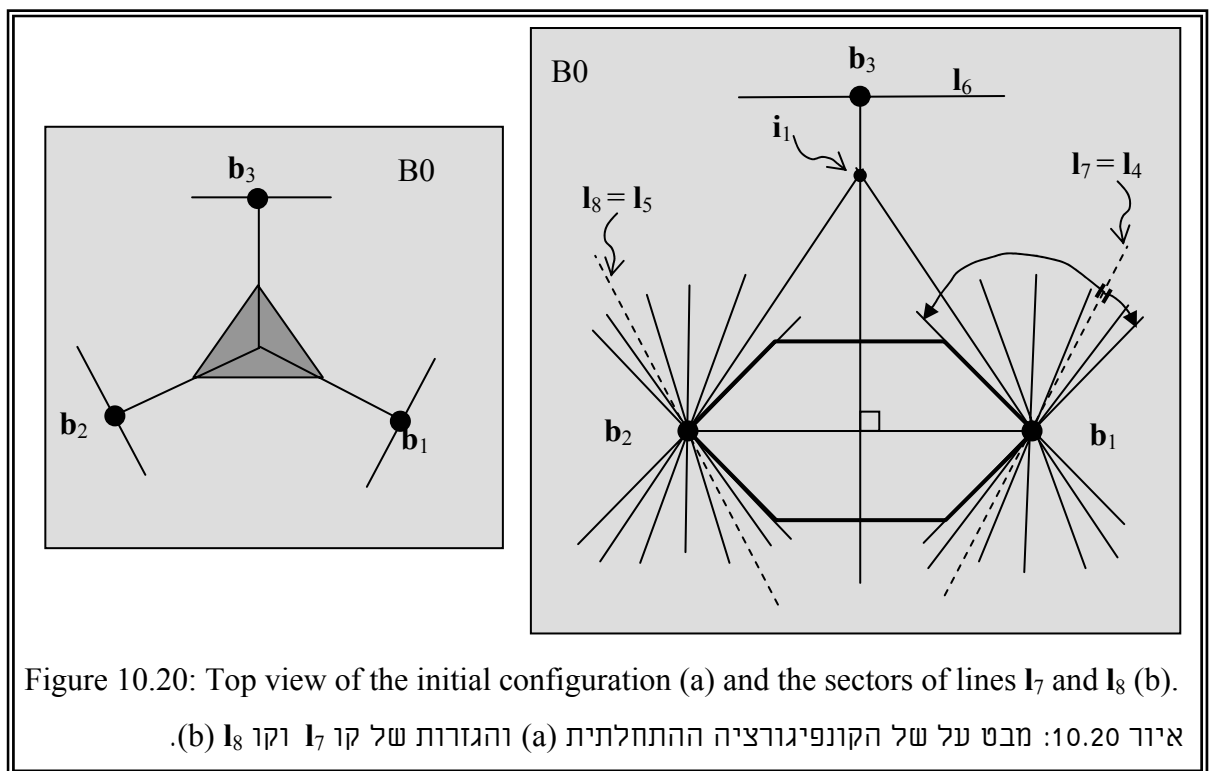
We note that the condition for this singularity is easily expressed as the condition for having the four planes ${}^pF_{14}$, ${}^pF_{25}$, ${}^pF_{36}$, and B_0 in one planar bundle, therefore, any one of these planes is linearly dependent on the other three planes.

We resort to a simple case study to show that this singularity is possible even for configurations with points $b_1 \neq b_2 \neq b_3$. This example is simple and it is solved using a geometric approach. The objective of this example is to answer the question whether this singularity is local or it is a full-cycle singularity. In local singularity we mean that in the singular configuration the general mobility of the mechanism is different than the full cycle mobility only in local neighborhood of the singular configuration. In local parallel singularity the moving platform performs undesirable infinitesimal motions relative to its singular position. Another objective of this simple example is to answer the question regarding possible methods for eliminating this singularity.

Consider the tripod in Fig. 10.19. This tripod has two fixed angles, β_1 and β_2 , between links A_1 and A_2 and the tripod platform, respectively. It has also two rigid links, A_1 and A_2 , having the same length.



Imagine that we rotate the platform of the tripod together with links A_1 and A_2 about line $\mathbf{b}_1\mathbf{b}_2$ such that the angles β_1 and β_2 are kept constant. We start from a configuration in which lines \mathbf{l}_4 and \mathbf{l}_5 lie in B_0 and we rotate the platform and links A_1 and A_2 about $\mathbf{b}_1\mathbf{b}_2$ as a rigid body until lines \mathbf{l}_1 and \mathbf{l}_2 lie in plane B_0 . In the initial configuration lines \mathbf{l}_7 and \mathbf{l}_8 are the same as lines \mathbf{l}_4 and \mathbf{l}_5 , respectively Fig. 10.20. In the final configuration (i.e. line \mathbf{l}_1 and \mathbf{l}_2 lie in B_0) lines \mathbf{l}_7 and \mathbf{l}_8 are the same as lines \mathbf{l}_1 and \mathbf{l}_2 , respectively. This means that during the process of rotation the intersection lines \mathbf{l}_7 and \mathbf{l}_8 of planes ${}^P F_{14}$ and ${}^P F_{25}$ with plane B_0 lie in angular sectors as shown in Fig. 10.20. Performing the same operation in the

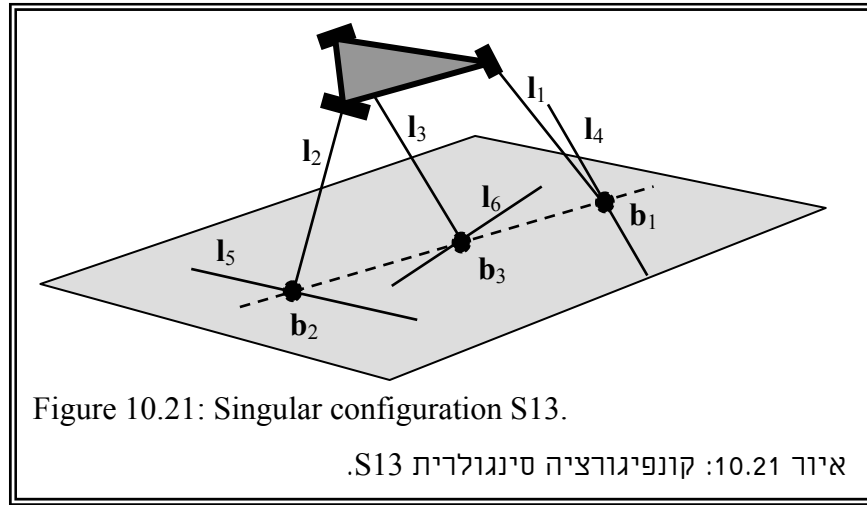


opposite direction results in two other angular sectors of lines \mathbf{l}_7 and \mathbf{l}_8 .

Because of the symmetry in this example every two homothetic lines in these angular sectors intersect along the normal bisector of $\mathbf{b}_1\mathbf{b}_2$. Also because of the symmetry of the equilateral platform this normal bisector is the intersection line of P_3 with B_0 . Therefore if we keep the two links and the platform in a given position, we can alter the position of point \mathbf{b}_3 such that is copunctal with an intersection point of such two lines. In such configuration lines \mathbf{l}_7 , \mathbf{l}_8 , and \mathbf{l}_9 belong to one flat pencil with a center at \mathbf{b}_3 . We note that any movement relative to this singular configuration changes lines \mathbf{l}_7 and \mathbf{l}_8 therefore this singularity is local.

Case 2 Six lines in a special linear complex (5B):

A group of six lines includes three permanent flat pencils of type F. All the lines in Γ intersect a common line if this line is the line of intersection of planes ${}^P F_{14}$, ${}^P F_{25}$, and ${}^P F_{36}$ or if points \mathbf{b}_1 , \mathbf{b}_2 , and \mathbf{b}_3 are collinear. Because of the geometry of the moving platform the planes ${}^P F_{14}$, ${}^P F_{25}$, and ${}^P F_{36}$ do not have a common intersection line. Therefore, the only possible singular configuration occurs when points \mathbf{b}_1 , \mathbf{b}_2 , and \mathbf{b}_3 are collinear, Fig. 10.21.



Singular configuration S13: $A\mathbf{b}_1 + B\mathbf{b}_2 + C\mathbf{b}_3 = \mathbf{0}$

$$A, B, C \in \mathbb{R} . (A, B, C) \neq (0, 0, 0)$$

10.2.8 Concluding remarks

The analysis of the parallel singularities led to 13 singular configurations. However, not all these singular configuration are independent. This is because the method of analysis increases the number of lines in a variety. Hence, some singular configurations are special cases of the others. Table 10.3 presents the independent singular configurations:

Table 10.3: Summary of parallel singular configurations.			
טבלה 10.3: סיכום מצבים סינגולריים מקביליים.			
Singular configuration	Geometric description	figure	Dependency
S1	$B0 = P0 \Rightarrow \mathbf{I}_n \in T_{jk}.$ $j, k, n = 1, 2, 3. j \neq k \neq n.$	10.4	Independent

S2	${}^pT_{jk} = P0, \mathbf{b}_j = \mathbf{o}_p \Rightarrow \mathbf{l}_n \in T_{jk}$ (j, k, n) $\in \{(1, 2, 4), (2, 1, 5), (2, 3, 5), (3, 2, 6), (3, 1, 6), (1, 3, 4)\}$	10.5	Special case of S9
S3	$\mathbf{b}_1 = \mathbf{b}_2 = \mathbf{b}_3. \mathbf{r}_i \parallel \mathbf{p}_j \mathbf{p}_k \Rightarrow \mathbf{l}_n \in T_{jk}$ (j, k, n) $\in \{(1, 2, 6), (2, 3, 4), (3, 1, 5)\}$. i, j, k=1,2,3. i \neq j \neq k	10.6	Special case of S13
S4	${}^pT_{jk} = B0. \mathbf{r}_i \parallel \mathbf{p}_j \mathbf{p}_k. \mathbf{b}_i = {}^cT_{jk} \Rightarrow \mathbf{l}_n \in T_{jk}$. (j, k, n) $\in \{(1, 2, 6), (2, 3, 4), (3, 1, 5)\}$. i, j, k=1,2,3. i \neq j \neq k.	10.7	Special case of S12
S5	First set: ${}^pF_{jk} = P0, \mathbf{b}_{j+1} \in P0 \Rightarrow \mathbf{l}_n \in F_{jk}$. (j, k, n) $\in \{(1, 4, 5), (2, 5, 6), (3, 6, 4)\}$. Second set: ${}^pF_{jk} = P0, \mathbf{b}_{j-1} \in P0 \Rightarrow \mathbf{l}_n \in F_{jk}$. (j, k, n) $\in \{(1, 4, 6), (2, 5, 4), (3, 6, 5)\}$. Note: index j follows a cyclic order such that for j = 3 \Rightarrow j+1 = 1 and for j = 1 \Rightarrow j-1 = 3.	10.8	Special case of S9
		10.9	
S6, S7	$B0 \parallel P0. \mathbf{l}_n \in S_{jk}$. j, k, n = 4, 5, 6. j \neq k \neq n.	10.10 10.11	Special case of S12
S8	$\mathbf{b}_j = \mathbf{b}_k$. j, k=1,2,3. j \neq k.	10.12	Special case of S13
S9	$\mathbf{l}_j \in P0, \mathbf{l}_k \in P0$. j, k = 1,2,3. j \neq k.	10.15	Independent
S10	$\mathbf{l}_n \in B0, {}^pF_{j,j+3} \cap {}^pF_{k,k+3} \cap B0 \in \mathbf{l}_n$ j, k, n = 1, 2, 3. j \neq k \neq n.	10.16	Special case of S12
S11	$\mathbf{l}_n \in B0, {}^pF_{j,j+3} \cap {}^pF_{k,k+3} \cap B0 \in \mathbf{l}_n$. (j, k, n) $\in \{(1, 2, 6), (2, 3, 4), (3, 1, 5)\}$.	10.17	Special case of S12
S12	${}^pF_{14} \cap {}^pF_{25} \cap {}^pF_{36} \cap B0 \neq \emptyset$	10.19	Independent
S13	$A\mathbf{b}_1 + B\mathbf{b}_2 + C\mathbf{b}_3 = \mathbf{0}$ A, B, C $\in \mathbb{R}$. (A, B, C) \neq (0, 0, 0)	10.21	Independent

We note that there are four independent singular configurations. One of the advantages of this tripod structure reflects in the fact that this architecture does not have the famous Hunt's singularity, which was presented in [Fichter, 1986] and [Merlet, 1989].

10.2.9 Design guidelines for minimizing parallel singularities

A successful design of a parallel robot provides a minimal number of singular configurations inside the physical workspace of the robot. The term physical workspace refers to the resulting workspace of the robot when we take into account joint limits, collisions between moving parts, and only one assembly mode. In general, the design should not permit assembly mode transitions because each transition is associated with a singular configuration.

These simple guidelines are of great importance when designing the class of parallel robots to which the USR and the RSPR robots belong. Table 10.4 presents all six independent singular configurations and the design guidelines, which prevent reaching these singular configurations.

Table 10.4. Design guidelines for minimizing parallel singularities טבלה 10.4: שיקולי תכן למינימיזציה של מספר המצבים הסינגולריים.		
Singular case	Geometrical condition for preventing singularity.	Suggested method for preventing singularity.
S1	Prevent the lines 1,2,3 from lying in the tripod base plane.	Limit the spherical joint range, or limit the revolute joint range.
S9	Prevent lines i, j from simultaneously lying in the moving platform's plane. $i, j \in 1, 2, 3$.	Limit the lengths of lines i, j and pick suitable paths for points $\mathbf{b}_i, \mathbf{b}_j$.
S12	Prevent the planes ${}^pF_{14}$ ${}^pF_{25}$ ${}^pF_{36}$ and B_0 from intersecting in one point.	Perform simulations to determine the required limits on β_i in order to prevent this singular configuration.
S13	Prevent points \mathbf{b}_i from being collinear.	Choose correct paths for points \mathbf{b}_i .

10.3 Analysis of serial singularities for the RSPR and USR robots

All the robots listed in Fig. 5.14 share the same parallel singularities, but differ in terms of their serial singularities. This is because every robot architecture has a distinct instantaneous inverse kinematics matrix \mathbf{B} .

10.3.1 Serial singularities of the RSPR robot

The instantaneous inverse kinematics matrix, \mathbf{B} , of the RSPR robot is given by Eq. (7.21) and it is rewritten in Eq. (10.3).

$$\mathbf{B} = \begin{bmatrix} \mathbf{I} & \mathbf{Cn}_1 \\ \mathbf{0} & \mathbf{Cn}_2 \end{bmatrix} \quad (10.3)$$

\mathbf{Cn}_1 and \mathbf{Cn}_2 are 3x3 diagonal matrices. The elements on the main diagonals of these matrices were given in Eq. (7.19).

$$\mathbf{Cn}_{1i} = (\hat{\mathbf{s}}_{1i} \times \hat{\mathbf{s}}_{ni})^t \mathbf{l}_{bi} \quad i=1,2,3. \quad (10.4)$$

$$\mathbf{Cn}_{2i} = (\hat{\mathbf{s}}_{2i} \times \hat{\mathbf{s}}_{ni})^t \mathbf{l}_{bi} \quad i=1,2,3. \quad (10.5)$$

Where $\hat{\mathbf{s}}_{1i}$ is the unit vector along the i 'th tripod link A_i . $\hat{\mathbf{s}}_{2i}$ is a unit vector through the center of the spherical joint of the i 'th kinematic chain and parallel to the axis of the upper revolute joint $\hat{\mathbf{r}}_i$. \mathbf{l}_{bi} is the vector from the center of rotation of link B_i to the center of the i 'th spherical joint. $\hat{\mathbf{s}}_{ni}$ is a unit vector along the rotation axis of link B_i , see Fig. 7.3 and Fig. 7.4.

It is obvious from inspecting the matrix \mathbf{B} that it is singular whenever one of the scalars \mathbf{Cn}_{2i} is zero; Therefore, the condition for serial singularity of the RSPR robot is given by Eq. (10.6).

$$\mathbf{Cn}_{2i} = (\hat{\mathbf{s}}_{2i} \times \hat{\mathbf{s}}_{ni})^t \mathbf{l}_{bi} = 0 \quad i=1,2,3 \quad (10.6)$$

Singularity of matrix \mathbf{B} indicates serial singularity of one of the kinematic chains. This singularity is characterized by loss of a degree of freedom. The singularity of the matrix \mathbf{B} is not sufficient to indicate singularity of the whole robot. This is because we must keep in mind that the singularity of \mathbf{B} indicates singularity of one or more kinematic chains and we must verify that this singular configuration is allowed by the selected assembly mode. Therefore, the serial singularities must be given geometric interpretation in addition to the mathematical analysis.

Rewriting Eq. (10.6) in the form of Eq. (10.7) indicates that it is satisfied in four cases.

$$\mathbf{Cn}_{2i} = (\hat{\mathbf{s}}_{2i} \times \hat{\mathbf{s}}_{ni})^t \mathbf{l}_{bi} = (\mathbf{l}_{bi} \times \hat{\mathbf{s}}_{2i})^t \hat{\mathbf{s}}_{ni} = (\hat{\mathbf{s}}_{ni} \times \mathbf{l}_{bi})^t \hat{\mathbf{s}}_{2i} \quad i=1, 2, 3. \quad (10.7)$$

The four cases are:

Case a: \hat{s}_{2i} lies in the plane of \mathbf{l}_{bi} and \hat{s}_{ni} .

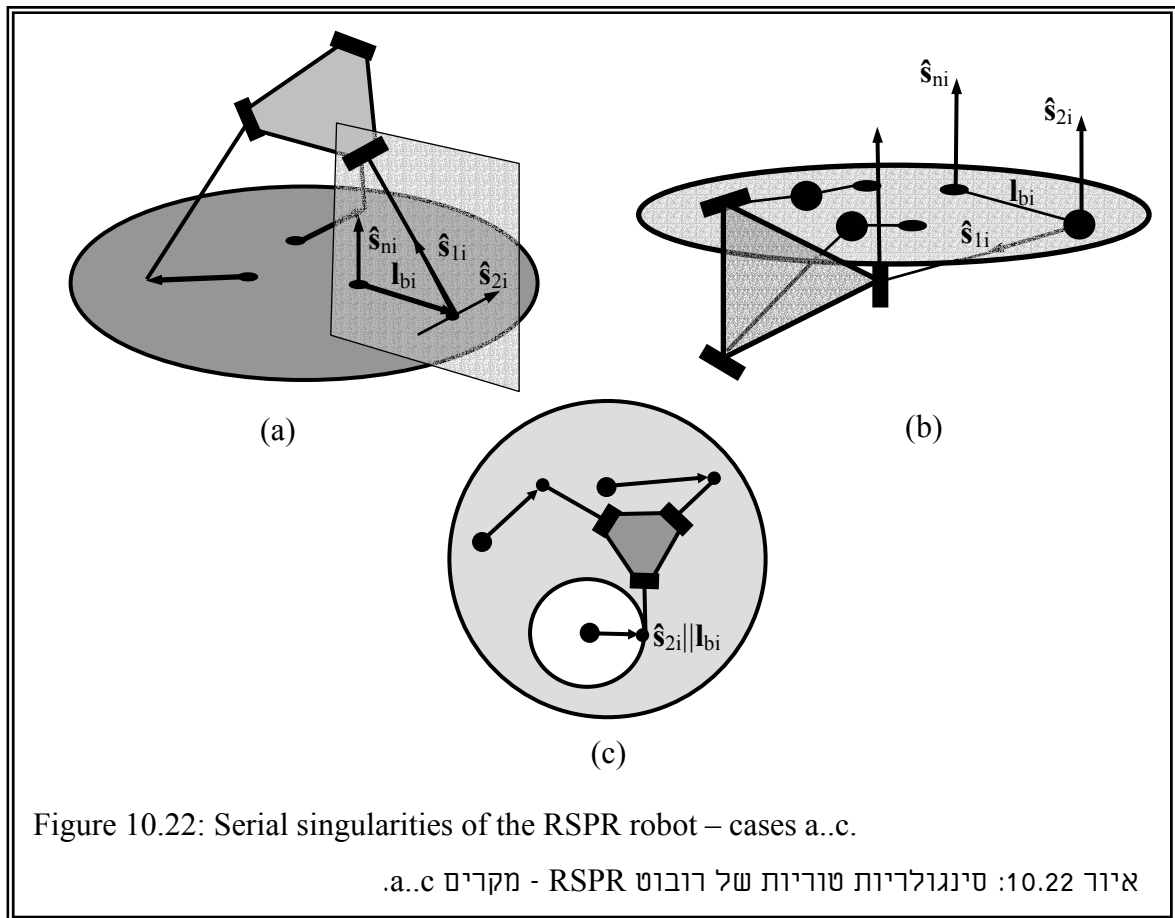
Case b: $\hat{s}_{2i} \parallel \hat{s}_{ni}$.

Case c: $\mathbf{l}_{bi} \parallel \hat{s}_{2i}$.

Case d: $\mathbf{l}_{bi} \parallel \hat{s}_{ni}$.

Case d is not possible for the RSPR robot since \hat{s}_{ni} is the rotation axis of \mathbf{l}_{bi} . Case a is the general case and it includes cases b and c. Cases a, b, and c are demonstrated in Fig. 10.22.

In case a, the actuator of rotating link can not apply force in the direction of \hat{s}_{2i} . In case b, the actuators can not produce any motion of the kinematic chain extremity in a direction normal to the base platform. In case c, the prismatic actuator lies in a plane tangent to the circle of the rotating link and the two solutions of the inverse kinematics meet. In all these cases any force acting on the kinematic chain extremity in the direction of the upper revolute joint produces zero force/moment in the actuators.



10.3.2 Serial singularities of the USR robot

The instantaneous inverse kinematics matrix \mathbf{B} of the USR robot was given in Eq. (7.31) and it is rewritten in Eq. (10.8).

$$\mathbf{B} = \begin{bmatrix} \mathbf{Cn}_1 & \mathbf{Cr}_1 \\ \mathbf{Cn}_2 & \mathbf{Cr}_2 \end{bmatrix}_{6 \times 6} \quad (10.8)$$

\mathbf{Cn}_1 , \mathbf{Cn}_2 , \mathbf{Cr}_1 , and \mathbf{Cr}_2 are 3 by 3 diagonal matrices given in Eq. (7.32) and Eq. (7.33) with the following elements on the main diagonal:

$$(10.9) \quad \mathbf{Cn}_{2i} = (\hat{\mathbf{s}}_{2i} \times \hat{\mathbf{s}}_{ni})^t \mathbf{l}_{bi} \quad \mathbf{Cn}_{1i} = (\hat{\mathbf{s}}_{1i} \times \hat{\mathbf{s}}_{ni})^t \mathbf{l}_{bi}$$

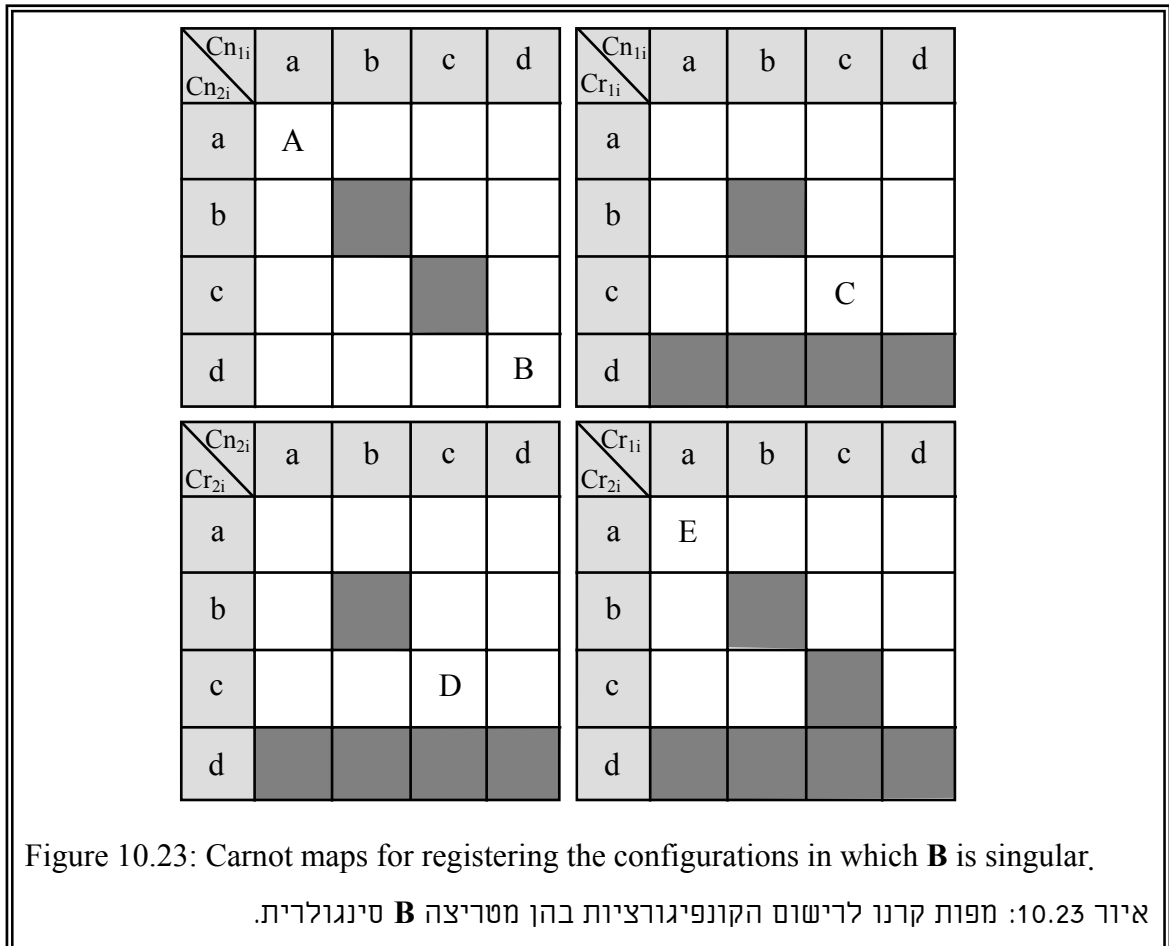
$$(10.10) \quad \mathbf{Cr}_{2i} = (\hat{\mathbf{s}}_{2i} \times \hat{\mathbf{s}}_{ri})^t \mathbf{l}_{bi} \quad \mathbf{Cr}_{1i} = (\hat{\mathbf{s}}_{1i} \times \hat{\mathbf{s}}_{ri})^t \mathbf{l}_{bi}$$

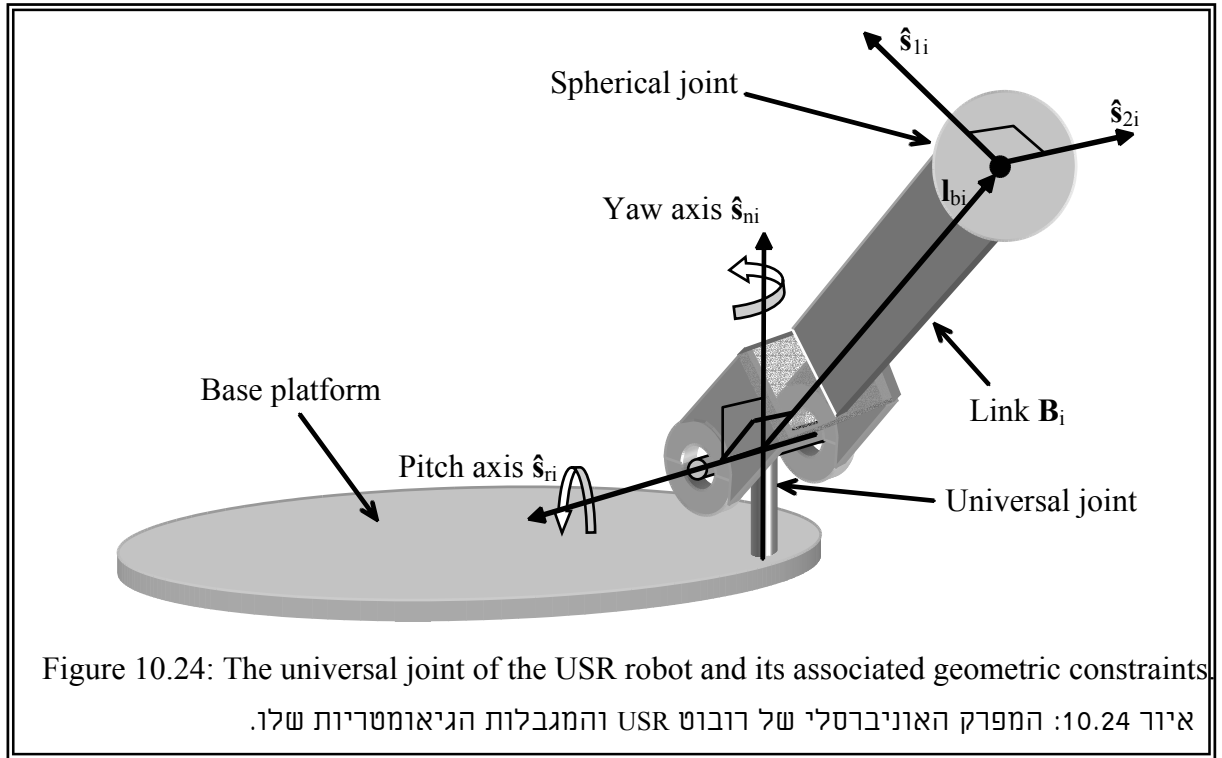
Where $\hat{\mathbf{s}}_{1i}$ is the unit vector along the i 'th tripod link A_i . $\hat{\mathbf{s}}_{2i}$ is a unit vector through the center of the spherical joint of the i 'th kinematic chain and parallel to the axis of the upper revolute joint $\hat{\mathbf{r}}_i$. \mathbf{l}_{bi} is the vector from the center of the universal joint to the center of the spherical joint of link B_i . $\hat{\mathbf{s}}_{ni}$, $\hat{\mathbf{s}}_{ri}$ are unit vectors along the yaw/pitch axes of the universal joint of link B_i , see Fig. 7.3 and Fig. 7.5.

The USR robot has a three-diagonal instantaneous inverse kinematics matrix, \mathbf{B} , and it is singular whenever one of its rows/columns is zero, or when a pair of its rows/columns is proportional. In a similar way to the analysis of Eq. (10.7) of the RSPR robot we register all the cases in which one of the elements in \mathbf{Cn}_1 , \mathbf{Cn}_2 , \mathbf{Cr}_1 , and \mathbf{Cr}_2 is zero. Each one of these cases, i.e., $\mathbf{Cn}_{1i}=0$, $\mathbf{Cn}_{2i}=0$, $\mathbf{Cr}_{1i}=0$, and $\mathbf{Cr}_{2i}=0$ is separated into four cases like the cases a..d of $\mathbf{Cn}_{2i}=0$ for the RSPR robot. The conditions for separately fulfilling $\mathbf{Cn}_{1i}=0$, $\mathbf{Cn}_{2i}=0$, $\mathbf{Cr}_{1i}=0$, and $\mathbf{Cr}_{2i}=0$ are registered in table 10.4.

10.5: The cases in which $\mathbf{Cn}_{1i}=0$, $\mathbf{Cn}_{2i}=0$, $\mathbf{Cr}_{1i}=0$, $\mathbf{Cr}_{2i}=0$ are fulfilled separately.				
טבלה 10.5: המקרים בהם מתקיימים לחוד $\mathbf{Cn}_{1i}=0$, $\mathbf{Cn}_{2i}=0$, $\mathbf{Cr}_{1i}=0$, $\mathbf{Cr}_{2i}=0$				
Condition	$\mathbf{Cn}_{1i}=0$	$\mathbf{Cn}_{2i}=0$	$\mathbf{Cr}_{1i}=0$	$\mathbf{Cr}_{2i}=0$
a	$\hat{\mathbf{s}}_{1i}$ lies in the plane of \mathbf{l}_{bi} and $\hat{\mathbf{s}}_{ni}$	$\hat{\mathbf{s}}_{2i}$ lies in the plane of \mathbf{l}_{bi} and $\hat{\mathbf{s}}_{ni}$	$\hat{\mathbf{s}}_{1i}$ lies in the plane of \mathbf{l}_{bi} and $\hat{\mathbf{s}}_{ri}$	$\hat{\mathbf{s}}_{2i}$ lies in the plane of \mathbf{l}_{bi} and $\hat{\mathbf{s}}_{ri}$
b	$\hat{\mathbf{s}}_{1i} \parallel \hat{\mathbf{s}}_{ni}$	$\hat{\mathbf{s}}_{2i} \parallel \hat{\mathbf{s}}_{ni}$	$\hat{\mathbf{s}}_{1i} \parallel \hat{\mathbf{s}}_{ri}$	$\hat{\mathbf{s}}_{2i} \parallel \hat{\mathbf{s}}_{ri}$
c	$\mathbf{l}_{bi} \parallel \hat{\mathbf{s}}_{1i}$	$\mathbf{l}_{bi} \parallel \hat{\mathbf{s}}_{2i}$	$\mathbf{l}_{bi} \parallel \hat{\mathbf{s}}_{1i}$	$\mathbf{l}_{bi} \parallel \hat{\mathbf{s}}_{2i}$
d	$\mathbf{l}_{bi} \parallel \hat{\mathbf{s}}_{ni}$	$\mathbf{l}_{bi} \parallel \hat{\mathbf{s}}_{ri}$	$\mathbf{l}_{bi} \parallel \hat{\mathbf{s}}_{ri}$	$\mathbf{l}_{bi} \parallel \hat{\mathbf{s}}_{ni}$

To find serial singularities of the USR robot we inspect the intersection of the conditions in table 10.4 that lead to zeroing of a row or a column in **B**. We produce four Carnot maps to register all the cases in which a row or a column is zero. The four Carnot maps are shown in Fig. 10.23. Theoretically, there are 64 possible intersections in these tables, but we exclude the cases that do not fulfill the geometrical constraints. In these maps, the cells with dark background represent impossible configurations because of the geometry of the universal joint, Fig. 10.24, and because \hat{s}_{1i} is perpendicular to \hat{s}_{2i} . From this figure, it is clear that \hat{s}_{ni} is perpendicular to \hat{s}_{ri} and that \hat{s}_{ri} is perpendicular to \mathbf{l}_{bi} . We inspect the cases for dependence and we find that there are only five independent configurations. These configurations are indicated in the maps by letters A..E. All the empty cells in these maps represent configurations that are dependent on configurations A..E.





The serial singularities of the USR robot in which a row or a column of the instantaneous matrix, \mathbf{B} , is zero are:

Configuration A: both \hat{s}_{1i} and \hat{s}_{2i} lie in the plane of \hat{s}_{ni} and \mathbf{I}_{bi} , Fig. 10.25-(A).

Configuration B: $\mathbf{I}_{bi} \parallel \hat{s}_{ni}$, i.e., the lower link is coincident with the yaw axis of the Hooke's joint, Fig. 10.25-(B).

Configuration C: \hat{s}_{1i} coincides with \mathbf{I}_{bi} , Fig. 10.25-(C).

Configuration D: \hat{s}_{2i} coincides with \mathbf{I}_{bi} , Fig. 10.25-(D).

Configuration E: both \hat{s}_{1i} and \hat{s}_{2i} lie in the plane of \hat{s}_{ri} and \mathbf{I}_{bi} , Fig. 10.22-(E).

In configurations A and B $C_{n1i}=C_{n2i}=0$ and the corresponding column out of columns 1..3 in \mathbf{B} is zero. In configurations E $C_{r1i}=C_{r2i}=0$ and the corresponding column out of columns 4..6 in \mathbf{B} is zero. In configurations C the corresponding row out of rows 1..3 in \mathbf{B} is zero. In configuration D $C_{r2i}=C_{n2i}=0$ and the corresponding row out of rows 4..6 in \mathbf{B} is zero.

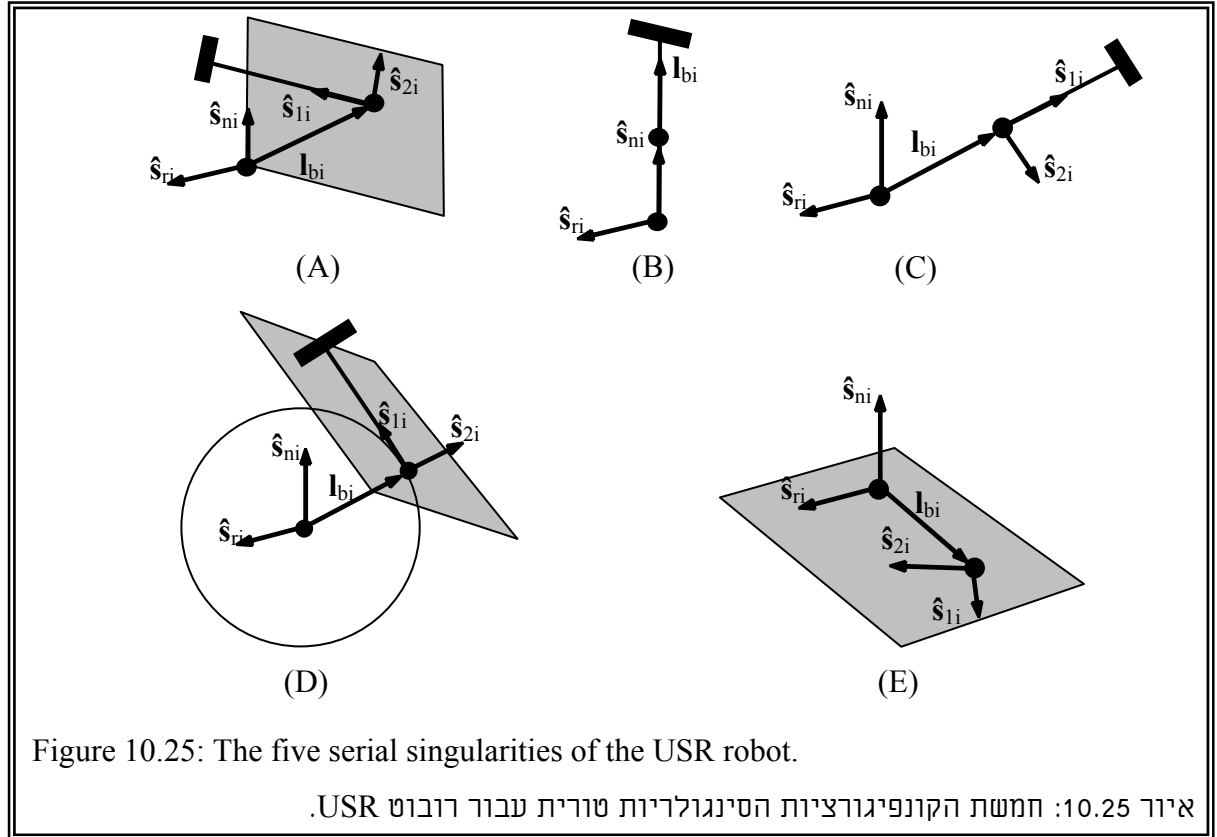
In configuration D, the two branches of the solution to the inverse kinematics problem meet. In case B the lower rotating link coincides with the yaw axis of the active Hooke's joint and the motor of this axis can not move the tip of this link. In cases A and E the forces of the upper rotating link produce zero moment in one of the axes of the Hooke's joint. In case C the two links of the singular kinematic chain are collinear.

In addition to the serial singularities in Fig. 10.25 there is an additional singularity that occurs when two columns of \mathbf{B} are proportional, Eq. (10.11).

Configuration F:

$$Cn_{1i} Cr_{2i} - Cr_{1i} Cn_{2i} = 0 \quad (10.11)$$

The condition in Eq. (10.11) is the general condition for singularity of one of the kinematic chains, therefore it includes all the singular configurations A..E in Fig. 10.25.



10.4 Conclusions

In this chapter, we analyzed the parallel singularities of the manipulators in Fig. 5.14. We found thirteen parallel singularities for all these manipulators out of which only four are independent. We analyzed the serial singularities of the USR and the RSPR robots and we showed that the RSPR has less serial singularities than the USR robot. We formulated the conditions for the serial and parallel singularities. These conditions can be used for designing a robot without singularities.

Chapter 11

The RSPR Prototype Robot

11.1 Introduction

This chapter presents the experimental setup and the control method of the RSPR prototype robot that was built according to the characteristic dimensions of chapter 8. We will show that the prototype fulfills the objectives of the design task that were presented in chapter 4. The technical drawings of the prototype are in a separate appendix to this work[§].

11.2 The RSPR prototype robot – design characteristics and specifications

The RSPR prototype robot is based on the selected robot in table 8.2. For convenience, the characteristic dimensions of this robot are re-listed in Table 11.1. Table 11.1 lists the height range of the prototype robot based on the kinematic model (without taking into account the additional parts below the base platform). The design of the robot included design of customized linear actuators to achieve the desired minimal length and stroke. To reduce the weight of the robot unnecessary material was removed by milling holes in the aluminum base platform. This resulted in 30% weight reduction in the weight of the base platform. Figure 11.1 presents the RSPR prototype holding a medical tool for demonstration purposes. Figure 11.2 presents a top view of the RSPR robot showing the details of the base platform.

Table 11.1: Characteristic dimensions of the RSPR prototype.			
טבלה 11.1: מידות אופייניות של רובוט אב הטיפוס מסוג RSPR.			
Eccentricity- e	20 mm	Minimal actuator length- L_{\min} .	144 mm
Rotating link length- r_b	90 mm	Minimal height (kinematic model)	130.9 mm
Radius of the moving platform - r_p .	50 mm	Maximal height (kinematic model)	201.2 mm

§ Robotics Laboratory - Technion.

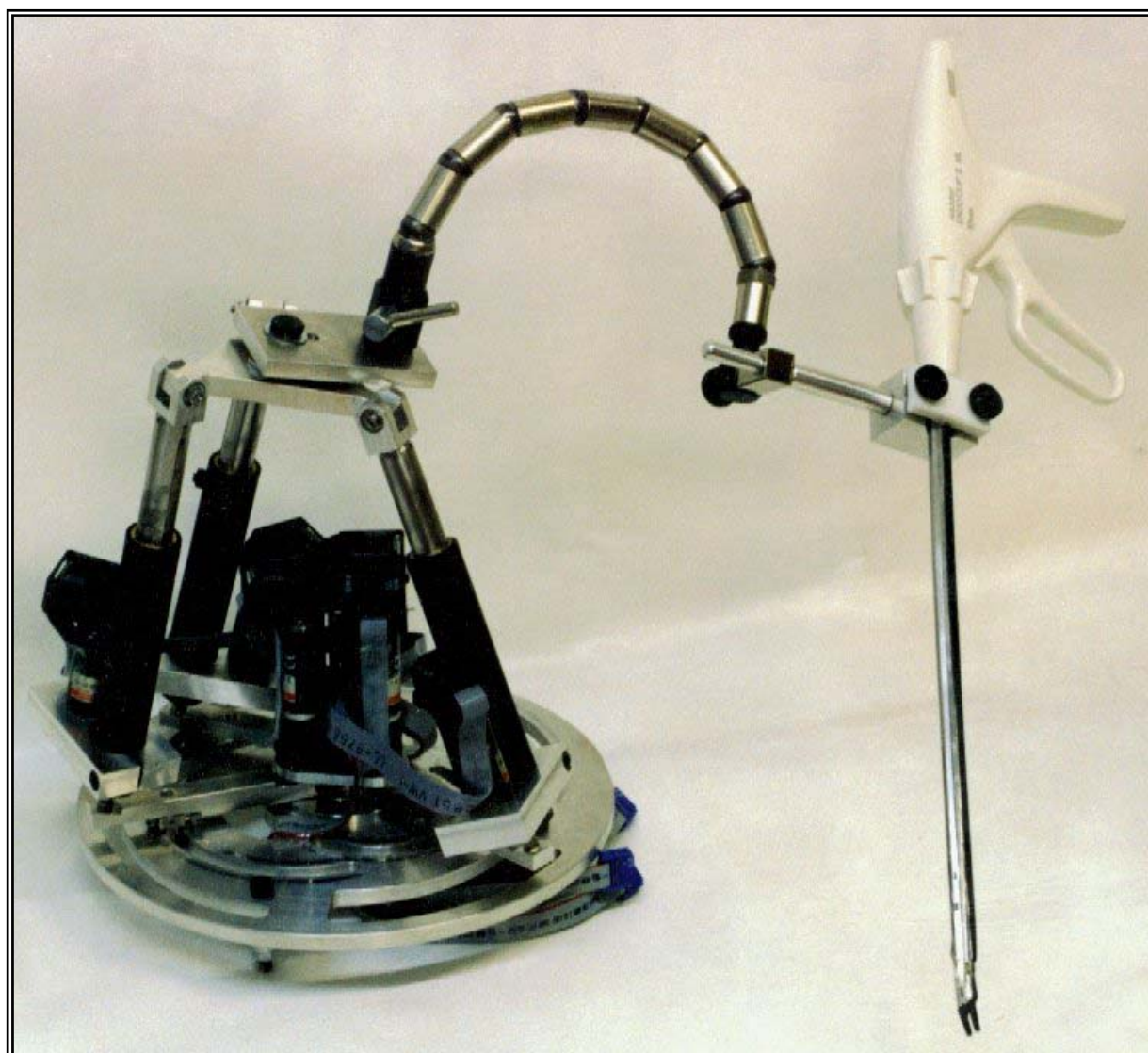


Figure 11.1: The RSPR prototype robot demonstrating surgical tool positioning.

איור 11.1: רובוט אב טיפוס RSPR מדגים מיקום כלי ניתוחי.



Figure 11.2: Top view of the RSPR prototype robot showing weight reduction voids in the base platform.

איור 11.2: מבט על לרובוט RSPR המראה את פלטפורמת הבסיס עם המגרעות להורדת משקל.

11.3 Mechanical properties of the prototype

The prototype robot has the physical properties listed in table 11.2. To achieve maximal accuracy we use anti-backlash gearing for the linear actuators and high precision gears for the rotating links. We use low friction PTFE coated lead screws for the linear actuators to reduce the friction in the system. The backlash of the linear actuators limits the accuracy of the robot, but replacing the lead screws with preloaded ball screws can easily solve this problem.

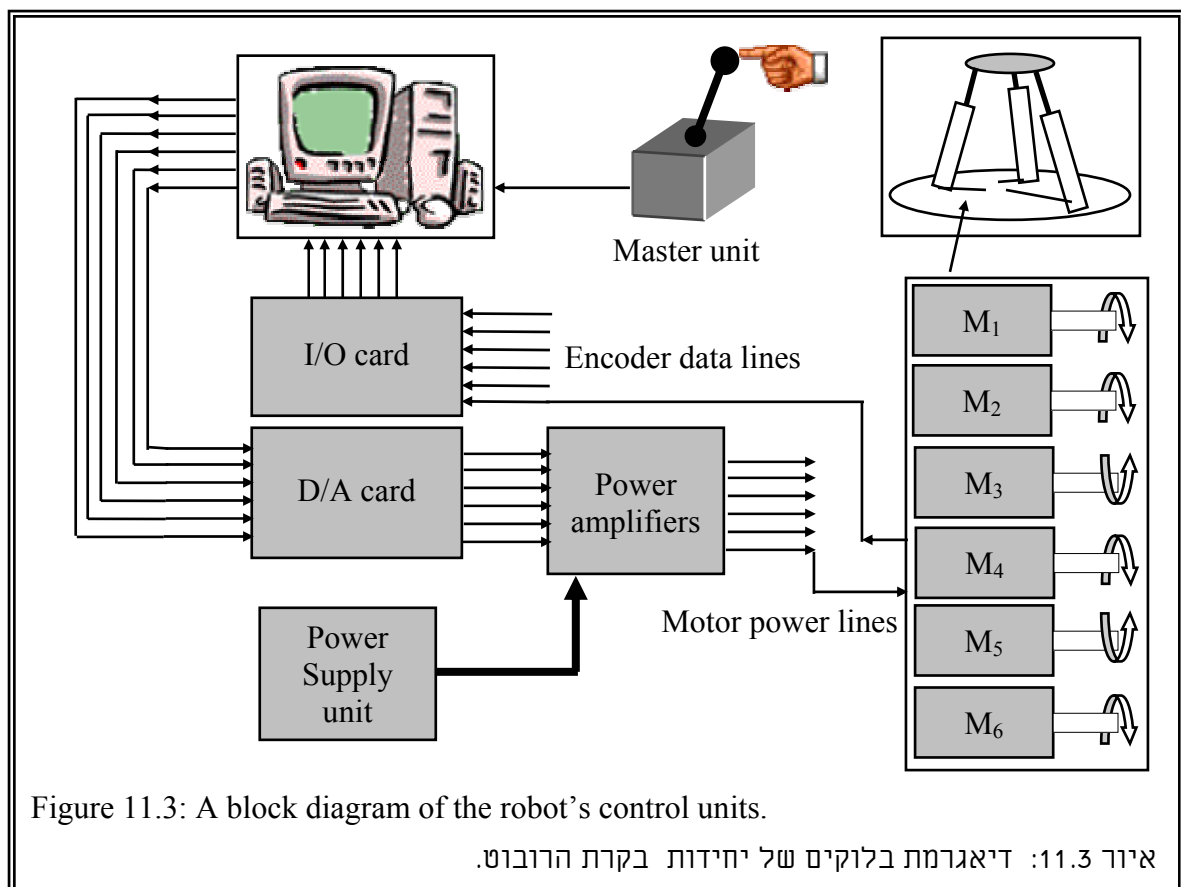
Table 11.2: Physical properties of the RSPR prototype	
טבלה 11.2: תכונות פיזיקליות של רובוט אב טיפוס מסוג RSPR.	
Weight	3 [Kg]
Physical dimensions of enveloping cylinder (diameter, height).	250, 200 [mm]
Maximal continuous torque of the rotating links at the gear output	0.5 [Nm]
Maximal force of linear actuators in continuous operation	220 [N]
Resolution of the optical encoders.	500 [encoder counts/revolution]
Resolution of the linear actuators	0.0015 [mm/encoder count]
Resolution of the rotating links	0.005 [degree/encoder count]
Linear actuator backlash	0.08-0.2 [mm]
Rotating links backlash	20''

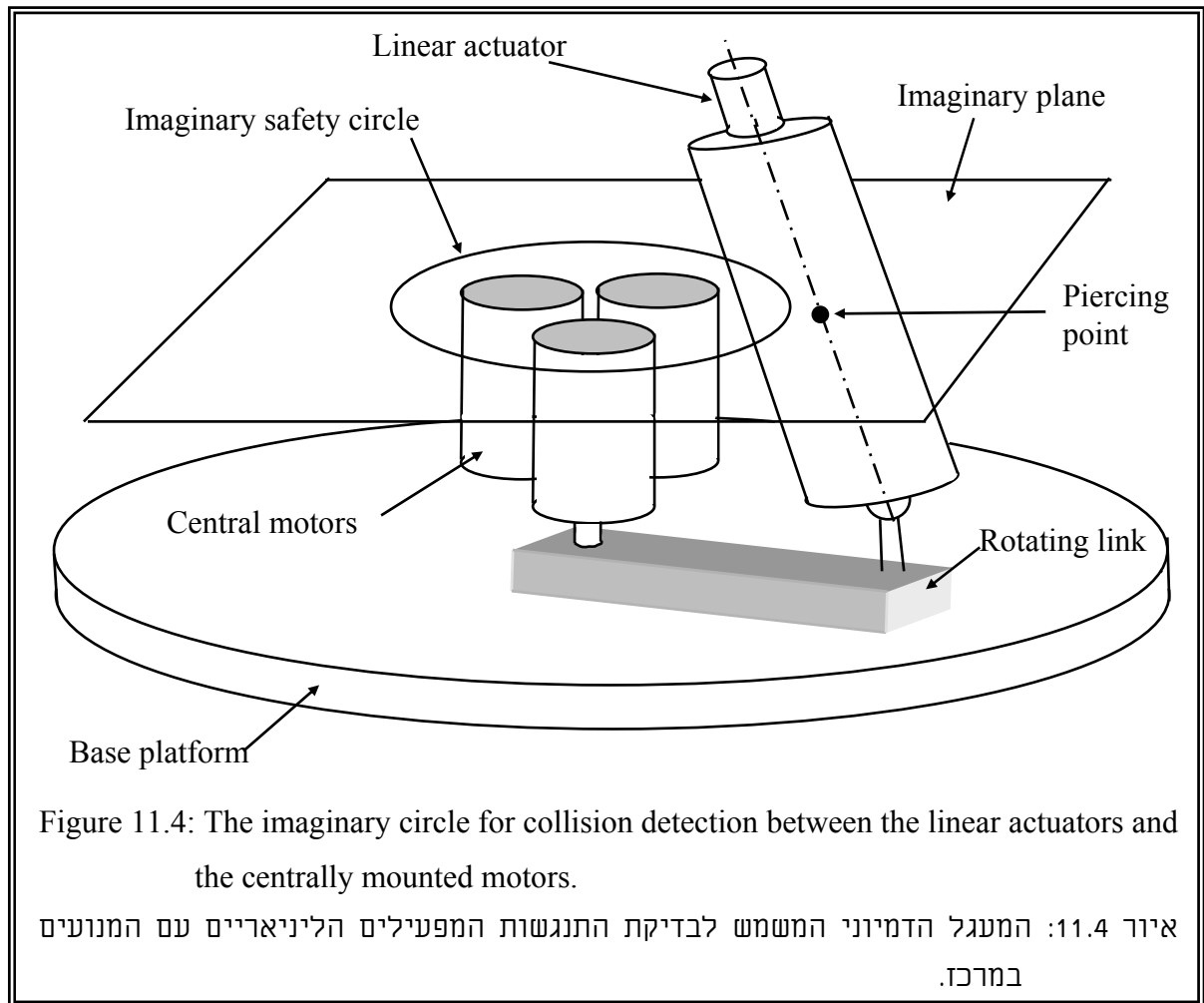
11.4 Experimental setup

The motion of the prototype robot is controlled in a Master-Slave mode. Our experimental system includes the computer control program in its core, a 12 bit 8 channel digital to analogue D/A converter, input output I/O card, six power amplifiers, the power supply unit, and the robot, Fig. 11.3.

The computer program reads the desired position/orientation of the moving platform as an input signal initiated by the user (the Master). The control program calculates the positional error and uses a PID control algorithm to compute the control signal, which is in turn converted by the D/A card to an analogue signal. This analogue signal is feeded to the power amplifiers and translated into a PWM signal for the DC motors $M_1 \dots M_6$.

The control program also checks the inverse kinematics solution and determines whether an actuation limit has been reached. Additionally, the program prevents collision between the linear actuators and the centrally located motors. This is achieved by computing the piercing points of the linear actuator axes with an imaginary plane that is perpendicular to the motors and defined by the upper extremities of the three central motors, Fig. 11.4. We define an imaginary safety circle that lies in this plane. This imaginary circle has a radius larger than the actual radius of the cylinder that envelops the three central motors. If the piercing point of a linear actuator axis lies inside this imaginary circle this means that the linear actuator collides with the upper extremity of one of the three centrally located motors. This approximation is appropriate because the linear actuators retain an inclination towards the centrally located motors and the inclination angle of the actuators does not reach high values. Therefore, this method is a sufficient and a fast method for solving the collision problem. We determined the required imaginary radius experimentally by manipulating the robot in many positions that bring the linear actuators into collision with one of the centrally located motors and we registered the upper limit of the result of the imaginary circle.





11.5 Future work and experimentation

The prototype robot will be tested in the future in medical tasks such as manipulating a laparoscope and an orthroscope in Orthroscopic knee surgery. To achieve this goal we need a convenient means to translate the commands of the surgeon to the robotic assistant. One possible method for manipulating the robot is by integrating a six degrees of freedom hand controller that enables easy scaling of the motions performed by the surgeon. The prototype also has not been exactly calibrated and in final stages of experimental setup we need exact calibration of the robot. Additional work should be invested in designing an extension mechanism that holds the tool.

11.6 Conclusion

The RSPR prototype was successfully designed, constructed, and controlled to meet the design goals. The final dimensions and weight of the robot promise good portability, which is an advantage in the operating room. The accuracy of the robot exceeds the accuracy

achieved by manual manipulation of surgical tools. This points out the potential embedded in this robot for medical applications.

Chapter 12

Conclusions

12.1 perspective overview of the work

This work incorporated two new fields of research: the field of robotic assisted surgery, and the subject of parallel manipulation. The requirements of a robotic assistant were formulated according to evaluations of the required workspace for laparoscopic surgery. Based on these requirements we sought the best robotic architecture for our design task. We first compared the serial architecture with the parallel one and based on the architecture-inherent characteristics of both architectures we concluded that the parallel architecture better suits the requirements of a medical robot. Then we searched for new parallel manipulators that fit the task. The synthesis process led to a family of 14 distinct parallel robots, with common kinematic features. Based on design guidelines we chose two possible candidate robots, the USR and the RSPR robots, for dimensional synthesis. The dimensional synthesis phase included scanning a vast array of manipulators with different characteristic dimensions and resulted in 22 possible RSPR robots and 95 admissible USR robots. Although the dimensions of the USR admissible robots were smaller than for the RSPR robots, we chose the RSPR robot because of two reasons. The first reason was that the RSPR robot requires less actuator effort. The second reason was based on design guidelines regarding mechanical simplicity and feasibility. Another important advantage of the RSPR robot over the USR robot was revealed in the phase of singularity analysis.

The dimensional synthesis simulations were based on the inverse kinematics solutions and the static Jacobian formulations for the USR and the RSPR robots. The aforementioned family of 14 manipulators was shown to have a common Jacobian matrix formulation with the same instantaneous direct kinematics matrix. This matrix was shown to be determined solely by the common tripod mechanism.

The line-based formulation of the tripod mechanism Jacobian allowed the analysis of the uncertainty configurations (parallel singularities) of all the 14 manipulators using line geometry method. The analysis of parallel singularities of this family of manipulators showed that these manipulators have 13 parallel singularities of which only 6 are independent and general. The use of line-based singularity analysis provided the geometrical insight, which allowed deducing design guidelines for minimizing the parallel singularities of these manipulators by altering the design variables.

The analysis of serial singularities of the RSPR and the USR robots showed that the RSPR robot has less serial singularities than the USR robot.

The design phase of a medical robotic assistant was based on the results of the dimensional synthesis of the RSPR robot. Based on actuator size and spherical joint limits we built a compact RSPR parallel robot prototype (over all weight less than 3 kg) which allows good portability in the surgery room.

After the prototype was successfully designed and constructed, we wrote a control program that allows activating it in a Master-Slave mode. The mechanical and architectural characteristics of the prototype indicate that this prototype is more accurate than a human hand. These features of the parallel robot prototype highlight its embedded potential for implementation in Laparoscopic and certain Orthroscopic surgeries.

12.2 Future work

The RSPR parallel robot prototype is currently an efficient tool, but it needs future adaptations before entering the experimental phase. Before commencing with surgical experiments, an exact calibration of the robot must be performed and an efficient interface and hand controller is necessary. The development of an efficient hand controller or an alternative solution for conveying the commands of the surgeon to the robot is a key prerequisite for ensuring the success of the medical robotic assistant. For surgical procedures incorporating tactile tasks, an efficient force-feedback system must be designed in order to convey information to the surgeon regarding the tactile forces exerted by the robot on the patient's body.

Appendix A

DESIGN CONSIDERATIONS OF NEW SIX DEGREES-OF-FREEDOM PARALLEL ROBOTS

N. Sima'an, D. Glozman, M. Shoham

Department of Mechanical Engineering .

Technion - Israel Institute of Technology, Haifa 32000, Israel

Email : shoham@tx.technion.ac.il

Abstract

This paper describes the structure of three types of parallel robots and compares their performances in the sense of size and static forces. The motivation for this investigation is to construct a robot that best fits a given medical application. The requirements are to cover a given work volume with a given orientation and to maintain the robot within the smallest cube possible. Among the structures examined, three are presented since two are modifications of known structures and the third is a new one.

1 Introduction

The exponential growth of publication on parallel robots in the last five years points to the potential embedded in this structure that has not yet been fully exploited. A survey of papers whose title includes the word robots, reveals that the number of papers dealing in particular with parallel structure has gone up from 1% in 1985 to 9% in 1996. This clearly indicates the trend of the research in the field. A typical example is the manufacturing area. The recently introduced parallel structured machine tools by Ingersoll-Rand [7] and Giddings-Lewis [11] opens the door for much research on the application of parallel robots in manufacturing as appears for example in the 1997 CIRP Annals.

Numerous investigations were aimed at new structures of parallel robots. We refer the reader to Merlet's comprehensive study where he collected and grouped different parallel structures by their Degrees Of Freedom (DOF) (see Merlet - web page [9]). In the six DOF section, different structures are grouped by their types of joints e.g. RRPS, RRRS, etc. (where R stands for Revolute, P for Prismatic and S for Spherical joint). The ones not falling within these categories are collected under the title of "robots with various kinematic chains".

Some structures use flexible members thus reducing their mechanical complexity by saving joints (e.g. [6,10]).

The three structures presented here are not included in the above mentioned list. Two structures are modifications of the USR and RSPR robots (where U stands for a Universal joint), and the third is a new structure which utilizes double planar robots. The idea of this structure stems from Merkle's [8] and Daniali's [5] works.

The structures of the new parallel robots are presented next. In Section 3 the Jacobian matrices of the three presented robots are derived. These matrices were used to derive the static forces and examine singularity. Section 4 presents simulation results from which minimal dimensions and actuating forces of each robot structure needed to achieve the given task are derived.

2 Kinematic structure of the robots

In this section the kinematic structures of the three suggested robots are given. The kinematic chains are described by abbreviations of the joint types, starting from the base platform and ending at the moving platform. All letters denoting joint types are encircled and shown in figures corresponding to each robot. (see Figs. 2.1, 2.2, 2.3).

2.1 USR robot

The USR robot consists of three identical kinematic chains connecting the base and the moving platform, each one has two links. One link is connected to the base platform by a U joint, the other link is connected to the moving platform by an R joint, and the two links are connected in between by an S joint. The lower link of each kinematic chain is oriented in space by a differential drive, controlling its yaw and pitch angles relative to the base platform.(Fig. 2.1)

This structure is a variation of the structure described by Cleary [4] which uses URS joint combination for each

kinematic chain, controlling the pitch and roll of the lower links. The structure we examined has, however, a reverse order of joints - a revolute joint connecting the links to the moving platform, and a spherical joint between the links. This modification prevents collision between links.

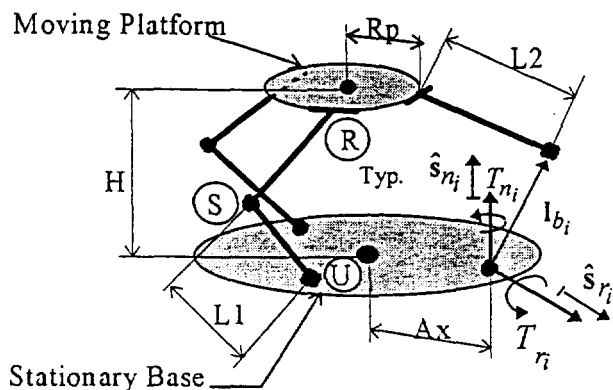


Figure 2.1: USR parallel robot

2.2 RSPR robot

This structure consists of three identical kinematic chains connecting the base and the moving platform. Each chain contains a lower link rotating around a pivot perpendicular to the base platform, and is offset placed from the center of the base. At the other end of the lower link a prismatic actuator is attached by a spherical joint. The upper end of the prismatic actuator is connected to the moving platform by a revolute joint. The revolute joints axes constitute an equilateral triangle in the plane of the moving platform (see Fig. 2.2).

This structure is distinguished by the location of the lower link revolute axes being placed offset from the center of the base platform. Comparison between RSPR structure and the structure suggested by Alizade [1] which uses RRPS kinematic chains, shows that due to the different order of joints, RSPR robot overcomes certain singularities (90° rotation about a vertical axis) that exist in RRPS arrangement, and reduces actuator forces as will be shown in section 4. On the other hand it should be noticed that the work volume of the RRPS is larger. Using the swept volume analysis [12] reveals that when eccentricity is eliminated in RSPR robot then both RSPR and RRPS have the same swept volume of the kinematic chains' upper extremities. Since RSPR robot has an R joint at the end of each kinematic chain, which imposes additional perpendicularity constraints, it results in a smaller vertex space and work volume than RRPS robot.

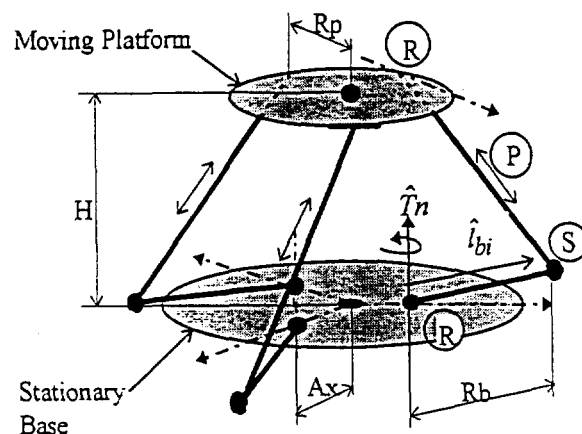


Figure 2.2: RSPR parallel robot

2.3 Double circular-triangular robot

This new structure is composed of two 3 DOF planar mechanisms. These planar mechanisms are different from the planar mechanism suggested by Daniali [5] since they use a circular-triangular combination rather than triangular-triangular one, thus providing much higher orientation capability (theoretically unlimited). The robot (shown in Fig. 2.3) has two similar planar mechanisms each one consists of a stationary circle and a moving triangle which is connected to the circle by three passive sliders pivoted on axes. The active joints actuate the location of these three pivot axes along the circumference of the stationary circle.

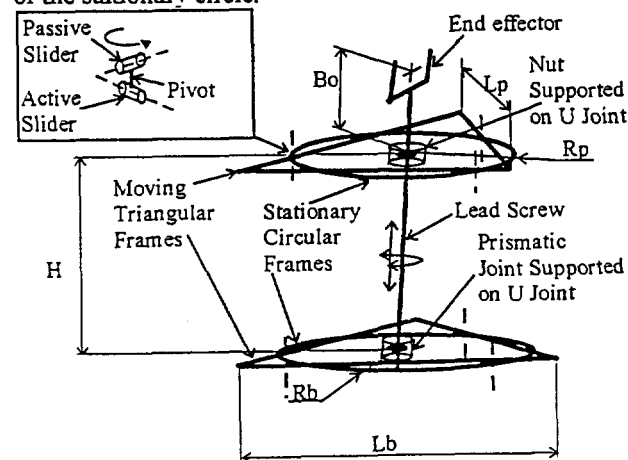


Figure 2.3 : Double circle-triangle robot

Two sets of this structure are used to construct a six-DOF robot. Each structure contributes three-DOF, namely, moves the triangle in a plane and rotates the triangle about an axis normal to this plane. With two such sets, a line connecting the triangle's centers is actuated in four-DOF. The output link is located along this line and the additional two-DOFs are obtained by controlling the

rotational motion of the moveable triangles. Each triangle's center contains a U joint and is connected to the output link at one triangle's center through a prismatic joint and at the other through a helical joint (nut and a lead screw). Rotational motion of the output link about the line connecting the centers is achieved by rotating the first movable triangle (the prismatic joint) while motion along the line is achieved by rotating both triangles at different angles. Unlike the planar mechanism suggested by Daniali [5], which allows maximum 60° rotation, the planar circle-triangle based mechanism allows full rotation and therefore practical use of the lead screw.

3 Robot performances

In the present research we aim at designing a robot for accurate remote manipulation of a laparoscopic laser dissection tool. Laparoscopic surgery has gained increasing popularity in recent years and many operative procedures are nowadays performed by this minimally invasive approach, requiring fine dexterity and accurate micro surgical technique. Utilizing laser for cutting operations is a highly demanding task since it requires the surgeon to manipulate the bulky apparatus of laparoscope, camera and laser guiding system in a constrained environment with high accuracy. Manipulating the laparoscope with an accurate robotic manipulator controlled remotely by the surgeon is therefore, an attractive approach. A parallel robot structure better fits these medical requirements. This robot structure is much more compact than the commonly used serial one, more rigid and accurate and its inherent limitation of small work volume is an advantage in medical applications where the required motion is small and safety is of utmost importance.

We examined the different parallel robots performances from several aspects: the ability to access a given work volume with a given orientation, the required forces/torques at the active joints and limitations due to singularities and spherical joints mechanical limitation. To check for robot's work volume we used the trivial inverse kinematics solution. We avoid the singularity where the Plucker coordinates of the lines stemming from the Jacobian matrices are four in a plane and hence dependent. This is the only singularity observed in the neighborhood of the work volume we examined (For a detailed singularity analysis of a series of parallel robots using line geometry, see [2]). For the static forces/torques analysis we used the Jacobian matrices the derivation of which are given below.

The Jacobian matrix transforms forces exerted by the moving platform into active joint's forces/torques.

For parallel robots the equation :

$$\tau = J^T s_e \quad (1)$$

determines the relation between the actuators generalized forces 6x1 vector, τ , and the external wrench, s_e , exerted by the moving platform on the environment. This equation is used next to determine the Jacobian matrices of the three structures.

For both USR and RSPR robots the upper part is identical, therefore we derive Jacobian matrix \tilde{J} of this common part.

Fig. 3.1 shows only one kinematic chain out of identical three. The moving platform is connected to a link A_i via a revolute joint. The moving platform exerts a wrench s_e on the environment, the lower end of the link is connected to another link B_i by a spherical joint.

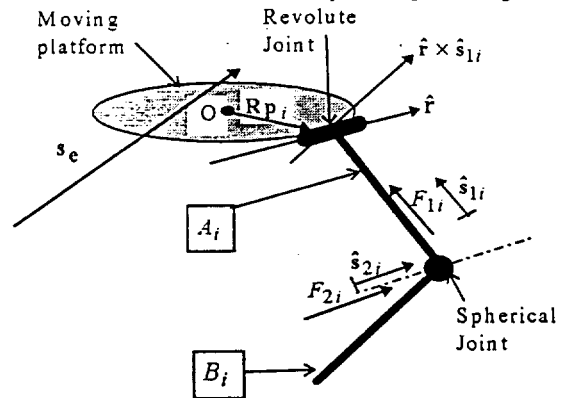


Figure 3.1: Common part of USR and RSPR robot structures

We will use the following symbols in our discussion:

'^' - unit vector.

\hat{s}_{1i} - unit vector along link A_i .

\hat{r} - unit vector along revolute joint axis.

\hat{s}_{2i} - unit vector parallel to \hat{r} passing through the spherical joint S.

R - rotation matrix from the moving platform to world coordinate system.

p_i - vector from moving platform's center to 'i'th revolute joint.

Since Link A_i is connected to link B_i by a spherical joint and to the moving platform by a revolute joint, it is capable of exerting force in the direction of \hat{s}_{1i} and moment in the direction of $\hat{r} \times \hat{s}_{1i}$ on the moving platform. Link B_i can exert on link A_i forces of magnitude F_{1i} in the direction of \hat{s}_{1i} and F_{2i} in the direction of \hat{s}_{2i} .

After some algebraic manipulation one obtains :

$$\tilde{\mathbf{J}} = [\mathbf{p}_{11}, \mathbf{p}_{12}, \mathbf{p}_{13}, \mathbf{p}_{21}, \mathbf{p}_{22}, \mathbf{p}_{23}]^T \quad i = 1, 2, 3 \quad (2)$$

where \mathbf{p}_{1i} and \mathbf{p}_{2i} are 6x1 plucker coordinates of lines $\hat{\mathbf{s}}_{1i}$ and $\hat{\mathbf{s}}_{2i}$, respectively, written relative to point 'o' and represented in world coordinates by:

$$\begin{aligned} \mathbf{p}_{1i} &= [\hat{\mathbf{s}}_{1i}, \mathbf{R}\mathbf{p}_i \times \hat{\mathbf{s}}_{1i}]^T \\ \mathbf{p}_{2i} &= [\hat{\mathbf{s}}_{2i}, (\mathbf{R}\mathbf{p}_i - \mathbf{s}_{1i}) \times \hat{\mathbf{s}}_{1i}]^T \end{aligned} \quad i = 1, 2, 3 \quad (3)$$

3.1 Jacobian matrix of USR robot

Let Tn_i and Tr_i be scalar quantities representing the magnitudes of the moments applied by the active U joint on link B_i along $\hat{\mathbf{s}}_{ni}$, $\hat{\mathbf{s}}_{ri}$ respectively (see Fig. 2.1), where $\hat{\mathbf{s}}_{ni}$, $\hat{\mathbf{s}}_{ri}$ are unit vectors along the rotation axes of the U joint. Let \mathbf{l}_{bi} denote a vector representing the lower link B, from the U to the S joint.

Static equilibrium at point U yields:

$$Tn_i = (\mathbf{l}_{bi} \times (F_{1i}\hat{\mathbf{s}}_{1i} + F_{2i}\hat{\mathbf{s}}_{2i})) \cdot \hat{\mathbf{s}}_{ni} \quad i = 1, 2, 3 \quad (4.1)$$

$$Tr_i = (\mathbf{l}_{bi} \times (F_{1i}\hat{\mathbf{s}}_{1i} + F_{2i}\hat{\mathbf{s}}_{2i})) \cdot \hat{\mathbf{s}}_{ri} \quad i = 1, 2, 3 \quad (4.2)$$

Using Eqs. (1),(2) one obtains :

$$\begin{bmatrix} F_{1i} \\ F_{2i} \end{bmatrix} = \tilde{\mathbf{J}}^T \mathbf{s}_e \quad i = 1, 2, 3 \quad (5)$$

Define \mathbf{v}_i as a 1×6 vector having 1 at the i 'th column and zeroes otherwise, then :

$$F_{1i} = \mathbf{v}_i \tilde{\mathbf{J}}^T \mathbf{s}_e \quad i = 1, 2, 3 \quad (6.1)$$

$$F_{2i} = \mathbf{v}_{i+3} \tilde{\mathbf{J}}^T \mathbf{s}_e \quad i = 1, 2, 3 \quad (6.2)$$

Substituting in Eqs. (4.1),(4.2) yields :

$$\begin{aligned} Tn_i &= \left(\mathbf{l}_{bi} \times \left(\mathbf{v}_i \tilde{\mathbf{J}}^T \mathbf{s}_e \hat{\mathbf{s}}_{1i} + \mathbf{v}_{i+3} \tilde{\mathbf{J}}^T \mathbf{s}_e \hat{\mathbf{s}}_{2i} \right) \right) \cdot \hat{\mathbf{s}}_{ni} \\ Tr_i &= \left(\mathbf{l}_{bi} \times \left(\mathbf{v}_i \tilde{\mathbf{J}}^T \mathbf{s}_e \hat{\mathbf{s}}_{1i} + \mathbf{v}_{i+3} \tilde{\mathbf{J}}^T \mathbf{s}_e \hat{\mathbf{s}}_{2i} \right) \right) \cdot \hat{\mathbf{s}}_{ri} \end{aligned} \quad i = 1, 2, 3 \quad (7)$$

after some algebraic manipulation one obtains:

$$\begin{bmatrix} Tr_1 \\ Tr_2 \\ Tr_3 \end{bmatrix} = \begin{bmatrix} \left[(\hat{\mathbf{s}}_{1i} \times \hat{\mathbf{s}}_{ri}) \cdot \mathbf{l}_{bi} \mathbf{v}_i + (\hat{\mathbf{s}}_{2i} \times \hat{\mathbf{s}}_{ri}) \cdot \mathbf{l}_{bi} \mathbf{v}_{i+3} \right] \tilde{\mathbf{J}}^T \\ \left[(\hat{\mathbf{s}}_{1i} \times \hat{\mathbf{s}}_{ri}) \cdot \mathbf{l}_{bi} \mathbf{v}_i + (\hat{\mathbf{s}}_{2i} \times \hat{\mathbf{s}}_{ri}) \cdot \mathbf{l}_{bi} \mathbf{v}_{i+3} \right] \tilde{\mathbf{J}}^T \\ \left[(\hat{\mathbf{s}}_{1i} \times \hat{\mathbf{s}}_{ri}) \cdot \mathbf{l}_{bi} \mathbf{v}_i + (\hat{\mathbf{s}}_{2i} \times \hat{\mathbf{s}}_{ri}) \cdot \mathbf{l}_{bi} \mathbf{v}_{i+3} \right] \tilde{\mathbf{J}}^T \end{bmatrix} \mathbf{s}_e \quad (8)$$

and the inverse transpose of the Jacobian matrix of the USR robot is given by the matrix in the right hand side.

3.2 Jacobian matrix of RSPR robot

Since the upper part of this robot is identical to the previous one, Eq. (6) is used and substituted in the expression of the moments at the lower link.

The moments at the lower rotating links are:

$$Tn_i = (\mathbf{l}_{bi} \times (F_{1i}\hat{\mathbf{s}}_{1i} + F_{2i}\hat{\mathbf{s}}_{2i})) \cdot \hat{\mathbf{s}}_{ni} \quad i = 1, 2, 3 \quad (9)$$

Following the same steps as for the USR robot one obtains the inverse transpose of the Jacobian matrix, on the right hand side of the following equation:

$$\begin{bmatrix} F_{1i} \\ F_{2i} \end{bmatrix} = \begin{bmatrix} \mathbf{v}_i \tilde{\mathbf{J}}^T \\ \left[(\hat{\mathbf{s}}_{1i} \times \hat{\mathbf{s}}_{ri}) \cdot \mathbf{l}_{bi} \mathbf{v}_i + (\hat{\mathbf{s}}_{2i} \times \hat{\mathbf{s}}_{ri}) \cdot \mathbf{l}_{bi} \mathbf{v}_{i+3} \right] \tilde{\mathbf{J}}^T \end{bmatrix} \mathbf{s}_e \quad i = 1, 2, 3 \quad (10)$$

3.3 Jacobian matrix of the double circular-triangular robot

This robot has two similar planar mechanisms at its upper and lower parts hence it is useful to derive the Jacobian matrix for the planar robot and utilize this matrix to derive the Jacobian matrix of the spatial robot.

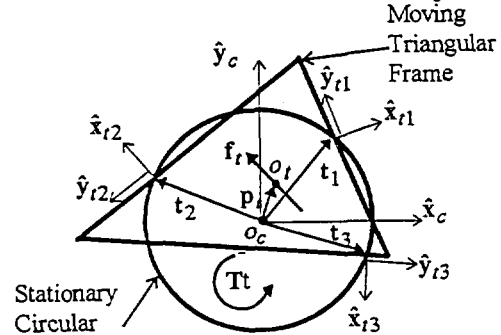


Figure 3.2 : Planar circular-triangular robot

The following additional symbols will be used in this section :

$\tilde{\mathbf{J}}$ - Jacobian matrix of the planar robot.

o_c, o_t - center points of the base circle and the moving triangle respectively.

\mathbf{p}_i - position vector from o_t to o_c .

t_i - active sliders position vectors $i = 1, 2, 3$.

\mathbf{s}_e - external force and torque exerted by the robot on the environment.

\mathbf{f}_i - force applied by the planar robot in the plane of the moving triangle.

T_i - magnitude of torque applied by the planar robot, perpendicular to the moving triangle.

${}^j R_i$ - rotation matrix, transforming vectors from i to j coordinate system.

g_j - function which relates between input moment and the output moment of the U joint ($T_{in} = g_j * T_{out}$).

l - screw lead with a right handed helix.

η - efficiency of lead screw.

From static equilibrium the Jacobian matrix of the planar robot is obtained as:

$$\bar{J} = \begin{bmatrix} c_1 & c_2 & c_3 \\ d_1 & d_2 & d_3 \\ e_1 & e_2 & e_3 \end{bmatrix}^T \quad \begin{aligned} c_i &= (\hat{x}_{ti} \cdot \hat{x}_0) * (\hat{x}_{ti} \cdot (\hat{z}_0 \times \hat{t}_i)) \\ d_i &= (\hat{x}_{ti} \cdot \hat{y}_0) * (\hat{x}_{ti} \cdot (\hat{z}_0 \times \hat{t}_i)) \\ e_i &= a_i \hat{x}_{ti} \cdot (\hat{z}_0 \times \hat{t}_i) \end{aligned} \quad (11)$$

$$a_i = (\hat{t}_i \times \hat{x}_{ti}) \cdot \hat{z}_0 - (\hat{x}_{ti} \cdot \hat{y}_0)(\hat{P}_{ti} \cdot \hat{x}_0) + (\hat{x}_{ti} \cdot \hat{x}_0)(\hat{P}_{ti} \cdot \hat{y}_0) \quad i = 1, 2, 3$$

The relation between actuator forces and exerted forces/moments by the moving triangle f_t, T_t is given by:

$$\begin{bmatrix} \tau_1 \\ \tau_2 \\ \tau_3 \end{bmatrix} = \bar{J}^T \begin{bmatrix} f_{tx} \\ f_{ty} \\ T_t \end{bmatrix} \quad (12)$$

For the spatial robot we will use indices p and b to refer to the upper and the lower planar robots.

First we decompose the exerted force/torque in end effectors coordinate system (see Fig. 2.3). From static equilibrium for the lead screw one obtains:

$$\mathbf{M}_p = \begin{bmatrix} \frac{h}{l_s} & 0 & 0 & 0 & \frac{1}{l_s} & 0 \\ 0 & \frac{h}{l_s} & 0 & -\frac{1}{l_s} & 0 & 0 \\ 0 & 0 & 1 & 0 & 0 & 0 \end{bmatrix}; \quad \mathbf{M}_b = \begin{bmatrix} (1-\frac{h}{l_s}) & 0 & 0 & 0 & -\frac{1}{l_s} & 0 \\ 0 & (1-\frac{h}{l_s}) & 0 & \frac{1}{l_s} & 0 & 0 \\ 0 & 0 & 0 & 0 & 0 & 0 \end{bmatrix} \quad (13)$$

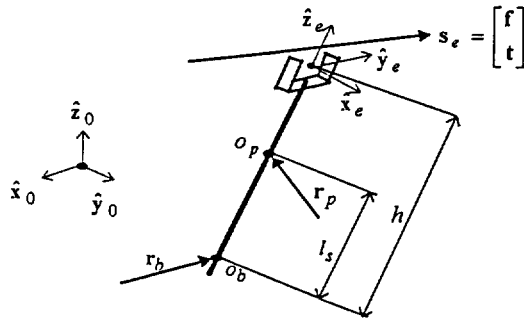


Figure 3.3: Parameters of lead screw

Where r_p and r_b are forces applied by the upper and lower planar robots on the screw, written in end effector attached system.

Using Eqs. (12-14) one obtains:

$$\begin{bmatrix} \tau_{1p} \\ \tau_{2p} \\ \tau_{3p} \end{bmatrix} = \bar{J}^T N_p s_e; \quad \begin{bmatrix} \tau_{1b} \\ \tau_{2b} \\ \tau_{3b} \end{bmatrix} = \bar{J}^T N_b s_e \quad (14)$$

where matrices N_p and N_b are given by Eq. (15), and vector v_i is a 1×3 row vector with 1 at the i 'th column and zeroes otherwise.

$$N_p = \begin{bmatrix} v_1^0 R_e M_p \\ v_2^0 R_e M_p \\ 0, 0, \frac{-g_j l}{2\pi\eta}, 0, 0, 0 \end{bmatrix}; \quad N_b = \begin{bmatrix} v_1^0 R_e M_b \\ v_2^0 R_e M_b \\ 0, 0, \frac{g_j l}{2\pi\eta}, 0, 0, g_j \end{bmatrix} \quad (15)$$

Defining generalized forces as $[\tau_p, \tau_b]^T$ we find the inverse transpose of the Jacobian matrix, given in the right hand side of the following equation:

$$\begin{bmatrix} \tau_p \\ \tau_b \end{bmatrix} = \begin{bmatrix} \bar{J}_p^T N_p \\ \bar{J}_b^T N_b \end{bmatrix} s_e \quad (16)$$

4 Simulation goal and results

The goal of this investigation was to design a robot that can manipulate surgical tools within a given work volume, with a given force and accuracy, to minimize its size and to obtain a robot which can be realized from design point of view.

The desired work volume is a $40 \times 40 \times 20$ mm cube. The robot has to reach all points within this cube with an orientation of up to 20° . The robot should fit into a cube smaller than $200 \times 200 \times 200$ mm.

All simulations use the inverse kinematic solution of each structure to check for accessibility while different robot dimensions, such as: base radius, moving platform radius and initial height, were examined. The simulations excluded robots which contain singular points within the desired work volume, and robots which exceed the limitation of 30° spherical joint inclination angle.

The dimensions of the smallest robot of each structure are shown in table 4.1. All dimensions are in millimeters and correspond to figures at section 2. Smaller robots were also found, but design considerations such as joint and motor sizes and mechanical feasibility excluded them from the final list.

In initial position the platforms are parallel at a distance H , and the center of the moving platform coincides with the center of the workspace cube.

Forces for each robot were computed along a diagonal linear path from the lower corner of the workspace cube, (point $[-20, -20, -10]$) to the upper corner of the cube (point $[20, 20, 10]$), while keeping the moving platform with an orientation of 20° rotation about $[1, 1, 1]$ axis.

The results are shown in Figs. 4.1 to 4.4, The external wrench applied by the robots is $s_e = [7,7,7 \text{ N}, 0.7,0.7,0.7 \text{ Nm}]$.

Table 4.1					
USR		RSPR		Double planar	
Rp	30	Rp	50	Rb, Rp	199,138
Ax	30	Rb	90	Lb,Lp	460,320
H	80	H	160	H	60
L1	60	Ax	20	Lead	25
L2	80	-----	-----	Bo	50

Fig. 4.4 shows a comparison between RSPR and RRPS robot [1] with RSPR having zero eccentricity. This figure with Fig. 4.2 shows that placing the R joints on the moving platform requires less torques at the active R joints (about 37%) while the linear actuator forces in both robots are almost the same.

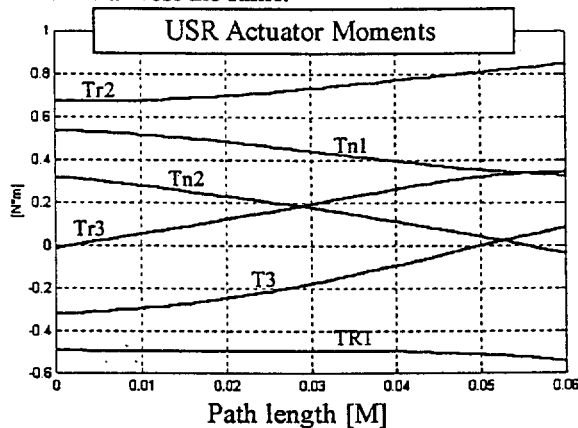


Figure 4.1

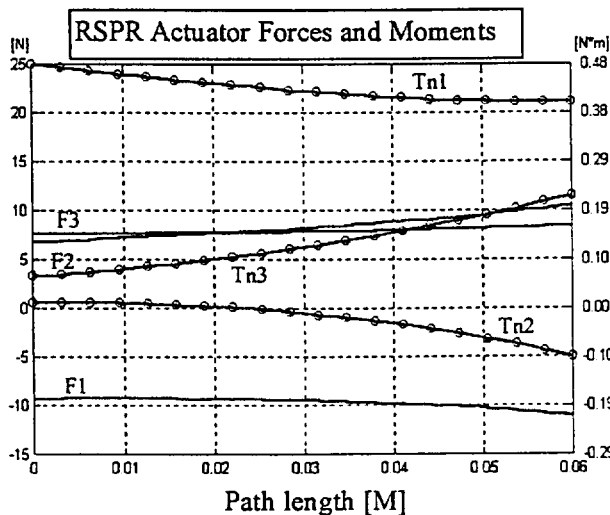


Figure 4.2

Figs. 4.5 to 4.7 show models of each robot (The USR robot in this figure is in a singular position as one of the links is coplanar with the moving platform).

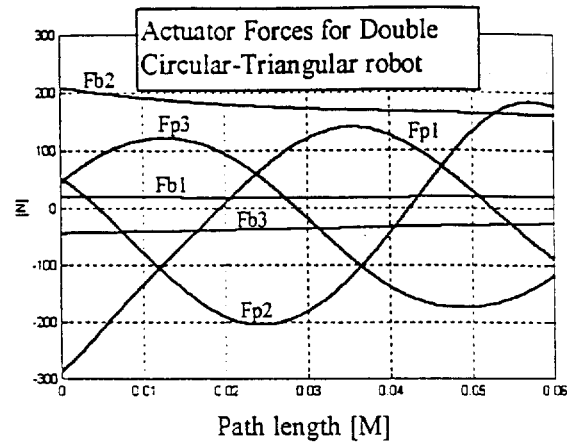


Figure 4.3

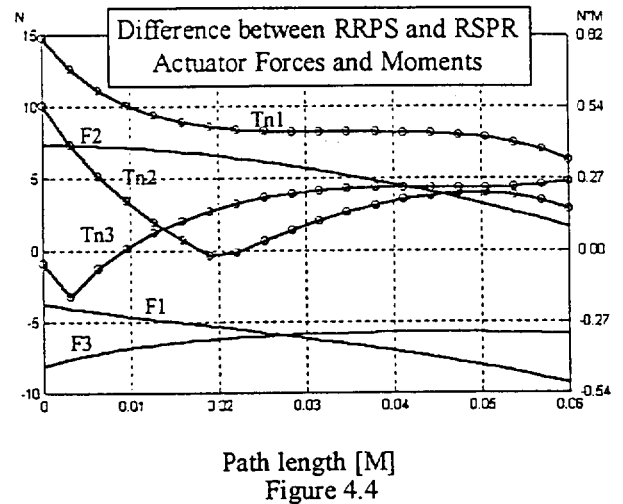


Figure 4.4

5 Conclusions

The goal of this investigation was to construct a robot that best fits a given medical application. Among several structures that were investigated three parallel robots are presented. The Double circular-triangular Robot is a novel structure with a considerably different structure than the Gough, Stewart platform. The RSPR robot is a variation of a known structure with a different location and order of joints that reduces required actuator forces and reduces singular positions. By changing the order of the joints the USR robot enhances the performances of a known structure.

Jacobian matrices of all three robots were derived. Simulation results compare the three structures from desired work volume and active joints forces/torques points of view.

Among the three presented robots, the RSPR robot best fits the required task. This robot has the simplest design and the largest work volume. The USR robot has

one practical limitation at the spherical joints because of large inclination angles and the use of differential drive. The Double-Planar robot exceeds the task limitations with its enveloping volume and requires large actuator forces.

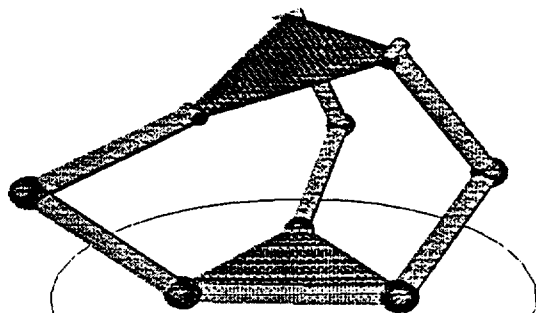


Figure 4.5: USR robot

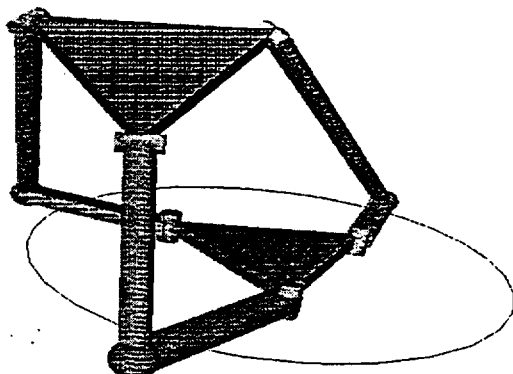


Figure 4.6 : RSPR robot

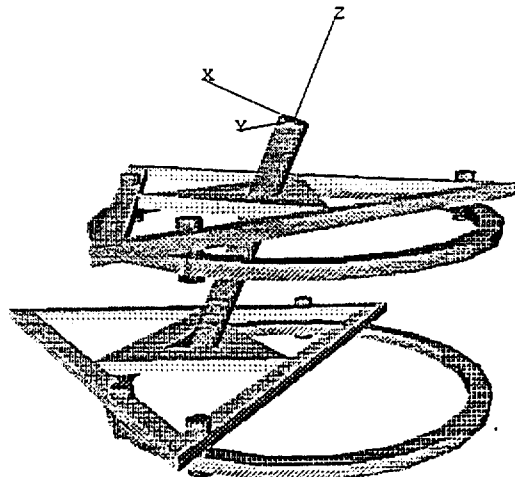


Figure 4.8: Double circular-triangular robot

Acknowledgments

This research was supported by the Mitchel-Sorf Foundation and by the fund for the promotion of research at the Technion.

References

- [1] Alizade, R.I. and Tagiyev, N.R. - "A Forward and Reverse Displacement Analysis of a 6-DOF in-Parallel Manipulator", *Mechanism and Machine Theory*, Vol.29, No.1, 1994, pp. 115-124.
- [2] Ben-Horin, R. "Design Parameters of Parallel Robots", Ph.D. Thesis, Technion, Haifa, Israel, 1998.
- [3] CIRP Annals. Vol. 46, 1997.
- [4] Cleary, K., Uebel, M., - " Jacobian Formulation for a Novel 6-DOF Parallel Manipulator " , Proc. IEEE Conference on Robotics and Automation, 1994, Vol. 3, pp. 2377-2382
- [5] Daniali, M.H.R., Zsombar-Murray, P.J., and Angeles, J : " The Kinematics of a Three DOF Planar and Spherical Double Triangular Parallel Manipulators", *Computational Kinematics*, eds. Angeles, J., Kovacs, P., Hommel, G., Kluwer Academic Publishers, 1993, pp. 153-164.
- [6] Hara, A. and Sugimoto, K., "Synthesis of Parallel Micromanipulators", *Asme Transactions. Journal of Mechanisms, Transmissions and Automation in Design*, Vol.111, 1989, pp. 34-39.
- [7] Lindem, T. J., : "Octahedral Machine with a Hexapodal Triangular Servostrut Section". US patent 5401128, Ingersoll Milling Machine Company, Rockford, IL, 1995.
- [8] Merkle, R.C., " A New Family of Six Degrees of Freedom Positional Devices " , *Nanotechnology*, Vol. 8, No. 2, 1997, pp. 47-52.
- [9] Merlet, J.P., Web Page 1997
http://inria.fr/prisme/personnel/merlet/merlet_eng.html.
- [10] Pernette, E., Henein, S., Magnani, I., Clavel, R., "Design of Parallel Robots in Microrobotics", *ROBOTICA*, Vol.15, pp. 417-420, July-August 1997.
- [11] Sheldon, P.C., " Six Axis Machine Tool ". US patent 5388935. Giddings & Lewis, Inc., Fond du Lac, WI, 1995.
- [12] Zhiming, J., "Workspace Analysis of Stewart Platforms via Vertex Space", *Journal of Robotic Systems*, Vol. 11(7), pp. 631-639, 1994.

References

- [Alizade, Tagiyev, and Duffy, 1994] Alizade, R. I., Tagiyev, N. R., "A Forward and Reverse Displacement Analysis of a 6-DOF In-Parallel Manipulator," *Mechanism and Machine theory*, Vol. 29, No. 1, pp. 115-124, 1994.
- [Basu and Ghosal, 1996] Basu, D., Ghosal, A., "Singularity Analysis of Platform-Type Multi-Loop Spatial Mechanisms," *Mechanism and Machine Theory*, Vol. 32, No., 3, pp. 375-389, 1997.
- [Behi, 1988] Behi, F., "Kinematic Analysis for a Six-Degrees-of-Freedom 3-PRPS Parallel Mechanism," *IEEE Journal of Robotics and Automation*, Vol. 4, No. 5, pp. 561-565.
- [Ben-Horin and Shoham, 1996] Ben-Horin, R., and Shoham, M., "Construction of a Six Degrees-of-Freedom Parallel Manipulator with Three Planarly Actuated Links." *Proceedings of the 1996 ASME Design Engineering Technical Conference and Computers in Engineering Conference*, August 18-22, 1996.
- [Ben-Horin, 1997] Ben-Horin, R., *Criteria for Analysis of Parallel Robots*, Ph.D. dissertation, The Technion, Israel, 1997.
- [Brandt, et al., 1997] Brandt, G., Radermacher, K., Lavallee, S., Staudte, H.-W., Rau, G., "A Compact Robot for Image Guided Orthopedic Surgery: Concept and Preliminary Results." *Lecture notes in Computer Science 1205*, CVRMed-MRCAS'97, Troccaz, J., Grimson, R., and Mosges R., eds., 1997, Springer, pp. 767-776.
- [Brodsky, Glozman, and Shoham, 1998] Brodsky, V., Glozman, D., Shoham, M. "Double Circular-Triangular Six-Degrees-of-Freedom Parallel Robot." *Advances In Robot Kinematics: Analysis and Control*, Lenarčič, J. and Husty, M. L., eds., , Kluwer Academic Publishers, 1998, pp. 155-164.
- [Burton, 1979] Burton, P., *Kinematics and Dynamics of Planar Machinery*, Prentice-Hall, 1979.

References

- [Byun and Cho, 1997] Byun, Y. K., Cho, H. S., "Analysis of a Novel 6-DOF, 3-PPSP Parallel Manipulator." *The international Journal of Robotics Research*, Vol.16, No. 6, December 1997, pp.859-872.
- [Ceccarelli, 1996] Ceccarelli, M., "A Study of Feasibility For A new Wrist," *World Automation Congress WAC'96*, Vol. 3, pp. 161-166, 1996.
- [Ceccarelli, 1997] Ceccarelli, M., "A New 3 D.O.F. Spatial Parallel Mechanism." *Mechanism and Machine Theory*, Vol. 32, No. 8, 1997, pp. 895-902.
- [Chablat and Wenger 1998] Chablat, D., Wenger, Ph., "Working Modes and Aspects in Fully Parallel Manipulators," *IEEE International Conference on Robotics and Automation*, pp. 1964-1969, 1998.
- [Cleary and Uebel, 1994] Cleary, C., Uebel, M., "Jacobian Formulation For A Novel 6-DOF Parallel Manipulator." *IEEE International Conference on Robotics and Automation*, 1994, Vol.3, pp.2377-2382.
- [Collins and Long, 1995(a)] Collins, C. L., Long. G. L., "The Singularity Analysis of an In-Parallel Hand Controller for Force-Reflected Teleoperation." *IEEE Transactions on Robotics and Automation*, Vol. 11, No. 5, 1995, pp. 661-669.
- [Collins and Long, 1995(b)] Collins, C. L., Long. G. L., "On the Duality of Twist/Wrench Distributions in Serial and Parallel Chain Robot Manipulators," *IEEE International Conference on Robotics and Automation*, pp. 526-531, 1995.
- [Dandurand, 1984] Dandurand, A., "The Rigidity of Compound Spatial Grid," *Structural Topology*, Vol. 10, pp. 41-56, 1984.
- [Daniali, Zombar- Murray, and Anjeles, 1993] Daniali, M. H. R., Zsombar-Murray, P. J., Anjeles, J., "The Kinematics of 3-Dof Planar and Spherical Double-Triangular Parallel Manipulators." *Computational Kinematics*, Anjeles, J., Kovacs, P., eds., Kluwer Academic Publishers, 1993, pp. 153-164.

References

- [Dario, et al., 1997] Dario, P., Paggetti, C., Troisfontaine, E., Papa, T., Ciucci, M. C., Carrozza, M. M., "A Miniature Steerable End-Effector for Application in Integrated System for Computer-Assisted Arthroscopy." IEEE International Conference on *Robotics and Automation*, 1997, pp. 1573-1579.
- [Dietmaier 1998] Dietmaier, P., "The Stewart-Gough Platform of General Geometry Can Have 40 Real Postures," *Advances in Robot Kinematics: Analysis and control*, Lenarčič, J., and Husty, M. L., eds., pp. 7-16, Kluwer Academic Publishers, 1998.
- [Dunlop and Jones, 1997] Dunlop, G. R., Jones, T. P., "Position Analysis of a 3-DOF Parallel Manipulator," *Mechanism and Machine Theory*, Vol. 32, no. 8, pp. 903-920, 1997.
- [Dunlop, Jones, and Lintott, 1994] Dunlop, G. R., Jones, T. P., Lintott, A. B., "Three DOF Parallel Robots for Linear and Spherical Positioning," *ISRAM*, pp. 655-660, Hawaii, 1994.
- [Earl and Rooney, 1983] Earl, C. F., Rooney, J., "Some Kinematic Structures for Robot Manipulator Designs," *Journal of Mechanisms, Transmissions, and Automation in Design*, 1983, Vol. 105, pp. 15-22.
- [Ebert and Gosselin, 1998] Ebert, U., Gosselin, C. M., "Kinematic Study of a New Type of Spatial Parallel Platform Mechanism," *ASME Design Engineering Technical Conference*, Atlanta, 13-16, September 1998.
- [Faraz and Payandeh, 1998] Faraz, A., Payandeh, S., "A Robotic Case Study: Optimal Design for Laparoscopic Positioning Stands." *International Journal of Robotics Research*, Vol. 17, No. 9, 1998, pp. 986-995.
- [Fichter, 1986] Fichter, E. F., "A Stewart Platform-Based Manipulator: General Theory and Practical Construction." *Int. J. Robotics Research*, Vol. 5, No. 2, 1986, pp. 157-182.
- [Finlay and Ornstein, 1995]. Finlay, P. A., Ornstein, M. H., "Controlling the

- Movement of a Surgical Laparoscope,” IEEE *Engineering in Medicine and Biology*, May/June 1995, Vol. 14, pp. 289-291.
- [Gosselin and Angeles, 1990] Gosselin, C., Angeles, J., “Singularity Analysis of Closed-Loop Kinematic Chains,” IEEE Transactions on *Robotics and Automation*, Vol. 6, No. 3, pp. 281-290, 1990.
- [Gough and Whitehall, 1962] Gough, V. E. and Whitehall, S. G., ”Universal Tyre Test Machine.” Proceedings, Ninth International Technical Congress F.I.S.I.T.A. May 1962, 117 (Institute of Mechanical Engineers)
- [Grace, et al., 1993] Grace, K. W., Colgate, J. E., Glucksberg, M. R., Chun, J. H., “A Six Degree of Freedom Micromanipulator for Ophthalmic Surgery.” IEEE International Conference on *Robotics and Automation*, 1993, pp. 630-635.
- [Graustein, 1930] Graustein, W. C., *Introduction to Higher Geometry*, The Macmillan Company, 1930.
- [Hao and McCarthy, 1998] Hao, F., McCarthy, J. M., “Conditions for Line-Based Singularities in Spatial Platform Manipulators,” *Journal of Robotic Systems*, Vol. 15, No. 1, pp. 43-55, 1998.
- [Harris, et al., 1997] Harris, S. J., Lin, W. J., Fan, K. L., Hibberd, R. D., Cobb, J., Middleton, R., Davies, B. L., “Experiences With Robotic Systems for Knee Surgery.” Lecture notes in Computer Science 1205, CVRMed-MRCAS’97, Troccaz, J., Grimson, R., and Mosges R., eds., 1997, Springer, pp. 757-766.
- [Ho, et al., 1995] Ho, S. C., Hibberd, R. D., Davies, B. L., “Robot Assisted Knee Surgery.” IEEE *Engineering in Medicine and Biology*, May/June 1995, Vol. 14, pp. 292-299.
- [Hon-Cheung, 1981] Hon-Cheung, Y., “The Bennett Linkage, its Associated Tetrahedron and the Hyperboloid of its Axes,” *Mechanism and Machine Theory*, Vol. 16, pp. 105-114, 1981.

References

- [Honegger, et al., 1997] Honegger, M., Codourey, E., Burdet, E., "Adaptive Control of the Hexaglide, a 6 dof Parallel Manipulator," IEEE International Conference on *Robotics and Automation*, Vol. 1, pp. 543-548, 1997
- [Hunt, 1978] Hunt, K. H., *Kinematic Geometry of Mechanisms*. Clarendon Press, Oxford, 1978.
- [Hunt, 1983] Hunt, K. H., "Structural Kinematics of In-Parallel-Actuated Robot arms," *Journal of Mechanisms, Transmissions, and Automation in Design*, 1983, Vol. 105, pp. 705-712.
- [Hunt, Samuel, McAaree, 1991] Hunt, K. H., Samuel, A. E., McAree, P. R., "Special Configurations of Multi Freedom Grippers – A kinematic Study," *The International Journal of Robotics Research*, Vol. 10, No. 2, pp. 123-134, 1991.
- [Innocenti and Parenti-Castelli, 1994] Innocenti, C., Parenti-Castelli, V., "Exhaustive Enumeration of Fully Parallel Kinematic Chains." ASME trans. Dynamic Systems and Control, Vol. 2, 1994, pp. 1135-1141.
- [Jensen et al., 1994] Jensen, P. S., Glucksberg, M. R., Colgate, J. E., Grace, K. W., Attariwala, R., "Robotic Micromanipulator for Ophthalmic Surgery." 1st International Symposium on Medical Robotics and Computer Assisted Surgery, pp. 204-210. Pittsburgh, 22-24 September, 1994.
- [Karger, 1998] Karger, A., "Architecture Singular Parallel Manipulators," *Advances In Robot Kinematics: Analysis and Control*, Lenarčič, J. and Husty, M. L., eds., Kluwer Academic Publishers, 1998, pp. 445-454.
- [Kavoussi, et al., 1996] Kavoussi, L. R., Moore, R. G., Adams, J. B., Partin, A. W., "Comparison of Robotic Versus Human Laparoscopic Camera Control." 2nd Annual International Symposium on Medical Robotics and Computer-Assisted Surgery (MRCAS'95), pp. 284-287.
- [Kazanzides, et al., 1995] Kazanzides, P., Mittelstadt, B. D., Musits, B. L., Bargar,

- W. L., Zuhar, J. F., Williamson, B., Cain, Ph. W., Carbone, E., J., "An Integrated System for Cementless Hip Replacement." *IEEE Engineering in Medicine and Biology*, May/June 1995, Vol. 14, pp.307-312.
- [Khodabandehloo, et al., 1996] Khodabandehloo, K., Brett, P. N., Buckingham, R. O., "Special-Purpose Actuators and Architectures for Surgery Robots", *Computer-Integrated Surgery*, Taylor, R., Lavllée, S., Burdea, G., Ralph Mösges, eds., pp. 263-274, 1996.
- [Kholi, et al., 1988] Kholi, D., Lee, S-H, Tsai, K-Y, Sandor, G. N., "Manipulator Configurations Based on Rotary-Linear (R-L) Actuators and Their Direct and Inverse Kinematics," *Journal of Mechanisms, Transmissions, and Automation in Design*, Vol. 110, pp. 397-404, 1988.
- [Kienzle, et al., 1995] Kienzle, T. C., Stulberg, S. d., Peshkin, M., Quaid, A., Lea, J., Goswami, A., Wu Chi-haur, "Total Knee Replacement." *IEEE Engineering in Medicine and Biology*, May/June 1995, Vol. 14, pp.301-306.
- [Kienzle, et al., 1996] Kienzle III, T., Stulberg, D., Peshkin, M., Quaid, A., Lea, J., goswami, A., Wu, Ch., "A Computer-Assisted Total Knee Replacement Surgical System Using a Calibrated Robot." in *Computer Integrated Surgery*. Taylor, Lavallee, Burdea, and Mosges, eds., MIT Press, 1996. pp. 410-416.
- [Lallemand et al., 1997] Lallemand, J. P., Goudali, A., Zeghloul, S., "The 6-Dof 2-Delta Parallel robot." *Robotica*, 1997, Vol. 15, pp. 407-416.
- [Lazard, 1993]. Lazard, D., "On The Representation Of Rigid-Body Motions And Its Application To Generalized Platform Manipulators," *Computational kinematics*, Anjeles, J., Hommel, G., and Kovács, eds., pp. 175-181, Kluwer Academic Publishers, 1993.
- [Lee, 1995] Lee K. L., "Design of a High Stiffness Machining Robot

- Arm using Double Parallel Mechanisms.” IEEE International Conference on *Robotics and Automation*, 1995, Vol. 1, pp.234-240.
- [Lindem, 1995] Lindem, T. J., “Octahedral Machine With a Hexapodal Triangular Servostrut Section.” US patent 5401128, Ingersoll Milling Machine Company, Rockford, IL, 1995.
- [Lipkin and Duffy, 1985] Lipkin, H., Duffy, J., “A Vector Analysis Of Robot Manipulators,” Recent Advances In Robot Kinematics, Beni, G., and Hackwood, S., eds., pp. 175-241, 1985.
- [Ma and Angeles, 1992] Ma, O., Angeles, J., “Architecture Singularities of Parallel Manipulators,” International Journal of *Robotics and Automation*, Vol. 7, No. 1, 1992.
- [Malik and Kerr, 1992] Malik, A. N., Kerr, D., “A new Approach to Type Synthesis of Spatial Robotic Mechanisms,” Robotics, Spatial Mechanisms, and Mechanical Systems, Kiezal, Reinholtz, Lipkin, Tsai, Pennock, Cipra, eds., DE – Vol. 45, pp. 387-395, 1992.
- [Merkle, 1997] Merkle, R. C., ”A New Family of Six Degrees of Freedom Positional Devices.” *Nanotechnology*, Vol. 8, No. 2, 1997, pp. 47-52.
- [Merlet, 1989] Merlet, J. P., “Singular Configurations of Parallel Manipulators and Grassmann Geometry,” The International Journal of *Robotics Research*, Vol. 8, No. 5, 1989.
- [Merlet, web page] <http://www-sop.inria.fr/saga/personnel/merlet/Archi/node2.html>
- [Mimura and Funahashi, 1995] Mimura, N., Funahashi, Y., “A New Analytical System Applying 6 DOF Parallel Link Manipulator For Evaluating Motion Sensation.” IEEE International Conference on *Robotics and Automation*, 1995, pp. 227-333.
- [Nakashima, 1994] Nakashima, k. “A Six-Axis Motion Base and a Study of

References

- a Parallel Manipulator.” *Advanced Robotics*, 1994, Vol. 8, No. 6, p. 609.
- [Notash, 1998] Notash, L., “Uncertainty Configurations of Parallel Manipulators,” *Mechanism and Machine Theory*, Vol. 33, No. 1, pp. 123-138, 1998.
- [Pernette, et al., 1997] Pernette, E. Henein, S., Magnani, I., Clavel, R., “Design of Parallel Robots in Microrobotics.” *Robotica*, 1997, Vol. 15, pp.417-420.
- [Phillips, 1990] Phillips, J., *Freedom In Machinery*, Cambridge Press, 1990.
- [Romiti and Soreli, 1990] Romiti, A, Soreli, M., “Flexible Sensorized Micro-Assembly by a Small Parallel Manipulator,” *Int. FAMOS Seminar*, pp. 181-189, 1990.
- [Roth, 1984] Roth, B., “Screws, Motors, and Wrenches that Cannot be Bought in a Hardware Store,” *Robotics Research: The 1st International Symposium*, Brady, M. and Paul, R., eds., pp. 679-693, 1984.
- [Schmidt, et al.,]
- [Shainpoor, 1992] Shahinpoor, M., “Kinematics of a Parallel-Serial (Hybrid) Manipulator,” *Journal of Robotic systems*, Vol. 9, no. 1, pp. 19-36. 1992.
- [Sheldon, 1995] Sheldon, P. C., “Six Axis Machine Tool.” US patent 5388935. Giddings & Lewis, Inc., fon du Lac, WI, 1995.
- [Shoham and Roth, 1997] Shoham, M., Roth, B., “Connectivity in Open and Closed Loop Robotic Mechanisms,” *Mechanism and Machine theory*, Vol. 32, No. 3, pp. 279-293, 1997.
- [Simaan, Glozman, and Shoham, 1998] Simaan, N., Glozman, D., Shoham, M., “Design Considerations of New Six Degrees-Of-Freedom Parallel Robots.” *IEEE International Conference on Robotics and Automation*, 1998, Vol. 2, pp. 1327-1333.
- [Slutski, 1998] Slutski, I. L., *Remote Manipulation Systems Quality Evaluating and Improvement*, Kluwer Academic

References

- Publishers, 1998.
- [Sommerville, 1934] Sommerville, D. M. Y., *Analytical Geometry of Three Dimensions*, Cambridge Press, 1934.
- [Soreli, et al., 1997] Soreli, M., Ferraresi, C., Kolarski, M., Borovac, C., Vukobratovic, M., "Mechanics of Turin Parallel Robot." *Mechanism and Machine Theory*, Vol. 32, No. 1, 1997, pp. 51-77.
- [Stewart,1965] Stewart, D., "A Platform With Six Degrees-of-Freedom." *Proc Inst. Mech. Engrs.*, Vol. 180 Part 1, No. 15, 1965, pp. 371-386.
- [Tahmasebi and Tsai, 1992] Tahmasebi, F., Tsai, L.W., "Jacobian And Stiffness Analysis of A Novel Class of Six-DOF Parallel Minimanipulators," *ASME DE-Vol. 47, Flexible Mechanisms, Dynamics and Analysis*, pp. 95-102, 1992.
- [Tahmasebi and Tsai, 1994(a)] Tahmasebi, F., Tsai, L.W., "Closed-Form Direct Kinematics Solution of a New Parallel Minimanipulator," *Transactions of the ASME, Journal of Mechanical Design*, Vol. 116, pp. 1141-1147, 1994.
- [Tahmasebi and Tasi, 1994(b)] Tahmasebi, F., Tsai, L.W., "Jacobian And Stiffness Analysis Of A Novel Class Of Six-DOF Parallel Minimanipulators." *DE-Vol. 47, Flexible Mechanisms, Dynamics, and Analysis*, ASME 1992, pp. 95-102.
- [Tahmasebi and Tsai, 1995] Tahmasebi, F., Tsai, L.W., "On the Stiffness Of a Novel Six-DOF Parallel Minimanipulator." *Journal of Robotic Systems*, 1995, Vol. 12, No. 12, pp. 845-856.
- [Taylor, et al., 1995] Taylor, R. H., Funda, J., Eldridge, B., Gomory, S., Gruben, K., Larose, D., Talamini, M., Kavoussi, L., Anderson, J., "A Telerobotic Assistant for Laparoscopic Surgery." *IEEE Engineering in Medicine and Biology*, May/June 1995, Vol. 14, pp. 279-287.
- [Tsai and Tahmasebi, 1993] Tsai, L-W, Tahmasebi, F., "Synthesis and Analysis of a New Class of Six-Degree-of-Freedom Parallel Minimanipulators," *Journal of Robotic Systems*, Vol. 10,

- No. 5, pp. 561-580, 1993.
- [Tsai, 1998] Tsai, L-W., "The Jacobian Analysis of Parallel Manipulators Using Reciprocal Screws," *Advances in Robot Kinematics: Analysis and Control*, Lenarčič, J., and Husty, M. L., eds., pp. 327-336, Kluwer Academic Publishers, 1998.
- [Veblen and Young, 1910] Veblen, O., Young, J. W., *Projective Geometry*, Boston: The Athenaeum Press, 1910.
- [Waldron and Hunt, 1991] Waldron, K. J., Hunt, K. H., "Series-Parallel Dualities in Actively Coordinated Mechanisms," *The International Journal of Robotics Research*, Vol. 10, No., 5, pp. 473-480, 1991.
- [Wei et al., 1997] Wei, G.-Q., Arbter, K., Hirzinger, G., "Automatic Tracking of Laparoscopic Instruments by Color Coding," *Lecture notes in Computer Science 1205*, CVRMed-MRCAS'97, Troccaz, J., Grimson, R., and Mosges R., eds., 1997, Springer, pp. 357-366.
- [Woo et al., 1998] Woo, K. Y., Jin, B.D., Kwon, D-S, "A 6 DODF Force-Reflecting Hand Controller Using the Fivebar Parallel Mechanism," *IEEE International Conference on Robotics and Automation*, 1998, Vol. 2, pp. 1597-1602.
- [Xu, Kholi, and Weng, 1992] Xu, Y-X., Kholi, D., and Weng, T-Ch., "Direct Differential Kinematics of Hybrid-Chain Manipulators Including Singularity and Stability Analyses," *Robotics, Spatial Mechanisms, and Mechanical Systems*, Kiezel, Reinholtz, Lipkin, Tsai, Pennock, Cipra, eds., DE – Vol. 45, pp. 65-73, 1992.
- [Zanganeh, Sinatra, and Anjeles, 1997] Zanganeh, K. E., Sinatra, R., Anjeles, J., "Kinematics and Dynamics of a Six-Degrees-of-Freedom Parallel Manipulator With Revolute Legs." *Robotica*, 1997, Vol. 15, Part 4, pp. 385-394.
- [Zhiming, 1994] Zhiming, J., "Workspace Analysis of Stewart Platforms via Vertex Space," *Journal of Robotic Systems*, Vol. 11,

References

- No. 7, pp. 631-639, 1994.
- [Zlatanov, et al., 1992] Zlatanov, D., Dai, M. Q., Fenton, R. G., Benhabib, B., "Mechanical Design and Kinematic Analysis of a Three-Legged Six Degree-of-Freedom Parallel Manipulator," *Robotics, Spatial Mechanisms, and Mechanical Systems*, Kiezel, Reinholtz, Lipkin, Tsai, Pennock, Cipra, eds., DE – Vol. 45, pp. 529-536, 1992.
- [Zlatanov, et al., 1995] Zlatanov, D., Fenton, R. G., Benhabib, B., "A Unifying Framework for Classification and Interpretation of Mechanism Singularities," *Transactions of the ASME Journal of Mechanical Design*, Vol. 117, pp. 566-572, 1995.